UNIVERSITY OF CANTERBURY
Te Whare Wananga o Waitaha
CHRISTCHURCH NEW ZEALAND

Department of Civil Engineering

Experimental and financial investigations into the further development of Damage Avoidance Design

A thesis submitted in partial fulfilment of the requirements for the
Degree of Master of Engineering in Civil Engineering
at the University of Canterbury

by
Kevin M. Solberg

Supervised by

Professor John B. Mander
Chair of Structural Engineering

Dr. Rajesh P. Dhakal
Senior Lecturer

January 2007

Table of contents

Acknowledgements

This thesis is the culmination of research conducted at the University of Canterbury, Christchurch, New Zealand. The research was funded through the Future Building Systems research project. The public and private contributors to this project are gratefully acknowledged, specifically the Foundation for Research, Science, and Technology (FRST), Fletcher Buildings, Fifth Concrete, and Holms Consulting Group.

Throughout the course of this research I have been fortunate enough to have the support of many individuals for whom I am deeply grateful. I would first like to thank my supervisors, Professor John Mander and Dr. Rajesh Dhakal, for guiding me towards my final goal with support, patience, and faith in my abilities. I will carry with me a renewed appreciation and passion for structural engineering thanks to the energetic time and effort expended by you both on my behalf.

A big thanks to Tim Perigo and his fellow technicians in the Structural Engineering Laboratory at UC. Your work ethic is second to none, and I consider myself very lucky to have had the privilege of working side-by-side with the best technician on campus. Thank you.

The wide scope of research reported herein could not have been achieved without the teamwork put forth by my peers. Specifically, I'd like to thank Naoto Mashiko (concept development and specimen construction of the DAD pier), Katheryn Roberson (development of the IDA logarithm), Luoman Li (test setup and specimen development of the DAD beam-column joint), Brendon Bradley (analytical analysis of the DAD prototype building), and Geoff Rodgers (LE damper device development). Each one of you have helped in the growth

of this thesis in one way or another, and without that help I would not have completed even half as much.

Finally, I would like to thank my friends and family for supporting me though this adventure. My partner, Allison Ryan, pushed me to new and exciting bounds and supported me throughout the journey. Mom and Dad, you supported me and encouraged me to succeed. Without that support, I would not be where I am today. Thank you.

Abstract

Multiple experimental and computational tests are performed on precast concrete structures designed for damage avoidance. These structures are designed to accommodate non-linear behaviour by rocking at specially detailed connections. Unbonded prestress is employed to provide a restoring force and supplemental devices are used to dissipate energy. Tests are performed on a 30 percent scale bridge pier and an 80 percent scale 3D beam-column joint subassembly. Several detailing strategies are developed and tested. Straight and draped tendon profiles are considered. Supplemental energy dissipation is provided by yielding mild steel devices or lead-extrusion dampers. The lead-extrusion dampers are tested both externally and internally. Detailing at the joint region is refined in an effort to provide a cost-effective and simple solution. A closure pour is considered to simply the construction process. Results indicate it is possible to eliminate virtually all damage at the beam-column joint with minor increased cost from steel armouring. The lead-extrusion damper is shown to be ‘resetable’, and therefore would not have to be replaced following a seismic event.

Two seismic financial risk methodologies are developed to investigate the enhanced performance inherent to ductile jointed structures. A rapid method is introduced which simplifies the intensive computational effort necessary to perform loss studies. A distribution-free computational method is also examined. The methods are demonstrated with a case study of bridge piers designed to different seismic design codes and a bridge designed for damage avoidance. The bridge pier designed for damage avoidance is shown to have an expected annual loss of approximately 25 percent that of the conventional ductile piers.

Preface

The research reported herein is part of a multi-year research project entitled Future Building Systems, with financial support and guidance supplied by both the public and private sector. The Future Building Systems project is dedicated to the development of ductile jointed precast concrete systems in New Zealand. Such systems have been investigated overseas and have shown (through laboratory testing) to provide seismic performance superior to conventional monolithic systems. This is accomplished by accommodating structural deformation through a single gap opening at joints, thus allowing members to remain elastic, with the inclusion of unbonded post-tensioning to provide a restoring force to the system. Employing steel armouring at the joint interface, *Damage Avoidance Design* (DAD) is investigated with the intent of further eliminating damage from large contact forces and reducing any stiffness degradation at the joint under cyclic displacements.

WHAT IS PARTICULARLY NEW IN THIS THESIS?

In a broad sense, the research reported in this thesis is a culmination of studies on several aspects of jointed precast concrete systems. As the concept of jointed systems has been validated by past researchers, the aim in this case is to refine the body of knowledge of such systems by providing more efficient detailing schemes and to investigate the long-term financial benefits of such systems. Specifically, this is accomplished by investigating three different detailing strategies for beam-column joints and rocking columns (bridge piers) utilizing different energy dissipation devices, tendon profiles, and armouring sections. The research on bridge piers is extended analytically to investigate the expected financial loss of these systems as compared to conventional monolithic systems by developing two new methods of calculating *expected annual loss* (EAL).

STRUCTURE OF THIS THESIS

This thesis will investigate the application of DAD structures in several contexts. Each chapter of the thesis has been written to stand alone, therefore some concepts are repeated The research is presented in seven main chapters:

Chapter 1: An introduction to the concept of ductile jointed systems is provided. A hand method for predicting response is presented and a brief discussion of practical design and construction issues is given.

Chapter 2: Two loss estimation methods are developed: an advanced computational method and a simpler rapid method. The methods are illustrated using a case study of three bridge piers designed to conventional monolithic standards.

Chapter 3: Experimental bi-directional testing of a 30 percent scaled DAD bridge pier is presented. A loss study employing the methods described in Chapter 2 is conducted to examine the financial seismic risk of the DAD pier.

Chapter 4: A 3D beam-column joint subassembly is developed using a bent tendon-coupling system. A Multi-level Seismic Performance Assessment is conducted using bi-directional testing.

Chapter 5: The specimen introduced in Chapter 4 is modified to accommodate external lead-extrusion damping devices. Tests are conducted with two different levels of damping. The results are compared to the steel devices reported in Chapter 4.

Chapter 6: This chapter builds on findings of Chapter 4 and 5 by developing a new specimen employing internal lead-extrusion dampers and other design alternatives in the joint region. A Multi-level Seismic Performance Assessment is performed.

Chapter 7: The findings of this and previous research is discussed, comparing the various detailing methods and their performance. Recommendations are made for industry implementation of DAD. Further research avenues are discussed.

1 Introduction and theory

1.1 RESEARCH MOTIVATION

Under current earthquake engineering design philosophies found implicitly in codes around the world, structures in seismic zones are designed to accommodate earthquake induced displacements by forming plastic hinges at specially detailed plastic hinge zones. During earthquakes, plastic hinge zones are subjected to significant inelastic rotations. These zones provide a fuse to protect other essential elements of the structure. The plastic hinge zones, through yielding, dissipate earthquake energy thus reducing displacements, particularly in short period structures. In building frames, these plastic hinge zones are usually located at beam ends, while in bridges, they are typically found at the base of the piers. While the main structural elements are protected from being damaged, the plastic hinge zones themselves sustain a degree of damage. Under large earthquakes this damage could be extensive and irreparable. This philosophy, termed capacity design, aims to ensure life safety while allowing the engineer to reduce the strength of members – and in turn the structure's cost – by providing sufficient ductility.

Earthquakes of the past two decades such as the Northridge earthquake in 1994 and the Kobe earthquake in 1995 have validated capacity design principles with the ductile detailing approach; few deaths have been reported due to structural collapse. However, in both cases the economic costs due to uninhabitable or damaged structures (largely as a result of excessive residual displacements) has been substantial. Because of this, engineers are now beginning to explicitly consider multiple building performance objectives which, in addition to life safety, give emphasis to the economic consequences of earthquakes in the form of damage and lost productivity.

The development of jointed precast structural systems may be one such alternative that ensures minimal damage and residual displacement while still providing an economical system exhibiting non-linear force-displacement characteristics. This is accomplished by eliminating the formation of a plastic hinge, and instead accommodating deformation by gap openings through rocking. Unbonded prestress is used to clamp members together, thus providing a restoring force, while other elements (such as mild steel reinforcing bars) across the joint absorb earthquake energy.

The research explained herein will further develop the concept of ductile jointed precast concrete systems with the specific intent of eliminating all damage to the system while still maintaining labour and material costs similar to current standards. In addition, the life cycle cost savings of systems that resist damage will be investigated to help clarify their advantages over conventional monolithic systems.

1.2 LITERATURE REVIEW

1.2.1 Previous research in the United States

Some of the earliest work related to ductile jointed precast concrete systems was conducted by Priestley and Tao (1993). This conceptual study notes that by using partially unbonded prestressed tendons, it is possible to prevent effective prestress losses by ensuring the tendons remain elastic at the maximum displacement of the system. Thus, the system would return to its original position following a design level earthquake with no residual displacement. The study goes on to note that there will be an inherent reduction in energy dissipation as compared to conventional systems, due to the bi-linear elastic hysteretic response. This effect is investigated by comparing the dynamic performance of analytical single degree of freedom oscillators exhibiting various hysteresis loops and natural periods. It is found the reduced energy dissipation of such systems would slightly increase (100% increase) the maximum displacement response for long period structures, as compared to

elasto-plastic hysteresis loops. For medium period structures the effect would be more severe (200% increase). This study however, has not considered the potential variation in stiffness of monolithic or ductile jointed systems for members of the same dimension.

The concepts developed by Priestley and Tao (1993) were experimentally validated by Priestley and MacRae (1996) using uni-directional testing of beam-column joint subassemblies. Two cases were considered: an exterior joint and an interior joint, both utilizing straight unbonded post-tensioning. The beam and column were precast using a concrete-concrete interface at the joint. The maximum residual displacement of the specimen was found to be 2.2 percent of the maximum drift, thus confirming the re-centring characteristics of the system. Damage to the specimen was small compared to conventional monolithic systems; some spalling occurred at top and bottom of the beams and superficial cracks were observed across the joint and beam ends. This damage was seen in the hysteretic curve as a gradual stiffness degradation through each cycle. Energy dissipation, presumably from cracking and spalling of concrete, as well as slight yielding of the transverse reinforcement, was greater than expected, but still markedly less than conventional systems.

Shortly after experimental validation of the unbonded system, Stanton *et al.* (1997) proposed a 'hybrid' system. The concept of the system is described in Figure 1-1. By combining the bi-linear elastic hysteresis effect of unbonded post-tensioning with the elasto-plastic effect from mild steel across the joint region, the resulting hysteresis loop exhibits considerable energy dissipation yet still re-centres. Experimental tests confirmed the theory.

The hybrid concept was integrated into a 5 storey 3D test frame developed as part of the US–Japan *Precast Seismic Structural Systems* (PRESSS) Program (summarized in Priestley *et al.*, 1999). This specimen consisted of a wall system in one direction and a frame in the other, using four different detailing configurations. All detailing schemes utilized a concrete-concrete or concrete-grout interface at the joint and friction due to the clamping

force to provide shear resistance at the joint face. The researchers observed overall damage to the frame was comparatively less than expected from an equivalent monolithic system. Some spalling and cracking was observed in the beams and across the joint of the columns plus some crushing of the grout pads at the beam ends. Residual displacement was recorded to be .06 percent, less than 4 percent of the peak drift of 1.8 percent.

In an effort to fully eliminate damage, Mander and Cheng (1997) proposed a ductile jointed precast system using the concept of *Damage Avoidance Design* (DAD). In this application, contact surfaces at the joints were armoured with steel in an attempt to mitigate the high concrete compression stresses typical of such systems. The concept was tested on a reinforced concrete bridge pier utilizing a steel-steel rocking interface at its base. Uni-directional quasi-static and shake table tests were performed. Damage to the pier was negligible and it exhibited good bi-linear elastic force-displacement behaviour, with minor strength degradation. The researchers predicted the pier's response using a combination of elastic theory and rigid body kinematics, assuming the rocking action would be essentially rigid due to the inclusion of steel armouring.

1.2.2 Recent work at the University of Canterbury

Recently, attempts have been made to extend the concept of DAD to reinforced concrete frame structures. The first applications of this can be found in Davies (2003) and Arnold (2004) where analytical and physical investigations were performed. These studies developed subassemblies taken from a 9 storey frame structure, considering seismic loading in one direction and the inclusion of gravity loads from one-way floor panels in the other. A draped tendon profile was adopted for the gravity loaded frame. Uni-directional testing was performed on the 80 percent scale subassemblies. An extensive armouring system at the joint was utilized which consisted of 20mm thick full depth plates with stiffener plates provided to help spread the compressive point loads developed during rocking. The specimen performed

very well, with virtually no cracking or spalling and little residual drift. The researchers noted the rocking zone was over-designed, and suggested limiting the extensive amount of welding and steel employed in their specimens.

Li (2006) set out to refine the detailing scheme at the rocking zone with the intent of reducing material and labour costs. In addition, a new testing apparatus was developed, capable of simulating a more representative loading scenario through bi-directional loading and consideration of torsion. The experimental subassembly consisted of two beams in the seismically dominated direction and a beam with gravity load in the orthogonal direction. As presented in Figure 1-2, Li's joint employed a bent coupler system. The intent of this was to allow members to be constructed off site and connected onsite via a 'bolt bar' running through the ducts in the column at an angle and connected to the beam's tendons with the coupler. Joint armouring was reduced by introducing steel angles at beam ends, thereby eliminating the full depth steel plate used in the previous tests.

In parallel to Li's studies, Amaris *et al.* (2006) investigated the bi-directional behaviour of a corner joint utilizing a full steel plate 'cruciform' interface designed for external mild steel damping devices. Tests were conducted at various prestress levels and with a multitude of damping configurations. A floor slab was incorporated to investigate compatibility issues between the frame and slab.

As part of a multi-bridge pier comparison study, Mashiko (2006) tested a DAD pier similar to the pier previously developed by Mander and Cheng (1997). Mashiko used a bi-directional testing apparatus and pseudodynamic testing to investigate the behaviour of the pier under more representative loading profiles. Earthquake records were selected using a probabilistic analytical method to represent demand at multiple performance objectives. Detailing of the armoured interface was concluded to be deficient; significant cracking occurred along the pier's base, in addition to crushing of the concrete behind the armoured

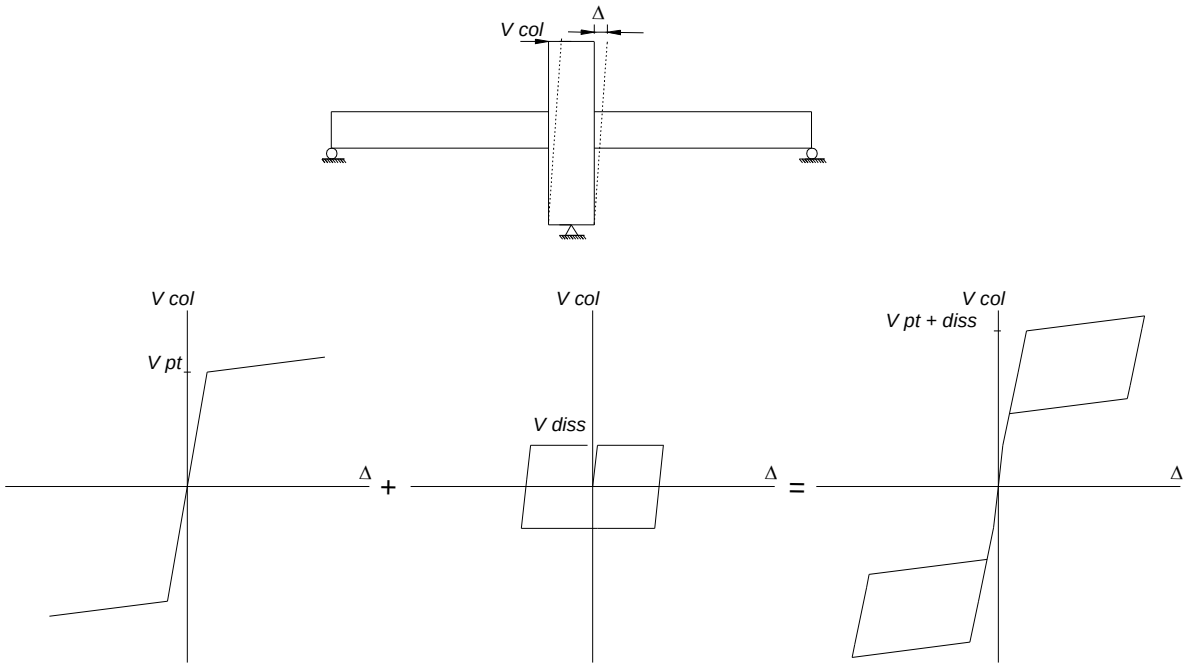

Figure 1-1: A combination of bi-linear elastic behaviour (left) from unbonded post-tensioning and elasto-plastic behaviour (middle) from yielding devices results in a 'flag shaped' hysteresis loop (right).

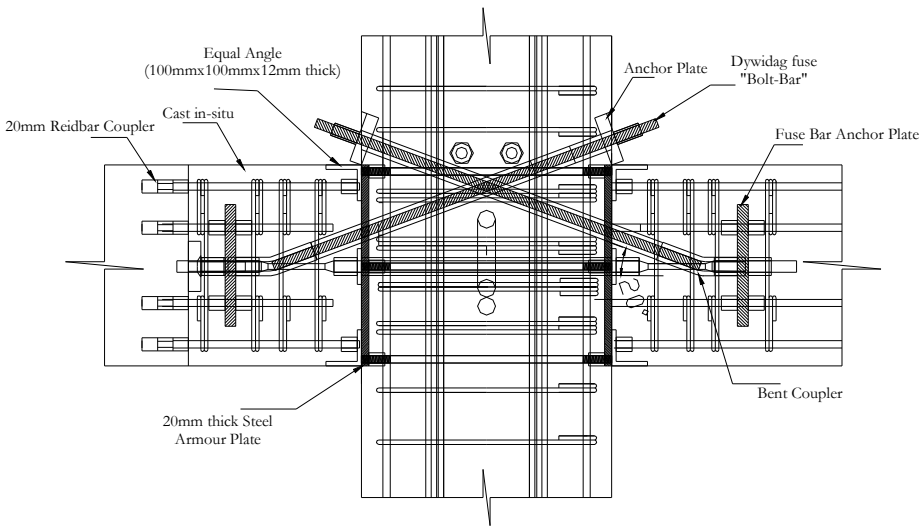

Figure 1-2: Subassembly joint detail employed in previous research (Li, 2006).

plate. Further work in this area is being conducted by Marriot *et al.* (2006) considering various levels of damping using buckling restrained mild steel dissipaters and different armouring configurations.

1.3 THEORETICAL RESPONSE OF A DUCTILE JOINTED PRECAST CONCRETE SYSTEM

1.3.1 Previous work on modelling

The theoretical behaviour of ductile jointed precast systems has been investigated by many researchers and several methods of varying complexity have been developed to model behaviour of such systems. Priestley and Tao (1993) theorized the force-deformation response of a partially unbonded system utilizing a concrete-concrete interface. Three points were defined: (1) the decompression point (first cracking of the extreme fibre); (2) the linear limit point (the point where the neutral axis at the joint is at the same location of the tendons); and (3) limit of proportionality of the steel tendons (assumed concrete ultimate conditions are reached). The three points are easy to calculate based on assumptions common of reinforced concrete, however, it was noted that between points 2 and 3 the force-deformation relationship is difficult to determine, since steel and concrete strains are not linearly related. Pampanin *et al.* (2001) addressed this by proposing the 'monolithic beam analogy'. To solve the strain compatibility issue, the full member behaviour was considered, thus equating it to a monolithic beam. Using this assumption, an iterative process was developed to find the neutral axis position based on section equilibrium. The procedure was validated against moment-rotation response of specimens tested by Stanton *et al.* (1997). In addition, Pampanin *et al.* (2001) proposed a simple analytical model which considered the response due to unbonded post-tensioning and energy dissipation devices. The model consisted of two parallel springs, calibrated for the respective elements of the system.

More complex modelling has also been developed. El-Sheikh *et al.* (1999) used finite element analysis to develop a fibre model which considered each material independently. The model was checked against experimental data and showed good correlation. Speith *et al.* (2004) developed a multi-spring model for incorporation in Ruaumoko (Carr, 2006), an inelastic dynamic analysis program. This element was designed to act as a contact element, using up to ten springs to model the contact surface accounting for beam elongation, local stress and strains, and damage in the contact area. These more complex modelling options will not be considered as part of this study, however it will be demonstrated a simple hand method is sufficient for predicting the moment-rotation and force displacement response of rocking systems with steel armouring.

1.3.2 Moment-rotation behaviour

By building on the findings of early researchers as given above and expanded on by Davies (2003) and Arnold (2004), the following pages will give an overview of a hand method used to predict the response of ductile jointed systems with steel armoured interfaces. Due to the relatively high strength of the steel armouring, the compression zone when rocking will be very small, such that it is acceptable to assume elements will rock in a rigid fashion. Using this assumption, one can calculate the moment-rotation response by taking forces about the extreme edges of the section. Although this assumption is slightly non-conservative, it greatly simplifies the design of such connections, and has been shown in previous research (e.g. Arnold, 2004) to be an acceptable approximation. This is illustrated in Figure 1-3 for a typical beam-column joint utilizing unbonded post-tensioning only.

The moment capacity of a beam to column connection is generally provided by two components: the post-tensioned tendons and the energy dissipation devices. Considering these components independently, their moment contributions are simply given by:

$$M_{PS}^{\pm} = P_{PS} e_{PS} \tag{1-1}$$

$$M_{diss}^{\pm} = P_{diss} e_{diss} \tag{1-2}$$

where P_{PS} and P_{diss} are the forces in the post-tensioned tendons and energy dissipaters, respectively, and e is the vertical distance of the tendon or dissipaters from the rocking edge of the beam section. This yields a total moment capacity of the connection of:

$$M = \sum M_{PS} + \sum M_{diss} \tag{1-3}$$

where the summation indicates independent consideration of multiple tendons or dissipation devices.

As the connection begins to open, the tendon is forced to elongate by a length of Δ (see Figure 1-3). This increase in strain will increase the force in the tendon. Due to the unbonded post-tensioning, it is not possible to use strain compatibility across the section to determine P_{PS}. Instead, a relationship between gap opening and the tendon's length is used:

$$P_{PS} = P_i + \frac{A_{PS} E_{PS}}{L_t} e_{PS} \theta_{con} n \tag{1-4}$$

where P_i = initial post-tensioning force; E_{PS} = elastic modulus of the tendon; L_t = unbonded length of the tendon; A_{PS} = cross sectional area of the tendon; θ_{con} = connection rotation; and n = number of joint openings spanned by the tendon. For example, if the tendon is unbonded through a column, it will elongate by Δ across each face for a total elongation of $n\Delta$.

The force exerted by dissipaters, P_{diss} will to some extent vary with the type of device and its elastic stiffness. For example, mild steel dissipaters, with their high elastic modulus and relatively short length effectively means they will yield shortly after gap opening. This allows one to simply assume each device exerts a force of:

$$P_{diss} = A_{diss} f_y \tag{1-5}$$

where A_{diss} = the cross sectional area of the mild steel dissipation device; and f_y = yield stress of the steel (without consideration for strain hardening). Using a simple assumption such as this is reasonable for predicting moment-rotation response, but, as will be shown later, may

prove problematic when considering the force-displacement response of the system, particularly when attempting to determine the system's elastic stiffness.

Figure 1-4 illustrates the typical moment-rotation response of a rocking connection. Once the moment is great enough to counter the clamping force provided by the initial post-tensioning, the member will begin to rotate and a gap will begin to open. At this point, assuming there is no initial load in the energy dissipation devices, they will load to their yield limit. Once they yield, a post-rocking stiffness will remain, governed primarily by elongation of the tendons. Finally, the tendons will yield and there will be no additional moment capacity of the connection.

1.3.3 Force-displacement response of a subassembly

To investigate the behaviour of a typical joint in a frame, consider the cruciform taken from the inflection points of a typical frame beam to column connection shown in Figure 1-5(a). The column lateral force, V_{col}, can be found from geometry of the section and the moment at the joint:

$$V_{col} = 2M \frac{L}{L_b L_c} \tag{1-6}$$

where M = the moment at a single joint, defined in Equation (1-3). The 2 denotes there are two joints contributing to the lateral resistance of the system, such as the system illustrated in Figure 1-5(a). An evaluation of the bending moment resulting from a lateral force, V_{col}, is given in Figure 1-5(b), showing the maximum positive and negative moment at the column face.

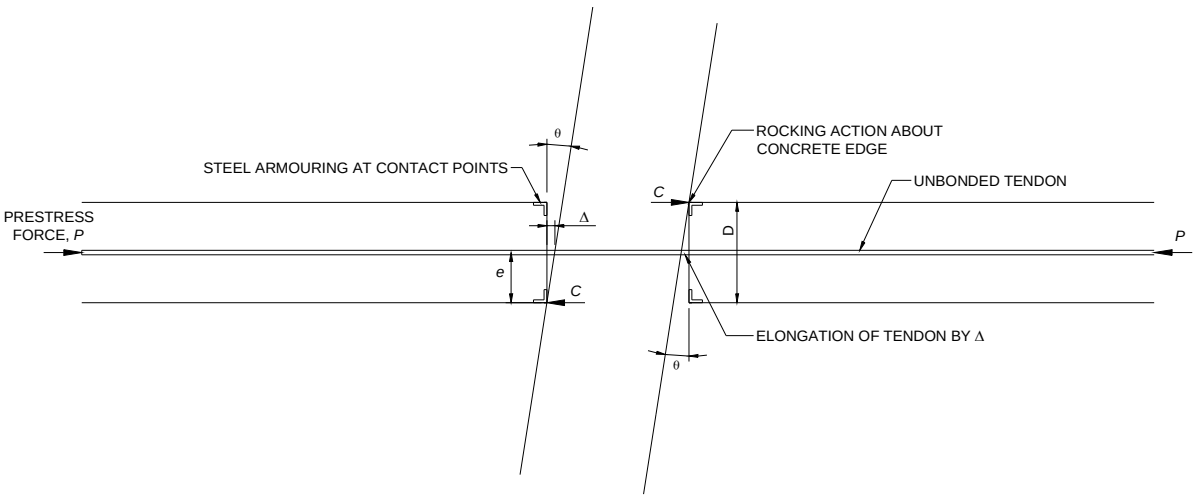

Figure 1-3: Details of beam-column joint rocking connection.

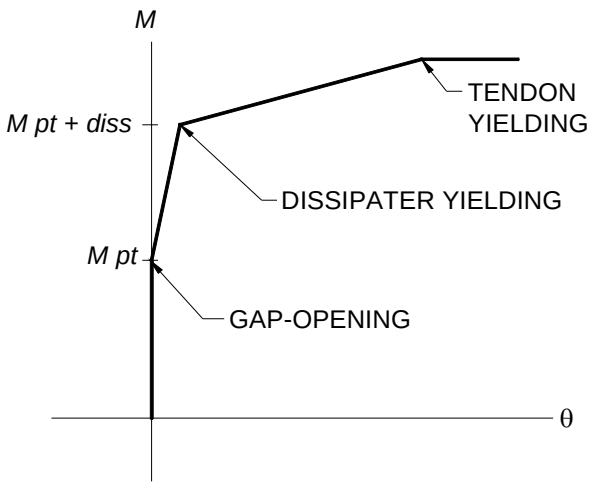

Figure 1-4: Idealized moment-rotation response of a typical rocking connection.

Considering elastic deformation, a typical force-displacement response is illustrated in Figure 1-6. In this case, the system's stiffness is governed by its elastic properties until a gap begins to open at the joints. This occurs at approximately V_{pt}. With the onset of gap opening, the energy dissipation devices engage and eventually yield, at which point the system 'yields'. Depending on the type of dissipaters employed in the system, the specimen, upon unloading, will force the dissipation devices into compression and eventually yield them. The ideal behaviour of these devices is shown in Figure 1-6 by the solid line, with the behaviour of buckling dissipaters and / or the softening Bausching effect of steel given by the dashed line.

Using the moment area method, $\Delta_{elastic}$ (Figure 1-5c) can be calculated as a function of V_{col} (Davies, 2003):

$$\Delta_{elastic} = \frac{V_{col}}{12}\left[\frac{(L_c - D)^3}{EI^*_{col}} + \frac{L_c{}^2 L_b{}^3}{L^2 EI^*_{bm}}\right] \tag{1-7}$$

where EI^*_{bm} and EI^*_{col} are the effective stiffness of the beam and column, respectively, D is the depth of the beam,,and L_c, L_b, and L are defined in Figure 1-5(a). This can be rearranged to give the elastic stiffness of the system:

$$K_e = \frac{12EI^*_{bm} / L_b{}^3}{\left(\frac{L_c}{L}\right)^2 + \left(\frac{L_c - D}{L_b}\right)^3 \left(\frac{EI^*_{bm}}{EI^*_{col}}\right)} \tag{1-8}$$

As is typical of reinforced concrete design, the effective stiffness of the beams and columns is generally taken based on its cracked section properties. This is often on the order of 35 to 60 percent of the gross section properties (Paulay and Priestley, 1992). Li (2006) found these assumptions resulted in an over prediction of the elastic stiffness of a rocking system. St. Venant's principle assumes the high contact compression forces will propagate through the concrete at approximately 45 degrees. Using this theory, it is possible to account for an effectively reduced section along this disturbed region. Consequently, it was recommended

by Li (2006) to use and effective beam stiffness of approximately 25 percent of the gross section properties.

Once the dissipaters have yielded, the rocking stiffness, K_2 is a function of the elastic properties of the post-tensioned tendons and the previously defined elastic stiffness of the system:

$$K_2 = \frac{K_{p2} K_e}{K_{p2} + K_e} \tag{1-9}$$

where K_{p2} is the stiffness of the system from elongation of unbonded post-tensioning alone:

$$K_{p2} = \left(\frac{L}{L_b}\right)^2 \left(\frac{D}{L_c}\right)^2 \frac{A_{PS} E_{PS}}{L_t} \tag{1-10}$$

These basic equations will be used in subsequent chapters to aid in the design and prediction of experimental subassemblies.

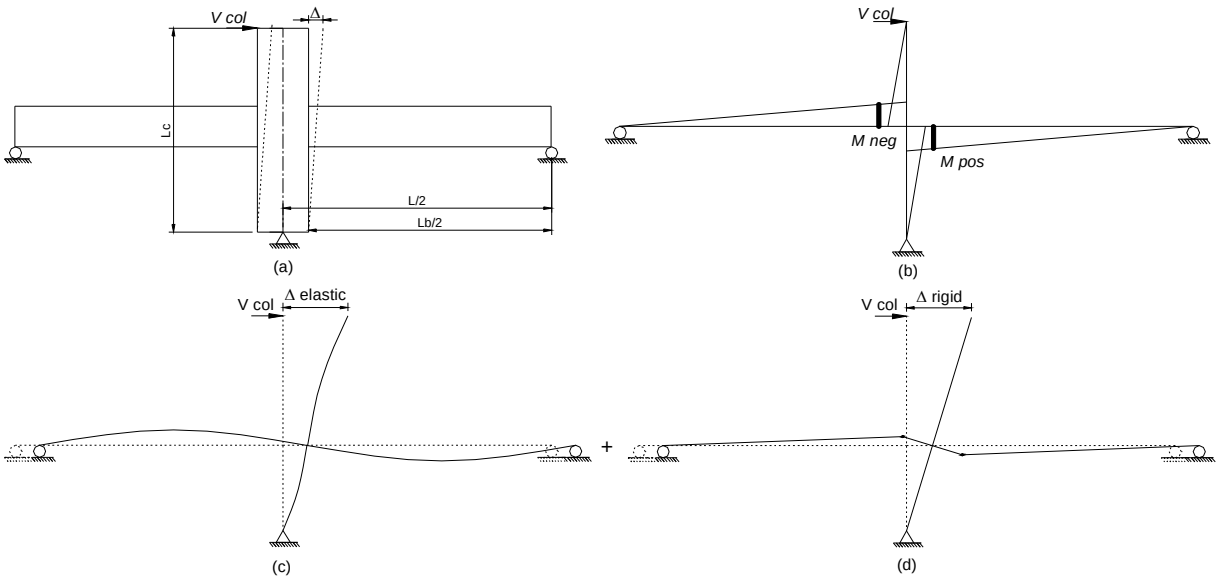

Figure 1-5: A cruciform subassembly showing (a) definition; (b) moment diagram; (c) elastic deformation; and (d) rigid body deformation.

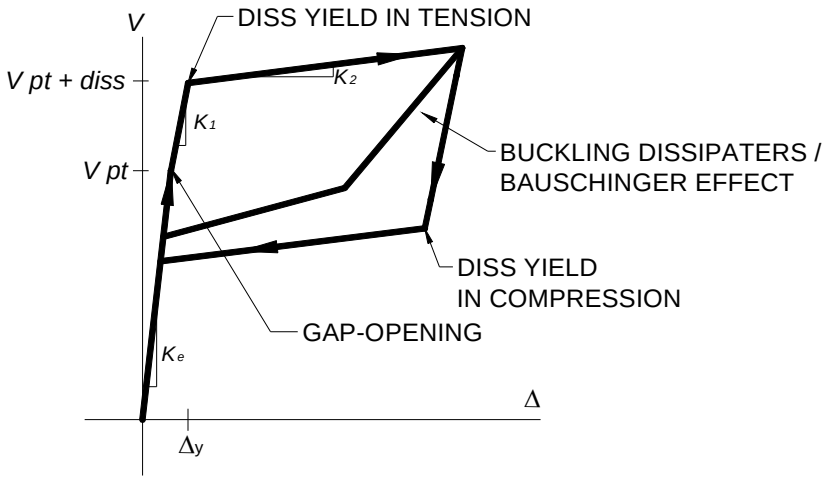

Figure 1-6: Idealized force-displacement response of a rocking connection.

1.4 DESIGN AND CONSTRUCTION ISSUES

The concept of ductile jointed precast systems is relatively new, and therefore only a few applications of such technology exist. Early applications of rocking structures without post-tensioning can be found in New Zealand: the South Rangitikei Rail Bridge and an industrial chimney at Christchurch International Airport. Both structures were fitted with damping devices to restrain uplift and attenuate the number of rocking cycles. A good overview of these structures can be found in Skinner *et al.* (1993).

With the conclusion of the PRESSS program in the United States, Pankow Builders constructed the Third and Mission Apartments in San Francisco, California. To the author's knowledge, this structure was the first to employ PRESSS technology in a high seismic region. The 39 storey structure consists of *precast hybrid moment resisting frames* (PHBRF) in both directions, grouted mild steel for energy dissipation, unbonded post-tensioning, and grout pads at beam ends. Limited information exists regarding the construction of this building, nevertheless, it stands as an early application of the emerging technology.

Efforts are underway to encourage use of these systems in New Zealand. Some key advantages of ductile jointed structural systems are:

- Competitive cost of materials to conventional systems;
- Reduction / elimination of damage to the structural frame;
- Improved life-cycle cost savings of the structure;
- Potentially longer floor spans due to post-tensioning;
- Precast construction will speed on-site erection;
- Design flexibility.

However, there are several issues related to constructability and design which must be considered, these include:

- Shear transfer at the joints;
- Tolerance requirements to ensure flush connections;
- Displacement compatibility issues between the frame and floor slabs;

- Lack of engineering knowledge; a new way of thinking about design;
- No established design procedure available to engineers;
- Construction complications compared to monolithic construction with the inclusion of damping devices and unbonded post-tensioning.

The following will give a brief overview of some of these issues, and how they have been accommodated for by researchers.

1.4.1 Shear transfer

The transfer of gravity and seismic induced shear forces at the joints has been considered in many ways. An early application of unbonded post-tensioning (Priestley and MacRae, 1996) relied on friction due to the tendon clamping force to provide shear resistance. This same concept was employed in the design of the PRESSS frame structure, with consideration of dowel action of the mild steel energy dissipaters to provide some additional resistance. This eliminated the need for a corbel, typical of similar precast construction. This approach seemed adequate for the subassembly, however with the inclusion of a floor slab in the PRESSS frame, it was inadequate to resist torsion forces resulting from the eccentric connection of the precast floor slabs. Relying on friction is heavily penalized by requiring stringent upper and lower bounds in the prestress forces, since the approach could result in substantial reductions of gravity load carrying capacity if the clamping force is lost. The New Zealand Concrete Standard (NZS:3101, 2006) has recently incorporated ductile jointed precast systems into an appendix. This standard requires gravity loads be resisted by shear keys or corbels, but allows seismic induced shear to be carried by friction.

As alternative to concrete corbels in the columns, steel corbels or shear keys could be used to resist gravity loads. The Brooklyn system, developed in Italy for gravity dominated frames (Pampanin *et al.*, 2004), employed a steel corbel to seat the beam. Other options considered by Davies (2003) included a single ‘shark fin’ design using a slot to seat the

connecting beams, and shear pintles which could be screwed into a plate in the column through the beam. Another approach was used by Li (2006) in consideration of both gravity induced shear and torsion. In this case, four tapered shear keys located at the corners of the beam were used.

All of these approaches rely on considerably tight construction tolerances and may reduce the speed of on-site erection. Shear transfer is still an issue being considered by researchers, and is addressed further in later sections of this thesis.

1.4.2 Floor slabs

Ductile jointed precast systems designed to rock about both top and bottom, will inevitably cause beam elongation, similar to the phenomena found in yielding longitudinal steel of a monolithic beam's plastic hinge region. When gap opening occurs along the top of the beam, it must be accommodated by the entire system. Therefore the floor slab must elongate by the same amount. If this is not considered in design, cracking would occur along the floor slab connection, and potentially unseat the precast slabs. This has been extensively studied previously (Matthews, 2004), and is therefore not addressed in this study. Nevertheless, it should be noted that such a phenomena will occur in jointed systems. Research is currently underway at the University of Canterbury to address this issue through the development of a non-tearing floor solution. This alternative design pins the system at the top of the beam, with gapping accommodated entirely at the bottom of the beam.

1.4.3 Construction tolerances

As with any engineering endeavour, the consideration of constructability should always play a critical role throughout the design process. Ductile jointed precast concrete systems offer an attractive option of casting all members off-site, thus eliminating the need for large on-site closure pours. In a typical PRESSS system, this is possible by providing a grout pad at the joint region; this allows for slight misalignment issues (either by inconsistent

member length or slightly out of plum columns) to be accommodated. If armouring is used in the contact region, this is no longer an option, and misalignment will need to be corrected in another way. It is plausible that precasters could cast members to a much tighter tolerance. However, as the steel interface must be aligned perfectly flush, even being off by 1mm at the beam face could cause misalignment of 15-20mm at the opposite end. Furthermore, tighter tolerances equals more effort, which also means additional cost.

In response to this, it is considered necessary to provide a cast insitu closure pour at at least one end of the beams. This can ensure all contact surfaces are flush, while still allowing most concrete to be cast offsite. Furthermore, this option allows access to coupling devices which may simplify the installation of supplemental damping and PT tendons. These issues will be discussed in greater details later in this thesis.

1.4.4 Energy dissipation

Due to the inherent lack of energy dissipation provided by the unbonded post-tensioning, it is generally accepted that ductile jointed systems must employ some form of supplemental energy dissipation. This is especially necessary for short and medium period structures, where displacement amplifications can be double that of a system exhibiting elasto-plastic hysteretic behaviour (Priestley and Tao, 1993).

The first application of a ductile jointed system with energy dissipation (Stanton *et al*., 1997) used mild steel reinforcing running through the joint region in corrugated ducts which were later grouted. Test results showed such an approach provided good energy dissipation thanks to the grout providing an efficient anti-buckling encasing. From a constructability standpoint, this system may not be ideal, since access holes must be provided to move the steel rods into position prior to grouting.

Other options have been considered by various researchers (Davies, 2003; Arnold, 2004; Amaris, 2006). These have included the use of external devices which could be more

easily replaced. Figure 1-7 presents three such devices. Two of these are designed to yield in tension and compression while the ‘dog bone’ dissipater will yield in flexure. These devices, however, will eventually buckle in compression and thus provide dissipation only at larger subsequent cycles. It is possible to combat this using techniques found in steel buckling restrained braced frames. The steel dissipation device can be encased in a tube of grout or epoxy to restrain buckling. This has been demonstrated to work quite well in experiments. (Armaris, 2006). However, connecting these devices to reasonable tolerances and developing them into the respective members may be difficult and aesthetically unattractive. Furthermore, they may need to be replaced following an earthquake.

Another mechanical device, developed in parallel to this study and discussed in detail in a later section, is the lead extrusion damper. This device, capable of providing a very large force compared to its compact size, has been shown to offer stable energy dissipation in a relatively small device.

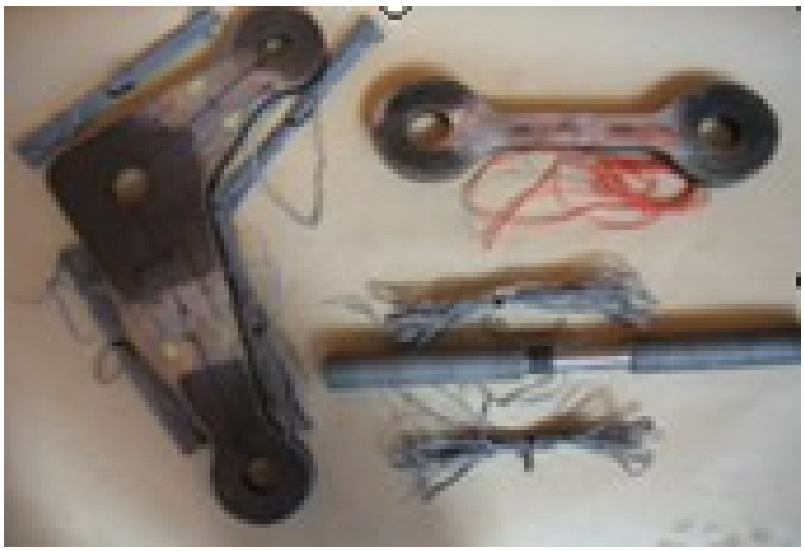

Figure 1-7: Sacrificial supplemental mechanical energy dissipaters (Arnold, 2004)

1.5 CLOSURE

This section has offered the reader an overview of precast concrete structural systems. The development of these systems from the late eighties to present time has been discussed, identifying some of the key findings of the various research literature available. A simple hand method has been described to predict the performance of DAD systems which employ steel armouring, which will later be used to predict the performance of subassemblies developed as part of the current research. Finally, some of the key design and construction issues of these systems have been addressed, specifically challenges relating to shear transfer at the joint, tolerances, and energy dissipation. The remainder of this thesis will build on these findings and address some of the construction issues described.

REFERENCES

Amaris A, Pampanin S, Palermo A. 2006. Uni and bi-directional quasi-static tests on alternative hybrid precast beam column joint subassemblies. *Proceedings of the 2006 New Zealand Society for Earthquake Engineering* (NZSEE) *Conference*. Napier, New Zealand, Paper #24.

Arnold DM. 2004. Development and Experimental Testing Of a Seismic Damage Avoidance Designed Beam to Column Connection Utilising Draped Unbonded Post-Tensioning. *Master of Engineering Thesis*. University of Canterbury, Christchurch, New Zealand.

Carr AJ. 2006. RUAUMOKO: Inelastic Dynamic Computer Program. Computer Program Library, Department of Civil Engineering, University of Canterbury, Christchurch, New Zealand.

Davies MN. 2003 Seismic Damage Avoidance Design of Beam-Column Joints using Unbonded Post-Tensioning: Theory, Experiments and Design Example. *Master of Engineering Thesis*. University of Canterbury, Christchurch, New Zealand.

EI-Sheikh M, Sause R, Pessiki S and Lu LW. 1999. Seismic Behaviour and Design of Unbonded Post-Tensioned Precast Concrete Frames. *PCI Journal*, **44**(3):54-71.

Li L. 2006. Further experiments on the seismic performance of structural concrete beam-column joints designed in accordance with the principals of damage avoidance. *Master of Engineering Thesis*. University of Canterbury, Christchurch, New Zealand.

Mander JB and Cheng CT. 1997 Seismic Resistance of Bridge Piers Based on Damage Avoidance Design, *Technical Report NCEER-97-0014*, Department of Civil, Structural and Environmental Engineering, State University of New York at Buffalo, New York, USA.

Marriot D, Boys A, Pampanin S, Palermo A. 2006. Experimental validation of high-performance hybrid bridge piers. *Proceedings of the 2006 New Zealand Society for Earthquake Engineering* (NZSEE) *Conference*. Napier, New Zealand, Paper #19.

Mashiko N. 2006. Comparative performance of ductile and damage protected bridge piers subjected to bi-direction earthquake attack. *Master of Engineering Thesis*. University of Canterbury, Christchurch, New Zealand,.

Matthews, J. 2004. Comparative performance of ductile and damage protected bridge piers subjected to bi-direction earthquake attack. *PhD Thesis*. University of Canterbury, Christchurch, New Zealand.

NZS:3101-06. 2006. *Concrete Structures Standard: NZS3101*. Standards New Zealand, Wellington, New Zealand.

Pampanin S, Priestley NJ, and Sritharan S. 2001. Analytical modelling of the Seismic Behaviour of Precast Concrete Frames Designed with Ductile Connections. *Journal of Earthquake Engineering*, **5**(3):329-367.

Pampanin S, Pagani C, and Zambelli S. 2004. Cable-Stayed and Suspended post-tensioned Solution for Precast Concrete Frames: The Brooklyn System. *Proc of New Zealand Concrete Industry Conference*, Queenstown.

Paulay T and Priestley MJN. 1992. *Seismic Design of Reinforced Concrete and Masonry Buildings*. John Wiley & Sons, New York, NY.

Priestley MJN and Tao JRT. 1993. Seismic Response of Precast Prestressed Concrete Frames with Partially Debonded Tendons. *PCI Journal*, **38**(1):58-69.

Priestley MJN and MacRae GA. 1996. Seismic Tests of Precast Beam-to-Column Joint Subassemblages with Unbonded Tendons. *PCI Journal*, **41**(1):64-81.

Priestley MJN, Sritharan S, Conley JR, Pampanin S. 1999. Preliminary Results and Conclusions from the PRESSS Five-Storey Precast Concrete Test Building. *PCI Journal*, **44(**6):43-67.

Skinner RI, Robinson, WH, and McVerry GH. 1993. *An Introduction to Seismic Isolation*. John Wiley & Sons, Inc., New York, NY.

Spieth HA, Arnold D, Davies M, Mander JB, and Carr AJ. 2004. Modelling of post-tensioned precast reinforced concrete frame structure with rocking beam-column connections. *Proceedings of the 2004 New Zealand Society for Earthquake Engineering* (NZSEE) *Conference*. Paper #32.

Stanton JF, Stone WC, and Cheok GS. 1997. A Hybrid Reinforced Precast Frame for Seismic Regions. *PCI Journal*, **42**:20-32.

2 Computational and rapid loss estimation methodologies with application to reinforced concrete bridges

SUMMARY

Expected annual loss (EAL), which can be expressed in dollars, is an effective way of communicating the seismic vulnerability of constructed facilities to owners and insurers. A simplified method for estimating EAL without conducting time consuming non-linear dynamic analyses is presented. Relationships between intensity measures and engineering demand parameters resulting from a pushover analysis and a modified capacity-spectrum method are combined with aleotoric variability and epistemic uncertainty to arrive at a probabilistic demand model. Damage measures are established to determine thresholds for damage states from which loss ratios can be defined. Financial implications due to damage can then be quantified in the form of EAL by integrating total probable losses for all likely earthquake scenarios. This rapid loss estimation method is verified through customary computational Incremental Dynamic Analysis where results are processed using a distribution-free methodology. To illustrate the application of the proposed methods, the seismic vulnerability of three highway bridge piers is compared; the piers are designed to the governing standards of three different countries. Through the case study, strength, rather than ductility, is shown to have a significant effect on EAL. The rapid method is shown to be a good tool for comparison purposes, but may not provide an accurate approximation of EAL.

2.1 INTRODUCTION

One primary aim of *performance based earthquake engineering* (PBEE) is to predict, with a certain level of confidence, the seismic performance of structures at various levels of earthquake excitation (seismic demand). This requires the engineer to understand seismic risk and its inherent uncertainty. As an adjunct to conventional design it is desirable that the engineer be able to communicate that risk in a way easily understood by stake-holders such as owners, bankers, and insurers. The *Pacific Earthquake Engineering Research* (PEER) *Centre's* probability framework equation, which can be used to arrive at a mean annual frequency of a decision variable, is a good starting point. An early application and theory outlining the PEER framework equation is given in Deierlein *et al.* (2003), while a history of the evolution of this theory along with certain problems pertaining to the non-ergodicity of the assumptions is outlined in Der Kiureghian (2005). For example, this equation can be used to determine the closure probability of a building given a specified level of shaking. This is done by interrelating the level of ground shaking with the column response, and the column response with damage, and by quantifying the likelihood of the facility being closed given a certain level of damage. Thus, it is apparent that the triple integral equation can be broken into four subtasks: (i) assessment of seismic hazard; (ii) analysis for structural response; (iii) quantification of damage; and (iv) estimation of damage consequence in terms of a chosen decision variable. Implicit in the formula is a probabilistic analysis, incorporating both randomness and uncertainty and combining this variability in accordance with the total probability theorem. The manner in which this formula is applied, its limitations, and its potential expansion, have been the subject of rigorous research, both within and outside PEER. A good overview of such developments is given in Krawinkler and Miranda (2004).

One expansion of the framework formula would be the inclusion of time, resulting in quantification of seismic risk in terms of an *expected annual loss* (EAL), which can be

calculated by performing a fourth integration where the earthquake intensity is related to a recurrence rate (i.e. annual frequency). Recently Der Kiureghian (2005) has noted that such an expansion of the PEER equation had not been conducted. The advantage of EAL is that it incorporates a range of seismic scenarios, return rate, and expected damage into a single median dollar loss. Therefore, EAL is especially useful to decision makers for financial analysis of design alternatives and general inclusion into operating budgets.

Although several methods of financial risk assessment have been presented, no method has yet been widely adopted. One detailed method introduced by Porter *et al.* (2001) is *assembly based vulnerability* (ABV). This method is especially good at estimating the overall damage to a building based on the damage to its individual components. Uncertainty is usually expressed by fragility curves, which show the probability of a variable (i.e. earthquake intensity or interstory drift) exceeding a certain limit. Most uncertainty can be approximated by a distribution function with a median and a standard deviation function. For example, spalling can be defined to occur at a certain local curvature, yet for a given specimen it may occur at a range of curvatures which can be defined by a lognormal distribution with a lognormal standard deviation. If uncertainty is considered in each of the subtasks in the risk assessment process, the calculation can become complicated. Attempts have been made to simplify the process. Cornell *et al.* (2002) used data generated from a series of non-linear time-history analysis and proposed an equation for the median curve. If the hazard-recurrence relationship is also expressed in a similar algebraic form, it is possible to combine the two equations and arrive at a closed form solution that can be used to determine the probability of exceeding a demand parameter (i.e. interstory drift) given a period of time.

A primary step within PBEE is defining a relationship between specified demand levels and a hazard environment. This relationship, termed the demand model, has gained a lot of attention in the past decade. Vamvatsikos and Cornell (2002) have researched the feasibility

of *Incremental Dynamic Analysis* (IDA) as a means of relating these parameters. An IDA basically consists of performing a series of time-history analyses to arrive at a set of demand parameters, obtained by scaling a suite of earthquake records to various intensities. It is similar (though far superior) to a static pushover in that it encompasses the entire range of likely behaviour, from pre-yield to collapse. This method has gained some acceptance since its inclusion in emerging regulations (FEMA 350, 2000). Another simplified method has been proposed by Porter and Beck (2004). Assuming that seismic risk is dominated by non-structural damage from moderate events, they proposed a simple linear elastic analysis to replace the often cumbersome non-linear dynamic analysis. The non-linear dynamic procedure is considerably more time consuming and requires uncommon skills for practicing engineers, whereas the linear approach is relatively simple. Nevertheless, the assumptions made in the linear method may not be valid for all structures, specifically those designed to behave well in the non-linear range.

A generic procedure is needed that will consider non-linear behaviour and a range of uncertainty, while retaining a degree of simplicity. Vamvatsikos and Cornell (2005) have established that it is possible to relate a static pushover curve to IDA. This chapter will set out to estimate EAL using a rapid analysis approach, referred to hereafter as the *Rapid IDA-EAL* approach. The Rapid IDA-EAL method will be verified by a rigorous computational IDA. For this verification analysis, in order not to bias the latter through *a priori* assumptions in the choice of probability density functions, a distribution-free analysis method is introduced. Hereafter, this is referred to as the *Computational IDA-EAL* distribution-free approach. A case study of three different bridge piers will illustrate the effectiveness of the two approaches for estimating EAL.

2.2 EAL THEORY

In order to conduct a financial risk analysis, it is necessary to form relationships between the multiple facets of the assessment process, including time. This can be accomplished by implementing the PEER triple integral equation:

$$\lambda(dv) = \int\int\int G(dv \mid dm) \mid dG(dm \mid edp) \parallel dG(edp \mid im) \parallel d\lambda(im) \mid \qquad (2\text{-}1)$$

in which *im* = intensity measure (e.g. peak ground acceleration, spectral acceleration); *edp* = engineering demand parameter (e.g. column drift angle); *dm* = damage measure (e.g. maximum drift without damage); *dv* = decision variable (e.g. loss ratio, repair cost, downtime); and $G(x|y)=P(x<X|y=Y)$; the conditional *cumulative distribution function* (CDF) (Der Kiureghain, 2005).

Der Kiureghian (2005) noted that it is possible to perform an additional integration giving the expected cumulative loss (represented by the variable *X*) in one year:

$$E[\sum X] = \int_0^\infty \lambda(x)dx \qquad (2\text{-}2)$$

In the context of financial loss assessment, this can be combined with Equation (2-1) to give:

$$E[L_r] = \int\int\int\int L_r dG(L_r \mid dm) \mid dG(dm \mid edp) \parallel dG(edp \mid im) \parallel d\lambda(im) \mid \qquad (2\text{-}3)$$

where L_r = loss ratio defined as the cost to repair a structure divided by the total replacement cost. This formula is the basis of the EAL calculations presented in this chapter.

2.3 RAPID IDA-EAL METHODOLOGY

The concept of the proposed Rapid IDA-EAL procedure is relatively straightforward. It is possible to generate the median *intensity measure* (IM) versus *engineering demand parameter* (EDP) relationship from a non-linear *static pushover* (SPO) analysis and employing a modified *capacity spectrum method* (CSM). Adopting the customary assumption that variability conforms to a lognormal distribution (Shome *et al.*, 1998; Mander *et al.*, 1999; Mander, 2004), fragility curves can be generated for discrete states of damage. The fragility curves are then transformed via a hazard-recurrence relationship into hazard-

survival curves for each damage state. Then, financial implications of the different damage states are considered together with the corresponding hazard-survival curves to arrive at the EAL. This general process is outlined in detail through the following steps.

2.3.1 Step 1: Conduct a pushover analysis

A non-linear SPO analysis is performed to assess the capacity of the system, as illustrated in Figure 2-1(a). From the SPO curve, it is possible to calculate the secant (equivalent elastic) period, *T*, in terms of normalized base shear capacity C_c and peak response displacement Δ as follows:

$$T = 2\pi\sqrt{\frac{M}{K}} = 2\pi\sqrt{\frac{W}{g}\frac{\Delta}{C_c W}} = 2\pi\sqrt{\frac{\Delta}{C_c g}} \tag{2-4}$$

in which C_c can be expanded as $C_c = F_y / W$ where F_y = base shear force; W = seismic weight; M = seismic mass, K = initial stiffness; and g = acceleration of gravity.

2.3.2 Step 2: Calculate the median IDA curve

The evaluation of seismic demand at various effective damping levels depends on the portion of the spectrum governing response. Figure 2-1(b) illustrates the seismic demand spectrum and the regions of constant spectral acceleration, spectral velocity, and spectral displacement as limited by T_a, T_v, and T_d. For a given effective (secant) period of vibration *T*, the normalized base shear demand C_d can be calculated as the lesser of:

$$C_d = \frac{F_a S_s}{B_a} \tag{2-5}$$

$$C_d = \frac{F_v S_1}{T B_v} \tag{2-6}$$

$$C_d = \frac{F_v S_1 T_d}{T^2 B_d} \tag{2-7}$$

where F_a and F_v are factors to adjust spectral acceleration for short and long period structures at different soil classes; S_s and S_1 are spectral acceleration at short periods and the one second period; and B_a, B_v, and B_d are factors based on effective viscous damping for the constant spectral acceleration, velocity, and displacement regions, respectively.

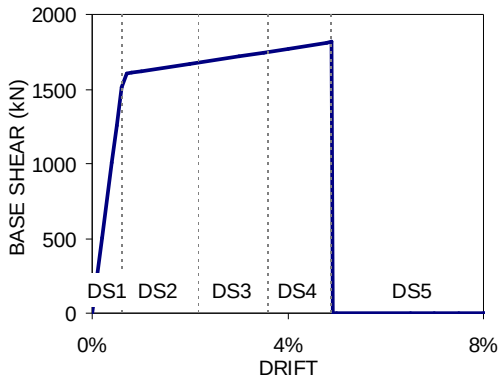

(a) Step 1:Conduct non-linear static pushover

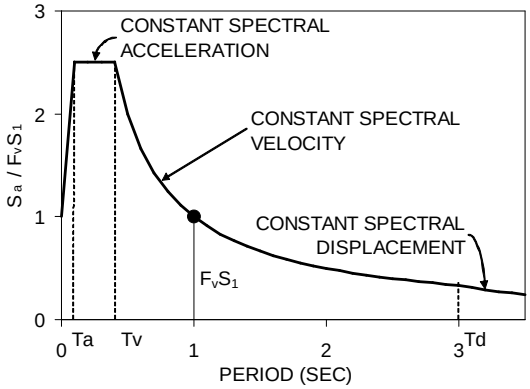

(b) Adopt standard spectral acceleration relationships

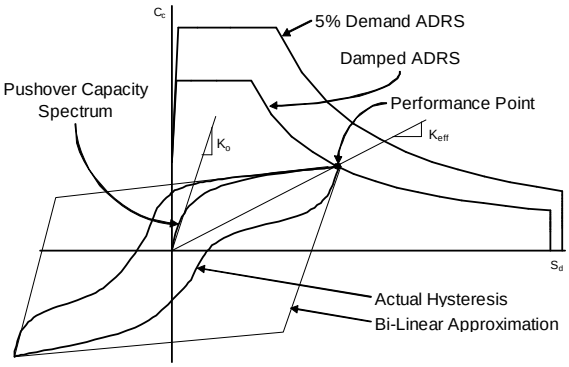

(c) Modified capacity spectrum method (Pekcan et al.,1999)

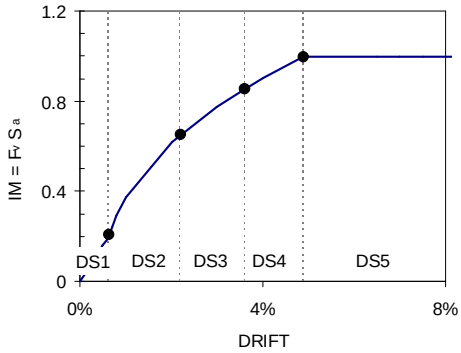

(d) Step 2: Calculate median curve
Step 3: Define damage states and limits

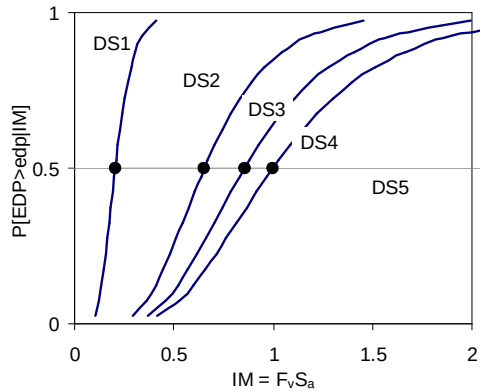

(e) Step 4: With assumed $\beta_{C/D}$ plot fragility curves

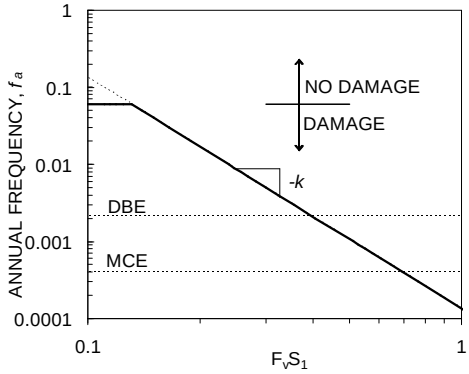

(f) Step 5: Define an earthquake recurrence relationship

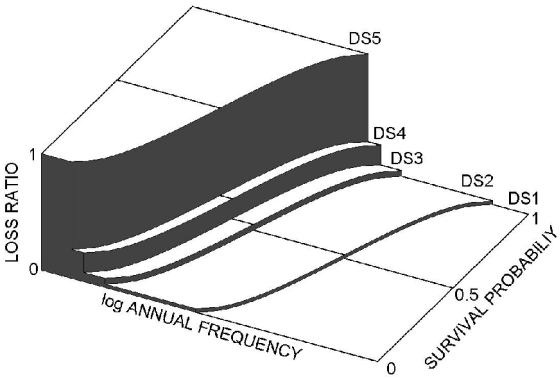

(g) Step 6a: Calculate hazard-survival curve.

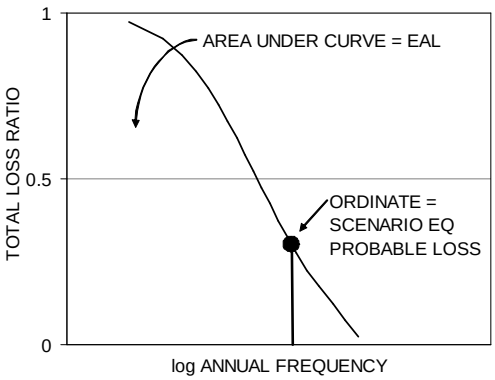

(h) Step 6b: Calculate EAL

Figure 2-1: Step for conducting a Rapid IDA-EAL risk assessment.

Employing the modified CSM, it is possible to relate the capacity-displacement curve (SPO curve) and the *acceleration-displacement response spectrum* (ADRS) curve by combining them into a single plot as illustrated in Figure 2-1(c). The "performance point" of the structure is estimated from the intersection of the SPO curve with the damping-reduced ADRS curve. The CSM, as presented in ATC-40 (1996), has come under considerable scrutiny due to inconsistent displacement predictions (Goel and Chopra., 2001; Miranda and Ruiz-Garcia, 2002). Such errors appear to be rectified by use of either the inelastic spectra or a modified CSM as described by Iwan (2002).

To further address these issues, this study has adopted modified damping approximations proposed by Lin and Chang (2004) coupled with the reduction in equivalent viscous damping due to the pinched nature of the real hysteresis curves, as introduced by Pekcan *et al.* (1999). Based on recent studies by Lin and Chang (2004), confirmed by Lin *et al.* (2005), and modified herein as part of the present study, the damping-related reduction factors, B_a, B_v, and B_d can be calculated as a function of effective damping, ξ_{eff} as follows:

$$B_a = \sqrt{\frac{2+\xi_{eff}}{7}} \tag{2-8}$$

$$B_d = \sqrt{\frac{8+\xi_{eff}}{13}} \tag{2-9}$$

The damping factor for the constant spectral velocity range, B_v can be calculated by linear interpolation between B_a and B_d based on period or spectral displacement. Total effective viscous damping can be estimated by using the method proposed by Pekcan *et al.* (1999):

$$\xi_{eff} = \xi_o + \xi_{hy} = \xi_o + \frac{2}{\pi}\eta\frac{(1-\alpha_s)(1-1/\mu)}{(1-\alpha_s+\mu\cdot\alpha_s)} \tag{2-10}$$

in which ξ_o = intrinsic damping of an elastic system; η = the efficiency factor defined as the ratio of the actual area within a hysteresis loop to that of the idealized bi-linear loop (Figure 2-1(c)); α_s = post-yield stiffness to initial stiffness ratio; $\mu = \Delta_{max} / \Delta_{yield}$ where Δ = displacement at the seismic centre of mass of the structure.

Setting C_c=C_d and substituting Equation (2-4) into (2-5), (2-6), and (2-7), the one second spectral acceleration *(F_vS_1)* for a given demand can be found. Thus for the median IDA curve shown in Figure 2-1(d), the IM (spectral acceleration) can be found for a given EDP (displacement) by the *greater* of the following three equations:

$$F_vS_1 = T_v \cdot B_a \cdot C_c \tag{2-11}$$

$$F_vS_1 = 2\pi\sqrt{\frac{C_c \cdot \Delta}{g}} \cdot B_v \tag{2-12}$$

$$F_vS_1 = \frac{4\pi^2}{g \cdot T_o} \cdot \Delta \cdot B_d \tag{2-13}$$

where generally, T_v, and T_d can be taken as 0.4 and 3.0 seconds, respectively.

2.3.3 Step 3: Define damage states and limites

This study adopts the five damage states (DS1 to DS5) defined by Mander and Basoz (1999) that have been adopted in Hazus, as summarised in Table 2-1. The damage state limits are also illustrated in Figure 2-1(d).

2.3.4 Step 4: Incorporate Sources of Variation using Assumed Distributions

Throughout this process numerous approximations are made regarding damping, material strengths, modelling simplifications, etc. These approximations can be grouped into epistemic uncertainty, where further investigation may lead to an increase in accuracy, and aleotoric variability (randomness), which cannot be reduced because of its random nature. An example of the former would be uncertainty in analytical modelling, and the latter would be the inherent record-to-record randomness of earthquake ground motions. As discussed earlier, previous studies have shown that these variations approximately conform to a lognormal distribution. This two-parameter distribution can be defined with a median ($\tilde{x}$) and a lognormal standard deviation (β), referred to herein as the dispersion factor. Since a formula relating EDP and IM is available, the median values have been established and only the dispersion is left to be determined. It is possible to assume a dispersion based on

Table 2-1: Damage states index as defined by *Hazus (*Mander and Basoz, 1999) and the loss ratios and range

	Damage State	*Failure Mechanism*	*Repair required*	*Outage*	*Drift Limit (%)*			*Loss Ratio (%)*
					NZ	*Japan*	*Caltrans*	
DS1	None	Pre-Yielding	None	None	--	--	--	0
DS2	Minor/Slight	Minor spalling	Inspect, Patch	< 3 days	0.62	0.53	0.53	3
DS3	Moderate	Bar buckling	Repair components	< 3 weeks	2.30	1.60	1.90	8
DS4	Major/Extensive	Bar fracture	Rebuild components	< 3 months	4.40	4.60	5.10	25
DS5	Complete/ Collapse	Collapse	Rebuild structure	> 3 months	5.64	5.66	6.16	100

established trends regarding the various uncertainties discussed. To determine the dispersion of all combined uncertainty and randomness, they are combined by the root-sum-squares method established by Kennedy *et al.* (1980) and adopted in FEMA 350 (Cornell *et al.*, 2002):

$$\beta_{c/d} = \sqrt{\beta_d^{\,2} + \beta_c^{\,2} + \beta_u^{\,2}} \tag{2-14}$$

where β_d = the variation of structural response due to the input motion, β_c = the aleotoric randomness in structural capacity (usually considered in the damage model), and β_u = epistemic modelling uncertainty. In this study, recommendations of FEMA 350 (2000) have been adopted; i.e. β_c = 0.2 and β_u = 0.25. Although β_d is difficult to quantify, it is likely to vary depending on the IM considered. Investigations into the variation of input motion have been conducted by the authors. It can be shown that the variation of β_d can be approximated by the relationship:

$$\beta_d = \beta_{DBE}\sqrt{\frac{IM}{IM_{DBE}}} \tag{2-15}$$

where β_{DBE} = lognormal standard deviation of the structural response due to ground motions scaled to the design basis earthquake level, IM_{DBE}. With the calculated median IM's and the resulting $\beta_{c/d}$, fragility curves are plotted as in Figure 2-1(e). Fragility curves are drawn to correlate the probability of exceeding a damage state given an IM. Unlike other vulnerability methods, all uncertainty and randomness are grouped into a single composite dispersion factor, $\beta_{c/d}$. This greatly simplifies the subsequent integration.

2.3.5 Step 5: Define an earthquake-recurrence relationship

To arrive at an EAL, it is necessary to define a relationship between an IM and annual frequency (f_a), which is commonly known as the hazard-recurrence relationship. It is possible to approximate the hazard-recurrence curve by fitting a straight line through two known points in a log-log scale:

$$f_a(IM) = k_o(IM)^{-k} \tag{2-16}$$

where k_o and k are empirical constants. Using the 1 second spectral acceleration (F_vS_1) as the IM, Figure 2-19(f) plots Equation (2-16) which can also be written as follows for a high seismic zone in New Zealand (k = 3):

$$f_a = \frac{1}{475}\left(\frac{F_v S_1}{0.4}\right)^{-3} \tag{2-17}$$

As noted by Der Kiureghian (2005), earthquakes are discrete, rather than continuous events, and should be modelled as a Poisson process. In this case, the hazard-recurrence relation formulated above, though conservative, is perhaps not strictly correct when $f_a > 0.01$ (T < 100 years). The aforementioned deficiency can be rectified by disregarding any damage below a certain threshold. In this chapter, this threshold is assumed to correspond to 90% probability of not sustaining any damage. In other words, this is the intersection of the 90th percentile curve and the line serving as the boundary between DS1 (no damage) and DS2 (slight damage). Although this cut-off point may be arbitrary, to the author's knowledge there are no simplified models appropriate for loss modelling which fully capture hazard relationship. This cut-off is at least a small improvement over the log-log linear relationship commonly adopted in loss modelling studies.

2.3.6 Step 6: Calculate EAL

In order to evaluate the EAL, financial implications of the different damage states must be quantified. This is done through a *loss ratio* (LR), which is the ratio of the repair cost to the total replacement cost. Selecting an appropriate LR for each damage state is a subjective process and the accuracy of results will depend largely on the amount of time devoted to researching historical repair costs and their variation with respect to the extent of damage, location of structure, etc.

Hazard-survival curves shown in Figure 1(g) relate the probability of not exceeding a damage state given an annual frequency, and these curves must be integrated and multiplied with the corresponding LR's to estimate EAL. In other words, EAL is the total volume

subtended by the hazard-survival curves for different damage states plotted in the horizontal plane and their corresponding loss ratios plotted in the vertical axis as shown in Figure 1(g). Using Gaussian quadrature principles, a direct expression for the numerical integration of a cumulative probability curve conforming to a lognormal distribution covering the total probability range (i.e. between 0 and 1) is:

$$EAL = \tilde{x}\left[0.75 + 0.125\left(7^{k\beta} + 7^{-k\beta}\right)\right] \tag{2-18}$$

where β = lognormal standard deviation from Equation (2-14) and k = hazard recurrence parameter defined above. In Equation (2-18), the median variable $\tilde{x}$ for n damage states is defined as:

$$\tilde{x} = \sum_{i=1}^{n} f_{a_i} \Delta LR_i \tag{2-19}$$

where $\Delta LR_i = LR_i - LR_{i-1}$ and f_{a_i} is the annual frequency corresponding to 50% survival probability of the i^{th} damage state boundary. Equation (2-18) was compared with numerical integration, which showed good agreement with results falling within 1% for $k\beta < 2$. This formula, however, is conservative and will lead to a higher EAL since it does not consider the cut-off of damage from frequent events. To account for this, Equation (2-18) can be modified to truncate the data above the 90% no-damage confidence threshold established in Section 2.3.5:

$$EAL = \tilde{x}\left[0.6 + 0.2\left(3.5^{k\beta} + 3.5^{-k\beta}\right)\right] \tag{2-20}$$

Figure 2-1(h) illustrates the resulting total loss ratio curve as a function of annual frequency. Taking a single value from this curve gives a scenario loss, similar to what the PEER triple integral equation (i.e. Equation (2-1)) does. Performing the additional integration yields the EAL, illustrated as the area under the curve.

To calculate EAL based on the proposed Rapid IDA-EAL, the engineer needs to define only two sets of parameters: the EDP limits for each damage state, and the associated LR's. Once the EAL contributions for each damage state have been calculated using Equations

(2-18) and (2-20), their summation will give the total EAL for the assumed dispersion. Note that all calculations are based on median values and can be computed by hand. The randomness and uncertainty are combined in a single parameter β which is introduced in the process only in the final step. This eliminates difficult integration steps and simplifies the process to such extent that it can be completed in a table.

2.4 COMPUTATIONAL IDA-EAL THEORY

To verify the accuracy of the Rapid IDA-EAL method, a rigorous Computational IDA-EAL procedure was developed that does not presume any distributions. Instead, the procedure implements a technique called spectral reordering to rank data generated from the computational IDA. The hazard-survival curves generated from these Computational IDA-EAL curves are then numerically integrated to arrive at EAL. A detailed explanation of this computational approach follows.

2.4.1 Incremental Dynamic Analysis

The basic concept of IDA has been well researched (Vamvatsikos and Cornell, 2002) and is not a focus of this study, but rather the data processing that follows. However, a brief description of the analysis technique is presented. Conducting an IDA consists of running a series of inelastic dynamic time-history analyses at various levels of excitation, over a suite of earthquake records. This results in a matrix of data from which probabilistic studies can be conducted. Choosing an appropriate IM is an important step, since it can have significant effect on the scatter of data. The best practice is to use the 5% damped spectral acceleration at the fundamental period of the structure being analysed. This IM is illustrated in Figure 2-2(a) by the spectral acceleration plots of twenty earthquake records (listed in Table 2) scaled to the same IM, which also shows the lognormal standard deviation of the spectral acceleration at various periods.

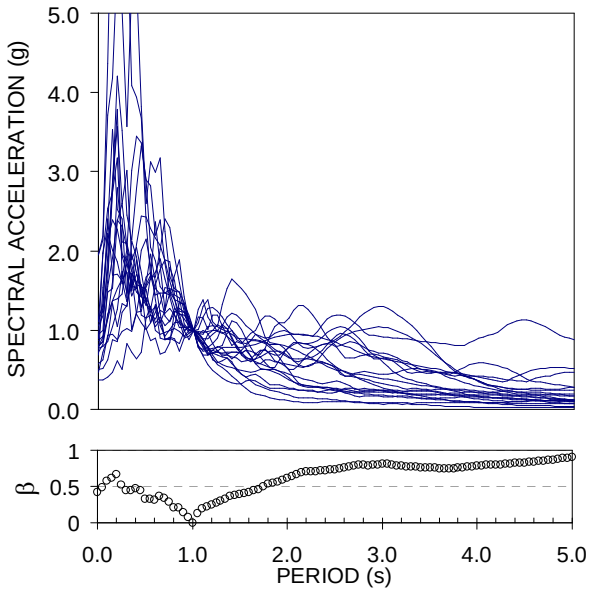

(a) Spectral acceleration of 20 ground motions and the lognormal standard deviation

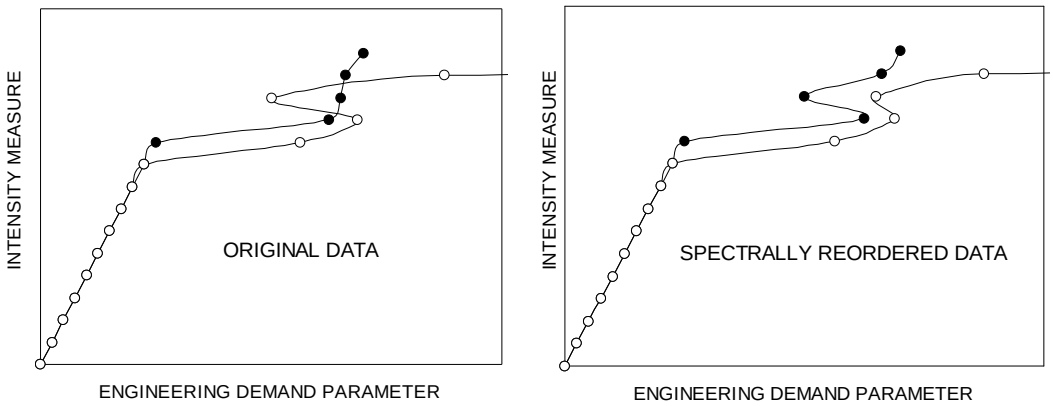

(b) The effect of spectral reordering on two nearby IDA curves that exhibit the cross-over phenomenon

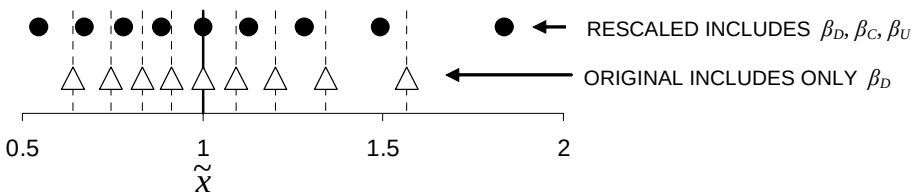

(c) Graphical interpretation showing the effect of spectral scaling

Figure 2-2: Computational IDA-EAL

2.4.2 Spectral reordering and accounting for other sources of variability and uncertainty

The EDP data points in the IDA curves at different IM levels are analysed using a procedure called spectral reordering to organize data and assign confidence bounds. For *n* earthquake records, this is accomplished by sorting the *n* EDP's at each IM in descending order and defining survival probability, *S*, by the following formula:

$$S_i = 1 - \frac{i - 0.5}{n} \tag{2-21}$$

where *i* = the rank of EDP's in descending order and *n* = number of earthquake records. This procedure is illustrated in Figure 2-2(b). No curve fitting is performed, as is typical (and necessary) to arrive at closed form solutions for integration. Though this method does not lend itself to an easily quantifiable curve (i.e. a simple median and dispersion) it is a more 'exact' representation of the data presented, though the size and relevance of the earthquake suite can dictate the accuracy of the results.

The variability of results from an IDA comes solely from the randomness in the input motion. However, other sources of uncertainty and randomness previously discussed must be considered. Knowing that the data will at least loosely conform to a lognormal distribution, it is possible to incorporate this additional uncertainty by modifying the data to incorporate a larger dispersion. Unfortunately, the lognormal CDF cannot be expressed by a single explicit equation. However, as part of the present research, a convenient equation has been formed to closely represent the lognormal CDF as follows:

$$P = \frac{1}{1 + \left(\frac{x}{\tilde{x}} \right)^{\frac{1.8}{\beta}}} \tag{2-22}$$

in which *P* = cumulative probability; $\tilde{x}$ = median; *x* = a random variable, and β = lognormal standard deviation. For consistent probabilities, before and after spectral scaling, Equation (2-22) can be utilised as follows:

$$P = \frac{1}{1+\left(\frac{x_u}{\tilde{x}}\right)^{\frac{1.8}{\beta_d}}} = \frac{1}{1+\left(\frac{x_s}{\tilde{x}}\right)^{\frac{1.8}{\beta_{c/d}}}} \tag{2-23}$$

where x_u = unscaled data points with group dispersion of β_d that arises from record-to-record randomness only; x_s = rescaled data that accounts for all sources of aleotoric randomness and epistemic uncertainty, $\beta_{c/d}$. Rearranging Equation (2-23) while utilising Equation (2-14) gives:

$$x_s = \tilde{x} \cdot \left|\frac{x_u}{\tilde{x}}\right|^{\frac{\beta_{c/d}}{\beta_d}} = \tilde{x} \cdot \left|\frac{x_u}{\tilde{x}}\right|^{\sqrt{1+\frac{\beta_c^2+\beta_u^2}{\beta_d^2}}} \tag{2-24}$$

An illustrative example of spectral scaling is given in Figure 2-2(c). Note that β_d is calculated at each IM, unlike the Rapid IDA-EAL method where it is approximated by an empirical relation.

2.4.3 Calculate EAL

For a given DM, the corresponding IM at each probability interval can be found by linear interpolation of the re-ordered data. Given the hazard-recurrence relationship, this can be expressed by a hazard-survival curve. EAL can be found by numerically integrating the given set of data points as:

$$EAL = \sum_{i=1}^{n}\sum_{j=1}^{m} f_{a_i} LR_j \frac{1}{n} \tag{2-25}$$

where n = total number of earthquake records; m = number of damage states; and j corresponds to each probability interval calculated in Equation (2-21). This formula is the area beneath the total loss curve presented in Figure 2-1(h).

2.5 CASE STUDY: REINFORCED CONCRETE BRIDGE PIERS

To illustrate the effectiveness of the two methods presented, a case study will be conducted to compare the financial seismic risk of three highway bridge piers. Building on a comparative study conducted by Tanabe (1999), the three piers were designed for similar

loading, material, and geological characteristics using governing specifications of New Zealand, Japan and the *California Department of Transportation* (Caltrans). All three piers are 7m high and were taken from a "long" multi-span highway bridge on firm soil with a 40m longitudinal span and a 10m transverse width. The weight of the super-structure at each pier is assumed to be 7000kN. Elevation views of the whole bridge and piers plus the design parameters for the three piers are given in Figure 2-3.

2.5.1 Damage and loss parameters

Maximum drift at the seismic centre of mass is considered to be an effective EDP for bridge piers. Drift is a good indicator of both global damage (toppling) and local damage (plastic hinging). Limit states were assigned as prescribed in Table 2-1, using the previously discussed *Hazus* guidelines. The damage state boundaries were calculated from the mechanisms illustrated in Figure 2-4. The first damage state (DS1) can be defined at the onset of damage defined as the computed yield drift (displacement) of the structure. This can be approximated considering elastic deformation of the pier and local curvature at yield. The final damage state, DS5, occurs when the structure becomes dynamically unstable and topples. This generally occurs when the lateral strength is exhausted as a result of longitudinal bar fracture from low cycle fatigue, or instability from the P-delta effect.

The other damage stages are more subjective in their definitions. It is suggested that the boundary separating DS=3 and DS=4 be defined at that level of drift where the structure would be deemed to have suffered irreparable damage such that the structure would likely be abandoned. This may be evidenced by: (i) excessive permanent (residual) drift at the end of the earthquake; (ii) severe damage to critical elements such as buckling of longitudinal reinforcing bars or the fracture of transverse hoops and/or longitudinal reinforcing bars.

The boundary separating DS=2 and DS=3 should be defined as that level of damage that would necessitate repairs that need to be undertaken. Such repairs lead to temporary loss of

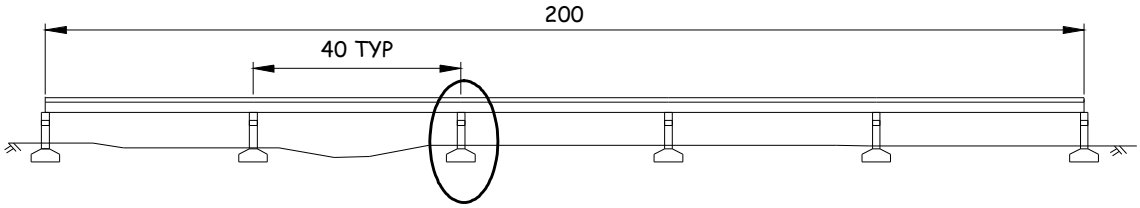

		NZ	Japan	Caltrans
D	mm	1700	2000	2000
D'	mm	1540	1834	1838
PHZ	mm	1700	4000	3000
$P/A_g f'_c$	-	0.15	0.11	0.11
Bar	-	28-D32	28-D51	32-D41
M_n	kN-m	11200	22400	19300
ρ_t	-	0.99%	1.82%	1.34%
Spiral	-	R20@170	R20@115	R20@85
ρ_s	-	0.49%	0.61%	0.78%
T_n	sec	0.86	0.61	0.66

ρ_s = ratio of the volume of the spiral to the volume of the confined concrete
ρ_t = the ratio of the longitudinal bars area to the pier's cross sectional area
T_n = natural period

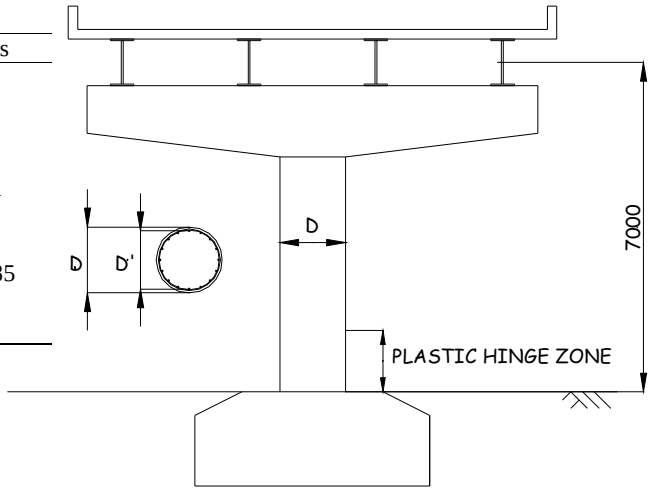

Figure 2-3: Case study bridge pier elevations and details.

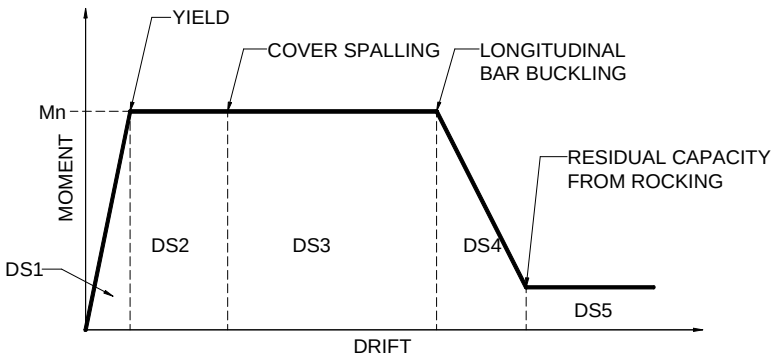

Figure 2-4: Damage state boundaries adopted in this study.

functionality. For reinforced concrete bridge substructures, this usually occurs when spalling of cover concrete is evident. This displacement can also be found from moment-curvature analysis when the cover concrete compression strain exceeds the spalling strain. At drifts below this boundary (i.e., DS=2) damage is considered to be slight and tolerable.

The yield limit (DS=1) is calculated considering elastic deformation of the pier and yield curvature as defined by Priestley *et al.* (1986). Based on recommendations given in Paulay and Priestley (1992), a compressive concrete strain of 0.008 was adopted to represent the spalling strain at the onset of DS3. The onset of longitudinal bar buckling was calculated based on a performance model of bar buckling given in Berry and Eberhard (2005). Finally, DS5 was assumed to occur at $\mu_{DS5} = \mu_{DS4} + 2$, where μ is defined as drift divided by the yield drift. In the present study, each of these limit state demarcation points have been verified through experiments on 30% scale models of all three bridge piers (Mashiko, 2006). The choice of these limits is somewhat subjective, and was based on the failure mechanisms described in Table 2-1.

The assigned LR's are given in the last column of Table 2-1. The LR's are based on actual repair data from the Northridge and Loma Prieta earthquakes as given by Mander and Basoz (1999). The same values were assigned for all three piers.

2.5.2 The Rapid IDA-EAL method

Comparative results for each step of the Rapid IDA-EAL procedure are presented in Figure 2-5. A non-linear SPO curve was obtained for each system as presented in Figure 2-5(a). Using the SPO curve and the methodology presented in Section 2.3, the median IDA curves correlating the spectral acceleration (IM) and drift (EDP) for the three piers are shown in Figure 2-5(b). The damping-related factors ξ_{in} and η were taken as 0.05 and 0.25, respectively, for all piers. This was calculated expecting the hysteresis behaviour of the pier to follow a modified Takeda hysteresis loop (Carr, 2006) with unloading and reloading

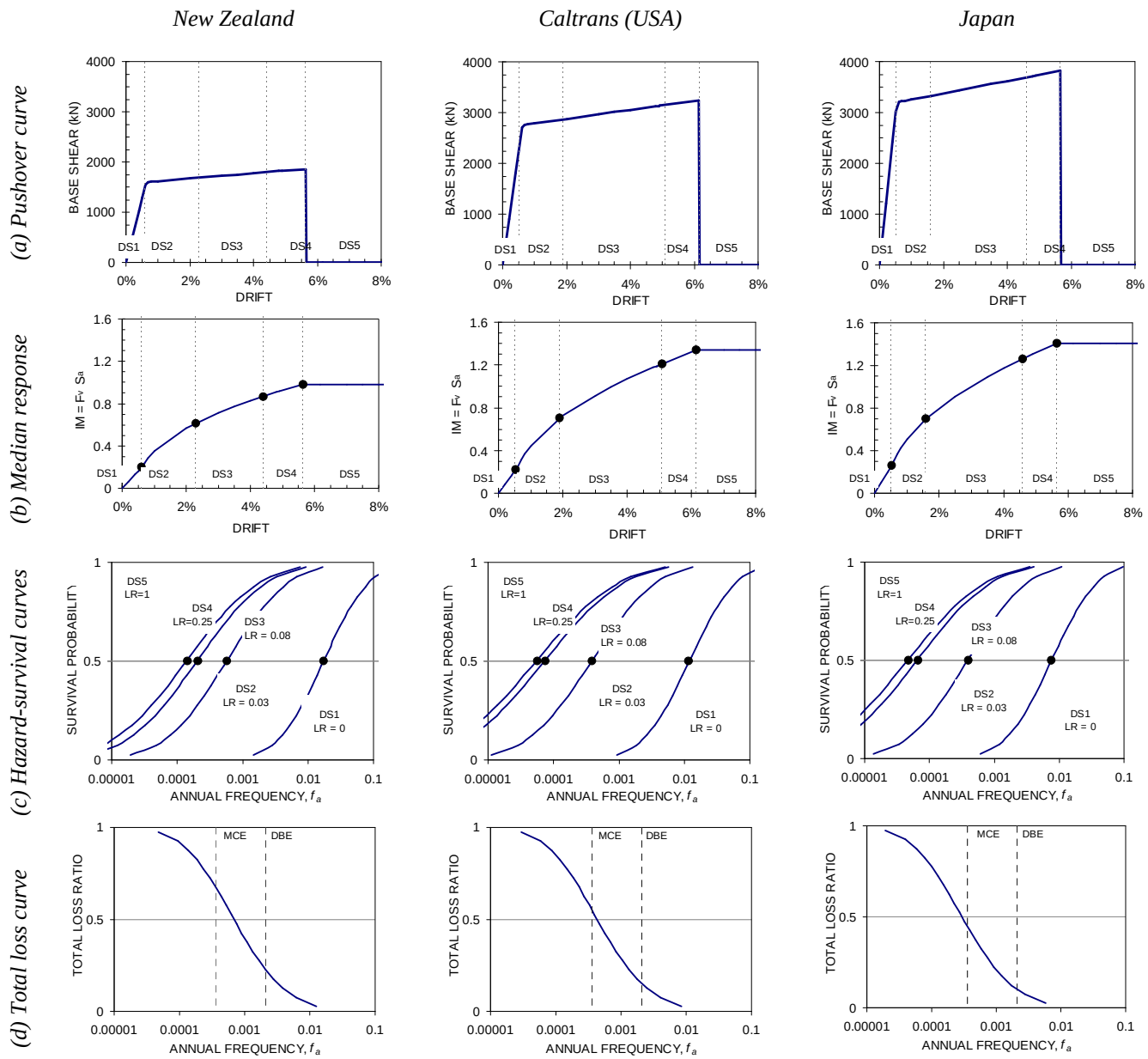

Figure 2-5: Rapid IDA-EAL applied to bridge piers.

behaviour modelled by $\alpha = \beta = 0.3$. T_a, T_v, and T_d were taken as 0.15s, 0.4s and 3s, respectively.

The hazard survival curves and total loss curves for the piers are given in Figure 2-5(c) and (d), respectively. These curves were generated using a constant hazard-recurrence relationship of k=3 so that a direct comparison of the piers' performance can be made. Finally, EAL was calculated using Equation (2-20). A generic value of β_{DBE}=0.38 was used to calculated β_d based on Equation (2-15). The EAL was found to be $1,920 per 1 million of value for the New Zealand pier, $1,270 for the Caltrans pier, and $880 for the Japanese pier.

2.5.3 The Computational IDA-EAL method

To perform the computational IDA, a non-linear structural model was developed. The pier was idealized as a single-degree-of-freedom system (i.e. a lumped mass centreline column with rotational springs at its base). The ductile pier was modelled using the a modified Takeda hysteresis loop (Carr, 2006) combined with strength degradation in accordance with the damage states outlined in Figure 2-4. Ruaumoko2D (Carr, 2006), an inelastic dynamic time-history analysis program, was used to conduct the analysis. The Rayleigh elastic damping was taken as 5 percent of critical damping. Soil-structure interaction was not considered (firm soil site was assumed).

As presented in Table 2-2, the same 20 records used by Vamvatsikos and Cornell (2002) were adopted for this study. These records range in magnitude between 6.5 and 6.9, have moderate epi-central distance, and were recorded on firm soil. For consistency between the three piers, PGA, rather than S_a, was adopted as the IM. Although this IM may not be the best choice in terms of dispersion of data, it is considered adequate in this case, since this is a comparative study of piers at different periods and the applicable design codes tend to relate return periods with PGA. The twenty records were scaled between 0.1g and 2.0g with an increment of 0.1g, resulting in 400 separate analyses. Figure 2-6 presents the data obtained

Table 2-2: Earthquake records adopted for IDA

No.	Event	Year	Station	ϕ^{1}	M^{*2}	R^{*3} *(km)*	PGA *(g)*
1	Loma Prieta	1989	Agnews State Hospital	90	6.9	28.2	0.159
2	Imperial Valley	1979	Plaster City	135	6.5	31.7	0.057
3	Loma Prieta	1989	Hollister Diff. Array	255	6.9	25.8	0.279
4	Loma Prieta	1989	Anderson Dam	270	6.9	21.4	0.244
5	Loma Prieta	1989	Coyote Lake Dam	285	6.5	22.3	0.179
6	Imperial Valley	1979	Cucapah	85	6.9	23.6	0.309
7	Loma Prieta	1989	Sunnyvale Colton Ave	270	6.9	28.8	0.207
8	Imperial Valley	1979	El Centro Array #13	140	6.5	21.9	0.117
9	Imperial Valley	1979	Westmoreland Fire Sta.	90	6.5	15.1	0.074
10	Loma Prieta	1989	Hollister South & Pine	0	6.9	28.8	0.371
11	Loma Prieta	1989	Sunnyvale Colton Ave	360	6.9	28.8	0.209
12	Superstition Hills	1987	Wildlife Liquefaction Array	90	6.7	24.4	0.180
13	Imperial Valley	1979	Chihuahua	282	6.5	28.7	0.254
14	Imperial Valley	1979	El Centro Array #13	230	6.5	21.9	0.139
15	Imperial Valley	1979	Westmoreland Fire Sta.	180	6.5	15.1	0.110
16	Loma Prieta	1989	WAHO	0	6.9	16.9	0.370
17	Superstition Hills	1987	Wildlife Liquefaction Array	360	6.7	24.4	0.200
18	Imperial Valley	1979	Plaster City	45	6.5	31.7	0.042
19	Loma Prieta	1989	Hollister Diff. Array	165	6.9	25.8	0.269
20	Loma Prieta	1989	WAHO	90	6.9	16.9	0.638

[1] Component, [2] Moment Magnitudes, [3] Closest Distances to Fault Rupture, and Source: PEER Strong Motion Database, http://peer.berkeley.edu/smcat/

from the IDA computational investigation which are plotted along with their respective dispersions for the three piers. The dispersions were calculated using standard statistical techniques (circles) or a least-squares analysis (triangles) when extreme (off-scale) data required fitting to an incomplete data set.

Using the IDA data, the Computational IDA-EAL results calculated using the methodology outlined in Section 2.4 are given in Figure 2-7. The data, plotted as triangles, is given alongside the Rapid IDA-EAL data, plotted as lines, so that a comparison can be made. The EAL, calculated using the proposed Computational IDA-EAL method was found to be $1,860, and $1,175, and $630 per $1Million of asset value for the New Zealand, Caltrans, and Japan piers, respectively. This corresponds to a difference between the two methods of 3, 8, and 40 percent, respectively.

2.6 DISCUSSION

2.6.1 The Rapid IDA-EAL method

A primary aim of this study was to develop a practical method to rapidly estimate financial seismic risk. The proposed Rapid IDA-EAL method has shown to be a very powerful, yet simple, procedure for seismic risk assessment. By means of pushover analysis and a modified CSM, a median EDP-IM relationship can be established. Using a constant lognormal standard deviation, structural fragility can be found for defined damage states. All sources of variability and uncertainty can be combined and related to the annual frequency in the form of hazard-survival curves which can be integrated and multiplied with the corresponding loss ratios to arrive at EAL.

The proposed method was verified using the Computational IDA-EAL method with no assumed distribution. Results showed reasonable correlation between the two approaches. For two of the three piers, EAL from the two methods differed by less than 10%. The third pier's EAL differed by 40% for the two methods. This difference can be attributed to the

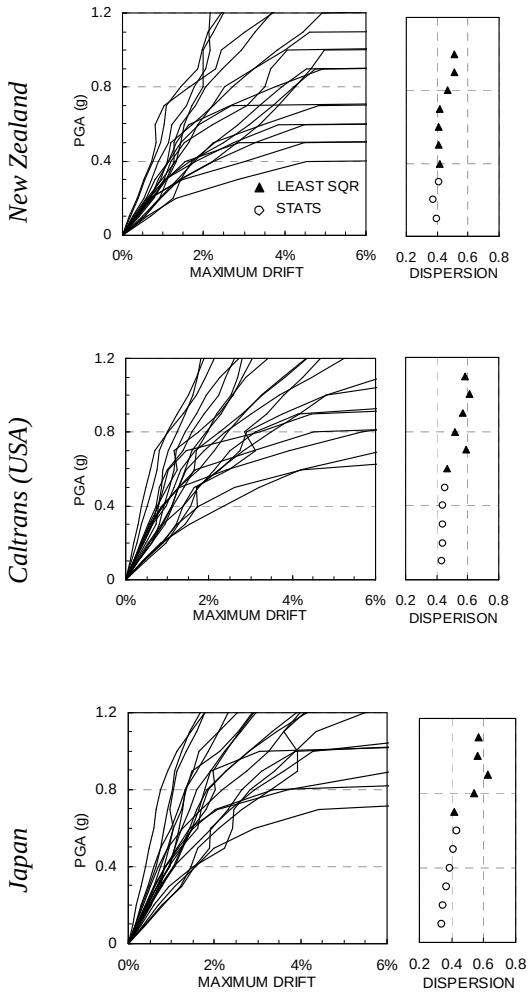

Figure 2-6: IDA applied to bridge piers.

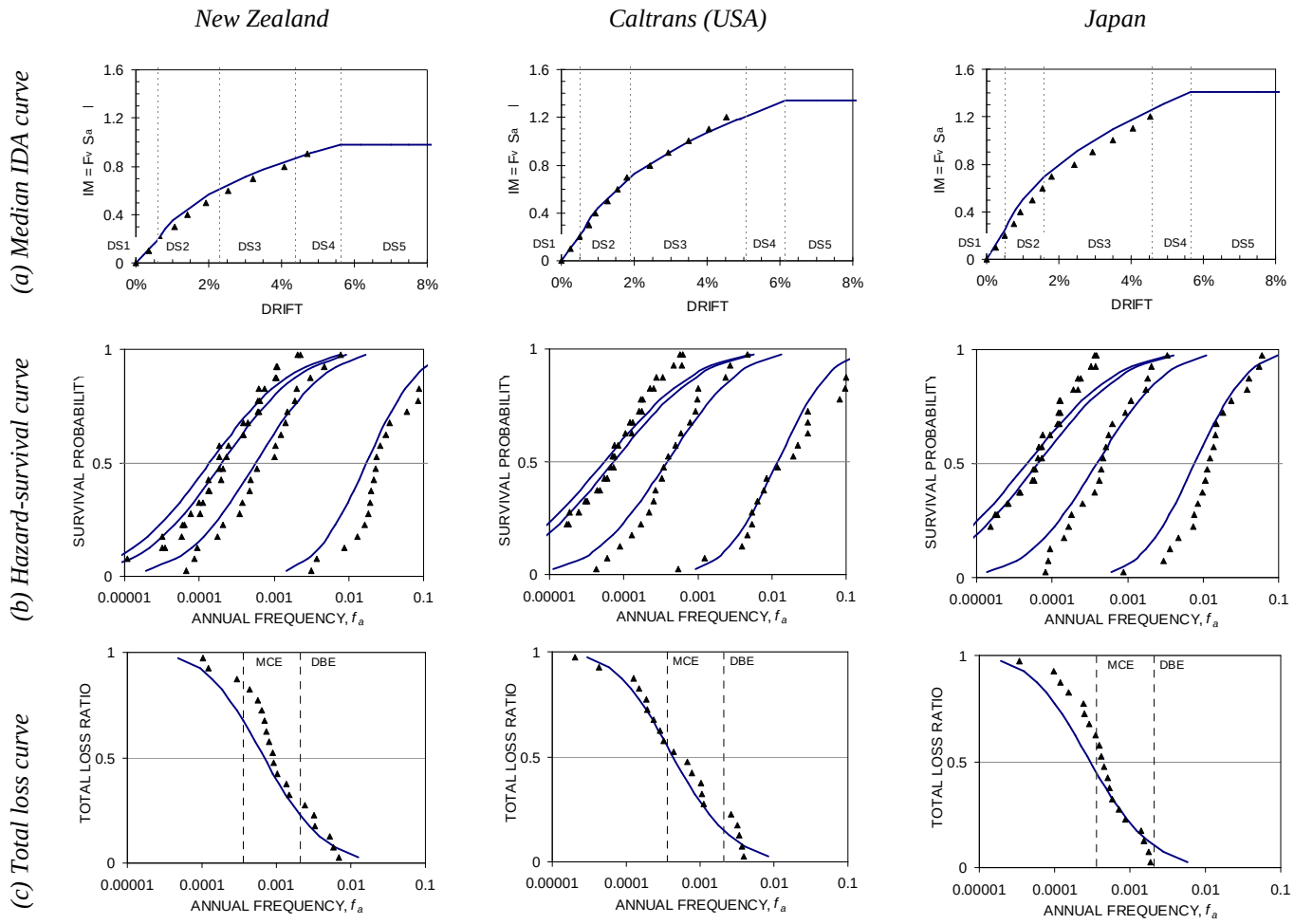

EAL_{rapid} =	*$1922 per $1M*	*$1272 per $1M*	*$880 per $1M*
EAL_{comp} =	*$1860 per $1M*	*$1175 per $1M*	*$630 per $1M*

Figure 2-7: Comparison between the rapid method (lines) and computational method (triangles).

random nature of data resulting from the Computational IDA-EAL method, where the data plotted for the Japanese pier in Figure 2-7(c) differs considerably at high annual frequencies. Figure 2-7(a) compares the median (50^{th} percentile) IDA responses from the two methods for the two piers. Both curves appear to be similar, especially at lower intensity levels. At higher intensity levels the variation in data increases somewhat; which can mainly be attributed to two reasons. First, as IM is scaled at the structure's fundamental elastic period, and the natural period elongates with the onset of inelastic behaviour, variations in response will increase due to an increased dispersion (see Figure 2(a)) Secondly, as the target displacement increases, the Rapid IDA-EAL method is more susceptible to error from hysteresis damping approximations. The fragility, hazard-survival, and total loss curves obtained from the two methods are compared in Figure 2-7(b), (c), and (d), respectively. Although differences between the two are evident, the data appears to conform reasonably well.

At this point, it is important to emphasize that the parameters adopted in the Rapid IDA-EAL method can be very sensitive to the final calculation of EAL. In particular β_c, and K (the elastic stiffness of the system), when increased by 20 percent, will increase EAL by 25-45 percent. Therefore, the Rapid IDA-EAL method, may need further investigation to address these types of sensitivities. Although further research may help to make the proposed procedures more robust, the methodologies, even in their present form, are a substantial improvement over current practice. For the purposes of comparison, as illustrated in the case study, the method will enable engineers to take into account the long-term financial implications of seismic risk. With very little computational effort, an engineer can vary parameters, such as strength, damage limits, or repair cost to help understand how these effect its seismic vulnerability. This will help engineers and stake holders to make informed decisions when weighing the pros and cons of various systems for new structures or retrofit options for existing ones.

2.6.2 The Computational IDA-EAL method

The Computational IDA-EAL method was used to verify the Rapid IDA-EAL method through a more computationally intensive analysis of the bridge piers. Data generated from IDA was directly incorporated into the final calculation of EAL, without fitting a cumulative distribution curve to the data. The intent of this was to eliminate any bias such an assumption may have on the final calculation of EAL. As evident from Figure 2-7, this resulted in curves that tend to "zig-zag" rather than transition smoothly. In theory, with the inclusion of many more analyses (i.e. thousands), the data should begin to conform to a distribution, resulting in less "kinks". If fewer data points are used, this will have the opposite effect. Therefore, for such an approach to be effective, it is recommended that at least 20 earthquake records be chosen, each scaled to at least 10 different intensities that take the structure through all the damage states in question.

As noted in the previous section, the Rapid IDA-EAL method developed herein may not be appropriate for determining the absolute EAL of a structure. For a more definite calculation of EAL, the Computational IDA-EAL method is more appropriate. However, there are some pitfalls associated with this method that must be addressed. For example, it is largely dependent on the earthquake records adopted for the study. This study adopted a generic set of earthquakes, as investigated by others. However, for more accurate future loss studies, site specific earthquakes must be considered. Furthermore, the hazard-recurrence relationship needs further development. It is accepted that a log-log linear relationship between intensity and annual frequency is reasonable over a short range (such as between the DBE and MCE); this may not be the case when considering frequent and very rare events. The truncation method developed as part of this study is a simple way of acknowledging this inaccuracy, but the cut-off is arbitrary. A more realistic hazard-recurrence model may lead to more accurate results.

2.6.3 Performance of the three piers

From the results of the analysis it is demonstrated that the designs for each country satisfy life-safety requirements. However, from an overall loss point-of-view, the results of this study suggest that the Japanese pier has a better performance than the other piers; and the NZ pier does not perform as well as the Caltrans pier does. Note, this hierarchy may not appear to agree with the general belief that the NZ concrete design specification with its sophisticated ductile detailing requirements should lead to superior seismic performance. Nevertheless, when it comes to strength, it is obvious from the tabular data listed in Figure 2 for the three piers that a small section combined with a lower reinforcement ratio renders the NZ pier significantly weaker than the other two. Furthermore, although the Japanese and Caltrans piers have the same cross-section, a higher reinforcement ratio makes the Japanese pier slightly stronger than its Caltrans counterpart.

Ductility based designs permit inelastic response and hence damage to occur, as long as collapse is prevented. It is thus not surprising to see the NZ pier resulting in a higher financial loss. This is mainly attributed to the repair cost of the minor to moderate damage states, DS2 and DS3. What is more worrying is that the implicit compromise of strength for additional ductility in the NZ code has resulted in rendering the NZ pier unable to withstand the 90^{th} percentile MCE. In a PBEE context, as the hierarchies of seismic performance and potential financial risk exposure of these three piers are in the same order as their strength (and not ductility), the following provocative questions are raised: Is there merit in moving away from highly deformable piers based on designs for high ductility? Or, is there merit in moving towards a damage avoidance design philosophy?

2.7 CONCLUSIONS

Based on the findings of this research, the following conclusions can be drawn:

1. A rapid method was established to assess seismic financial risk. A non-linear static pushover curve can be combined with the acceleration-displacement response spectrum using the capacity spectrum method to generate the median IDA curve. Given observed trends of data scatter, it can be used to calculate EAL through the use of simplified formulae.
2. A computational method was developed to verify the rapid method. This study has advanced the use of a distribution-free approach whereby data is reorganized without any pre-conceived probability distribution function. Other sources of uncertainty and randomness were combined into the analysis in an approximate sense.
3. The Rapid IDA-EAL method is best suited for comparison of different design parameters of structures, and may not give an accurate assessment of EAL. This was attributed to the dependence of the Rapid IDA-EAL method on several design key assumptions, which can significantly vary the resulting EAL
4. Both the rapid and full computational methods were compared through a practical application to reinforced concrete bridges. The Rapid IDA-EAL assessment approach showed reasonable agreement with the full Computational IDA-EAL approach. Results for the three piers varied by, 3, 10, and 40 percent.
5. Pitfalls associated with both proposed methods were discussed, identifying where further investigation may lead to more robust loss calculation methods. These pitfalls centred around approximations used to reduce computational effort in terms of distribution approximations in the rapid method and hazard-recurrence modelling and site-specific earthquake selection in the computational method.

REFERENCES

ATC-40. 1996. Seismic Evaluation and Retrofit of Concrete Buildings Volume 1. *Applied Technology Council Report No. ATC-40*.

Berry MP and Eberhard MO. 2005. Practical performance model for bar buckling. Journal of Structural Engineering – ASCE, **131**(7):1060-1070.

Carr AJ. 2006. RUAUMOKO: Inelastic Dynamic Computer Program. Computer Program Library, Department of Civil Engineering, University of Canterbury, Christchurch, New Zealand.

Cornell CA, Fatemeh JF, Hamburger RO, Foutch DA. 2002, Probabilistic Basis for 2000 SAC Federal Emergency Management Agency Steel Moment Frame Guidelines. *Journal of Structural Engineering, ASCE*, **128**(4):526-533.

Deierlein GG, Krawinkler H, Cornell CA. 2003. A Framework for Performance-based Earthquake Engineering. *Pacific Conference on Earthquake Engineering*. Christchurch, New Zealand.

Der Kiureghian A. 2005. Non-erogodicity and PEER's framework formula. *Earthquake Engineering and Structural Dynamics*, **34**(13):1643-1652.

Federal Emergency Management Agency (FEMA). 2000. Recommended seismic design criteria for new steel moment-frame buildings. *Rep. No. FEMA-350*. SAC Joint Venture: Washington, DC.

Goel RK and Chopra AK. 2001. Improved direct displacement-based design procedure for performance-based seismic assessment. *Proceedings of 2001 Structures Congress*. Washington DC.

Iwan, WD. 2002. The use of equivalent linearization in performance based engineering. *Proc. International Conference on Advances and New Challenges in Earthquake Engineering Research (ICAN-CEER)*. Harbin, China.

Kennedy RP, Cornell CA, Campbell RD, Kaplan S, Perla HF. 1980. Probabilistic Seismic Safety Study of an Existing Nuclear Power Plant. *Nuclear Engineering and Design*; **59**(2):315-338.

Krawinkler H and Miranda E. 2004. Performance-Based Earthquake Engineering. *Earthquake Engineering: From Engineering Seismology to Performance-Based Engineering*. Edited by Bozorgnia Y. and Bertero V.V. CRC Press: Boca Raton, FL.

Lin YY and Chang KC. 2004. Evaluation of Damping Reduction Factors. *Journal of Structural Engineering, ASCE*, **133**(9):1667-1675.

Lin YY, Miranda E, Chang KC. 2005. Evaluation of Dampening Reduction Factors for Estimating Elastic Response of Structures with High Dampening. *Earthquake Engineering and Structural Dynamics*, **34**:1427–1443.

Mander JB and Basoz N. 1999. Seismic fragility curve theory for highway bridges in transportation lifeline loss estimation. *Optimizing Post-Earthquake Lifeline System Reliability*, TCLEE Monograph No. 16. American Society of Civil Engineers: Reston, VA, USA; 31–40.

Mander JB. 2004. Beyond ductility: The quest goes on. *Bulletin of the New Zealand Society of Earthquake Engineering*, **37**(1): 35-44.

Mashiko N. 2006. Comparative performance of ductile and damage protected bridge piers subjected to bi-direction earthquake attack. Master of Engineering Thesis. University of Canterbury, Christchurch, New Zealand.

Miranda E and Ruiz-Garcia J. 2002. Evaluation of approximate methods to estimate maximum inelastic displacement demands. *Earthquake Engineering and Structural Dynamics*, **31**:539-560.

Paulay T and Priestley MJN. 1992. *Seismic Design of Reinforced Concrete and Masonry Buildings*. John Wiley & Sons, New York, NY, 744 pp.

Pekcan G, Mander JB, Chen SS. 1999. Fundamental Considerations for the Design of Non-Linear Viscous Dampers. *Earthquake Engineering and Structural Dynamics*, **28**:1405–1425.

Porter KA, Kiremidjian AS, LeGrue JS. 2001. Assembly-Based Vulnerability for Buildings and Its Use in Performance Evaluation, *Earthquake Spectra*; **17**(2):291-312.

Porter KA and Beck JL. 2004. Simplified Estimation of Economic Seismic Risk for Buildings. *Earthquake Spectra*; **20**(4):1239-1263.

Priestley MJN, Seible F, and Calvi GM. 1986. *Seismic Design and Retrofit of Bridges*. Wiley, New York, NY, 686 pp.

Shome N, Cornell CA, Bazzurro P, Carballo JE. 1998. Earthquakes, records, and nonlinear responses. *Earthquake Spectra*; **14**(3): 469-500.

Tanabe T. 1999. Comparative Performance of Seismic Design codes for Concrete Structures, Vol. 1, Elsevier, New York.

Vamvatsikos D and Cornell CA. 2002. Incremental Dynamic Analysis. *Earthquake Engineering and Structural Dynamics*, **31**:491–514.

Vamvatsikos D and Cornell CA. 2005. Direct Estimation of Seismic Demand and Capcity of Multidegree-of-Freedom Systems through Incremental Dynamic Analysis of a Single Degree of Freedom Approximation. *Journal of Structural Engineering*, **131**(4):589-599.

3 Performance of a damage-protected highway bridge pier subjected to bi-directional earthquake attack

SUMMARY

Bi-directional testing is performed on a 30 percent scaled rocking bridge pier designed and detailed for damage avoidance. The square base of the bridge pier is protected from being damaged by the presence of a steel armouring interface. The pier column-to-foundation joint region above the armouring is reinforced with a combination of reinforcing steel and high-strength concrete to help mitigate the high contact stresses that arise during rocking behaviour. Axial load from gravity and prestress is incorporated into the test setup. Pseudodynamic testing is performed where the earthquake records are selected probabilistically to represent multiple levels of seismic demand. Damage outcomes are compared to performance objectives related to each earthquake record. Results indicate negligible loss of stiffness and strength. The seismic performance of the rocking pier is compared to that of a conventional ductile pier. The resulting damage outcomes are incorporated into a financial seismic risk assessment and the *expected annual loss* (EAL) of the two piers is compared. The rocking pier is shown to have an EAL of approximately 20 percent of the conventional fixed-base ductile pier.

3.1. INTRODUCTION

Current seismic engineering standards for reinforced concrete bridge piers tolerate a degree of inelastic behaviour when subjected to design level ground motions, resulting in the formation of plastic hinges to provide ductile behaviour. As a direct consequence, damage to the pier is unavoidable and may also result in significant residual displacement and potential closure of the bridge as the pier is repaired or replaced. Although the ductile design methodology does afford economic (inelastic) structures with good life-safety (ductile) characteristics, damage is inherent and the financial losses due to repair or replacement coupled with down-time from closure of transportation arteries can be devastating. As the end-user community is now demanding more in terms of post-earthquake serviceability, a *Damage Avoidance Design* (DAD) philosophy is emerging which attempts to ensure that post-earthquake serviceability demands are met.

The concept of rocking structures is an effective solution to this problem. Original investigations by Housner (1963) examined the free vibration behaviour of rigid blocks. Subsequent studies considered flexibility (Meek, 1978) coupled with rocking systems and prestress (Aslam *et al.*, 1980) as a means of anchoring a structure to the ground and thus increasing its lateral capacity. More recently, these concepts have been carried over to bridge piers as presented by Mander and Cheng (1997) and Mander (2000 and 2004); the philosophy was similarly brought to precast concrete buildings using beam-column joints and structural walls by Priestley *et al.* (1999). Though still not common, two state-of-the-practice examples of rocking structures can be found in New Zealand: the South Rangitikei Railway Bridge and an industrial chimney at Christchurch International Airport (Skinner *et al.*, 1993).

Analytical and experimental investigations of such systems performed by Mander and Cheng (1997) adopt a displacement-based approach to design bridges for damage avoidance. They derived relationships through standard rigid-body kinematics. The method was

confirmed by uni-directional cyclic loading and shake-table tests performed on reinforced concrete bridge piers, with and without unbonded post-tensioned prestress, and steel interface plates between the pier and foundation. No damage to the specimen was observed in these tests. However, bi-directional tests were not performed which would better represent actual ground motions. Palermo *et al.* (2004) investigated the performance of the "hybrid" controlled rocking system applied to bridge piers and the global response of this system with regular and irregular pier configurations. Results indicated improved performance of rocking systems when compared to conventional ductile detailing.

As an extension to the uni-directional tests described by Mander and Cheng (1997) and Mander (2000 and 2004), Mashiko (2006) tested a scaled bridge pier with an armoured interface under bi-directional *pseudodynamic* (PD) loading regimes. Mashiko's pier was found to have insufficient reinforcement at its base. A considerable amount of crushing and cracking resulted. Although this slight degree of damage did not cause considerable strength or stiffness degradation, aesthetically the damage would be disconcerting to a bridge owner or user; some minor repairs may be necessary following a design level earthquake. To address this, this chapter will report on a second phase of testing on the DAD pier, strengthened at its base. Special attention is given to the large concentrated forces which are transmitted through a small region of the specimen's base due to bi-directional rocking behaviour.

3.2. EXPERIMENTAL PROGRAMME

The prototype DAD bridge pier was detailed using the principles of a damage avoidance philosophy and scaled to fit available experimental facilities. PD tests were performed, simulating the performance of the pier subjected to real earthquake ground motions. Earthquake records were chosen from a suite of twenty ground motions based on an *Incremental Dynamic Analysis* (IDA) (Vamvatsikos and Cornell, 2004). Following the procedure established by Dhakal *et al.* (2006), three particular earthquake records were

chosen to represent: (i) the 90th percentile *design basis earthquake* (DBE), with a 10 percent chance of occurrence in 50 years; (ii) the 50th percentile *maximum considered earthquake* (MCE), with a 2 percent chance of occurrence in 50 years; and (iii) the 90th percentile MCE. Damage to the pier was monitored and classified according to the *Hazus* damage states index described for bridges by Mander and Basoz (1999).

3.2.1. Prototype Design

The prototype design was conducted as part of another study (Mashiko, 2006), and is summarized here. The prototype bridge pier is 7m high and taken from a typical 'long' multi-span highway bridge on firm soil with 40m longitudinal spans and a 10m transverse width. Design details are presented in Table 3-1 and Figure 3-1(a). The seismic weight of the superstructure was calculated to be 7000kN. The pier was assumed to be located in a high seismic zone in New Zealand, with the DBE having a *peak ground acceleration* (PGA) of 0.4g. The moment demand was assessed according to the New Zealand seismic design standard (NZS1170.5, 2005; NZS:3101, 1995) considering a ductile monolithic pier; this was calculated to be 7440kN-m.

The lateral capacity of the DAD pier was satisfied by a combination of gravity load, longitudinal un-bonded tendons, and supplemental energy dissipation devices. Vertical un-bonded post-tensioned prestress was designed to provide a clamping force of 815kN. The dissipation devices were designed to act in tension only, providing a yield force of 128kN per device. These damping devices were designed previously by Mashiko (2006). Following the theory presented in Chapter 1, a pushover curve is given in Figure 3-2 with and without energy dissipation devices. Due to the high stiffness of the dissipaters, it is assumed they yield at the onset of rocking, therefore their stiffness contribution is not considered. Instead, the figure depicts the expected elastic stiffness of the pier and the post-rocking stiffness of the

Table 3-1: Dimensions and materials of the prototype bridge pier and specimen.

			DAD Pier	Ductile Pier (Mashiko, 2006)
Prototype				
Diameter	D	*mm*	1400	1700
Effective Diameter	D'	*mm*	1240	1540
Width of shoe block	B	*mm*	1700	---
Height of shoe block	H_s	*mm*	1500	---
Longitudinal reinforcing			20-D32	28-D32
Longitudinal reinforcement ratio	ρ_t		1.04%	0.99%
Transverse reinforcement			R20@190	R20@170
Specimen				
Diameter	D	*mm*	400	500
Gravity Load	P	*kN*	630	630
Longitudinal reinforcing bars			16-D10	24-D10
Longitudinal steel volume	ρ_t	*%*	1.00	0.96
Transverse spiral reinforcement			R6@55	R6@50[1]
Transverse steel volume	ρ_s	*%*	0.60	0.51
Shoe block steel			D16	---
Shoe block confinement (HS wire rope)			7x16	---
Concrete measured strength	f'_c	*MPa*	70.6	41.2
Shoe block concrete strength	f'_c	*MPa*	61.5	---
Shoe block tensile strength[2]	f_t	*MPa*	7.0	---
Longitudinal steel: yield strength	f_y	*MPa*	539	539
Ultimate strength	f_u	*MPa*	677	677
Strain hardening	ε_{sh}	*%*	1.8	1.8
Strain at ultimate strength	ε_{su}	*%*	14.6	14.6
Transverse Spiral Steel: yield strength	f_y	*MPa*	461	461
Ultimate strength	f_u	*MPa*	633	633
Strain hardening	ε_{sh}	*%*	1.4	1.4
Strain at ultimate strength	ε_{su}	*%*	19.6	19.6

[1] within the plastic hinge zone
[2] determined from split tension (Brazilian) test

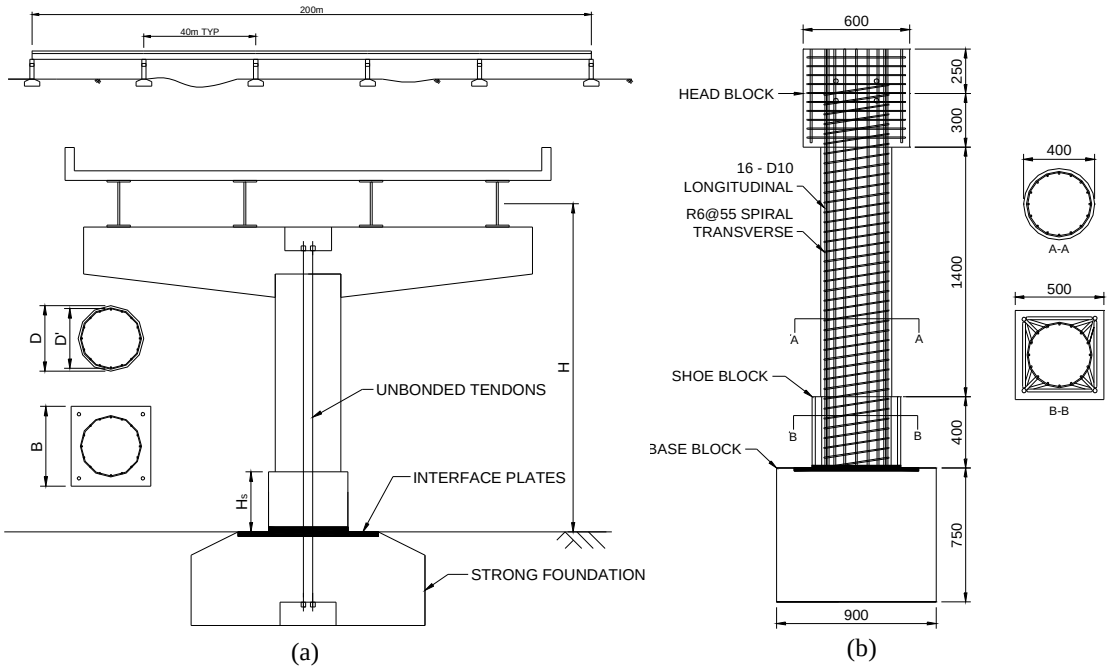

Figure 3-1: Bridge pier details: (a) prototype bridge pier; (b) 30% scaled specimen.

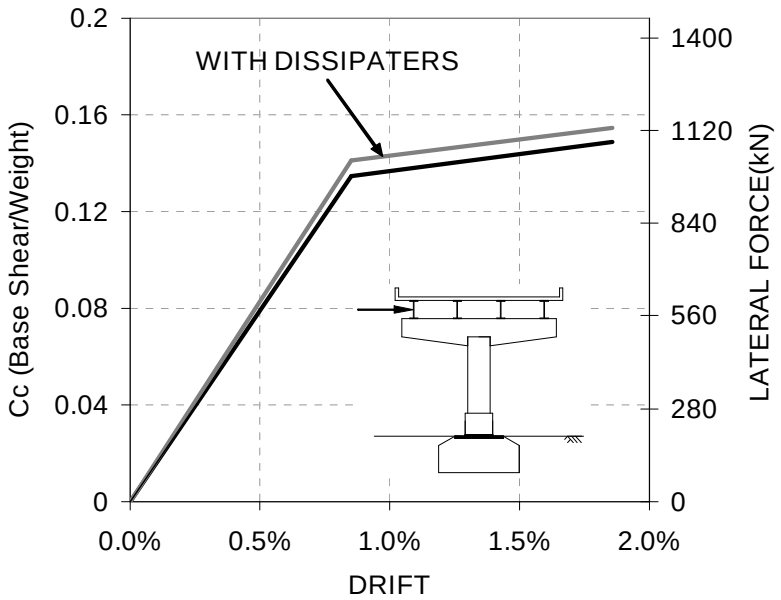

Figure 3-2: Theoretical pushover curve

system, provided by the longitudinal un-bonded post-tensioning. The moment capacity at uplift was calculated to be:

$$M_{uplift} = (P+F)\frac{B}{2} + \sum A_s \sigma_y \frac{2e+B}{2}$$
$$M_{uplift} = (7300kN + 815kN)\frac{1.7m}{2} + 2\left(\frac{415mm^2\,300MPa}{1000}\frac{2\cdot 0.4m + 1.7m}{2}\right) = 7200kNm \quad (3\text{-}1)$$

where P = axial load; F = effective prestress force; B = width of the rocking base; A_s = cross sectional area of the energy dissipaters; σ_y = yield stress of the energy dissipaters; and e = eccentricity of the energy dissipaters from the pier centreline. Since P is in effect fixed, the required moment capacity can be reached by modifying either the geometry of the rocking interface, adding additional prestress, or adding dissipaters. The post-uplift (rocking) behaviour of the pier is a function of the initial prestress and the elastic properties of the tendons.

To determine the displacement of the pier at the onset of rocking, it is necessary to consider the elastic stiffness of the pier. The pier can be characterized as a cantilever with a point load, thus its deflection can be found by:

$$\Delta = \frac{V_{pier} H^3}{3EI_{eff}} \quad (3\text{-}2)$$

where V_{pier} = the lateral force at the top of the pier; H = height of the pier; E = elastic modulus of the reinforced concrete; I_{eff} = effective moment of inertial of the pier's cross section. As noted in Chapter 1, this can be taken as $0.25I_{gross}$. The post-uplift displacement of the system was calculated considering elastic deformation of the pier, and local rotation from rocking.

Since the post-yield response of the DAD pier is limited to the rocking region, it is implied that the pier itself will not form a plastic hinge, and can therefore be detailed according to nominal longitudinal and transverse reinforcement requirements.

3.2.2. Specimen Construction

A scaled model of the prototype bridge pier was constructed. Figure 3-1 (b) presents an elevation of the specimen. Longitudinal and transverse reinforcement ratios were kept constant in the 30 percent scaled physical model and the prototype pier.

The specimen was constructed in four parts (Mashiko, 2006): (i) the base block; (ii) circular column; (iii) head block; and (iv) shoe block. As the base block and head block were considered part of the experimental testing apparatus, they were detailed to withstand the expected demands from testing. At the top of the base block, Plate C (illustrated in Figure 3-3), with a 350x350 mm hole in the centre, was placed flush to the top of the base block to act as the armoured rocking interface of the pier's foundation. To construct the interface at the base of the column, Plate B was bolted to Plate A to form the shear key which would rest in the square hole of Plate C. A 3mm gap was provided on each side to prevent the steel plates from binding during rocking. Longitudinal reinforcement was tack welded into holes drilled in Plate A. The R6 spirals were wrapped around these longitudinal bars.

After testing was complete as reported in Mashiko (2006), the pier's shoe block was stripped to the circular core using a jack hammer. It was found from Mashiko's tests that the pier was inadequate for resisting the large contact forces from rocking; excessive crushing and cracking was observed, particularly in the corners of the shoe block. Under bi-directional loading, this meant the entire axial load was being transmitted through one corner of the specimen. This corresponded to a point load of approximately 800kN. The aim of strengthening the pier was to reduce or eliminate crushing and cracking. As illustrated in Figure 3-3, this was accomplished in three ways: (1) diagonal reinforcing steel was used to help develop the expected strut mechanism from the shoe block corners to the pier's core; (2) high strength wire rope was wrapped in two layers to reduce the development of cracks and to help confine the concrete; and (3) high strength fibre reinforced concrete was used to reduce

crushing and decrease crack propagation. To accomplish this, three D16 grade 500MPa bars were tack welded to Plate A at each corner and to the pier's longitudinal reinforcement, creating a diagonal mechanism to resist the expected strut forces. Additional D16 'hoop' bars were placed parallel to each plate edge. The wire rope (7x19 construction) was hand wrapped around the inner diagonal reinforcement and the outer cage at a 35mm pitch. Finally, the shoe block was poured using a high strength concrete mix with 1 percent Dramix^{TM} steel fibres by weight. A photograph of the strengthened shoe block is given in Figure 3-4.

The energy dissipaters consisted of R12 threaded bars with the centre 300mm machined to a 7mm diameter (Figure 3-3). The dissipaters were designed by Mashiko (2006), where a more detailed account of their design is given. These devices were screwed vertically into Plate C through ducts at each corner of the shoe block, bolted in place, and stressed to $0.5f_y$ by torque wrench. The dissipaters were designed to perform in tension only, with the intent they could be easily replaced following a seismic event.

3.2.3. The Test Apparatus

An elevation and plan view of the test setup is given in Figure 3-5(a) and (b), respectively. The apparatus was designed to simulate actual seismic demands imposed on the prototype structure. To accomplish this, simultaneous lateral loads combined with axial load were applied to the specimen via two actuators mounted on reaction frames. These frames were assembled within the confines of a 10,000kN capacity Dartec^{TM} universal testing machine. At the top and bottom of the specimen, a ball joint transmitted a constant axial load of 777kN, consisting of the scaled weight of the superstructure (630kN) and the simulated force from un-bonded tendons (147kN). In reality, the tendon force would increase as the gap opens, however this was not considered in the axial load, which was constant throughout testing. The L-shaped reaction frames were attached to counter weight baskets by 30mm diameter high strength rods running through the base block. Lateral loads were applied via

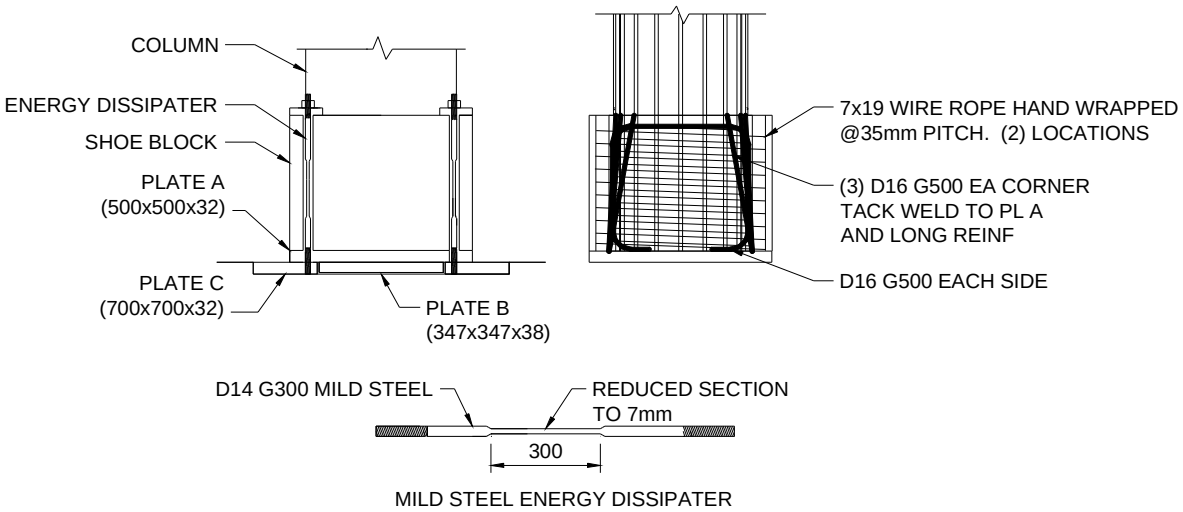

Figure 3-3: Shoe block and energy dissipater details.

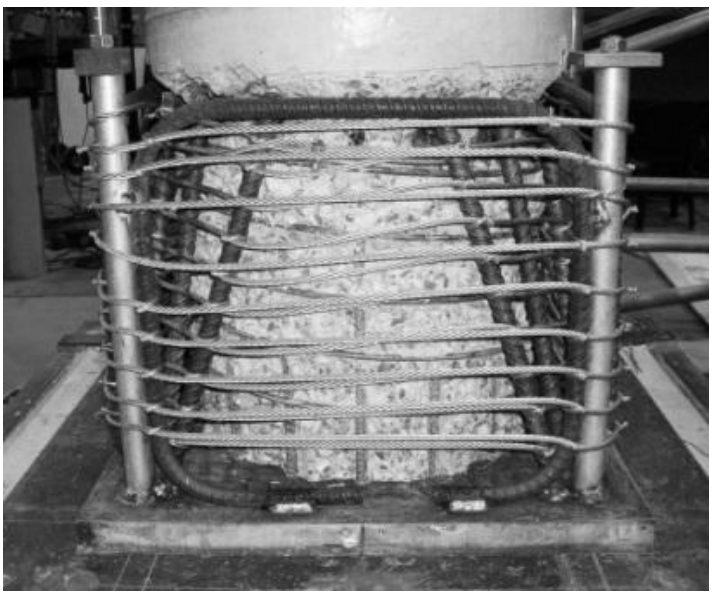

Figure 3-4: Photograph of the shoe block reinforcing.

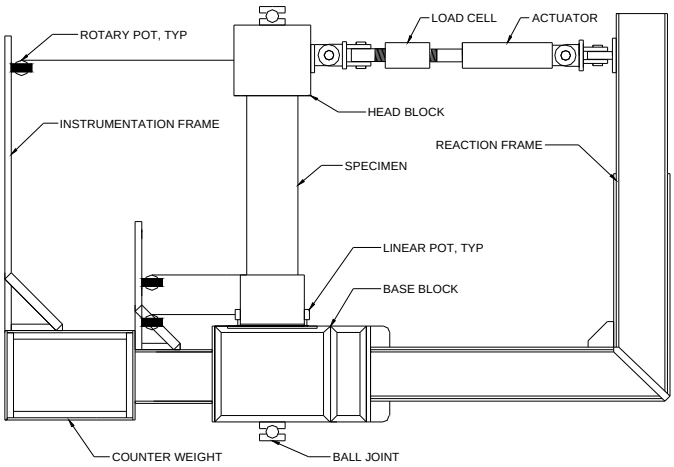

(a)

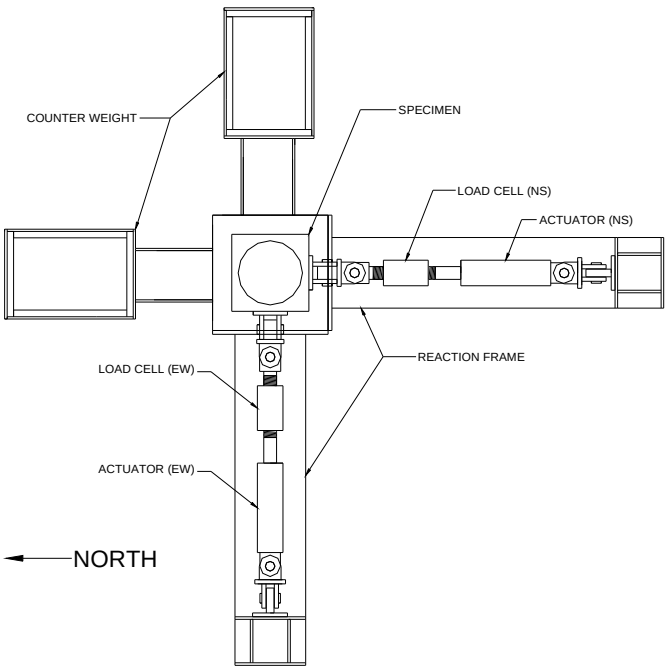

(b)

Figure 3-5: The testing setup: (a) EW elevation; (b) plan view.

Figure 3-6: Photograph of the specimen in the testing apparatus.

800kN capacity hydraulic actuators; each actuator was connected to the specimen's head block and reaction frame by universal joints. A photograph of the test setup is given in Figure 3-6.

The instrumentation plan is given in Figure 3-7. A primary rotary potentiometer was installed in line with each actuator to measure the displacement of the specimen to be used by the controller's PD algorithm. Two additional rotary potentiometers (pots) were installed at the top and bottom of the shoe block along with a series of spring pots at each corner to measure localized uplift. All instrumentation was isolated on the testing apparatus to measure relative displacement. Load cells (1000kN capacity) were installed in-series with the actuators. Eight strain gauges were installed on the longitudinal steel of the pier 500mm from the base of the pier.

3.2.4. Pseudodynamic Testing Method

The PD testing concept is illustrated in Figure 3-7. Two linked systems are required to perform testing: an analytical system and a physical system representing the analytical model. The process originates from the well-known equation of motion:

$$m\ddot{u} + c\dot{u} + ku = -m\ddot{u}_g(t) \tag{3-3}$$

where m = mass; c = damping; k = stiffness; $\ddot{u}_g$ = ground acceleration; u = displacement; $\dot{u}$ = first derivative of u (velocity); $\ddot{u}$ = second derivative of u (acceleration); and t = time.

Given an assumed m and c, it is possible to determine k through physical experimentation, and u can be solved. This was performed in a closed loop, whereby $\ddot{u}_g$ was input from an earthquake record consisting of a series of ground accelerations at a given time step. From a user-defined initial stiffness, the analytical system calculated u, then instructed the test apparatus to move the specimen to the calculated displacement, at which time the physical stiffness was recorded from the specimen. Calling this step n, the analytical system then applied $\ddot{u}_g$ at the next $n + 1$ time step using k_n to solve for $u_{(n+1)}$, thus completing the

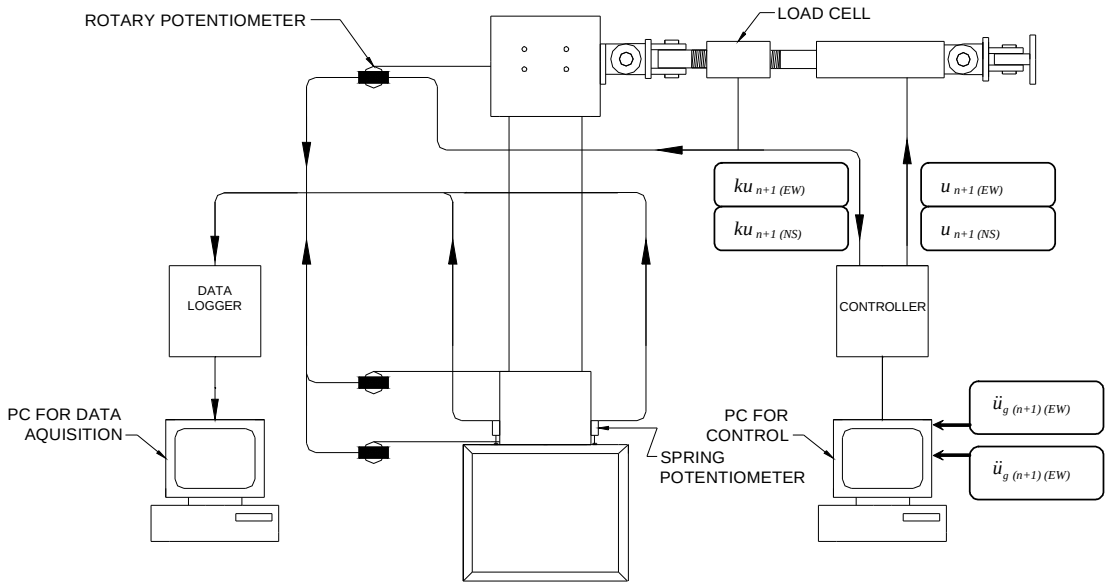

Figure 3-7: Schematic of acquisition hardware and the PD experimental procedure.

loop. This process was repeated until the acceleration data set terminated. A detailed explanation of the PD testing concept is given in Shing *et al.* (1996).

In the case of this study, calculations performed in the analytical system were consistent with the prototype (full scale) system. Displacements and forces were scaled when sent to or retrieved from the physical model; displacements were scaled by $\lambda = 0.3$ and forces by $1/\lambda^2 = 11.11$.

3.2.5. Input Data

For PD testing, the aforementioned mass, *m*, and effective viscous damping, ξ_{eff}, are required to solve the equation of motion. The latter can be assessed by:

$$\xi_{eff} = \xi_0 + \xi_{rocking} \tag{3-4}$$

in which ξ_0 = intrinsic damping; $\xi_{rocking}$ = effective viscous damping from the radiation of energy by rocking impacts. According to Mander and Cheng (1997), the following equation can be used:

$$\xi_{rocking} = \frac{2}{\pi}\left(\frac{D_c}{H_c}\right) \tag{3-5}$$

where D_c = the width of the shoe block and H_c = the height of the pier. For the present specimen $\xi_{rocking} = 3.75\%$. Herein it will be assumed $\xi_0 = 2\%$ which is customarily adopted for prestressed concrete structures, thus $\xi_{eff} = 5.75\%$.

3.2.6. Earthquake Records

To determine the earthquake records used for PD testing a procedure described by Dhakal *et al.* (2006) was adopted. In that study, PD tests were performed on a bridge pier where the earthquake records adopted for testing were selected based on IDA. Termed a *multilevel seismic performance assessment* (MSPA), the procedure determines appropriate earthquake records to represent the demand associated with multiple performance objectives. A suite of twenty earthquakes were adopted as potential candidates based on a previous study

conducted by Vamvatsikos and Cornell (2004). These records range in magnitude between 6.5 and 6.9, have moderate epi-central distance, and were recorded on firm soil. The IDA data from these records was analyzed probabilistically to identify those critical to the pier. Three records were chosen to represent the 90th percentile DBE (10%/50 years) and the 50th and 90th percentile MCE (2%/50 years). Since this study will highlight the enhanced performance of a DAD bridge pier, it is necessary to directly compare its performance to that of a conventional ductile pier. To accomplish this, specific earthquake selection for the DAD pier was not performed; the same earthquakes selected for the New Zealand ductile bridge pier (Mashiko, 2006) have been adopted for this study. These earthquakes, termed EQ1 (90% DBE), EQ2 (50% MCE), and EQ3 (90% MCE), are given in Table 3-2. In the test, the three records were applied consecutively, with 5 second intervals of zero acceleration between each record. The interval allowed the residual drift and natural period of the structure to be recorded.

3.2.7. Damage Limit States

All observed damage to the shoe block was classified according to the *Hazus* damage limit states index presented in Table 3-3 (Mander and Basoz, 1999). These *damage states* (DS) were developed for ductile monolithic bridge piers, and are modified here to apply to the DAD pier. DS1 represents pre-yield response and therefore no damage to the structure; hence a representative limit is the uplift drift of the structure. This is further defined as the point where the energy dissipation devices would require replacement. When considering a structure designed for damage avoidance, ideally the structure would not pass this limit until full collapse (i.e. DS5). The intermediate damage states, DS2, DS3, and DS4, are somewhat subjective and defined for various magnitudes of damage and the expected outage of the structure. The boundary for DS2 and DS3 is defined as being the point at which the structure would be unusable until repairs are made. Similarly, the boundary for DS3 and DS4 would be

Table 3-2: Earthquake records adopted for PD testing.

		PGA (g)	Component	Event	Year	Station	ϕ^1	M^2	R^3 (km)	PGA (g)
EQ1	90% DBE	0.376	EW	Imperial Valley	1979	Chihuahua	282	6.5	28.7	0.254
		0.400	NS				012			0.270
EQ2	50% MCE	0.800	EW	Loma Prieta	1989	Anderson Dam	270	6.9	21.4	0.244
		0.787	NS				360			0.240
EQ3	90% MCE	0.800	EW	Superstition Hills	1987	Wildlife Liquefaction	360	6.7	24.4	0.207
		0.700	NS				90			0.181

[1] component; [2] moment magnitudes; [3] closest distances to fault rupture

Table 3-3: Damage states index for bridges as defined by *Hazus*.

Damage State		Failure Mechanism	Repair required	Outage expected
DS1	None	First Yield	None	No
DS2	Minor/Slight	Cracking, Minor spalling	Inspect, Adjust, Patch	< 3 days
DS3	Moderate	Spalling, Bar buckling	Repair components	< 3 weeks
DS4	Major/Extensive	Degrading of strength, Bar fracture	Rebuild components	< 3 months
DS5	Complete/Collapse	Collapse	Rebuild structure	> 3 month

the point at which the structure is deemed irreparable; components must be rebuilt or the entire structure must be replaced. Finally, DS5 represents full collapse of the structure. In the case of a DAD structure, it should not experience DS3 or DS4 because of the rocking mechanism. However, DS3 may result when yielding of the post-tensioned tendons occurs, or aesthetic cracks and minor spalling excessive enough to merit aesthetic repairs.

3.3. EXPERIMENTAL RESULTS

The specimen was subject to two PD tests: the first without energy dissipaters and the second with energy dissipaters. Each test was a series of 3 earthquakes of increasing intensity, with 5 second intervals between records. Figure 3-8 presents results from the test with energy dissipaters. The results are plotted so that data from one graph is projected to the next, resulting in two force-displacement curves (Figure 3-8(a) and (b)), two displacement history curves (Figure 3-8(d) and (e)) and a plan view of bi-directional displacement (Figure 3-8(c)). In addition, the theoretical prediction given in Figure 3-2 is plotted along with the force-displacement curve of Figure 3-8(a). Good agreement between the prediction and the experimental result is evident. Maximum drifts observed during EQ1 in the EW and NS direction were 1.9 percent and -1.8 percent at 6.48 seconds and 14.94 seconds, respectively. The corresponding lateral forces were 91kN and -80kN. Some minor hairline cracks propagating diagonally from the bottom corners to top midsection of the shoe block were observed. Flexural cracking also occurred in the pier. All of these cracks closed after testing was complete. The energy dissipation devices yielded during testing. This was evident from an approximately 5mm elongation of the devices, as illustrated in Figure 3-9(a). Since the energy dissipation devices would have to be retightened or replaced, the pier was classified as being at DS2: slight damage.

The maximum drift observed during EQ2 in the EW and NS direction was 3.8 percent and 2.2 percent at 36.42 seconds and 38.34 seconds, respectively. The corresponding lateral

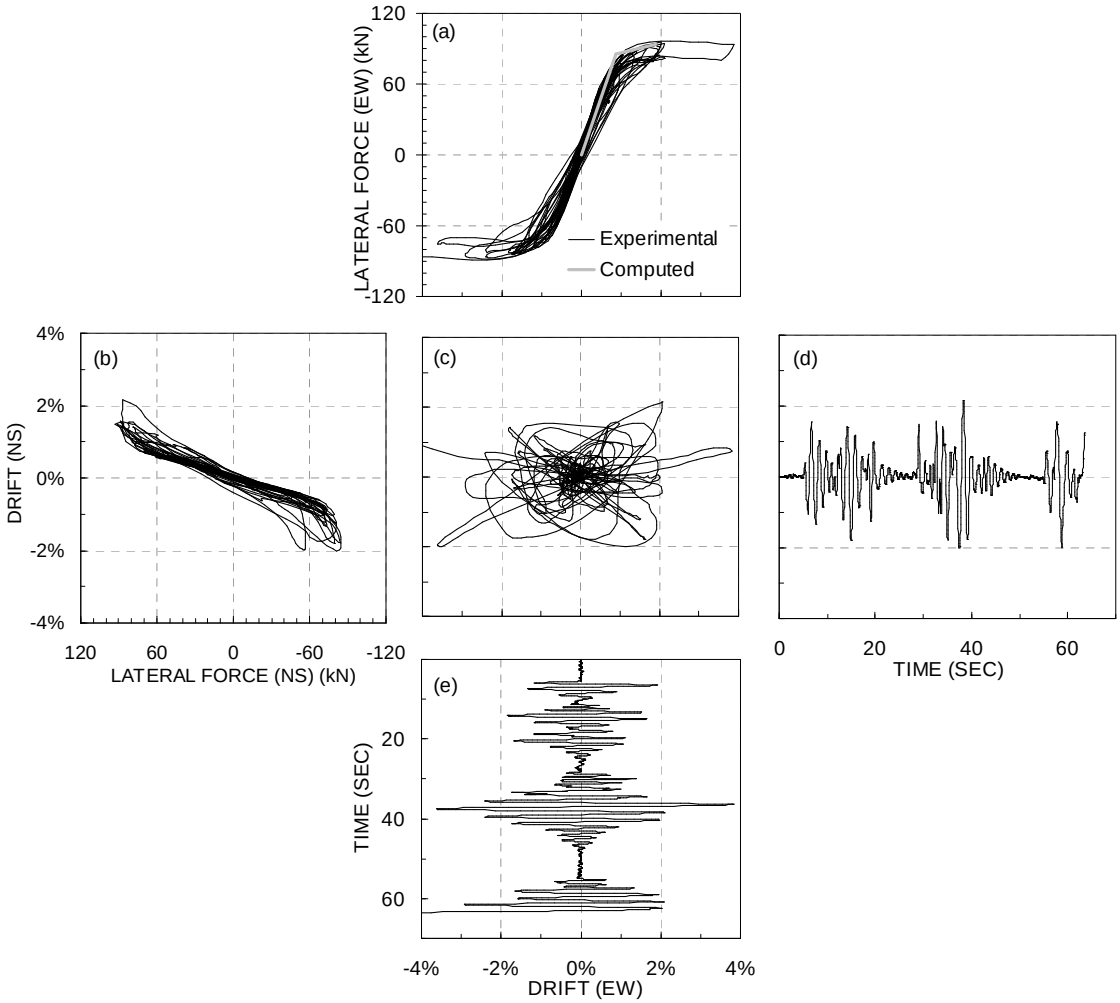

Figure 3-8: Test results of the DAD pier with energy dissipaters, subjected to EQ1, EQ2, and EQ3: force-displacement curves for (a) EW and the analytical prediction pushover curve, (b) NS direction; (c) plan view of drift; (d) NS and (e) EW displacement-time plots.

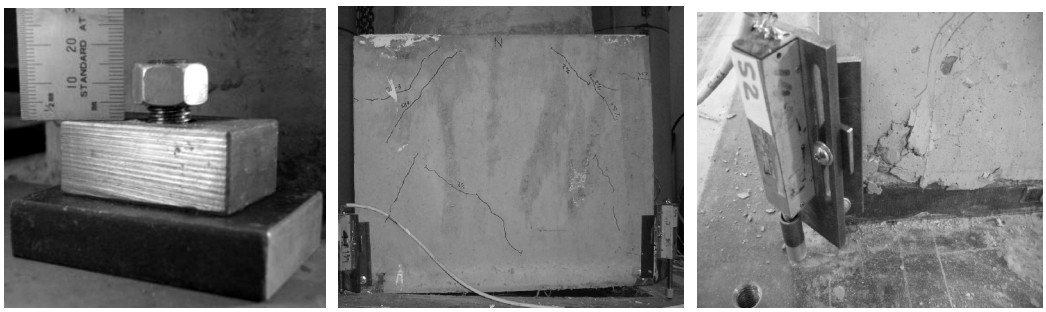

(a) (b) (c)

Figure 3-9: Photographs of the DAD specimen: (a) elongation of an energy dissipater after EQ1; (b) the shoe block rocking at 3.8% drift during EQ2; (c) localised crushing at the shoe block corner after testing.

loads were 96kN and 91kN. A photograph of the shoe block at approximately 3.8 percent drift (at 37 seconds) is given in Figure 3-9(b). At times the pier was rocking on a single corner of the shoe block, such as when the drift of the pier was at 2 percent in both the NS and EW direction at approximately 39 seconds. This resulted in minor crushing and additional hairline cracks at the diagonal, as shown in Figure 3-9(c). Such damage was largely aesthetic and did not cause noticeable degradation of strength or stiffness, thus the pier was classified as being at DS2: slight damage.

The pier did not survive EQ3. At 13.5 seconds the drift angle of the pier was 5.5 percent in the EW direction and 1.2 percent in the NS. It was deemed unsafe to continue testing, thus resulting in an assumed complete collapse of the structure under EQ3. Aside from this, there appeared to be only minor additional damage; further crushing and hairline cracks were observed. This was in the form of additional propagation of the cracks, expanding by another 1/3rd their length. These cracks tended to open to about 0.5mm during testing but closed after testing. However, since complete collapse was assumed due to termination of the test, the pier was classified at DS5.

Figure 3-10 presents a comparison of the hysteretic response of the pier with and without energy dissipaters. Results are presented for EQ1 and EQ2. The energy dissipation devices had a small contribution to the overall behaviour of the specimen. The maximum lateral force in the EW and NS direction for EQ1 increased 3 percent and 4 percent, respectively. For EQ2 there was a similar increase in strength, 7 percent and 4 percent for the EW and NS, respectively. This increase is consistent with initial calculations, which predicted a 5 percent increase in strength.

Strain gauges attached to the longitudinal steel 500mm from the base did not detect yielding, which would have occurred at approximately 1 percent drift had the specimen been a conventional monolithic pier. Using supplemental linear potentiometers, it was possible to

calculate the local rotation of the shoe block by measuring the uplift at its corners. It was found that the rotation of the shoe block accommodated most total drift past 1 percent. Thus, flexural deformation of the pier did not account for more that 1 percent drift. During the zero acceleration portion of testing no discernable residual displacements were observed.

3.4. COMPARISON WITH A MONOLITHIC DUCTILE PIER

To highlight the advantages of DAD, the specimen's performance was compared to that of a companion conventional monolithic pier (Mashiko, 2006) designed to the concrete structure design specification for New Zealand (NZS:3101, 1995). The prototype details are given in Table 3-1. The pier was subject to the same PD testing as the DAD pier. Figure 3-11 presents experimental results of the ductile pier for EQ1, EQ2 and EQ3. Similar to Figure 3-8, Figure 3-11(a) and (b) give force-displacement for the EW and NS, respectively, (c) gives a plan view of the drift orbit, and (d) and (e) gives displacement versus time. From this figure it is evident that the ductile pier had a higher stiffness and a higher moment capacity than the DAD pier. This is due to the different design procedures of the two piers. Consequently, the maximum displacement for the two piers varied considerably. However, in spite of greater displacements, the DAD pier suffered considerably less damage and no residual displacement. After EQ1 and EQ2, the ductile pier was classified as being in DS2. As is evident from Figure 3-8 and Figure 3-11, the residual drift for the DAD pier was essentially zero, while for the ductile pier this was approximately 0.25 percent. After EQ3, testing was terminated due to high drifts, resulting in DS5. Damage was comparably less for the DAD pier. Although the final collapse condition was similar during EQ3, considerably less damage was observed from EQ1 and EQ2.

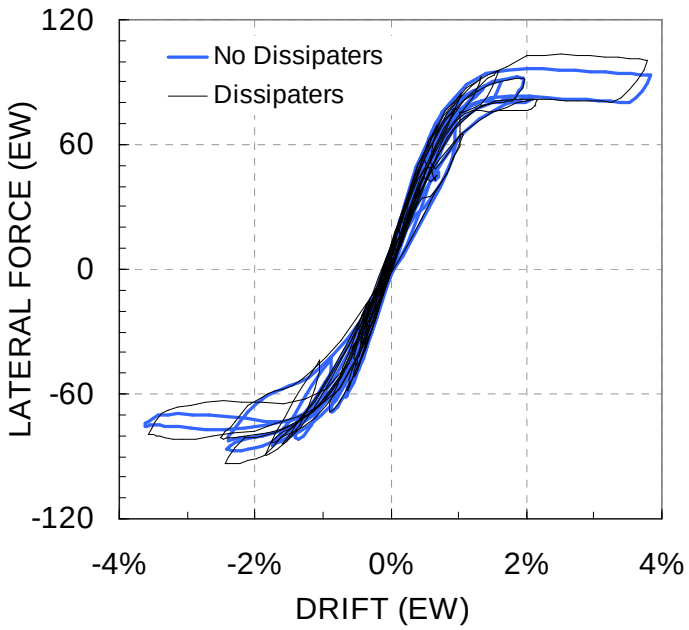

Figure 3-10: Hysteresis loop comparison for the EW direction with and without energy dissipation devices.

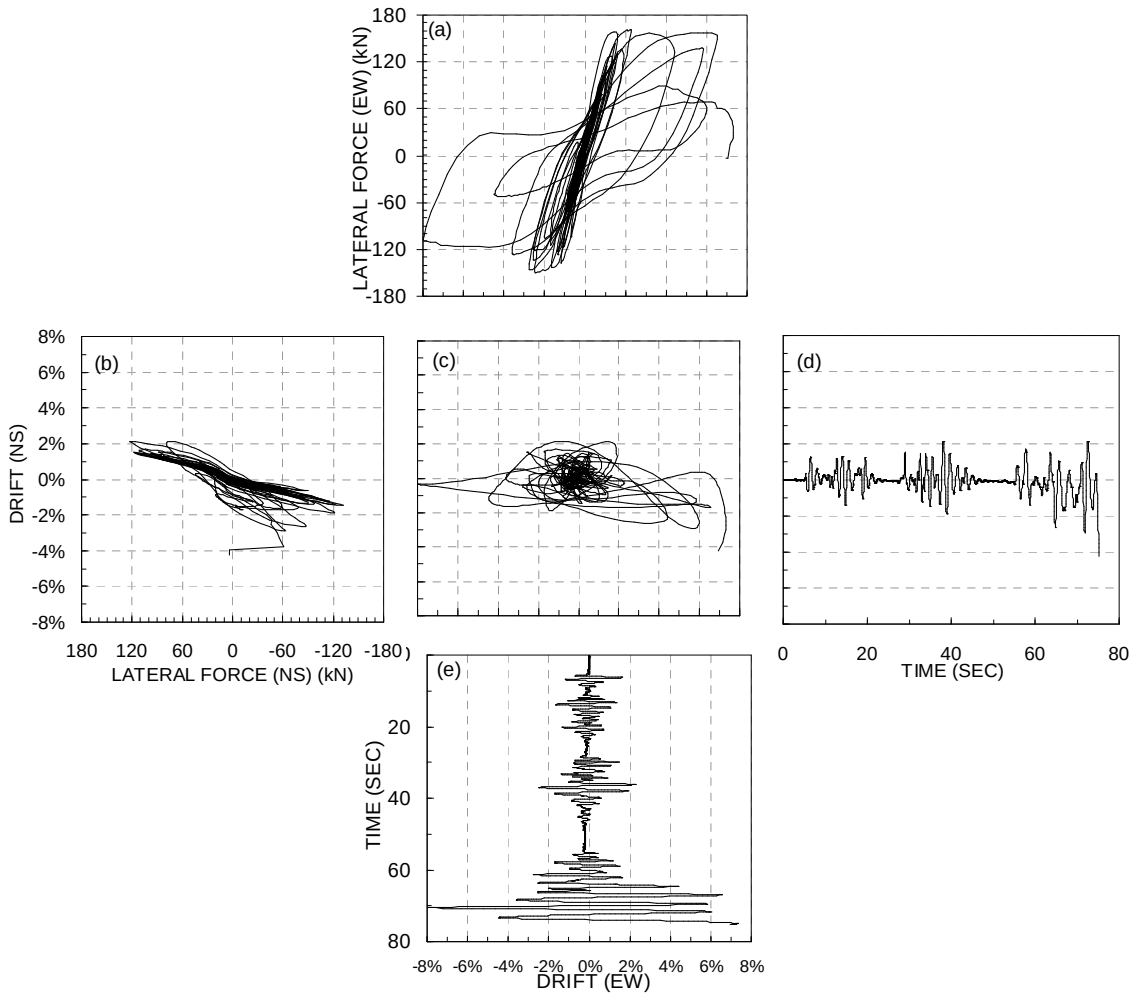

Figure 3-11: Test results of the ductile pier, subjected to EQ1, EQ2, and EQ3 (Mashiko, 2006): force-displacement curves for (a) EW and (b) NS direction; (c) plan view of drift; (d) NS and (e) EW displacement-time plots.

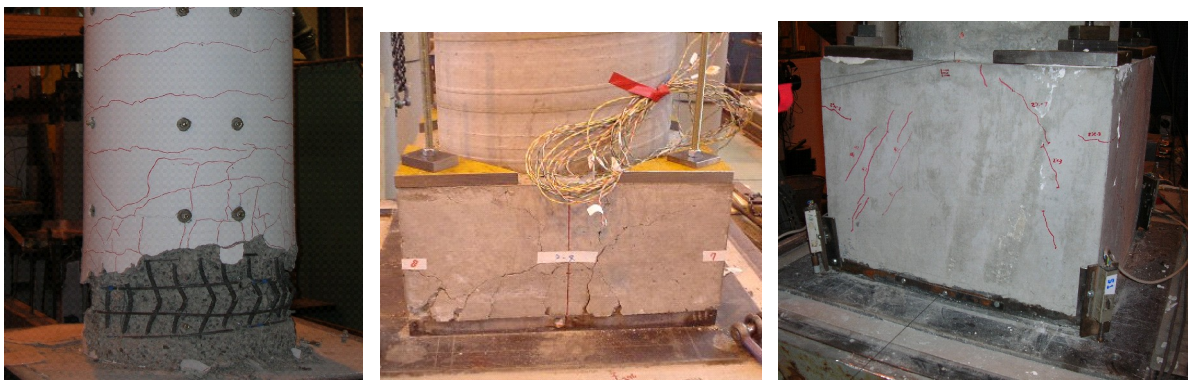

(a) (b) (c)

Figure 3-12: Comparison of damage between: (a) the NZ ductile monolithic pier; (b) the phase I DAD pier (Mashiko, 2006); (c) the phase II strengthened DAD pier

3.5. FINANCIAL RISK ANALYSIS

In an effort to further investigate the advantages of DAD, a loss study was performed using the theory introduced in Chapter 2. The Rapid IDA-EAL and Computational IDA-EAL method were employed to investigate the financial risk of the ductile New Zealand pier and the DAD pier.

3.5.1. Damage states and loss ratios adopted for the DAD pier

Damage states were selected based on the findings of the experimental investigation given in Section 3.3. Similar to the case study given in Chapter 2, the damage states are based off *Hazus* recommendations defining damage in terms of expected downtime. These limits are exactly the same for the ductile New Zealand pier. For the DAD pier the limits are modified slightly and defined as follows. Four basic stages of damage to the DAD pier were observed from testing. Firstly, with the onset of gap-opening, the energy dissipation devices yielded. Once yielded, these devices would need to be replaced or re-tightened. This could be categorized as slight damage (DS2). Since the devices were found to yield at approximately 1 percent drift, the boundary between DS1 and DS2 was taken as 1 percent. Secondly, minor cracking and crushing was found at the shoe block corners. If the cracking and crushing is significant, aesthetic repairs may be required. Thirdly, although simulated during testing, at a large drift the unbonded post-tensioning would yield. This would require further repairs to re-tension the tendons. Since both the damage to the concrete and the tendons is more significant, it can be classified as DS3. Combining these two forms of damage, a limiting drift of 3 percent was conservatively taken to represent the onset of these two forms of damage. The final form of damage results from complete collapse; this equates to DS5. Based on expected P-Δ effects, onset of DS5 was calculated to be 10 percent drift.

The loss ratios adopted for the monolithic piers in Chapter 2 were based on historical data given in *Hazus* (Mander and Bazos, 1999). This was not an option for the DAD pier

since no such data exists. Therefore, the loss ratios adopted for the DAD pier are based on engineering judgement. For DS2, a loss ratio of 0.5 percent was adopted. It is expected the energy dissipation devices would be relatively simple to repair. A crew would have to either re-tighten the devices or replace them. The devices would be relatively easy to access. Therefore, for a $3 Million bridge, $15,000 dollars would be necessary to repair or replace the devices. For DS3, a loss ratio of 5 percent was adopted. Damage to the concrete and tendons would require more substantial repairs, though still less than the cost of a monolithic bridge at the same damage state. Therefore, for a $3 Million bridge, around $150,000 dollars of repairs would be necessary. The loss ratios for the ductile New Zealand pier were kept the same as adopted in the previous study given in Chapter 2. These are given, along with the DAD pier's damage states and loss ratios, in Table 3-4.

3.5.2. Analysis procedures

The analysis procedures adopted for this study are essentially the same as adopted in Chapter 2. However, there are a few minor differences. In Chapter 2, *peak ground acceleration* (PGA) was used as the *intensity measure* (IM) because it was found to be most easily comparable between the three piers and their respective building codes. This study will adopt the spectral acceleration at a 1s period ($S_{a\ (T=1)}$) since both piers are governed by the same design code and have roughly the same fundamental period. By changing the IM used in analysis, the lognormal variation of data from demand will inevitably be affected. Therefore, it was necessary to evaluate a different β_{DBE} based on $S_{a\ (T=1)}$. As expected, using $S_{a\ (T=1)}$ as the IM resulted in a reduction of β_c overall and thus β_{DBE} was taken as 0.2 based on the variation of EDP given IM = 0.4g for the ductile pier.

Table 3-4: Summary of the Rapid IDA-EAL method with adopted damage state limits and loss ratios.

Damage State	θ (EDP) *User Defined*	IM *f(θ)*	f_a *f(IM)*	LR *User Defined*	ΔLR $LR_i - LR_{i-1}$	$\hat{x}$ $f(LR, f_a)$	EAL $/million $f(\hat{x}, \beta)$
Ductile Monolithic Pier							
DS1				0			
	0.64%	0.205581	0.015538		0.03	0.000466153	0.000653078
DS2				0.03			
	2.30%	0.670446	0.000446		0.05	2.23198E-05	4.78614E-05
DS3				0.08			
	4.40%	0.946587	0.000158		0.17	2.69359E-05	6.54295E-05
DS4				0.25			
	5.64%	1.068667	0.000110		0.75	8.25541E-05	0.00021181
DS5				1			
						Total EAL =	**$980**
DAD Pier							
DS1				0			
	1.0%	0.296774	0.005159		0.005	2.57969E-05	2.7478E-05
DS2				.005			
	3.0%	0.580728	0.000687		0.045	3.09239E-05	4.4734E-05
DS3				0.05			
	10.0%	1.162522	8.55E-05		0.950	8.1211E-05	1.7284E-04
DS5				1			
						Total EAL =	**$245**

As discussed in Section 3.4, the DAD pier specimen was considerably weaker than the New Zealand ductile pier. For comparison purposes, the DAD pier's strength was scaled to the same limit as the ductile pier so that a more realistic comparison could be made. The resulting pushover curves for the two piers are given in Figure 3-13(a).

To perform IDA, a non-linear structural model was developed. The pier was idealized as a single-degree-of-freedom system; i.e. a lumped mass centreline column with rotational springs at its base. The DAD pier was modelled using two springs, one representing the bi-linear elastic behaviour inherent in post-tensioned rocking systems and the other elasto-plastic spring representing energy dissipation. The hysteresis properties of the springs were calibrated based on experimental results given in Section 3.3. Ruaumoko2D (Carr, 2006), an inelastic dynamic time-history analysis program, was used to conduct the analysis. The Rayleigh elastic damping was taken as 5 percent of critical damping. Soil-structure interaction was not considered.

3.5.3. Analysis results

Results for the Rapid IDA-EAL method and the Computational IDA-EAL method are presented in Figure 3-13 and Figure 3-14, respectively. Figure 3-13(a), (b), (c), and (d) shows the pushover curve, median rapid IDA curve, hazard-survival curves, and total loss curves, respectively. The EAL, representing the area underneath the total loss curve, is given above Figure 3-13(d). This was calculated to be \$980 and \$245 per \$1million of asset value for the ductile New Zealand pier and the DAD pier, respectively. The step-by-step calculations for the Rapid IDA-EAL method are given in Table 3-4.

Figure 3-14(a), (b), (c), and (d) gives the raw IDA data, the spectral reordered data accounting for other sources of variation, hazard survival curves, and total loss curves, respectively. Based on the methodology given in Chapter 2, the EAL for the ductile New

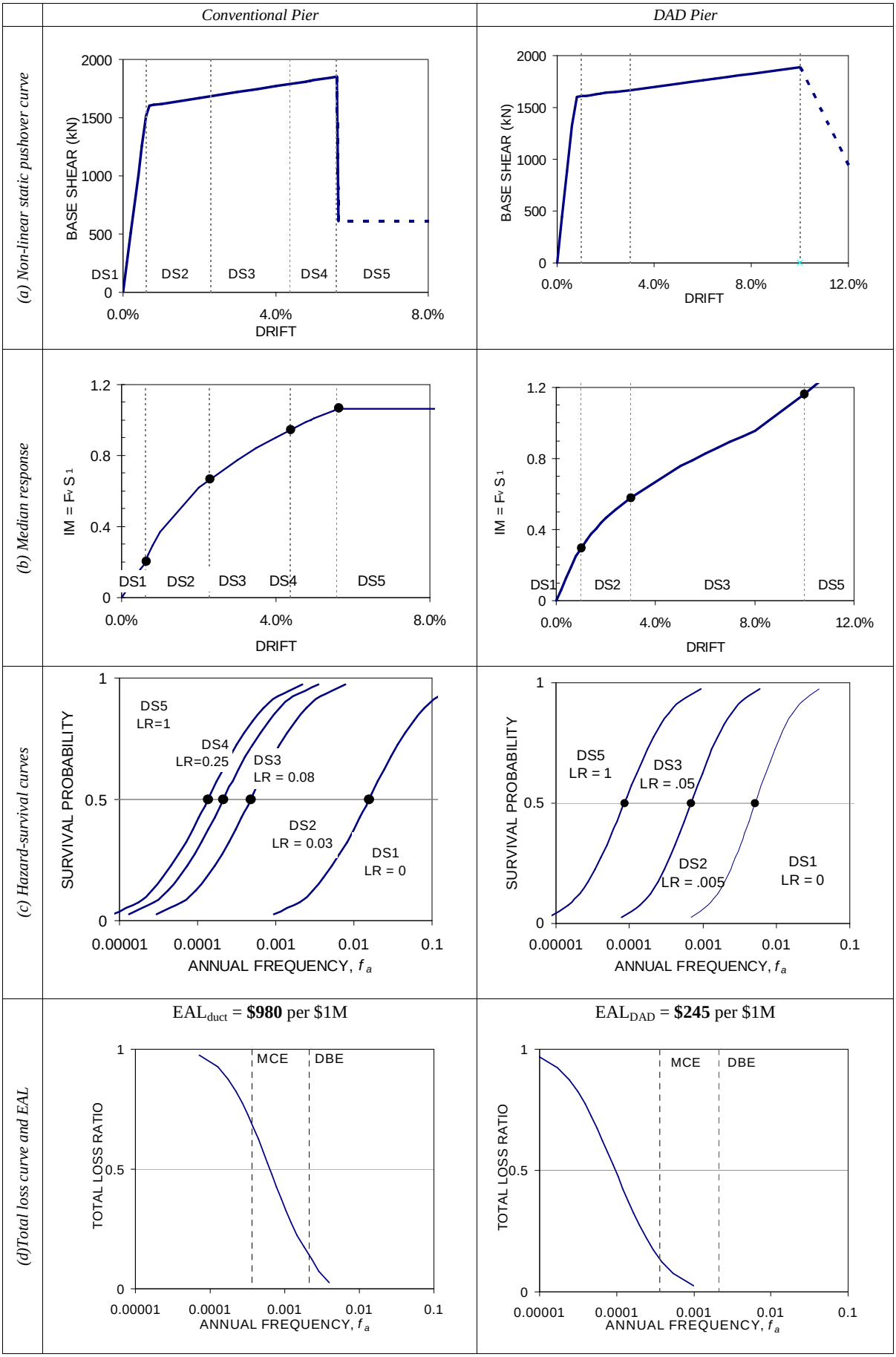

Figure 3-13: Rapid IDA-EAL case study of two RC bridge pier design alternatives.

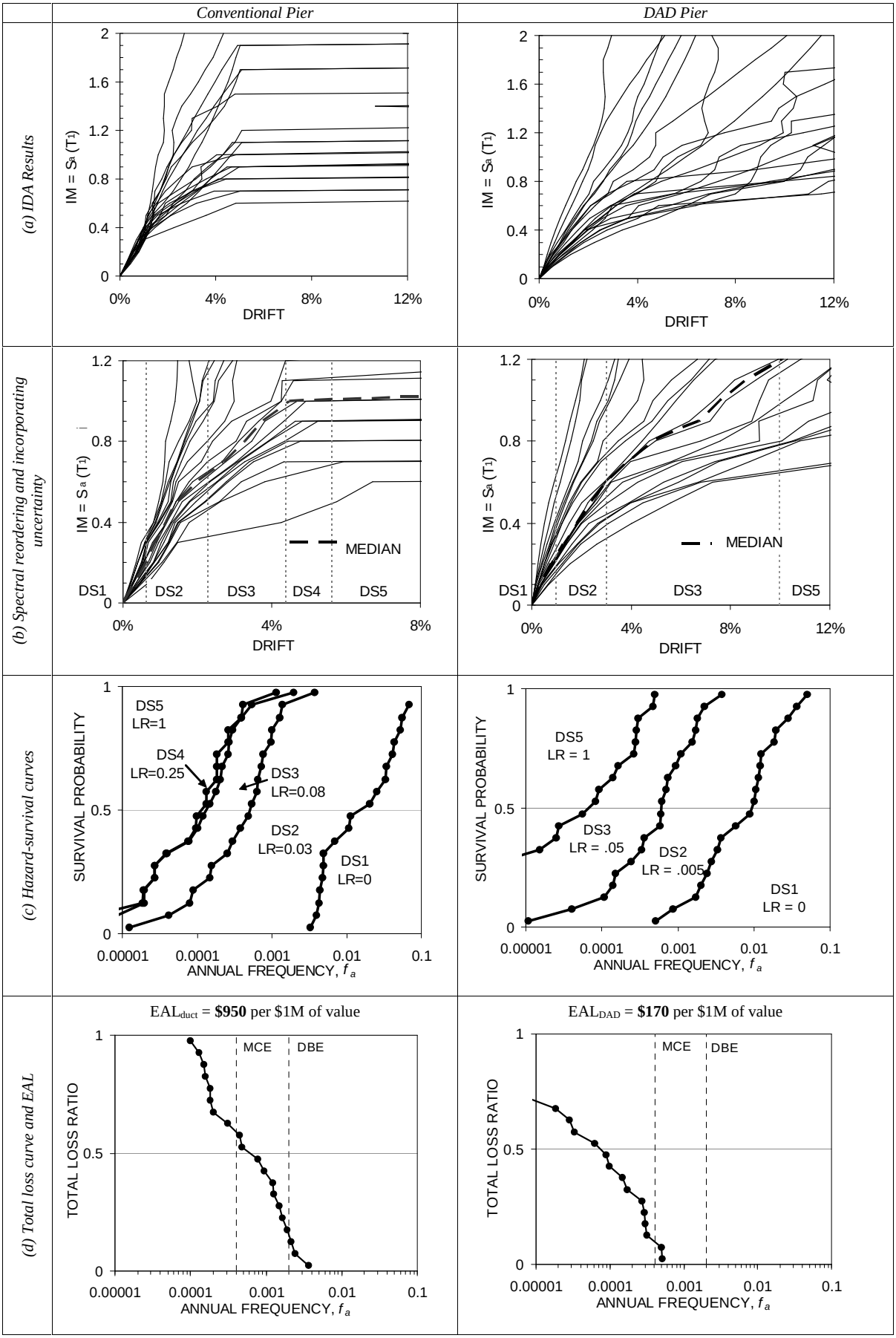

Figure 3-14: Results from computational IDA-EAL analysis

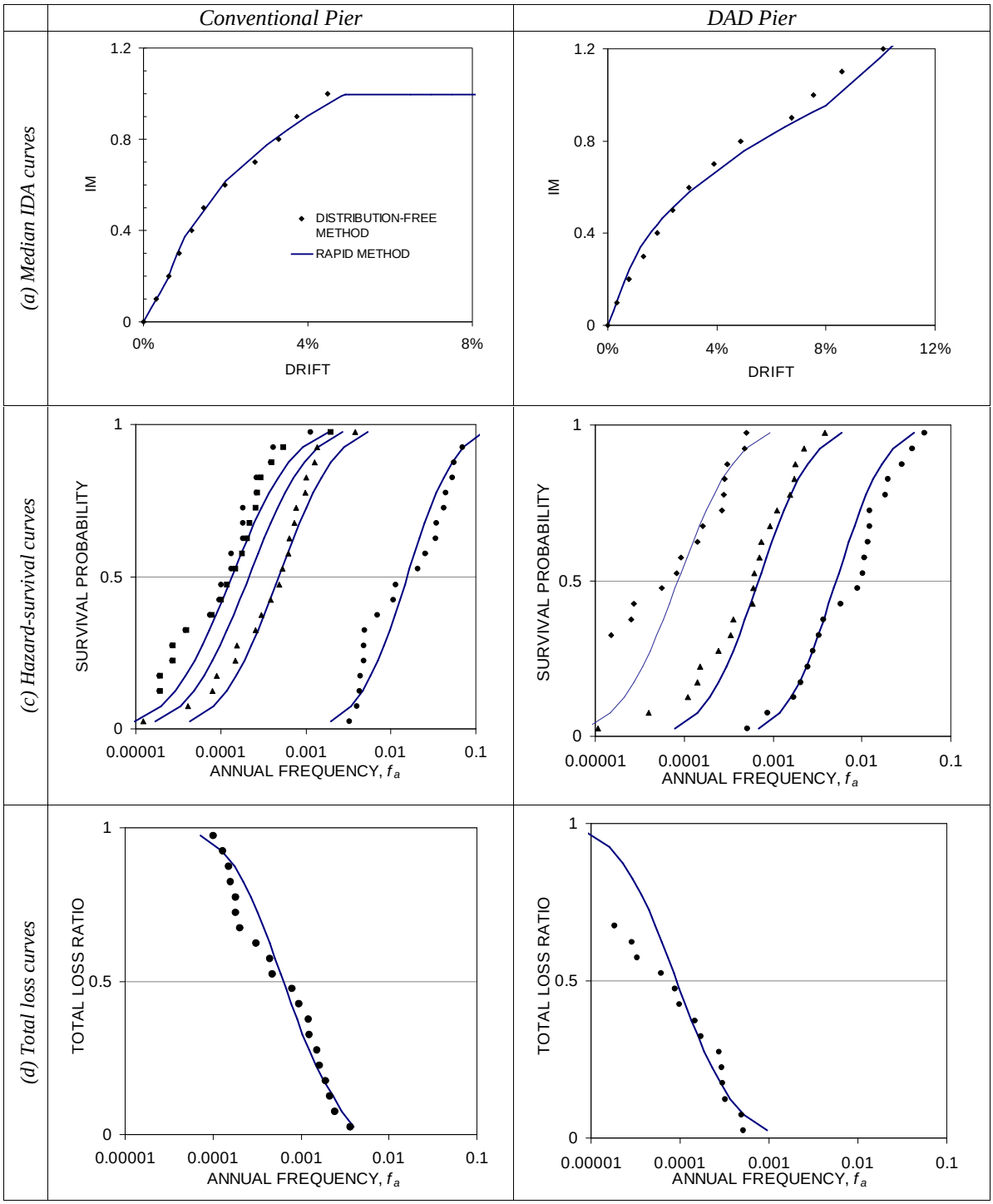

Figure 3-15: Comparison of Rapid IDA-EAL (solid lines) and the distribution-free method (symbols).

Zealand pier and the DAD pier was calculated to be $990 and $170 per $1million of asset value, respectively.

A visual comparison of the data from both methods is given in Figure 3-15. Results show reasonable correlation between the two methods. As found from the 3 bridge pier study conducted in Chapter 2, the Rapid IDA-EAL method over predicted EAL. This was on the order of 45 percent for the DAD pier and 3 percent for the ductile New Zealand pier. The large over prediction of the DAD pier can be partially attributed to the over prediction of EDP (drift) at IM's larger than about 0.5g. The relatively low loss ratios associated with DS2 and DS3 for this pier meant that EAL was governed by the ultimate condition where this over prediction was magnified.

3.6. DISCUSSION

3.6.1. Physical Testing

Results from physical testing confirmed the bi-linear elastic hysteresis behaviour of a rocking bridge pier. Throughout testing, there was no indication of stiffness degradation from multiple loading cycles. When the specimen was displaced in both directions to a drift of 2 percent, it was apparent the specimen had lost about 10-15 percent of its strength. When the specimen was displaced in one direction only its strength returned to the initial level. Therefore, the effect of bi-directional loading did lead to a slight loss in strength, but still retained its stiffness. Additionally, no residual displacement was observed.

As apparent from Figure 3-10, some hysteretic energy dissipation was observed when dissipaters were not installed. This was likely to be caused by friction within the testing apparatus, particularly at the ball joints. Damage to the pier was minor to a drift of approximately 5.5 percent. Toppling was assumed to occur when testing was terminated during EQ3 (90% MCE) due to safety considerations.

Special attention was given to the resistance of large concentrated compressive forces resulting from bi-directional rocking at an extreme corner of the steel-steel interface. Even at high drifts, only minor damage was observed in the form of superficial crushing and hairline cracks. This can be attributed to the diagonal reinforcing bars which transferred the strut forces into the pier and the steel fibres which impeded crack propagation. The energy dissipation devices did not significantly contribute to the pier's performance. Further development of these devices is needed to provide more efficient, reliable energy dissipation on both uplift and re-centring.

Based on the probabilistic nature of the earthquake selection process, it is possible to state the likely outcomes of damage to the bridge pier in a *performance-based earthquake engineering* (PBEE) context. For example, it can be stated that one can be 90 percent confident the DAD pier will survive an earthquake that has a 10 percent chance of occurrence in 50 years (DBE) with no damage to the structure, and minor damage to the dissipation devices. For an earthquake that has a 2 percent chance of occurrence in 50 years (MCE), one can be 50 percent confident that the structure will only sustain minor damage, yet it cannot be said that the structure will survive this level of earthquake with some 90 percent confidence. However, it should be noted that this could easily be mitigated by adopting a larger column in the original design and providing a higher overturning resistance. The decease in damage between the ductile monolithic pier, the Mashiko (2006) DAD pier, and the strengthened DAD pier presented in this section is illustrated in the photographs of Figure 3-12.

There are several obvious benefits of DAD apparent from this study: (i) a lack of damage can potentially lead to lower operating and repair costs; (ii) negligible residual displacement will ensure serviceability following a seismic event; (c) precast construction can be utilized to increase reliability and reduce initial (construction) costs. Related studies into these advantages and their expected financial benefits will be the topic of the next chapter.

3.6.2. Financial Risk Analysis

The resulting EAL for the ductile and DAD piers were of stark contrast, even though both piers had a similar design basis. The ductile pier's vulnerability was dominated by minor damage occurring at relatively low drifts and moderate ground shaking levels. The DAD pier was dominated by the ultimate failure condition, resulting in an annual risk of about 20 percent of that of the ductile New Zealand pier. Findings from this study suggest that current design practice, although adequate in protecting loss to life and limb, is deficient in protecting the structure from minor yet costly damage arising from medium frequency events. Ductile jointed precast structures employing DAD may offer some improvement for this type of loss.

Not considered in this study is the significant additional risk associated with non-structural damage, downtime, and loss of life. Bridges are especially vital for the flow of goods and people; closure of key transportation arteries can have severe economic consequences. Bridges designed according to DAD will incur little to no residual displacement, allowing full operation even after large earthquakes. Non-structural damage will need to be considered in buildings, where it is likely to contribute significantly to global financial loss. Studies in these areas are in their infancy, and further work regarding such risk is necessary to fully address the viability of ductile jointed precast conrete system, and more specifically DAD.

3.7. CONCLUSIONS

This research has further investigated the application of DAD to bridge piers. A 40m span prototype bridge was designed using discontinuous longitudinal reinforcement at the column-foundation interface to allow rocking at a specially detailed armoured column-foundation joint. Lateral forces were resisted by gravity load, post-tensioned tendons (simulated during testing) and supplemental energy dissipation devices. A 30 percent scaled

model was constructed and tested with PD bi-directional lateral forces and axial load. A financial risk analysis was conducted using two different methods. Based on this experimental and analytical investigation, the following conclusions can be drawn:

1. By providing ductile jointed bridge piers detailed according to DAD principles with similar strength to the conventional piers, it can be stated that owners can have some 90 percent confidence that such DAD piers will not sustain damage from a design basis earthquake. For a maximum considered earthquake, the structure may have minor damage and there would be at least 50 percent confidence the pier would not collapse.
2. Concentrated axial load was resisted by a combination of reinforcing steel and high strength fibre-reinforced concrete. Minor damage was observed under bi-directional loading up to 5.5 percent drift. This was in the form of yielding of the dissipation devices, hairline cracking, and slight spalling in the corners of the rocking interface.
3. The energy dissipation devices utilized in this study provided additional lateral resistance of approximately 5 percent. These or similar devices are recommended, though more efficient designs may increase their contribution to lateral resistance and dissipation of earthquake energy.
4. No stiffness degradation or residual displacement was observed. This was shown to be due to the rocking mechanism which resulted in bi-linear elastic hysteretic behaviour of the pier. Minor strength loss was observed due to bi-directional loading. No strength degradation was observed.
5. Bridge properly detailed according to DAD is more likely to remain operational following an earthquake than a conventional monolithic bridge.

6. A financial risk study was conducted comparing the EAL of a conventional ductile pier to a pier designed for damage avoidance. EAL was calculated using the Computational IDA-EAL method and the Rapid IDA-EAL method. Results indicate the DAD pier's EAL is only 20 percent of the ductile pier.

REFERENCES

Aslam M, Goddon WG, and Scalise DT. 1980. "Earthquake Rocking Response of Rigid Blocks." *Journal of Structural Engineering, ASCE*, **106**(2), 377-392.

Carr AJ. 2006. RUAUMOKO: Inelastic Dynamic Computer Program. Computer Program Library, Department of Civil Engineering, University of Canterbury, Christchurch, New Zealand.

Dhakal RP, Mander JB, and Mashiko N. 2006. "Identification of critical ground motions for seismic performance assessment of structures." *Earthquake Engineering and Structural Dynamics*, in press.

Housner GW. 1963. The Behavior of Inverted Pendulum Structure During Earthquake. *Bulletin of the Seismological Society of America*, **53**(2):403-417.

Meek JW. 1978. Dynamic Response of Tipping Core Buildings. *Earthquake Engineering & Structural Dynamics*, **6**(5):437-454.

Mander JB. 2000. Damage Avoidance Seismic Design of Bridge Piers. *New Zealand Concrete Society Conference*, Wairakei NZ, 13-15 October, NZCS Technical Report TR 23, pp 42- 49.

Mander JB. 2004. Beyond Ductility: The Quest Goes On. *Bulletin of the New Zealand Society of Earthquake Engineering*, **37**(1):35-44.

Mander JB. and Basoz N. 1999. Seismic fragility curve theory for highway bridges in transportation lifeline loss estimation. *Optimizing Post-Earthquake Lifeline System Reliability*, TCLEE Monograph No. 16. American Society of Civil Engineers: Reston, VA, U.S.A.; 31–40.

Mander, J.B., and Cheng, C.T. 1997. "Seismic Resistance of Bridge Piers Based on Damage Avoidance Design." *Technical Report NCEER-97-0014* (National Center for Earthquake Engineering Research), State University of New York, Buffalo, December 10.

Mander JB, Dhakal RP, and Mashiko N. 2006. Incremental dynamic analysis applied to seismic risk assessment of bridges. *8NCEE*, San Francisco, April 17-21. paper 770.

Mashiko N. 2006. Comparative performance of ductile and damage protected bridge piers subjected to bi-direction earthquake attack. *Master of Engineering Thesis*. University of Canterbury, Christchurch, New Zealand.

NZS:3101-95. 1995. *Concrete Structures Standard: NZS3101*, Standards New Zealand, Wellington, New Zealand

NZS:NZS:1170.5-05. 2005. *Loading Standard*, Standards New Zealand, Wellington, New Zealand

Palermo A., Pampanin S, Calvi GM., 2005. Concept and development of hybrid solutions for seismic resistant bridge systems. *Journal of Earthquake Engineering*, **9**(6):899-921.

Priestley MJN, Sritharan S, Conley JR, Pampanin S. 1999. Preliminary Results and Conclusions from the PRESSS Five-Story Precast Concrete Test Building. *PCI Journal*, **44**(6):42-67

Shing PB, Nakashima M, Bursi OS. 1996. Application of dynamic test method to structural research. *Earthquake Spectra*, **12**(1):29-54

Skinner RI, Robinson WH, and McVerry GH. 1993. *An Introduction to Seismic Isolation.* John Wiley & Sons, Inc., New York, NY.

Vamvatsikos D. and Cornell CA. 2004. Applied Incremental Dynamic Analysis. *Earthquake Spectra*, **38**(2):523-553.

4 Performance of damage protected beam-column joints subjected to bi-directional lateral loading

SUMMARY

An experimental and computational study of an 80 percent scale precast concrete 3D beam-column joint sub-assembly designed with damage protected rocking connections is presented. A prestress system is implemented whereby high-alloy high-strength unbonded thread-bars running through the beams are coupled to rods within the columns. The thread-bars are post-tensioned and supplemental energy dissipation devices are also installed. Both wet and dry joint solutions are considered. A *Multi-level Seismic Performance Assessment* (MSPA) is conducted considering three performance objectives related to occupancy and collapse prevention. First, bi-directional quasi-static cyclic tests are conducted and the specimen's performance is characterised. This data is then used in a 3D nonlinear *Incremental Dynamic Analysis* (IDA). Results from the IDA are used to select three critical earthquakes for further experimental bi-directional testing. Thus quasi-earthquake displacement tests are performed. Results indicate the system satisfies all performance objectives related to serviceability and life-safety. Further design improvements are discussed.

4.1. INTRODUCTION

Current seismic design accepts that damage will occur in moderate to large seismic events, although attempts are made via special detailing to limit this damage to specific plastic hinge zones. These zones, designed to sustain severe damage under multiple cyclic rotations, tend to act like a fuse, essentially protecting the structure from forming unfavourable mechanisms. Although this design philosophy ensures good protection to occupants by preventing collapse, there is a strong likelihood a moderate to large earthquake will render a structure irreparable. As a result, economic costs, both direct and indirect, can be significant; this has been confirmed from recent earthquakes in the United States (Northridge, 1994) and Japan (Kobe, 1995). To address this issue, alternative structural systems have been proposed where precast concrete elements are designed to remain essentially elastic, with inelastic behaviour accommodated for by rocking at specially detailed joints.

The theoretical basis of rocking systems have been investigated by many early researchers (e.g. Housner, 1963; Aslam *et al.*, 1980). Although it was not until more recently (Stone *et al.*, 1995) that so called "hybrid" systems were introduced. These systems utilize full or partially unbonded post-tensioned prestress to provide a restoring force and supplemental yielding devices to provide energy dissipation. By combining the hysteretic behaviour of these two components, it is possible for a joint to exhibit a combination of bi-linear elastic (post-tensioning) and elasto-plastic (yielding devices) hysteresis behaviour. The result is a flag shaped hysteresis loop, displaying good energy dissipation and re-centring characteristics.

As part of a large research project in the United States, the PRESSS program investigated the behaviour of these systems through testing of many sub-assemblages (Stone *et al.*, 1995) and a five-storey 3D frame and wall system (Priestley *et al.*, 1999). The system performed well with much less damage than would be expected with monolithic construction.

Little residual displacement was observed in both frames and walls. The joints, however, employed a concrete-concrete or high-strength grout interface, resulting in some damage at the joint region.

Mander and Cheng (1997) proposed an alternative seismic design and construction philosophy for bridges called *Damage Avoidance Design* (DAD). In this approach, joints are armoured with steel to protect them from damage incurred from rocking. This concept was validated by uni-directional tests performed on a scaled bridge pier. Results indicate little damage at the joint and good bi-linear elastic behaviour.

These concepts have been further developed in New Zealand and design guidelines for such ductile jointed precast concrete systems have been introduced into the concrete code as an appendix (NZS:3101, 2006). As part of an ongoing research program at the University of Canterbury, further experimental investigations have been conducted (Arnold, 2004; Davies, 2003; Li, 2006; Amaris *et al.*, 2006) with the goal of refining detailing at the joint and providing cost-effective alternative solutions. As a follow up to this previous work, this study presents results from a combined experimental and computational investigation on the bi-directional behaviour of DAD beam-column joints.

Two research objectives will be addressed herein. Firstly, previous research adopted quasi-static testing, in which loading was composed of regulated displacement cycles. These cycles however, are not completely representative of the displacement demands due to seismic excitation. Therefore, this study will adopt the *Quasi-Earthquake Displacement* (QED) test method (Dutta *et al.*, 1999), where the specimen will be subjected to displacement profiles found analytically using real ground motion records. Using this approach, a *Multi-level Seismic Performance Assessment* (MSPA) (Dhakal *et al.*, 2006) will be conducted, characterizing the performance of the specimen at multiple levels of seismic demand.

Secondly, further refinement of the beam-column joint details are needed to ensure a practical, cost-effective solution. Li (2006) investigated the behaviour of a beam-column joint using a bent coupler system whereby high-strength thead-bars in a beam are coupled to diagonal rods running through the column. The aim of such a system is to allow for rapid on-site erection, thereby reducing initial costs. From physical testing, it was found that its performance was satisfactory, however several design improvements relating to the coupler system and the armoured ends were suggested. This study implements these design improvements and ensures the provided detailing satisfies performance objectives relating to immediate occupancy and collapse prevention.

4.2. EXPERIMENTAL INVESTIGATION

4.2.1. Prototype structure

As shown in Figure 4-1, the prototype is a ten-storey reinforced concrete frame building with three 10m bays in each direction This generic structure, commonly known as the "red book" building (Bull and Brunsdon, 1998), was designed according to the New Zealand concrete standard (NZS:3101, 2006) for intermediate soil in Christchurch, New Zealand. Keeping all other variables constant, the same structure was designed and detailed according to damage avoidance principles, thereby resulting in precast beams and columns being connected via a post-tensioning system with other devices to provide supplemental energy dissipation. The DAD building was designed with precast flooring units running in the transverse direction and seated on the transverse beams, leaving the longitudinal beams to resist predominately seismic forces.

To help ensure rocking systems are adopted by the construction industry, the system must be relatively simple to erect. A major component of this is the post-tensioned prestress system. This study investigates the use of high strength thread-bars in beams coupled to fuse bolt-bars that pass through the joint.. In this design, it is possible for complete beam and

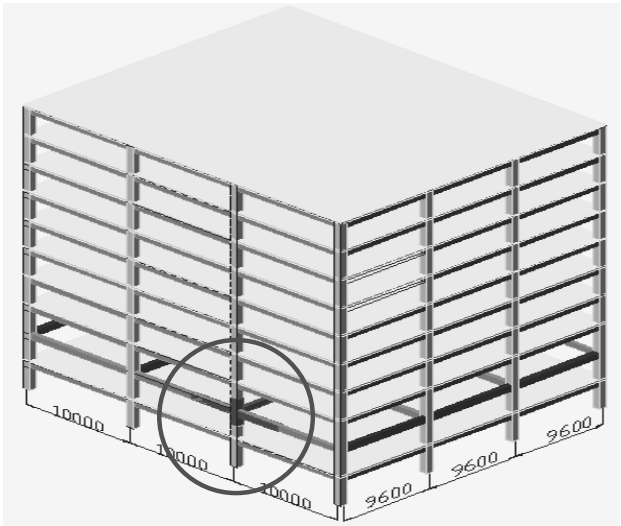

Figure 4-1: The prototype structure, showing the location of the subassembly (Li, 2006).

column sections to be cast off-site with rods already in place within the respective elements. Once on-site, the beam's thread-bars are connected via the coupler system to a short fuse-rod in the column and anchored to the column's opposite face. A detailed explanation of this, and other design elements follows.

4.2.2. Specimen sub-assemblage

An exterior joint on the second floor of the prototype structure was taken for the 3D beam-column subassembly. The joints were designed for a standard moment capacity of 500 kN-m. Using constant stress and strain similitude principles, the specimen was scaled to 80 percent of full size, and consisted of two beams in the longitudinal direction, and one beam in the transverse direction. Herein, the longitudinal and transverse beams are dominated by seismic load and gravity loads (carrying the one-way precast floor panels) and respectively are referred to as the east-west seismic and north-south gravity beams.

Reinforcing details of the column are given in Figure 4-2 and Figure 4-3. An axial load of 2000kN due to gravity loads of the above floors was simulated in the 700x700mm column by prestressed Macalloy^{TM} 32mm diameter high-strength thread-bars. Three 20mm thick mild steel plates were cast at the column faces where precast beams were joined. The minimum reinforcement ratio, ρ = 0.008 was provided using 12 HD20 (f_y = 500MPa) threaded rebars (Reidbars^{TM}). To transfer shear forces through the joint, five double HR12 hoops spaced at 100mm centres were provided. The design compression strength of the column was taken to be f'_c= 45MPa. PVC ducts were placed at a 20 degree angle in each seismic beam and horizontal through the gravity beam for the post-tensioning rods.

Reinforcing details of the seismic beams and gravity beam are given in Figure 4-2 and Figure 4-3, respectively. A cracked elastic design was used to detail longitudinal reinforcement in the precast beam segments. In this design approach, sufficient quantities of mild steel are provided to ensure that yield of longitudinal reinforcing is prevented and

concrete compressive stresses are below $0.7f'_c$. This ensures precast elements remain essentially elastic even when the connection reaches over-strength. Shear design of the precast elements followed the New Zealand concrete code (NZS:3101, 2006), with a total initial axial load of 400kN provided by the post-tensioning rods. Within the mid section of the beams, only minimal transverse steel was used, thus a stirrup spacing of $d/2$ was adopted. A tighter, 100mm spacing was provided at the ends. Additional stirrups near the joint were provided to confine the concrete to withstand large compressive stress expected in the end regions.

All beam specimens were 560mm deep by 400mm wide. The unbonded post-tensioned prestress was provided by two 26.5mm diameter high-strength thread-bars placed in 50mm PVC ducts. The seismic and gravity beams implemented two separate detailing strategies as explained below.

The gravity beam was detailed according to Li (2006). Instead of a straight coupler, a bent coupler was used for one of the rods. This was done to accommodate a draped tendon profile in the beam. As in the seismic beams, the shorter fuse bolt-bar section was machined to 75 percent of its effective area. A 100x100x12 steel angle was used, with the flange flush against the column face. This required the beam's longitudinal steel to be mechanically developed by plug welding it to the back edge of the angle's flange.

A detail of the seismic beam-column joint is given in Figure 4-4. The seismic beams utilized a straight coupler system where the tendons were pre-bent at the joint end to a radius of approximately 1.8m. This allowed proper alignment with the angled rod running through the column. The fuse bolt-bar, was machined to 75 percent of its effective area to ensure any yielding in the prestress system would be limited to the replaceable column bolt-bar. At the beam end, a 100x100x12 inverted steel angle was used at top and bottom of the joint and the face of concrete was recessed 5mm. This ensured that contact with the column was limited to

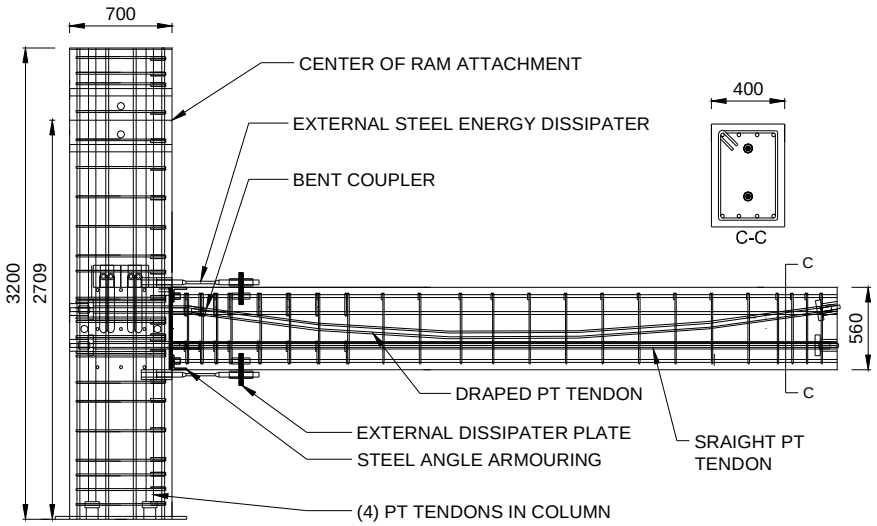

Figure 4-2: Elevation of the gravity beam and column.

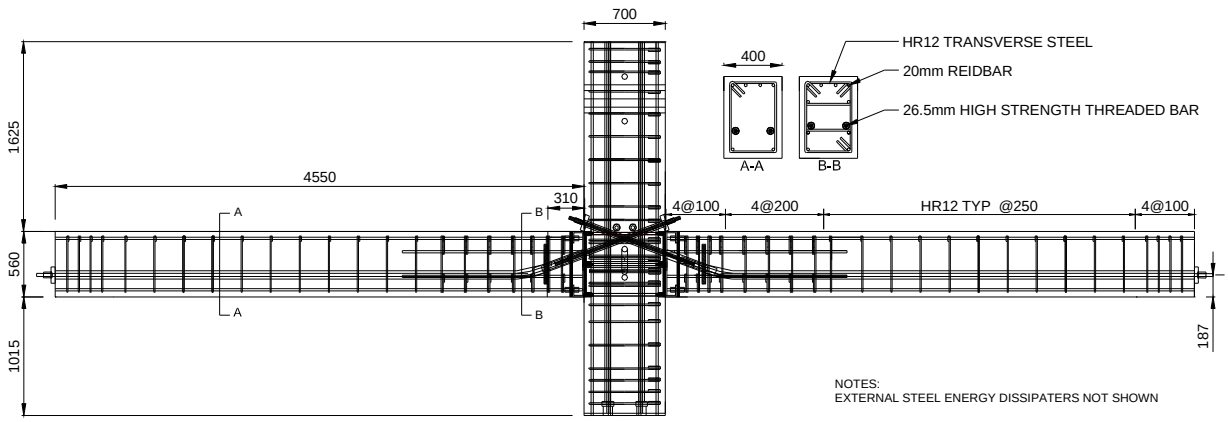

Figure 4-3: Elevation of the seismic beams and column.

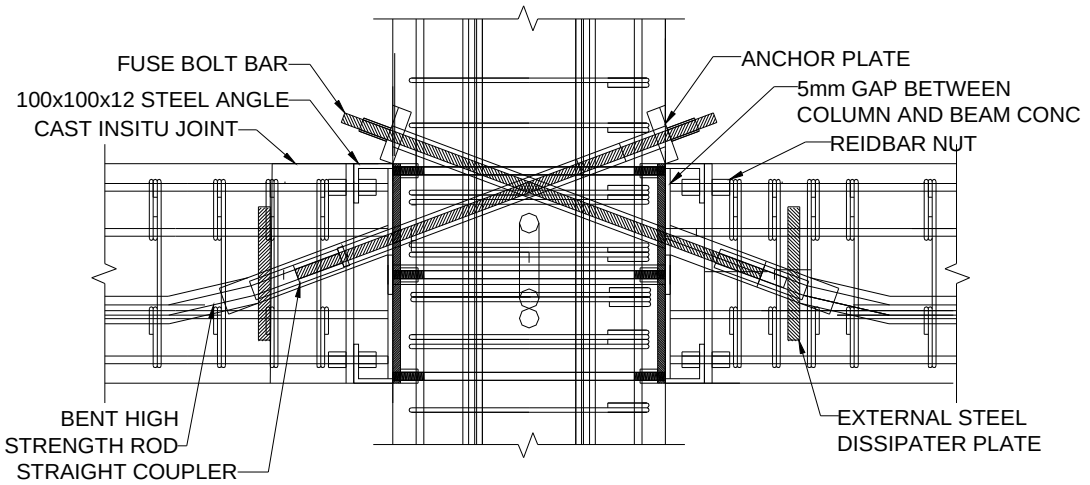

Figure 4-4: Detail of the seismic beam-column joint.

(a) (b)

Figure 4-5: Precast concrete beams showing: (a) the beam cage; and (b) the cast insitu closure pour.

the steel and allowed the angle's buried flange to mechanically develop the beam's longitudinal steel using Reidbar^{TM} nuts. A photograph of the east beam reinforcing cage is given in Figure 4-5(a).

By the nature of precast concrete and rocking connections, it is critical that the face of the beam be aligned flush with the column. Therefore, offsite erection of a full length beam section may lead to on-site misalignment issues which may affect rocking behaviour. To mitigate potential misalignment and to also allow for construction tolerances similar to current standards, a 310mm cast insitu closure pour was provided on the west seismic beam. This closure pour is expected to be cast on-site after the armouring angles have been adjusted to ensure a flush face at both ends and the post tensioning rods are coupled together. High strength, fibre-reinforced concrete was used in the insitu end to compare its behaviour to the regular strength concrete of the east beam. The compressive strength of the high strength concrete was tested and found to be f'_c= 70MPa. The east beam and the remainder of the west beam concrete was found to be f'_c= 37MPa. A photograph of the beam prior to pouring and the cast insitu closure pour is given in Figure 4-5(b).

At each joint, four 30mm diameter shear keys were installed, tapered 5° inward to ensure they do not jam when the specimen rocks. These were designed to be screwed into the face of the column via a cast in double nut. The shear keys were designed for gravity and seismic shear forces, as given in Li (2006). One shear key was located in each corner, providing resistance to torsion.

4.2.3. Supplemental energy dissipation

Supplemental energy dissipation was provided by mild steel bars designed to yield as the specimen rocks at its joints. To facilitate easy replacement, these devices were mounted externally. For the seismic beams, the dissipaters were located at centreline of the beam and anchored to a 32mm thick steel plate set back 300mm from the face of column. The

dissipaters ran through a duct in the column and were bolted at each end of the anchor plate and column face, ensuring the devices worked independently at each joint. For the seismic beam, dissipaters were located at top and bottom of the beam, anchored to the beam by a 32mm plate and screwed into nuts cast in the column. These devices were expected to buckle under significant cyclic loading. Although similar buckling-restrained devices are readily available (grout encased in a jacket would inhibit buckling), the chosen devices were chosen due to their relatively low cost.

To guarantee the prestressing thread-bars are capable of re-centring the system, the energy dissipation devices were designed not to exceed the critical moment capacity of the prestress system only. Note that the post-tensioned thread-bars do not cross the joint at centreline, but rather at the $h/3$ point. This meant the dissipaters had to be designed for the minimum eccentricity of the rods, 1/3 the beam depth. The seismic beam dissipaters were machined to a 15mm diameter over a 150mm length and the gravity beam dissipaters were machined to a 12mm diameter over a 200mm length. The devices were designed to buckle when subject to large inelastic cyclic strain.

4.3. THEORETICAL BEHAVIOUR

Two methods have been introduced for predicting the behaviour of rocking systems. Pampanin *et al*. (2001) proposed using a monolithic beam analogy approach. An iterative process is used to determine the neutral axis depth and strain in the compression concrete. Although it has been demonstrated this method agrees well with experimental results, it was developed for precast members without armouring. If armouring is considered, it is reasonable to assume rigid body behaviour at the joint. As investigated by Mander and Cheng (1997) and Li (2006), the theoretical behaviour of an armoured rocking system can best be determined from coupling elastic deformation with rigid body kinematics. In this method, the post-joint opening neutral axis is assumed to be negligible, thus allowing one to presume the

specimen rocks on an extreme edge. Using this approach, it is possible to calculate the moment capacity and stiffness at several key response milestones, namely initiation of gap-opening, yielding of the steel energy dissipaters and yielding of the prestressed tendons. As introduced in Chapter 1, the moment capacity of the joint is calculated by the summation of the contribution from post-tensioning and dissipation devices:

$$M = \sum M_{PS} + \sum M_{diss} \tag{4-1}$$

given that

$$M_{PS}^{\pm} = P_{PS} e_{PS}\,;\; M_{diss}^{\pm} = P_{diss} e_{diss} \tag{4-2}$$

where e is the vertical distance of the tendon or dissipaters from the rocking edge of the beam section and P is the force in the prestressed tendon or in the dissipater. Since the tendons at the joint were offset from centreline, e_{PS}^{+} = 187mm and e_{PS}^{-} = 373mm. The energy dissipation devices were at centreline, therefore, $e_{diss}^{+} = e_{diss}^{-}$ = 280mm. The force in the tendons can be calculated as:

$$P_{PS} = P_i + \frac{A_{PS} E_{PS}}{L_t} e_{PS} \theta_{con} n \tag{4-3}$$

where P_i = initial post-tensioning force (200kN); E_{PS} = elastic modulus of the tendon (170,000MPa); A_{PS} = cross sectional area of the tendon (552mm^2); L_t = unbonded length of the tendon (5.25m); θ_{con} = connection rotation; and n = number of joint openings spanned by the tendon (taken as 1 in this case for both directions). The force from the steel dissipaters was simply taken as the yield strength of the devices (60kN per device), and for a device on each side the combined total force was 120kN. For simplicity strain hardening of these devices was not considered.

The theoretical moment-rotation response of a typical rocking connection is given in Figure 4-6. The initial clamping force from P_i is used to calculate the moment capacity at gap-opening, M_{pt}, using Equation (4-2). This is illustrated by the thin dashed line in the figure. When the dissipation devices are considered, their contribution should be included in the calculation as shown in Figure 4-6. The yield elongation of the dissipation devices can be

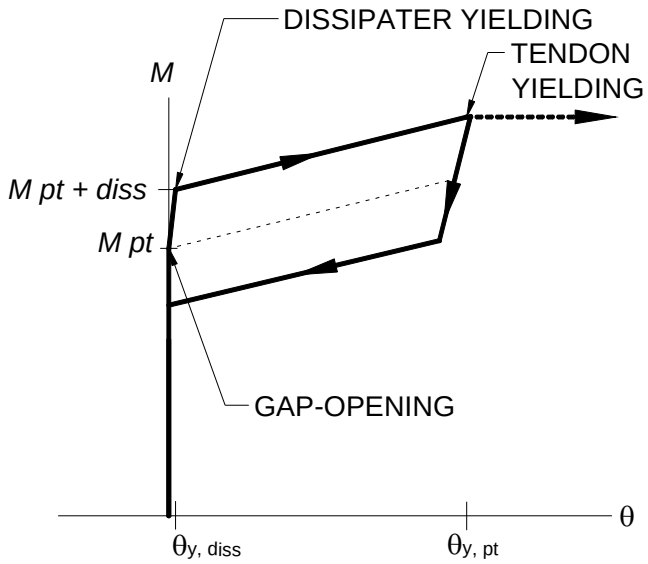

Figure 4-6: Theoretical moment-rotation reponse of the rocking connection.

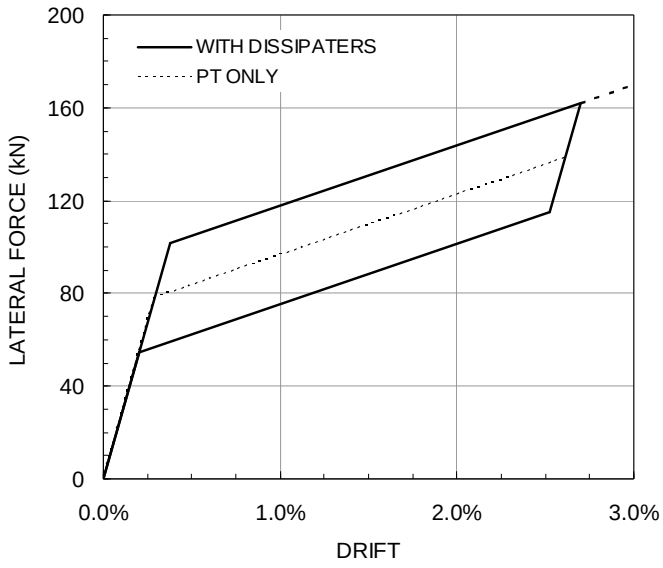

Figure 4-7: Theoretical force-displacement response of the subassembly in the EW direction.

shown to be very small. In this case, the length of the devices in the EW direction is 150mm. Given a yield strain of 0.0015, this equates to a rotation of 0.0008 for the beam depth and eccentricity provided in the specimen. This rotation is small enough to be neglected and the devices can be assumed to yield upon gap-opening. Upon unloading, the dampers will be forced into compression. The unloading moment capacity can now be calculated by taking the negative moment contribution of the dissipation devices, as shown by the unloading line of Figure 4-6. Finally, the rotation at which the thread-bars yield is found by back calculating given the yield strain of the thread-bars using Equation (4-3).

The moment capacity of the joint can be related to the lateral force, V_{col}, by:

$$V_{col} = 2M \frac{L}{L_b L_c} \tag{4-4}$$

where L = centreline length of the beam (9.8m); L_b = clear support length of the beam (9.1m); and L_c = storey height (2.8m).

The total top displacement of the system given V_{col} can be attributed to localised rotation at the joint and the total elastic deformation of the system:

$$\Delta = \Delta_{elastic} + \theta_j \frac{L_b}{L} L_c \tag{4-5}$$

where θ_j = joint rotation angle, and $\Delta_{elastic}$ is the elastic deformation of the system from flexure, which is limited to by the maximum lateral force at uplift. This is defined using the moment area theorem given in Chapter 1 by:

$$\Delta_{elastic} = \frac{V_{col,uplift}}{12}\left[\frac{(L_c - D)^3}{EI^*_{col}} + \frac{{L_c}^2 {L_b}^3}{L^2 EI^*_{bm}}\right] \tag{4-6}$$

where EI^*_{bm} and EI^*_{col} are the effective stiffness of the beam and column, respectively, and D is the depth of the beams (560mm). An effectives stiffness of $0.25I_{gross}$ was used for the beam, as recommended by Li (2006). Based on these equations, the theoretical pushover curve for the subassembly in the EW direction is given in Figure 4-7 up to a joint rotation of

0.02 radians. The thin dashed line indicates the theoretical force-displacement response from prestress alone.

4.4. TEST SETUP AND METHODS

Figure 4-8 gives a plan view of the test setup and Figure 4-9 presents two elevations. Loads were applied to the specimen by three hydraulic actuators. Actuators A and B were installed to the reaction frame and top of the east and south face of the column, respectively. Actuator C was installed in the east-west direction at the end of the gravity beam. This actuator was intended to keep the specimen movement in-plane during uni-directional testing and provide a measure of torsion in the specimen. Actuator C's movement was synchronised to approximately one half the displacement of Actuator A. A constant 120kN load was applied at midsection of the gravity beam through a 300kN hydraulic jack, simulating the weight of the precast flooring panels. The load was spread over a 1.5m timber block and developed into the strong floor through four high strength threaded rods. Load cells were installed in series with each actuator. Additional load cells were attached at the strut of each beam and the jacking point of each post-tensioned rod. A photograph of the specimen in the testing apparatus is given in Figure 4-10.

To measure rotation at the joint, 3 linear potentiometers were installed on both faces of each joint, totalling 18 devices. Two additional linear potentiometers were installed against the bottom face of each beam to measure vertical movement. At several locations around the specimen (see Figure 4-9) rotary potentiometers were installed to measure local displacement. Two 5mm strain gauges were installed on each bolt bar to measure any potential yielding that may occur during testing.

Due to the unique nature of a structural system designed to avoid damage, it was possible to conduct a wide range of tests on the specimen. These included uni-directional and bi-directional quasi-static tests, where the structure was deformed to controlled cyclic loading

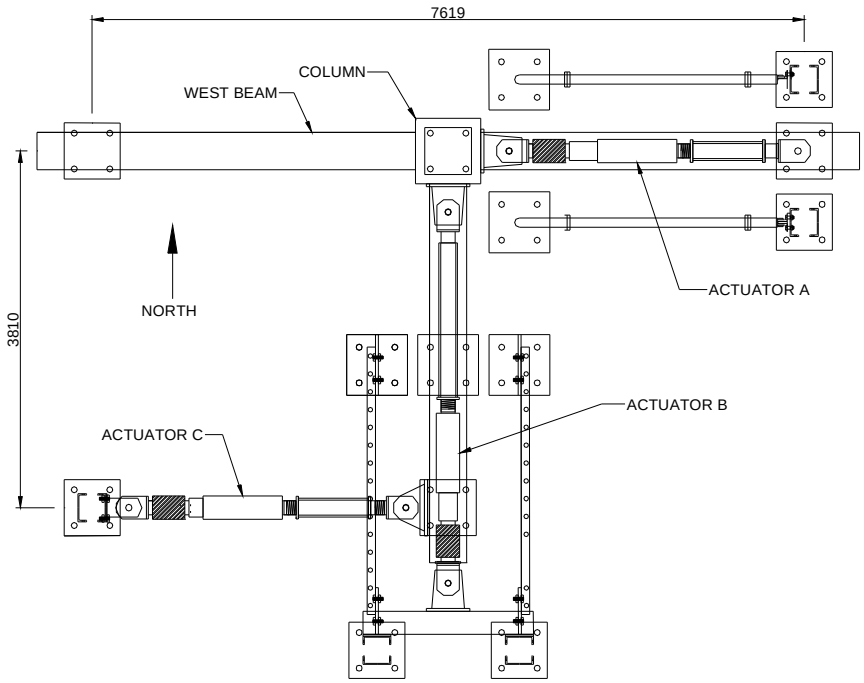

PLAN VIEW

Figure 4-8: Plan view of the specimen in the testing apparatus.

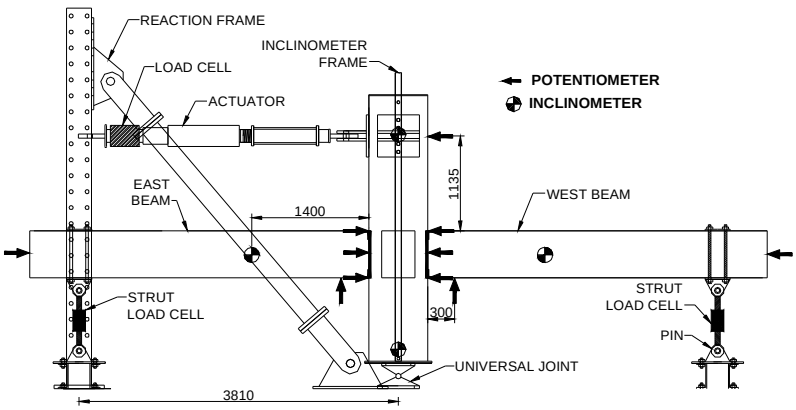

SOUTH ELEVATION

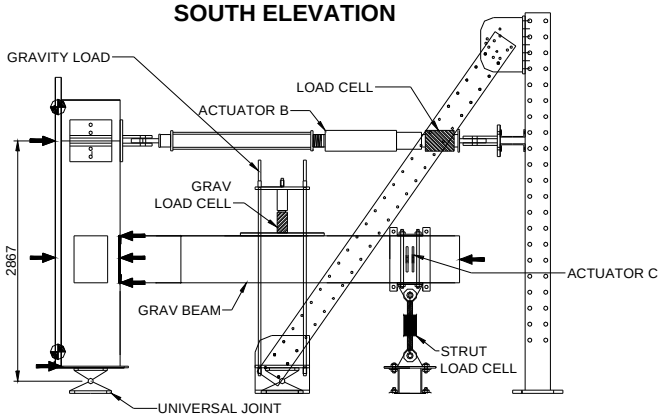

EAST ELEVATION

Figure 4-9: Elevations of the testing apparatus.

patterns, and QED tests where more realistic loading patterns were adopted. The latter method is similar to a pseudodynamic test in that the structure is displaced through 'real' seismic displacements. In QED testing, an inelastic analytical model of the prototype structure is created and subject to an earthquake record of interest. Displacement of the node representing the physical specimen is extracted and used as the displacement profile for physical testing.

A 3D analytical model of the prototype structure was developed using Ruaumoko3D (Carr, 2006), an inelastic dynamic analysis program. Development of this model was part of a parallel study conducted by a co-researcher; details can be found elsewhere (Bradley *et al.*, 2006). The hysteresis properties of the joint was calibrated based on uni-directional physical testing of the specimen. Figure 4-11 gives a comparison between the physical and analytical model up to an interstory drift of 2 percent.

In the case of a MSPA, it is necessary to select earthquake records that represent the desired level of ground excitation. Following current trends, three performance levels were considered. These levels correspond to an upper bound *design basis earthquake* (DBE), which has a 10 percent probability of occurrence in 50 years, and a median and upper bound *maximum considered event* (MCE), which has a 2 percent probability of occurrence in 50 years.

Current seismological studies predict *peak ground acceleration* (PGA) at various return periods. However, it is not correct to simply apply any earthquake record that conforms to this definition, as structural response is dependent on a multitude of factors. Therefore, it is necessary to extract earthquake records from a suite of likely candidates that will result in the most severe structural behaviour. Such a method has been proposed by Dhakal *et al.* (2006) whereby *Incremental Dynamic Analysis* (IDA) (Vamvatsikos and Cornell, 2002) is used to probabilistically determine earthquake records representing multiple

Figure 4-10: Photograph of the specimen in the testing apparatus.

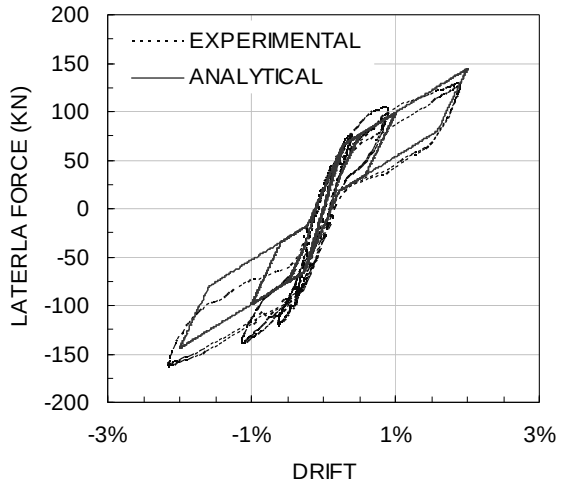

Figure 4-11: Experimental and analytical hysteresis loop comparison.

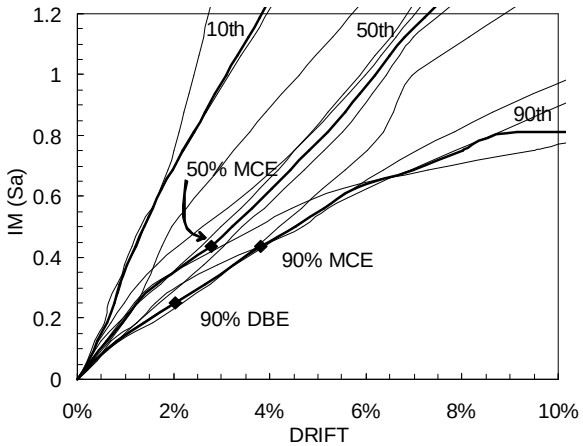

Figure 4-12: Earthquake record selection for the MSPA, using Incremental Dynamic Analysis (Bradley, 2006).

performance objectives. This method has been adopted herein and is illustrated in Figure 4-12. Once an IDA has been conducted earthquake records representing different percentile response at a given intensity measure (IM) can be extracted. In this study, records were chosen to yield responses that have non-exceedance probabilities of 90 percent at the DBE, 50 percent at the MCE, and 90 percent at the MCE, from a suite of 40 records consisting of medium and near-source ground motions.

Performance objectives must be defined for the MSPA. At the first level (90% DBE), there needs to be a high level or reliability that no damage needing repair will occur (i.e. immediate occupancy). This relates to the general philosophy that a structure should incur no damage from frequent earthquakes. The second and third levels of response relate to rare earthquakes. At this level, one should have moderate confidence that the structure will be repairable (50% MCE), and high confidence the structure will not collapse (90% MCE). Given these objectives, the DAD specimen will be monitored to ensure these objectives are met.

4.5. EXPERIMENTAL RESULTS

Results are presented only for a bi-directional quasi-static test to 2 percent drift and the QED tests using the earthquakes selected for MSPA. In all tests, each post-tensioned rod was stressed to 50 percent of its yield limit (200kN). This provided a total of 400kN of prestress force at each joint. The energy dissipaters were replaced after each test.

4.5.1. Quasi-static test results

Figure 4-13 presents results of bi-directional testing to the design level drift of 2 percent. The results shown are for a bi-directional “clover leaf” test, where total drift is calculated considering both X and Y components. Note that the individual plots are projected to one another, allowing an easy comparison to be made between the NS and EW direction.

During stressing of the rods, a 1mm crack formed at the bottom edge of each beam, running between the edge of each flange. This crack can be attributed to the vertical component of the diagonal tendons, approximately a 120kN upward force at the joint. This force in effect pulled the beam up the face of the column. The bottom steel flange however, resisted this due to high friction forces, causing tearing just above the angle, as evidenced by this crack. To combat this effect, the specimen was essentially wedged against the steel anchor plate above the beam. This reduced the effect, though vertical movement of the beam along the column was recorded to be about 5mm.

Opening of the gap was observed at approximately 0.5 percent drift, at which point the steel dissipaters yielded in tension almost immediately (as evidenced from strain gauges). In the east beam, two hairline cracks formed just before reaching the target drift of 2 percent, propagating 100mm out from the dissipater anchor plate. The west beam (high-strength concrete) did not suffer additional cracking. Due to the bi-directional rocking, localised crushing was observed behind the top angle of the east beam over a 10mm square area at the top concrete face. At approximately 1 percent drift, slight buckling of the steel dissipaters occurred as the gap began to close. This was more severe for the gravity beams than the seismic beams, attributed to their longer length. Throughout testing, no damage was observed on the column. A photograph of the east beam after testing is given in Figure 4-14.

As expected, the seismic beam exhibited bi-linear elastic hysteretic behaviour, with some energy dissipation, resulting in a flag-shaped response. Some residual displacement was observed, though this can be partially traced to movement of approximately 2mm in the column base pin, which was repaired for the remaining tests. The unsymmetrical hysteretic response of the gravity beam can be attributed to the inclusion of gravity load, causing an initial positive bending moment at the joint. The gravity beam did not fully re-centre upon

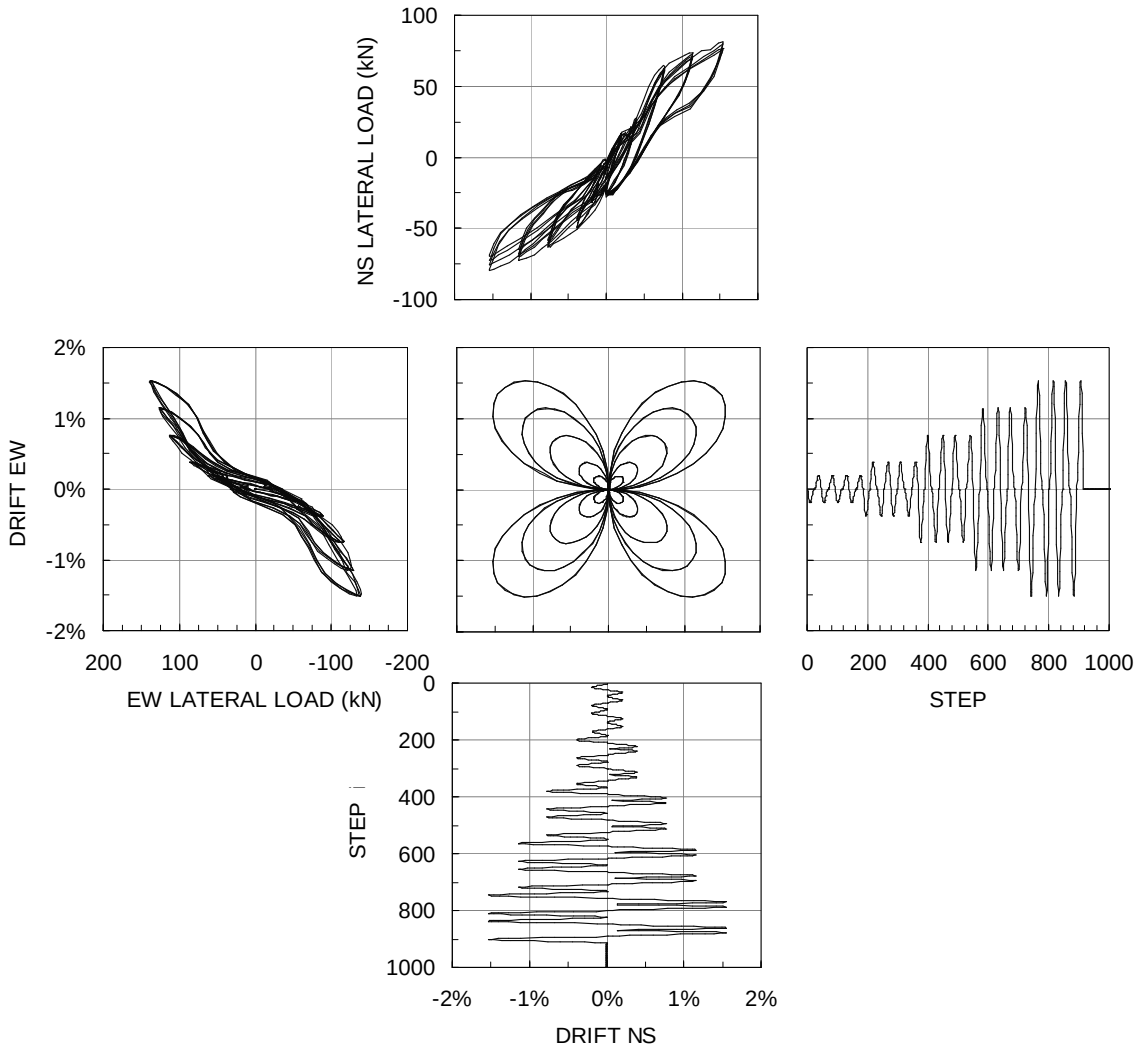

Figure 4-13: Force-displacement response from bi-directional 'clover leaf' test.

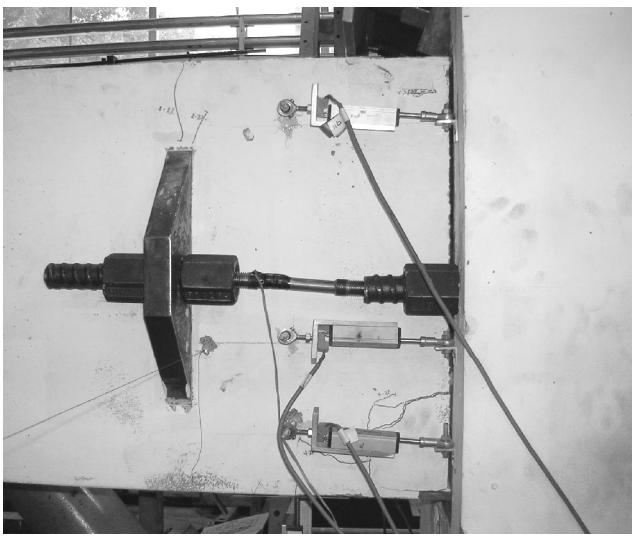

Figure 4-14: Photograph of the east beam after the bi-directional test to 2 percent drift.

removal of the lateral load, resulting in a residual drift of approximately 0.5 percent. This may be partially attributed to sliding of the base pin.

4.5.2. Quasi-earthquake displacement test results

Figure 4-15 presents results for the seismic beams from the three QED tests along with the earthquake records adopted. Since the gravity beam had been previously tested as part of a prior study, its response is omitted and can be found elsewhere (Li, 2006). Note that these tests were performed after the initial quasi-static tests (up to 2 percent drift), and therefore some damage to the specimen had already been observed. Nevertheless, these tests will give a more accurate assessment of response from 'real' loading patterns and any additional damage can be attributed to the given demand.

The 90th percentile DBE test consisted of an initial pulse (attributed to the near source record) to the maximum drift of 2.1 percent. Gap opening and yielding of the energy dissipaters occurred at around the same drift as in previous testing (~0.5%). No new cracks or additional crushing was observed on the seismic beams. A flag shaped hysteresis loop was observed during the initial pulse, however for the remainder of the test response was mostly elastic. Some post-gap opening stiffness degradation was observed, likely due to yielding and buckling of the energy dissipaters. The maximum gap opening, recorded from the potentiometers was approximately 5mm.

The 50th percentile MCE maximum drift was 2.8 percent, which, like the previous test, occurred in the first major loading cycle. This resulted in considerable yielding of the dissipaters and buckling upon unloading. Consequently, further cycles exhibited a lower capacity, resulting in strength degradation of approximately 20 percent on the second cycle. A hairline diagonal crack approximately 300mm long was observed on the east and west beam, appearing to be the result of a compression strut. Small (<100mm) hairline cracks formed along the corners of the steel angles of the east beam, but closed after testing. As

observed from the strain gauges, the fuse bolt-bars reached a maximum of 6000 μstrain (ε_{yield}~ 5500), resulting in slight yielding and an average loss of post-tensioning force of 5 percent.

The final test, the 90th percentile MCE was the most severe of all tests performed. The maximum drift was 4.7 percent. Additional crushing was observed along the top and bottom flange of the east beam's steel angle. This crushing was limited to an area of approximately 25mm measured from the flange edge. The bottom flange of the west beam suffered similar crushing, at one end, covering an area of approximately 10mm square. Some minor spalling was observed over a 25mm area along the angles of both beams. The diagonal cracks formed in the previous test approximately doubled in length and opened to about 1.5mm in the east beam, and 0.5mm in the west beam. At the end of testing, these cracks closed. As seen from the figure, a flag-shaped hysteresis loop was observed, with a maximum residual drift of about 0.1 percent.

The initial (pre-gap opening) stiffness of the specimen remained virtually unchanged, however. Some minor stiffness and strength degradation was observed in the post-gap opening range. The bolt bars reached a maximum strain of 0.009 and maximum force of 360kN, more than the yielding force of the fuse bar. This resulted in a loss of prestress force of some 35 percent and is the major cause of the observed strength degradation. Since the yield force of the regular 26.5mm tendon is about 400kN, the bolt bar 'fuse' protected the beam rods from yielding. Two photographs from testing are given in Figure 4-16.

Figure 4-17 presents a sample comparison of the experimental data and the prediction outlined in Section 4.3. The experimental data is for the 50th percentile MCE test. From this comparison it appears the prediction provides reasonable agreement with the experimental data. The transition between pre- and post-rocking is smooth for the physical specimen. Experimentally, the initial stiffness appears to vary slightly, but the prediction does seem to

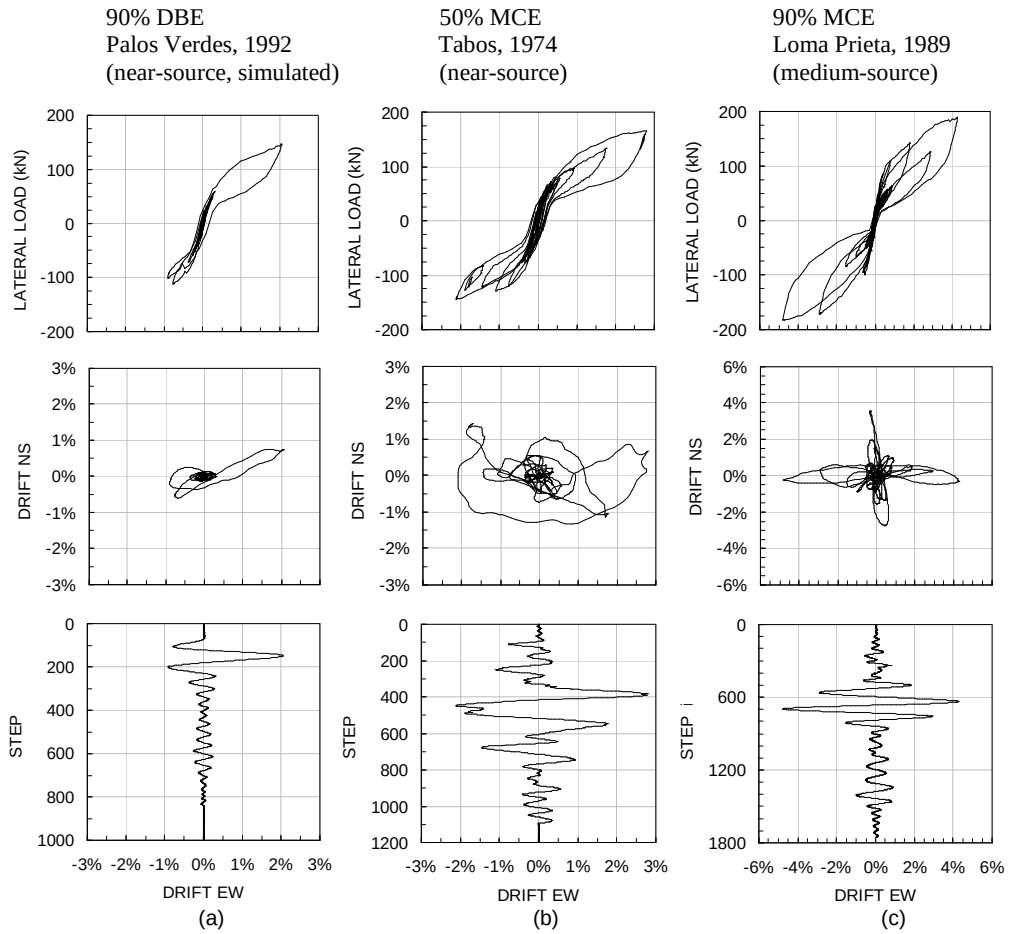

Figure 4-15: QED test results for the seismic beams (EW direction) for: (a) the 90 percent DBE; (b) the 50 percent MCE; and (c) the 90 percent MCE.

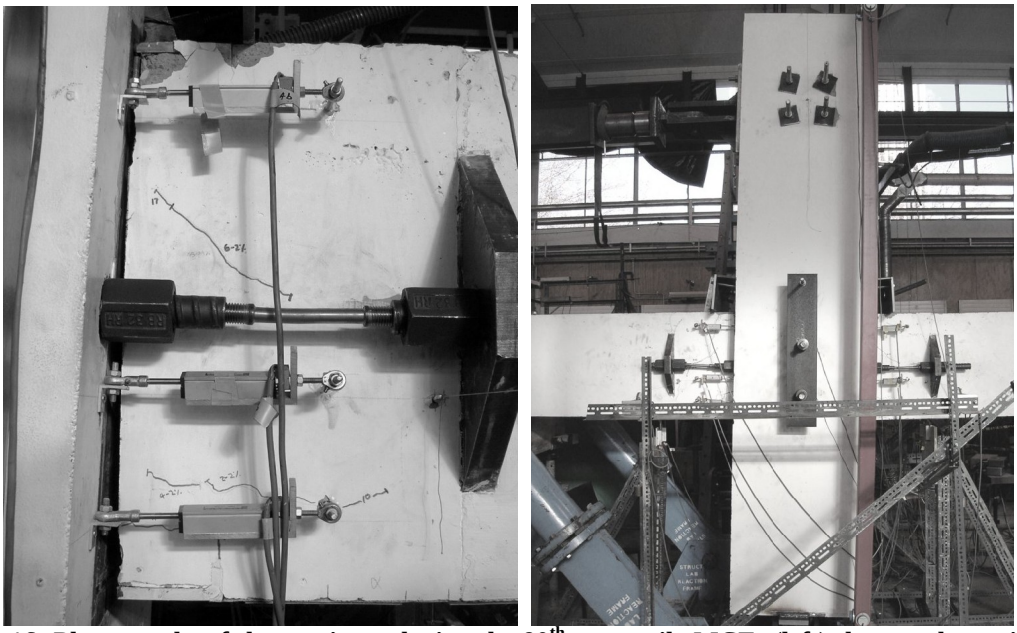

Figure 4-16: Photographs of the specimen during the 90th percentile MCE: (left) the west beam joint at 4 percent drift; and (right) the specimen looking south at the maximum drift of 4.7 percent.

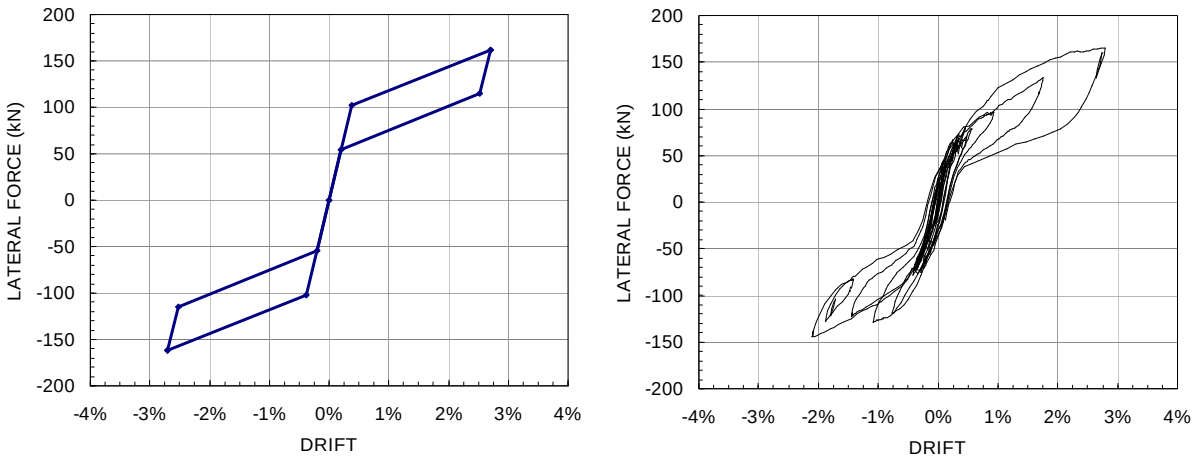

Figure 4-17: Comparison between (a) the hand method and (b) the experimental data for the 50th percentile MCE test.

capture the average stiffness. The energy dissipation is marginally more than expected; this is attributed to additional frictional losses within the prestress system itself that arise from relative movements in the vicinity of the bent tendon.

4.6. MULTI-LEVEL SEISMIC PERFORMACE ASSESSMENT

Test results suggest the specimen satisfied all performance objectives relating to occupancy and collapse prevention. By performing QED tests, whereby the specimen is displaced to patterns similar to those expected from real earthquakes, it is possible to provide some insight as to the damage outcomes of such a structure following seismic events.

Considering the first case of immediate occupancy, it was stated that the structure must be suitably reliable to remain operational following a design level earthquake. This case was represented by a 90th percentile DBE, with a peak drift of 2.1 percent. Aside from some aesthetic cracks, the structure did not sustain any damage that affected its response. Yielding of the energy dissipation devices occurred and therefore these would have to be replaced, which may be a costly undertaking in a multi-storey building. However, since the dissipaters did not sustain strains beyond an equivalent 2 percent drift, it is safe to conclude the structure remains life-safe, and therefore operational.

The second objective, ensuring with moderate confidence the structure can be repaired following an 'extreme' seismic event, was verified by the 50th percentile MCE. The maximum drift level for this test was 2.8 percent, at which point the dissipaters had buckled and slight yielding of the post-tensioning bolt bars had occurred. Since the structure lost some of its stiffness (as provided by the prestress effects) it would be prudent to close the structure until crews could re-tension the prestressing thread-bars and replace the dissipaters. The relative cost of these repairs would be moderate, since the jack points for the rods and the energy dissipaters are reasonably accessible.

The third and most important objective, ensuring with a high level of confidence that the structure will not collapse from an 'extreme' earthquake, was verified by a 90th percentile MCE. In this case, the structure was subject to an earthquake demanding a drift of 4.7 percent. Although the post-tensioned prestress system suffered considerable yielding (and hence loss of prestress), with the energy dissipaters also severely damaged, the specimen remained stable. Even after the extreme drift levels in excess of 4 percent, reasonably good hysteretic behaviour was exhibited. In this case, the energy dissipaters would need to be replaced and the post-tensioning system would need to be stressed back to initial conditions. Since the fuse bolt-bars underwent considerable plastic strain, it may be prudent to replace them. The integrity of the concrete, particularly for the high-strength cast insitu concrete joint, remained high.

4.7. DISCUSSION

Overall, the specimen met the stringent requirements outlined in the MSPA. Compared to traditional monolithic construction, the system performed exceptionally well. The most notable advantage of the DAD system was the significantly lower expected repair costs following the 90th percentile MCE. At 4.7 percent drift, a monolithic beam-column joint would likely experience severe cracking, spalling, and potentially even buckling of longitudinal steel. This would result in significant repair costs of each joint, or complete replacement of the structure. Conversely, the DAD system would need its prestressed thread-bars to be re-stressed and its energy dissipaters replaced. This would result in a much lower cost and would allow the structure to remain operational while any inspections and minor repairs were made.

Notwithstanding the success of the experiment, it is considered there is still room for improvement. The energy dissipation devices needed to be replaced following each event. These externally mounted devices facilitate rapid replacement when damaged. However,

such an arrangement may be too obtrusive in a real building. Alternative mounting locations should be examined or reusable internal devices should be considered. The joint detailing configuration tested has demonstrated that it is possible to reduce material and labour costs without sacrificing performance of the system. The unbonded prestress system was designed to yield at a reduced cross section bolt bar at large displacements. The aim was to provide additional energy dissipation in extreme events. However, as this would require the system to be re-stressed, it may be prudent to design the system to yield at very large (>8%) drifts and instead provide more robust supplemental energy dissipation devices.

Although the angled prestressing tendon alignment through the joint provided redundancy and easy access to jacking points, it significantly increased the complexity of the column joint. For example, due to the vertical component of the prestress force, the beam was observed creeping up the face of the column. This would have to be prevented by ensuring shear keys provided resistance both downward (gravity loads) and upward (prestress load). By utilizing a straight tendon profile, where bars are coupled at the cast insitu end, this problem would be eliminated.

The cast insitu closure pour that used high strength fibre-reinforced concrete performed better than the normal strength concrete joint. Only about 50 percent of the cracks were observed compared to the regular strength concrete, and those cracks which did form did not open or propagate as significantly as the other (dry) joint. For example, the crack formed by the diagonal compression strut in both beams opened to only one third the width in the west (high strength concrete) beam as in the east beam. Including such detailing strategies, possibly by casting all beam ends insitu with high strength concrete, would lead to a reduction in damage at the joint. It is considered that such an insitu joint located at least at one end is desirable to avoid potentially large on-site construction misalignment issues and allow the beams to be cast to reasonable tolerance.

4.8. CONCLUSIONS

Bi-directional quasi-earthquake displacement testing was performed on an 80 percent scale concrete frame sub-assemblage designed for damage avoidance. Critical earthquake records were selected probabilistically to represent multiple levels of demand and a Multi-level Seismic Performance Assessment was conducted. Based on this dual experimental-computational study, the following conclusions are drawn:

1. Three performance objectives were met: (i) with high confidence it can be stated the structure will remain operational following a design level earthquake; (ii) with moderate confidence the structure will be repairable following a very rare earthquake; and (iii) with high confidence the structure will not collapse following a very rare earthquake.
2. A cast insitu closure pour at one beam end helps alleviate construction tolerance issues and ensures the face of the beam is aligned properly with the column. The performance of this joint was satisfactory.
3. Steel energy dissipaters had to be replaced after each test. High efficiency, reusable energy dissipaters would further eliminate repair costs.
4. A hand method for predicting the subassembly response using rigid body kinematics was shown to provide reasonable agreement with results from testing. The results, however, showed more energy dissipation than predicted by the hand method. This was attributed to unpredictable friction forces from the bent tendons.

REFERENCES

Amaris A, Pampanin S, Palermo A. 2006. Uni and bi-directional quasi-static tests on alternative hybrid precast beam column joint subassemblies. *Proceedings of the 2006 New Zealand Society for Earthquake Engineering* (NZSEE) *Conference*. Napier, New Zealand, Paper #24.

Arnold DM. 2004. Development and Experimental Testing Of a Seismic Damage Avoidance Designed Beam to Column Connection Utilising Draped Unbonded Post-Tensioning. *Master of Engineering* Thesis, Department of Civil Engineering, University of Canterbury, Christchurch, New Zealand.

Aslam M, Goddon WG, and Scalise DT. 1980. Earthquake Rocking Response of Rigid Blocks. *Journal of Structural Engineering*, ASCE, **106**(2):377-392.

Bradley BA, Dhakal RP, Mander JB. 2006. Dependency of current Incremental Dynamic Analysis to source mechanisms of selected records. *19th Biennial Conference on the Mechanics of Structures and Materials*; Christchurch, NZ.

Bull D, and Brunsdon D. 1998. Examples of Concrete Structural Design to New Zealand Standards 3101. Cement and Concrete Association, New Zealand.

Carr AJ. 2006. Ruaumoko3D: Inelastic Dynamic Computer Program. Computer Program Library, Department of Civil Engineering, University of Canterbury, Christchurch, New Zealand.

Davies MN. 2003. Seismic Damage Avoidance Design of Beam-Column Joints using Unbonded Post-Tensioning: Theory, Experiments and Design Example. *Master of Engineering Thesis*, Department of Civil Engineering, University of Canterbury, Christchurch, New Zealand.

Dutta A, Mander JB, Kokorina T. 1999. Retrofit for control and reparability of damage. *Earthquake Spectra*, **15**(4):657-679.

Dhakal RP, Mander JB, Mashiko N. 2006. Identification of Critical Earthquakes for Seismic Performance Assessment of Structures, *Earthquake Engineering and Structural Dynamics*, **35**(8):989-1008.

Housner GW. 1963. The behaviour of Inverted Pendulum Structure During Earthquake. *Bulletin of the Seismological Society of America*, **53**(2):403-417.

Li L. 2006. Further Experiments on Damage Avoidance design of Beam-to-column joints. *Master of Engineering Thesis*, Dept. of Civil Engineering, University of Canterbury, Christchurch New Zealand

Mander JB, and Cheng CT. 1997. Seismic Resistance of Bridge Piers Based on Damage Avoidance Design. *Technical Report NCEER-97-0014* (National Centre of Earthquake Engineering Research), Department of Civil, Structural and Environmental Engineering, State University of New York at Buffalo, New York, USA

Pampanin S, Priestley MJN, Sritharan S. 2001. Analytical Modelling of the Seismic Behavior of Precast Conrete Frames Designed with Ductile Connections. *Journal of Earthquake Engineering*, **5**(3):329-367.

Priestley, M.J.N. Sritharan, S. Conley, J.R. Pampanin, S. 1999. Preliminary Results and Conclusions from the PRESSS Five-Story Precast Concrete Test Building. *PCI Journal*; **44**(6):42-67

Standards New Zealand. 1995. NZS 3101: Part 1: 1995: Concrete Structures Standard, Standards New Zealand, Wellington.

Stone WC, Cheok GS, Stanton JF. 1995. Performance of hybrid moment-resisting precast beam-column concrete connection subjected to cyclic loading. *ACI Journal*, **91**(2).

Vamvatsikos D, and Cornell CA. 2002. Incremental Dynamic Analysis. *Earthquake Engineering and Structural Dynamics*, **31**:491–514.

5 Performance of a damage-protected beam-column subassembly utilizing external lead-extrusion energy dissipation devices

SUMMARY

Ductile jointed connections, which often require some form of energy dissipation to alleviate displacement response, typically employ mild steel energy dissipation devices. These devices run the risk of low-cycle fatigue and would have to be replaced following an earthquake. This study presents an experimental investigation employing an alternative to mild steel: the *lead-extrusion* (LE) damping device. Tests are performed on an 80 percent scale beam-column joint subassembly utilizing externally mounted LE dampers. Two configurations are considered: an external joint with two beams framing into a central column, and a corner joint, with only one beam framing into a column. Quasi-static tests are performed to column drifts up to 4 percent. Testing validates the LE dampers' theoretical application, showing reasonable hysteretic energy dissipation. The response of the LE dampers are noted to be very sensitive to the stiffness of the anchorage elements.

5.1 INTRODUCTION

Precast jointed and rocking systems, which exhibit non-linear response by connection opening rather than by the formation of a plastic hinge, have markedly less inherent energy dissipation than ductile monolithic systems. Therefore, it is desirable to provide supplemental energy dissipation devices to help reduce displacement response from earthquakes. An early application of this was presented by Stanton *et al.* (1997), where mild steel rods, running across the connection and grouted in ducts were designed to yield in tension and compression. Test results revealed good hysteretic energy dissipation, however, because the bond between grout and steel deteriorated, some stiffness and strength degradation was observed. After repeated cycles, bar fracture occurred in some tests, due to low-cycle fatigue. Subsequent research at the University of Canterbury has highlighted alternative mild steel energy dissipation devices, bolted externally across the joint region. Amaris *et al.* (2006) demonstrated external buckling-restrained mild steel yielding devices could provide a stable hysteresis loop, with negligible stiffness or strength degradation. However, due to low-cycle fatigue and residual stresses these devices would still have to be replaced following an earthquake.

It then becomes apparent that a more robust form of energy dissipation is needed that satisfies several objectives: (i) energy dissipaters would not be at risk of low-cycle fatigue bar fracture; (ii) energy dissipaters could be located internally within the beam-column joint; (iii) residual forces in energy dissipater should either re-centre or creep back towards zero over time; and (iv) the cost of devices (materials and labour) should be economical. In response to these objectives, the *lead-extrusion* (LE) damper was developed as part of this study. A LE damper is a relatively simple device, as illustrated in Figure 5-1. It consists of a central shaft with a bulge encased in lead. When the shaft moves, the bulge displaces the lead. If properly designed, the device is capable of sustaining a constant force once a yield force is reached,

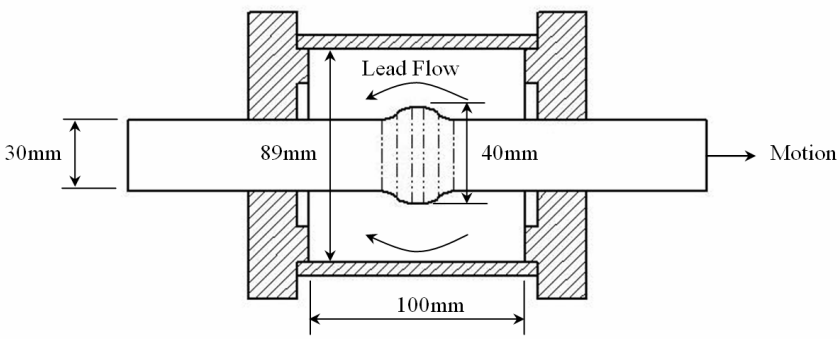

Figure 5-1: Section of a typical LE damper (Rodgers *et al*., 2006).

similar to the behaviour of the mild steel energy dissipation devices. These devices have been shown to be relatively insensitive to velocity. Given the relationship between LE damper force and velocity:

$$F = av^b \tag{5-1}$$

where F = the damper force; v = the velocity of the shaft; and a and b are empirical constants, b can be taken as 0.12 (Robinson and Greenback, 1976).

Historically these devices were considerably large, limiting their use to specific applications such as base isolation (Cousins and Porritt, 1993). More recently, researchers at the University of Canterbury have investigated the feasibility of such devices in tight volumetrically constrained applications, such as beam-column joints (Rodgers *et al.*, 2006).

The preceding chapter of this thesis has presented a beam-column joint subassembly designed for external mild steel energy dissipation devices. These devices were mounted externally to the specimen via a steel plate extruding from each side of the beams and a shaft in the column where the devices were anchored on the opposite end. In this addition, two LE dampers were designed and fabricated to be mounted on these anchor plates. The experimental testing presented herein is intended to confirm the benefits of such devices when incorporated into ductile jointed connections.

5.2 DESIGN DETAILS

The specimen utilized in this Chapter is the same as presented in Chapter 4. For sake of completeness, its design attributes will be repeated here.

5.2.1 The subassembly

A 3D subassembly representing an interior joint on a lower floor of a ten storey building was developed. The subassembly consisted of two beams cut at their midpoints and an orthogonal beam cut at its midpoint (the approximate location of the point of contraflexure), all framing into a central column. The orthogonal beam, referred to herein as

the gravity beam, was designed for supporting one-way precast flooring panels. The other two beams, referred to herein as the seismic beams, were designed for predominantly seismic forces. The dimensions of the prototype members were taken from previous research (Li, 2006); this corresponded to 850mm square columns, 700mm by 500mm beams, and a 3.6m storey height. The prototype joint was assumed to have a moment capacity of 500kNm (Arnold, 2004).

Given these constraints, the subassembly was scaled to 80 percent of the prototype building. The column was scaled to 750mm square and the beams scaled to 560mm by 400mm. A target longitudinal reinforcement ratio of 0.01 was taken for the column and the beams. Figure 5-2 illustrates the basic reinforcing layout for the beams and column. They were designed for the expected strength of the rocking joint from the dissipation devices and the prestress and were intended to remain elastic. Four D20 (f_y = 500MPa) longitudinal threaded rebars (Reidbar^{TM}) were provided top and bottom, thus providing a moment capacity of ϕM_n = 260kNm. Due to the presence of axial load from prestress, minimal transverse steel requirements governed (Davies, 2003). HR12 (f_y = 500MPa) stirrups were provided in the beam at a spacing of $d/2$ and a closer spacing at the ends. Additional transverse reinforcement was provided top and bottom 1.2m from the beam ends to confine the concrete in these high compression zones.

The unbonded post-tensioned prestress was provided by two 26.5mm diameter high-strength thread-bars placed in 50mm PVC ducts. A detail of the seismic beam-column joint is given in Figure 5-3. The seismic beams utilized a straight coupler system where the tendons were pre-bent at the joint end to a radius of approximately 1.8m. This allowed proper alignment with the angled rod running through the column. The fuse bolt-bar was machined to 75 percent of its effective area to ensure any yielding in the prestress system would be limited to the replaceable column bolt-bar. At the beam end, a 100x100x12 inverted steel

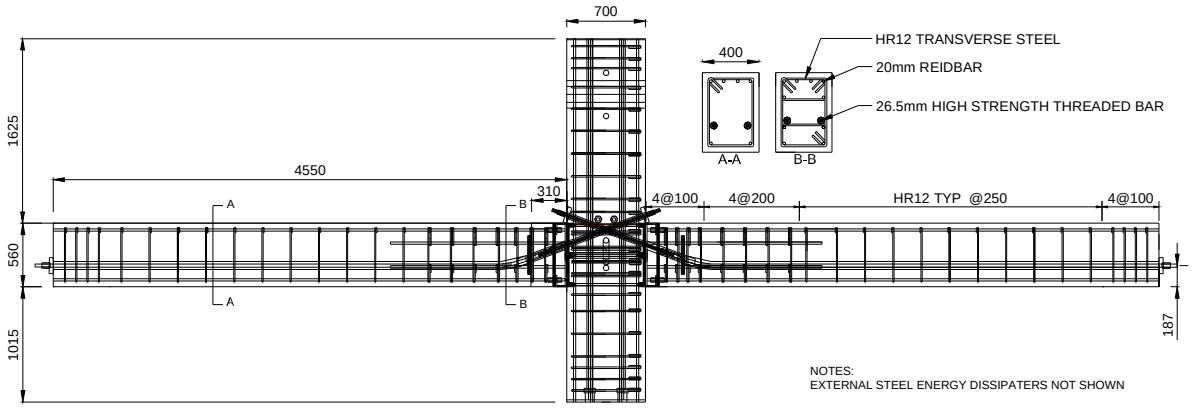

Figure 5-2: Elevation of the seismic beams and column.

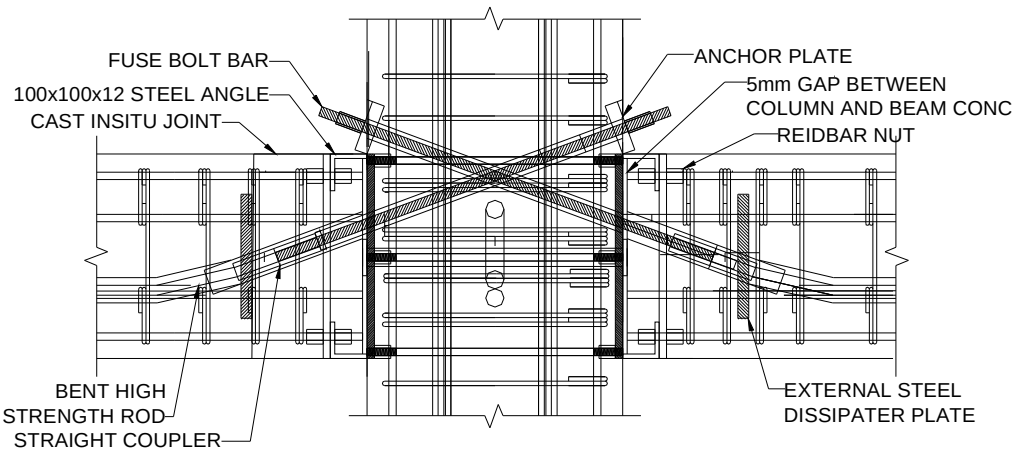

Figure 5-3: Detail of the seismic beam-column joint

angle was used at top and bottom of the joint and the face of concrete was recessed 5mm. This ensured that contact with the column was limited to the steel and allowed the angle's buried flange to mechanically develop the beam's longitudinal steel using Reidbar^{TM} nuts.

By the nature of precast concrete and rocking connections, it is critical that the face of the beam be aligned flush with the column. Therefore, offsite erection of a full length beam section may lead to on-site misalignment issues which may affect rocking behaviour. To mitigate potential misalignment and to also allow for construction tolerances similar to current standards, a 310mm cast insitu closure pour was provided on the west seismic beam. This closure pour is expected to be cast on-site after the armouring angles have been adjusted to ensure a flush face at both ends and the post tensioning rods are coupled together. High strength, fibre-reinforced concrete was used in the insitu end to compare its behaviour to the regular strength concrete of the east beam. The compressive strength of the high strength concrete was tested and found to be f'_c= 70MPa. The east beam and the remainder of the west beam concrete was found to be f'_c= 37MPa.

At each joint, four 30mm diameter shear keys were installed, tapered 5° inward to ensure they do not jam when the specimen rocks. These were designed to be screwed into the face of the column via a cast in double nut. The shear keys were designed for gravity and seismic shear forces, as given in Li (2006). One shear key was located in each corner, providing resistance to torsion.

5.2.2 The lead-extrusion damper

The lead-extrusion damper was designed to be mounted externally on pre-existing plates in the beams. An assembly of the LE damper is given in Figure 5-4. A detailed design of the LE damper was conducted by a co-researcher in the Mechanical Engineering Department of the University of Canterbury (Rodgers, 2006). A central shaft with a bulge was encased in a cylinder filled with lead. Rectangular endcaps were bolted together via two

attachment rods, which also anchored the device to the beam's anchor plate. One end of the central shaft was threaded, allowing it to be coupled to a threaded rod anchored to the column. The threaded rod running through the column was anchored on each end of the column face using a nut and steel plate washer. A photograph of the device and the mounting configuration is given in Figure 5-5(a) and (b), respectively.

To ensure the connection is capable of closing, the moment contribution from the initial prestress force must exceed the contribution from the dampers. This can be written as follows:

$$\phi M_{PS,i} \geq \Omega_{diss} M_{diss} \tag{5-2}$$

where $M_{PS,i}$ = moment contribution at the joint from the initial prestress force; M_{diss} = moment contribution at the joint from the energy dissipation devices in compression; Ω_{diss} = overstrength factor of the dissipation devices (taken as 1.5); ϕ = understrength factor for the prestress (taken as 0.85). Dividing the contribution from prestress by the contribution from the dissipation devices gives a ratio of their expected contribution:

$$\lambda = \frac{\phi M_{PS,i}}{\Omega_{diss} M_{diss}} \tag{5-3}$$

To ensure the system re-centres, $\lambda \geq 1$. The dampers were designed to provide the same level of energy dissipation as mild steel devices adopted in Li (2006). Therefore, the dampers were designed for a 120kN yield force. This corresponds to λ = 2.2 and 4.4 in the EW direction for positive and negative moment, respectively.

The force-displacement response of the LE dampers is shown in Figure 5-6. This plot was attainted by fixing the steel body and applying a compression force to the central shaft. Once the shaft had reached maximum travel, the device was flipped and the compression force was applied in the opposite direction. The devices exhibited an average initial stiffness of 200kN/mm.

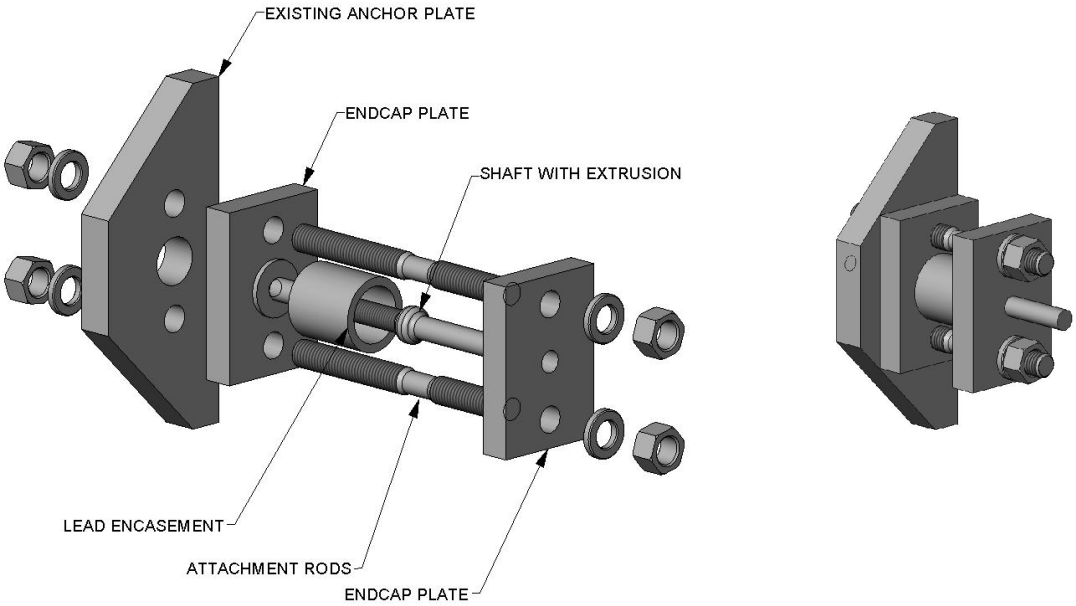

Figure 5-4: The lead-extrusion damper externally mounted to the beam's anchor plate (Rodgers, 2006).

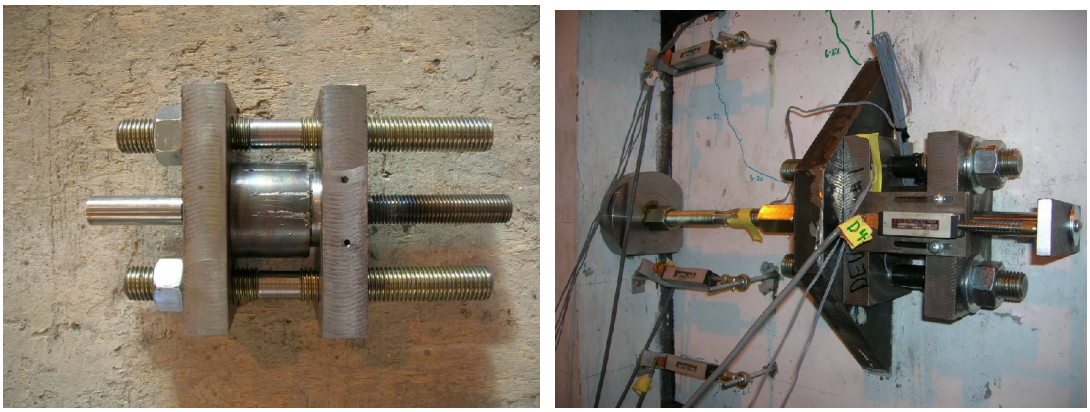

(a) (b)

Figure 5-5: Photographs of the external LE damper: (a) prior to installation; and (b) mounted on the east beam.

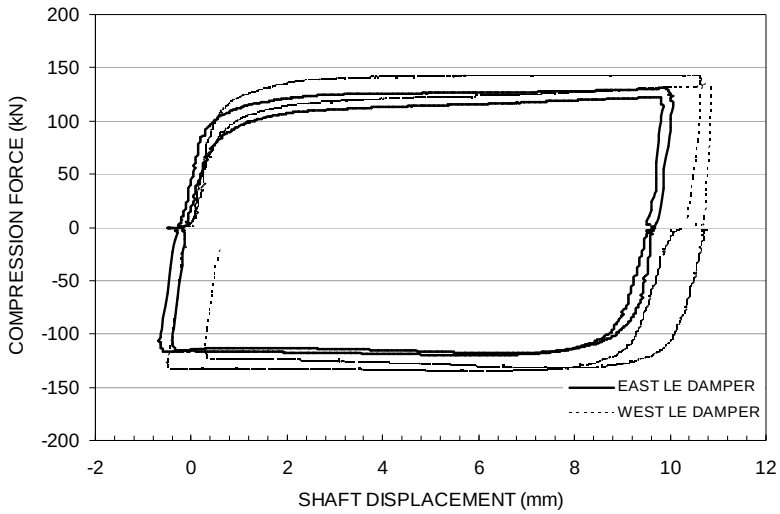

Figure 5-6: Force-displacement response of the LE dampers prior to testing.

5.3 TEST SETUP AND METHODS

Figure 5-7 gives a plan view of the test setup and Figure 5-8 presents two elevations. Loads were applied to the specimen by three hydraulic actuators. Actuators A and B were installed to the reaction frame and top of the east and south face of the column, respectively. Actuator C was installed in the east-west direction at the end of the gravity beam. This actuator was intended to stabilize the specimen. Actuator C's movement was synchronised to approximately one-half the displacement of Actuator A. Load cells were installed in-series with each actuator. Additional load cells were attached at the strut of each beam and the jacking point of each post-tensioned rod. A photograph of the specimen in the testing apparatus is given in Figure 5-9.

To measure rotation at the joint, 3 linear potentiometers were installed on both faces of each joint, totalling 18 devices. Two additional linear potentiometers were installed against the bottom face of each beam to measure vertical movement. At several locations around the specimen rotary potentiometers were installed to measure local displacement. Two 5mm strain gauges were installed on each bolt bar to measure any potential yielding that may occur during testing. To measure the response of the LE damper a load cell and strain gauges were attached to the anchor rod of each device. A spring potentiometer was mounted on the back of each device to measure the displacement of its central shaft.

The testing regime was relatively straightforward, and focuses entirely on the performance of the LE damper. Cyclic q*uasi-static* (QS) tests were performed at varying levels of drift. These tests were uni-directional in the EW direction. The NS direction is largely disregarded in this investigation, since its performance has already been reported in Chapter 4. The testing was done in two phases. First it was conducted with an LE damper attached to one side of each EW beam, as illustrated in Figure 5-7. Next, the east beam was removed and its LE damper was placed on the north face of the west beam, thus doubling its

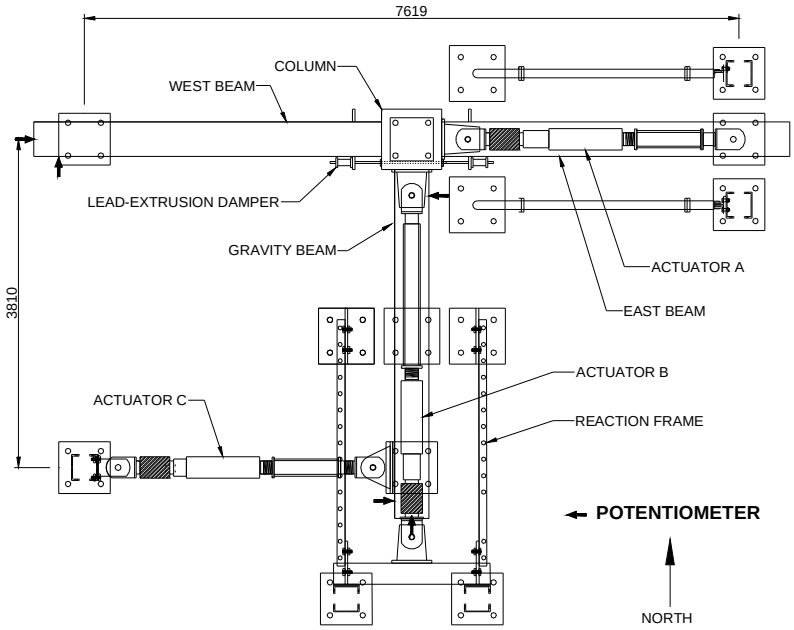

PLAN VIEW

Figure 5-7: Plan view of the bi-directional test setup.

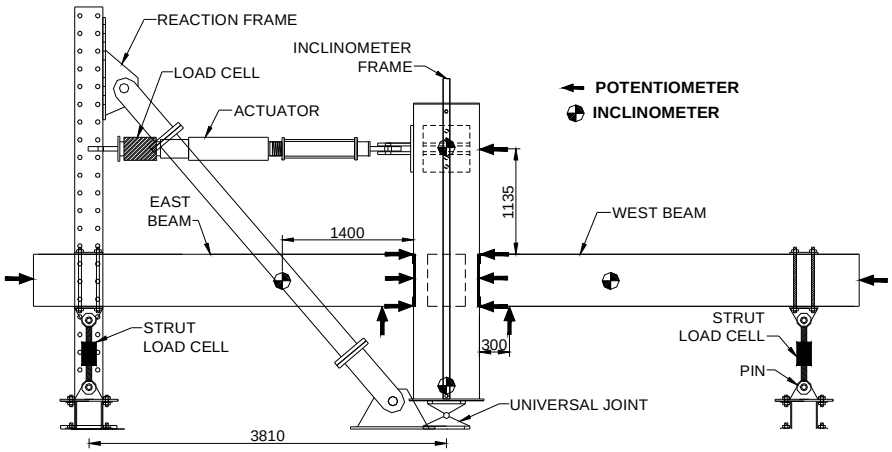

SOUTH ELEVATION

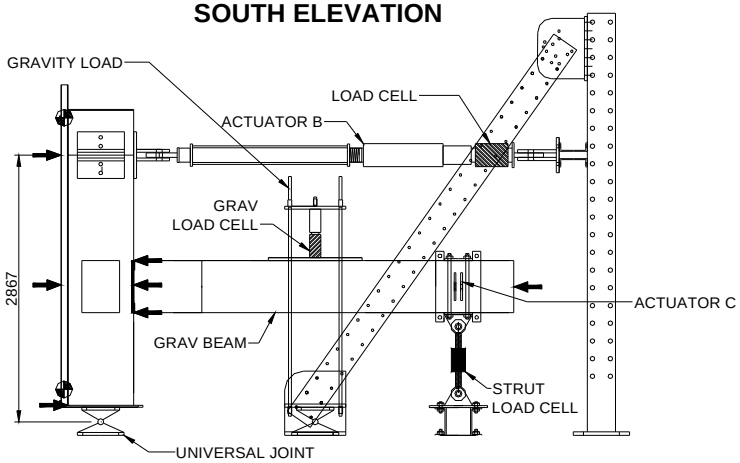

EAST ELEVATION

Figure 5-8: South and east elevation view of the test setup.

Figure 5-9: Photograph of the specimen in the testing apparatus.

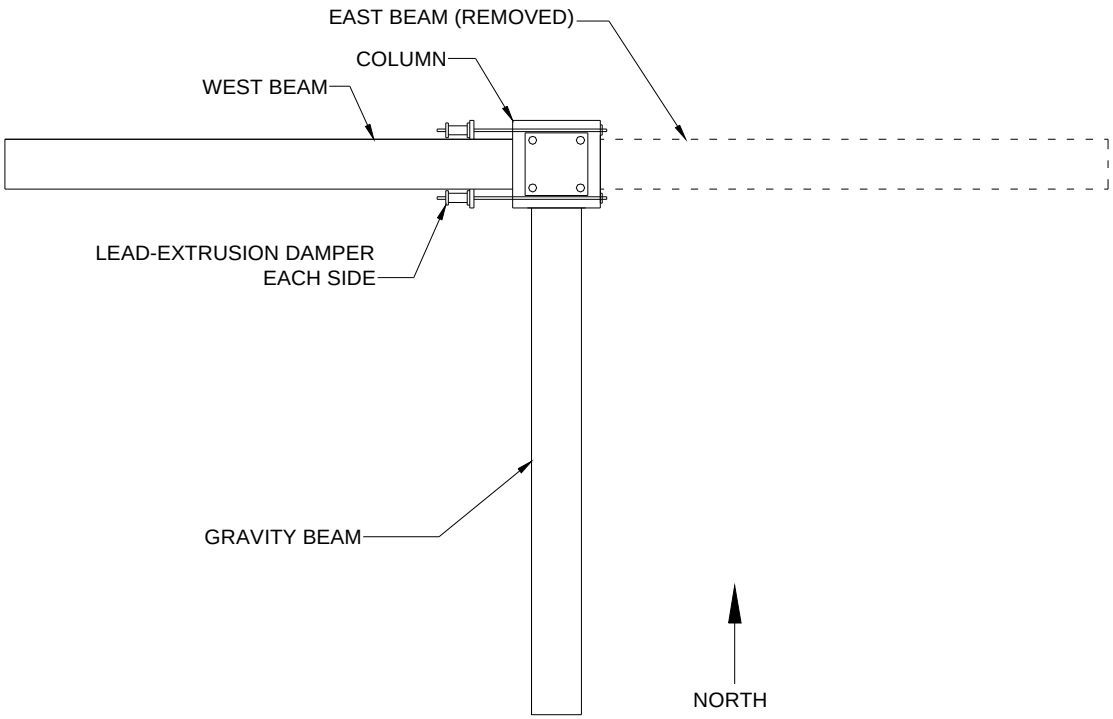

Figure 5-10: Plan view of the corner joint specimen; the east beam has been removed and its LE damper has been relocated.

damping capacity, (λ^+=1.1; λ^-=2.2). This is illustrated in Figure 5-10. The new setup essentially represents a corner joint of the prototype structure.

5.4 EXPERIMENTAL RESULTS

Experimental results from this section focus entirely on the global performance of the specimen and the local performance of the LE dampers. Since the local behaviour of the specimen (i.e. cracking, crushing, prestress, etc.) has been reported in the previous chapter, these aspects of the results were not reported.

For purposes of comparison, Figure 5-11 presents results of QS testing in the EW direction to a maximum column drift of 2 percent for three cases: (i) prestress only; (ii) mild steel energy dissipation as presented in Chapter 4; (iii) and the LE dampers. With prestress only it is apparent the system still provides some level of energy dissipation, likely due to friction of the bent thread-bar within the ducts. The steel devices provide the most hysteretic energy dissipation and the LE dampers provide slightly less. The specimen with steel devices exhibit some strength degradation. This can be traced to the fact that the devices will undergo plastic deformation in tension, and will not recover that deformation in compression due to buckling. The LE dampers do not exhibit this effect. The hysteresis loop is stable, showing only minor strength degradation.

On larger displacement cycles, the LE damper provided a significantly greater amount of hysteretic energy dissipation. This can be seen in Figure 5-12, where an additional two cycles to 3 percent drift reveals a markedly large change in response. The specimen exhibited some drop in strength during reloading to the previous peak, but no overall capacity was lost. This can be can be seen more clearly in the force-displacement response during testing of the LE damper given in Figure 5-13. Before the specimen reached a drift of 3 percent, the devices behaved essentially in an elastic manner. At 3 percent drift, the devices fully engaged and yielded. The shaft moved approximately 3.5mm. Upon subsequent loading and

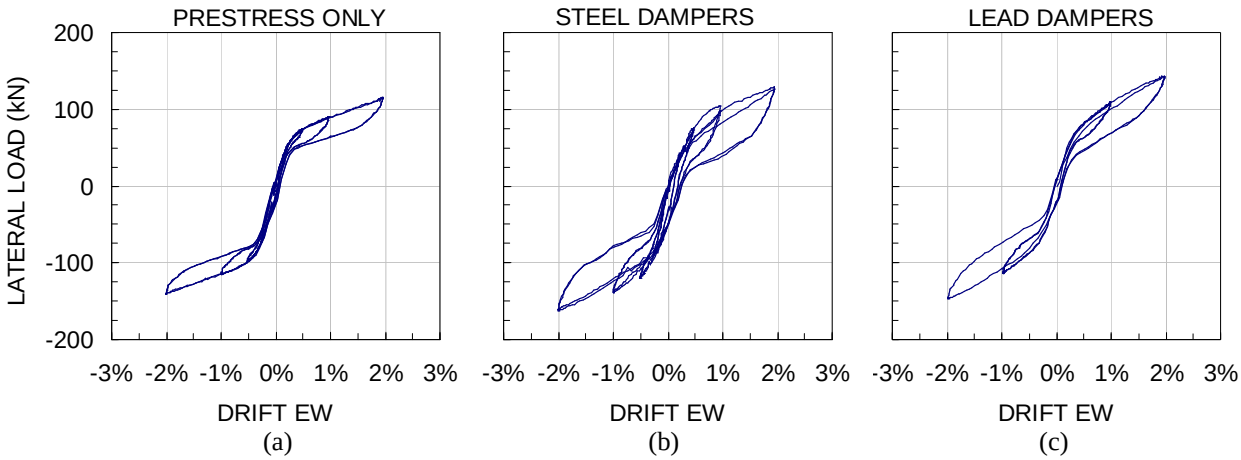

Figure 5-11: Comparison of the performance considering (a) prestress only; (b) steel dampers; and (c) lead dampers.

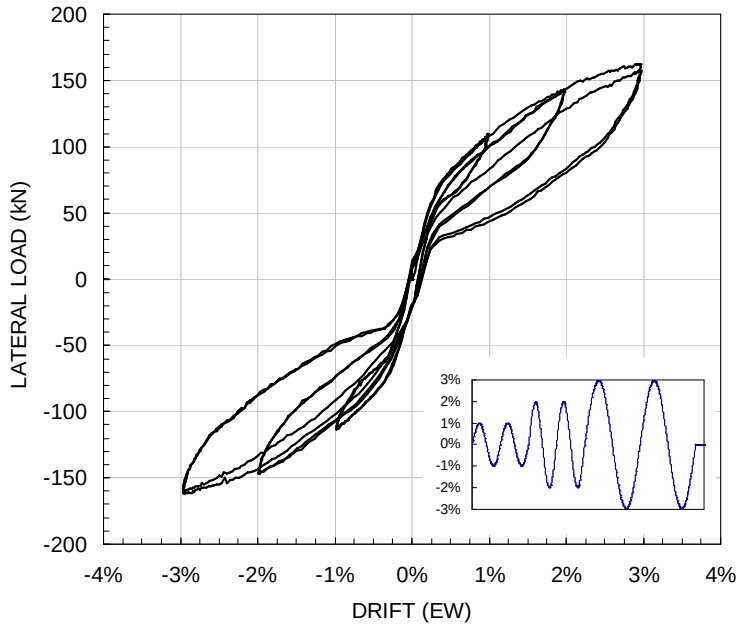

Figure 5-12: Response of the specimen with LE dampers to 3 percent drift.

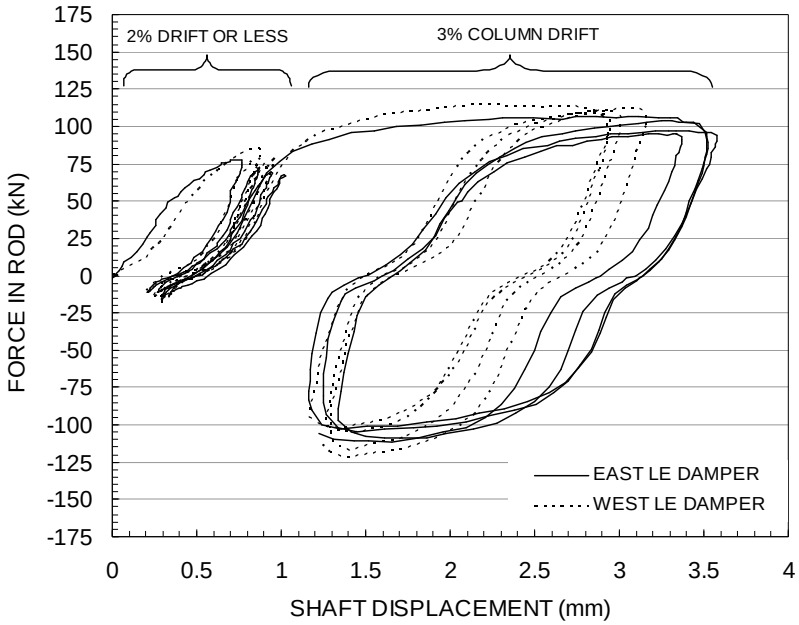

Figure 5-13: Force-displacement response of the LE dampers.

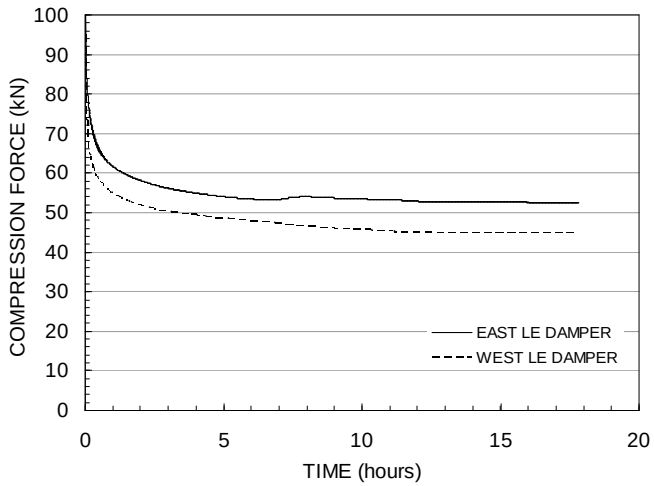

Figure 5-14: Damper force over time.

unloading, the device exhibits elasto-plastic response, with slight pinching at zero force. This can be attributed to slop within the connecting threaded elements of the device. The shaft does not return to its initial position, but upon completion of the test remains about 1.5mm from its initial position.

After testing, the residual compression force in the LE damper and anchor shaft was approximately 90kN. This force reduced over time, as shown in Figure 5-14. Within the first 5 hours the force in the devices had dropped by approximately 50kN – about 45 percent of the peak compression force.

As noted in the previous section, the east beam was removed and its LE damper was relocated to the west beam. Thus the beam's energy dissipation capacity doubled. Figure 5-15 presents the response of the specimen with and without LE dampers to 4 percent drift. Compared to previous tests, it is apparent that the specimen exhibits significantly more energy dissipation, as was expected. Some pinching was observed during the unloading phase. As evidenced by the load cells, this was be attributed to the relaxation of the threaded anchor rods. These were elastically stretched under tension during the loading phase, and then compressed prior to yield of the LE damper. As in previous tests, some strength degradation was observed. In this case, since the specimen had reached a peak drift of 4 percent, some yield of the reduced-section thread-bars occurred. This is the cause of strength degradation in the prestress-only case.

5.5 DISCUSSION

The performance of the specimen was satisfactory. This proof-of-concept experiment has validated the theoretical basis of a LE damper being incorporated into a beam-column joint to dissipate seismic energy. Although the devices were slow to 'engage', at higher drifts it was found that the specimen exhibited more stable, 'fatter' hysteresis loops than with the

mild steel devices, which buckled in compression. The fact these devices slowly lose the residual compressive force means the full moment capacity of the joint will be restored.

As noted, the devices were slow to 'engage'. This was evidenced by the stark difference in hysteretic energy dissipation shown in Figure 5-11 and Figure 5-12, between 2 percent and 3 percent column drift. This lag was traced to the anchoring system utilized. Given the properties of the anchor rod, its elongation at the yield force of the LE damper (120kN) would be approximately 2.5mm. Given a column drift of 2 percent, which corresponds to a connection rotation of about 0.015 radians, the maximum expected gap-opening at the location of the LE dampers is 4.5mm. The elongation of the rod would account for more than half this amount, thus seriously reducing the effectiveness of the device. This effect is magnified by the fact that each connecting element (the coupler, nuts, anchor plates) exhibit some degree of slop, which must also be accommodated before the full yield force of the dissipater can be reached. Given the already relatively low stiffness of the LE damper (200kN/mm), such effects can be extremely detrimental to the LE dampers' effectiveness at the joint.

This lag effect is also the reason the specimen exhibited strength degradation on secondary cycles. At the completion of a cycle, the LE damper and its connecting elements would be in compression. At the onset of a reversed cycle, the anchor rods would first have to transition from a fully elastic compression state to an elongation in tension. Thus requiring even greater displacement of the joint to allow the yield of the dissipation device to be reached. Obviously, this effect is considerable. This effect may be considerably reduced if the LE damper and its anchorage elements are prestressed, thus eliminating any slop. In future efforts, care should be taken when designing the dissipater anchorage, with specific attention given to eliminating any slop in the system.

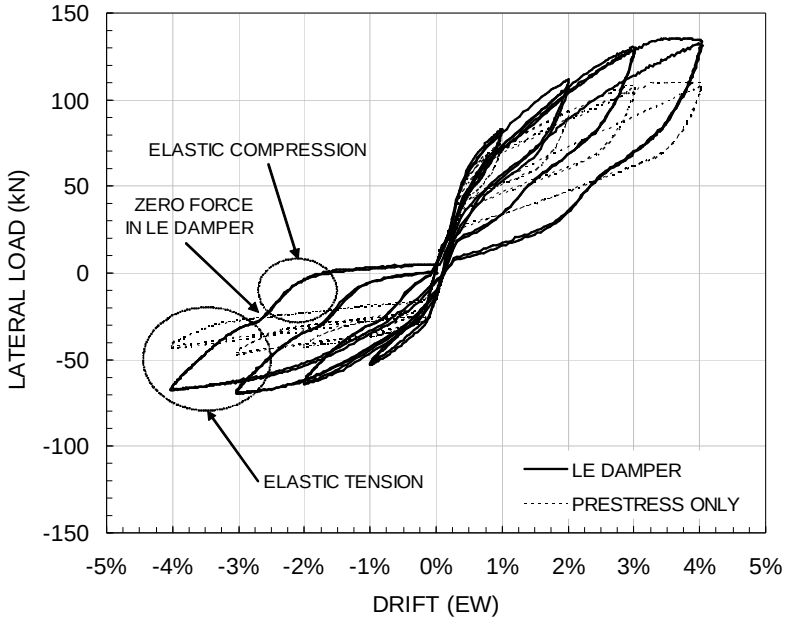

Figure 5-15: Response of corner joint specimen QS testing to 4% drift

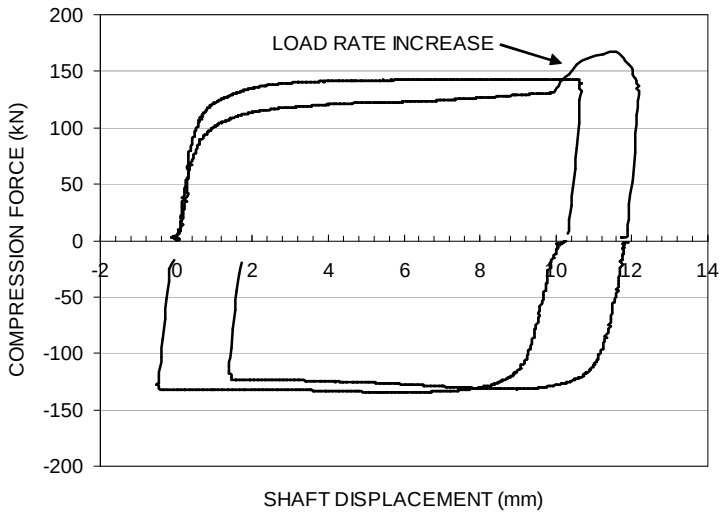

Figure 5-16: The effect of load rate on the LE damper.

During initial testing of the LE dampers (prior to mounting them to the specimen) it was found that the peak yield force of the devices was sensitive to the load rate. For example, upon loading the LE damper in compression at a constant rate, the rate was suddenly increased, resulting in the spike shown in Figure 5-16. In this case the load increased by 20 percent. This effect may be positive. Under very rapid displacements, such as would be expected in an earthquake, the device would provide additional damping to the structure. This allows the dampers to provide a force higher than the restoring force from prestress, while still allowing the connection to close upon unloading. Further investigations on this effect, and its implications to the dynamic response of the structure, is needed.

5.6 CONCLUSIONS

This study has presented a proof-of-concept experimental investigation. LE dampers, an alternative to mild-steel energy dissipation devices, were mounted externally across a joint. Based on the results of this study, the following conclusions can be drawn:

1. It was demonstrated through QS testing that the LE dampers could provide a level of energy dissipation comparable to mild steel devices designed for the same yield force.
2. LE dampers offer an attractive alternative to mild steel energy dissipation devices. These devices do not suffer from low-cycle fatigue and the force in the devices creeps back towards zero upon unloading. Therefore they would not need replacement following an earthquake and could be mounted internally.
3. The stiffness of these devices is lower than typical mild steel devices. Since gap-opening is generally 5-10mm, stiffness plays an important role in the effectiveness of supplemental energy dissipation. Care should be taken when designing the anchorage for these devices. Prestressing the devices may help alleviate the problem.
4. Further research to better investigate the dynamic loading effects of LE dampers is needed.

REFERENCES

Amaris A, Pampanin S, Palermo A. 2006. Uni and bi-directional quasi-static tests on alternative hybrid precast beam column joint subassemblies. *Proceedings of the 2006 New Zealand Society for Earthquake Engineering* (NZSEE) *Conference*. Napier, New Zealand, Paper #24.

Arnold DM. 2004. Development and Experimental Testing Of a Seismic Damage Avoidance Designed Beam to Column Connection Utilising Draped Unbonded Post-Tensioning. *Master of Engineering Thesis*. University of Canterbury, Christchurch, New Zealand.

Cousins WJ and Porritt TE. 1993. Improvements to lead-extrusion damper technology. *Bulletin of the New Zealand National Society for Earthquake Engineering*, **26**:342-348.

Davies MN. 2003 Seismic Damage Avoidance Design of Beam-Column Joints using Unbonded Post-Tensioning: Theory, Experiments and Design Example. *Master of Engineering Thesis*. University of Canterbury, Christchurch, New Zealand.

Li L. 2006. Further Experiments on Damage Avoidance design of Beam-to-column joints. *Master of Engineering Thesis*, Dept. of Civil Engineering, University of Canterbury, Christchurch New Zealand

Robinson WH and Greenback LR. 1976. An extrusion energy absorber suitable for the protection of structures during an earthquake. *Earthquake Engineering and Structural Dynamics*, **4**:251-259.

Rodgers GW, Denmead CS, Leach NC, Chase JG, Mander JB. 2006. Spectral evaluation of high force-volume lead dampers for structural response reduction. *Proc. New Zealand Society for Earthquake Engineering Annual Conference*, Napier, New Zealand, March 10-12.

Rodgers GW. 2006. Next generation structural technologies: implementing high force-to-volume energy absorbers. *PhD Dissertation*. University of Canterbury, Christchurch, New Zealand.

Stanton JF, Stone WC, and Cheok GS. 1997. A Hybrid Reinforced Precast Frame for Seismic Regions. *PCI Journal*, **42**:20-32.

6 Performance of a damage-protected beam-column subassembly utilizing internal lead-extrusion energy dissipation devices

SUMMARY

An experimental and computational study of an 80 percent scale precast concrete 3D beam-column joint sub-assembly designed with damage-protected rocking connections is presented. High-alloy high-strength unbonded thread-bars running through the beams and columns are implemented to prestress the system. The thread-bars are post-tensioned and supplemental energy dissipation is provided by internally mounted *lead-extrusion* (LE) dampers. A *Multi-level Seismic Performance Assessment* (MSPA) is conducted considering three performance objectives related to occupancy and collapse prevention. First, bi-directional quasi-static cyclic tests are conducted and the specimen's performance characterised. This data is then used in a 3D nonlinear *Incremental Dynamic Analysis* (IDA). Results from the IDA are used to select three critical earthquakes for further experimental bi-directional testing. Thus quasi-earthquake displacement tests are performed. Results indicate the specimen satisfies all performance objectives related to serviceability and life-safety. Damage to the specimen is negligible.

6.1 INTRODUCTION

Research and development of precast concrete rocking structures has gained considerable momentum over the past two decades, with significant research on so called PRESSS systems being conducted in the United States (Priestley *et al.*, 1999). These systems, designed to accommodate inelastic behaviour by rocking at specially detailed joints, have proven to provide a level of seismic resistance comparable to current standards while remaining almost damage-free. Furthermore, such systems do not suffer excessive residual displacement, a common occurrence in conventional systems that often leads to complete loss of the structure. However, these systems exhibit relatively low hysteretic energy dissipation. Although this may not be an issue with long period structures, studies have shown short to medium period rocking structures may undergo displacements double that of conventional ductile structures (Priestley and Tao, 1993). As a result, ductile jointed precast concrete systems require supplemental energy dissipation devices to dissipate earthquake energy, thus alleviating displacement response.

Energy dissipation devices of varying sophistication are available. Early applications of supplemental energy dissipation in ductile jointed connections are given in Stanton *et al.* (1997). In this case, energy dissipation was provided by mild steel reinforcing bars, grouted in ducts across the joint. The devices proved to work well, with the grout providing a degree of buckling resistance. However, de-bonding of the mild steel bars under cyclic loading caused some stiffness degradation of the system. Other options include simple tension-only mild steel devices (utilized in Chapter 3), external mild steel devices allowed to buckle (Chapter 4), and buckling-restrained external mild steel devices (Amaris *et al.*, 2006). Each of these options have limitations. In the case of mild steel devices allowed to buckle, part of the potential energy dissipation is lost upon buckling, resulting in comparably less hysteretic energy dissipation This does however have one advantage. Since the buckling restrained

devices provide stable resistance both in tension and compression, upon closing of the joint a residual compression force will remain. This force can alter the characteristics of the joint, leading to potential stiffness and/or strength loss which could lead to excessive displacement demand upon further seismic excitation. Furthermore, these devices run the risk of suffering from low-cylce fatigue fracture. Consequently these devices would have to be replaced following an earthquake.

The *lead-extrusion* (LE) damper may provide a good alternative to mild steel energy dissipation devices. A LE damper is a relatively simple device. It consists of a central shaft with a bulge which is encased in lead. When the shaft moves, the bulge displaces the lead. If properly designed, the device is capable of sustaining a constant force once a yield force is reached, similar to the behaviour of the mild steel energy dissipation devices. Unlike the mild steel devices, the LE damper is capable of creeping back to near zero force, thus providing a reusable device which would not have to be replaced following an earthquake.

Historically these devices were considerably large, limiting their application to specific applications like base isolation (Robinson and Greenback, 1976; Cousins and Porritt, 1993). More recently, researchers at the University of Canterbury have investigated the feasibility of such devices in tight volumetrically constrained applications, such as beam-column joints (Rodgers *et al.*, 2006). These LE dampers have promise as relatively insensitive to changes in velocity. Based on past tests, researchers have found that the velocity exponent (*b)* is on the order of 0.12 (Robinson and Greenback, 1976) given:

$$F = av^b \tag{6-1}$$

where F = the damper force; v = the velocity of the shaft; and a and b are empirical constants.

The study presented herein incorporates a culmination of findings from previous chapters, and focuses on the further development of cost effective, reliable energy dissipation and detailing schemes. As previous work related to beam-column joints has focused on external dissipation devices, this contribution will present an attractive alternative whereby

LE dampers are buried within the joint, providing a reliable form of energy dissipation and an architecturally pleasing finish. Detailing in the joint region is modified to accommodate the devices, with special attention given to further reduction of materials and constructability issues related globally to the prestress system and locally to congestion within the joint.

6.2 SUBASSEMBLY DEVELOPMENT

6.2.1 Construction considerations

For the class of modular precast building depicted in Figure 6-1, special attention was given to the manner in which the building would be constructed. The beam and column elements were designed to be precast, with limited concrete placement required on-site. If fully precast members are used, tolerances need to be considerably tighter and special shear key devices are be needed to lock the beam to the columns. To avoid this, this research adopted a cast insitu closure pour provided at one end of each beam. This was adopted for several reasons: (i) tolerances can be considerably less than fully precast members; (ii) the closure pour provides an access point for coupling the prestress thread-bars and the damping devices; (iii) high performance concrete could be used in the high stress zone at the beam end. This closure pour thus becomes the primary focus for on-site erection. Within this region the LE damper in each beam would be coupled to a threaded rod anchored in the column, the prestress thread-bars become coupled to one another, and the channels are tightened against the face of the column.

The sequencing of this operation is illustrated for a generic building in Figure 6-2. In this case, one end of the beam is precast and the other requires a closure pour approximately 300mm in length. The precast beams would be installed in series, with the opposite face of the column free for access. In Phase I, the beam would be brought into position and propped. The thread-bars would be sheeted through the end of the far column and anchored at the end of the opposing column. The damper devices in the ends of the beam would be anchored to

the column by coupling the shaft of the damper to a threaded rod in the column, accessible from the exposed end of the column. The rods coupling the dampers would then be prestressed to accommodate slop in the elements by tightening the anchor bolts. This would help ensure the dampers engaged upon gap-opening, rather than first accommodating any slack in the anchor or coupler. Once the elements were in place, in Phase II the second beam would be craned into position. The exposed prestress thread-bars and damper threaded rod would be coupled at the end with the closure pour allowing access. On the opposite end of the beam, the next set of prestress thread-bars would be sheeted through the beam. A threaded rod would be sheeted through the column and coupled to the LE damper shaft at the end of the precast beam. This would then be anchored. This process would continue across each bay, and the system would be anchored off at the end. Finally, the threaded rods connecting the LE dampers should be grouted, to help develop the damper forces and eliminate the possibility of elongation within the rod.

6.2.2 Specimen Design

A 3D subassembly representing an interior joint on a lower floor of a ten storey building was developed. The location of the subassembly is given in Figure 6-1. The subassembly consisted of two beams cut at their midpoints and an orthogonal beam cut at its midpoint (the approximate location of the point of contraflexure), all framing into a central column. The orthogonal beam, referred to herein as the gravity beam, was designed for one-way precast flooring panels, as shown in the figure. The other two beams, referred to herein as the seismic beams, were designed for predominantly seismic forces. The dimensions of the prototype members were taken from previous research (Li, 2006); this corresponded to 850mm square columns, 700mm by 500mm beams, and a 3.6m storey height. The prototype joint was assumed to have a moment capacity of 500kNm (Arnold, 2004).

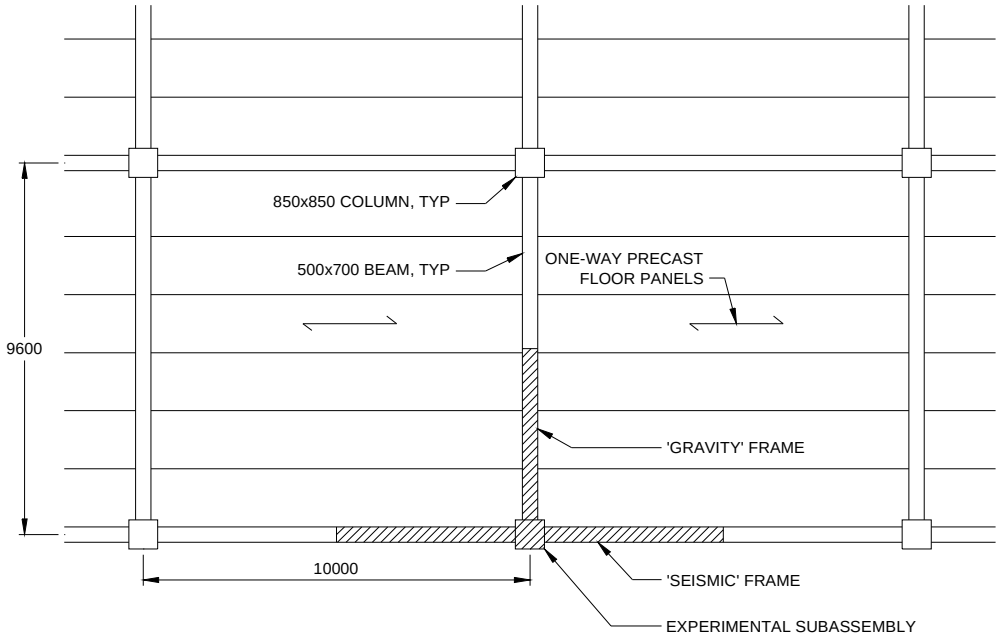

Figure 6-1: A plan view of the prototype structure, showing the location of the experimental subassembly.

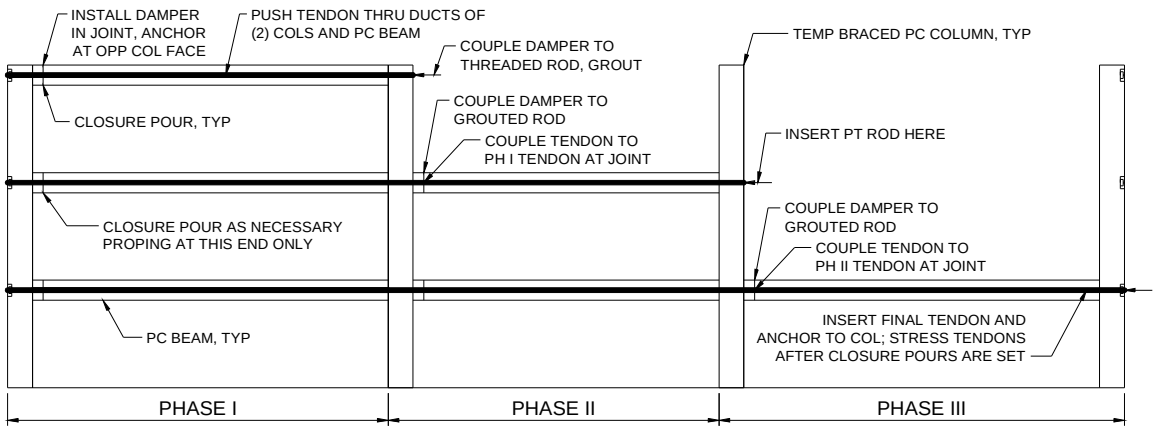

Figure 6-2: Possible construction sequencing scheme.

Given these constraints, the subassembly was scaled to 80 percent of the prototype building. The column was scaled to 700mm square and the beams scaled to 560mm by 400mm. A target longitudinal reinforcement ratio of 0.01 was taken for the column and the beams. Figure 6-3 illustrates the basic reinforcing layout for the beams. These members were designed for the expected strength of the rocking joint from the dissipation devices and the prestress and were intended to remain elastic. Four D20 (f_y = 500MPa) longitudinal threaded rebars (Reidbar^{TM}) were provided top and bottom, thus providing a moment capacity of ϕM_n = 260kNm. Due to the presence of axial load from prestress, minimal transverse steel requirements governed (Davies, 2003). HR12 (f_y = 500MPa) stirrups were provided in the beam at a spacing of half the beam depth (250mm) and a closer spacing at the ends (100mm). Additional transverse reinforcement was provided top and bottom 1.2m from the beam ends to confine the concrete in these high compression zones.

Two 45mm PVC ducts, spaced 200mm apart, were provided for the prestress system at the vertical centreline of the beams. Prestress was provided by two 26.5mm MacAlloy^{TM} thread-bars (f_y = 1100MPa). The prestress system in the seismic direction utilized a straight profile, along the longitudinal axis of the beams. This was adopted to ease congestion in the column and to provide a more constructible solution. The thread-bars in the gravity beam were draped to provide load balancing with the gravity loading from the one-way floor panels. This resulted in the thread-bar crossing the joint's centreline at a 30mm vertical offset. A photograph of the east beam reinforcing cage and the west beam cast insitu end is given in Figure 6-4 (a) and (b), respectively.

A 300mm cast insitu 'wet' joint was provided at the end of each beam. The detailing strategy of the cast insitu joint in the seismic direction is illustrated in Figure 6-5. This joint was designed to accommodate the LE damper with maximum dimensions of 150mm by 150mm. This space was provided in the centre of the joint in the seismic beams, and at a

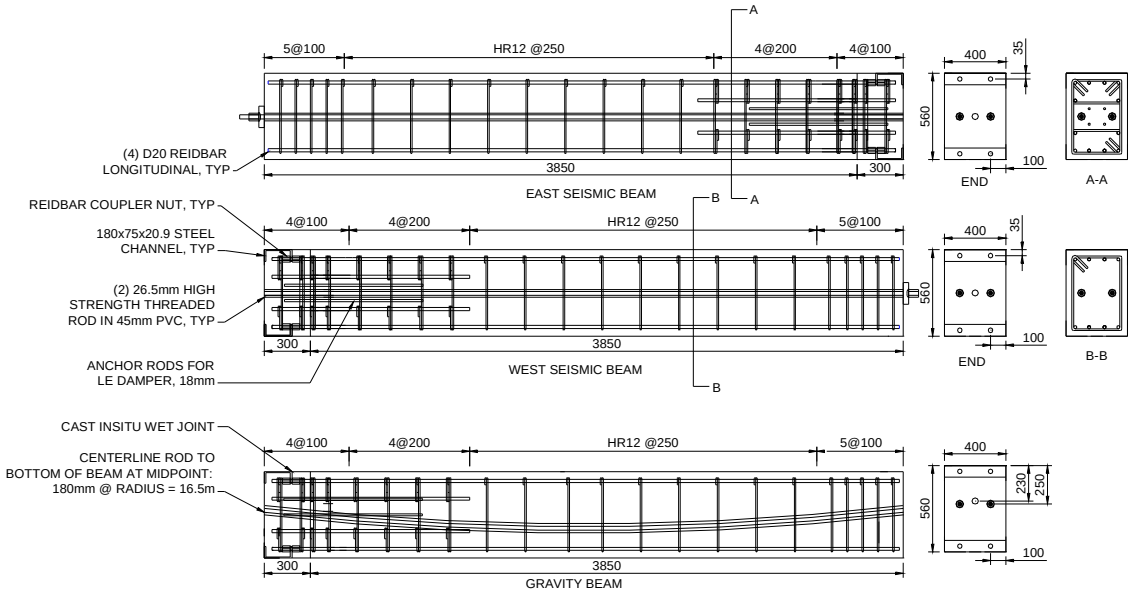

Figure 6-3: Reinforcing details of the beams.

(a) (b) (c)

Figure 6-4: Photographs of the specimen: (a) the west beam reinforcing; (b) the precast east beam cast insitu end; (c) the reinforcing in the column joint.

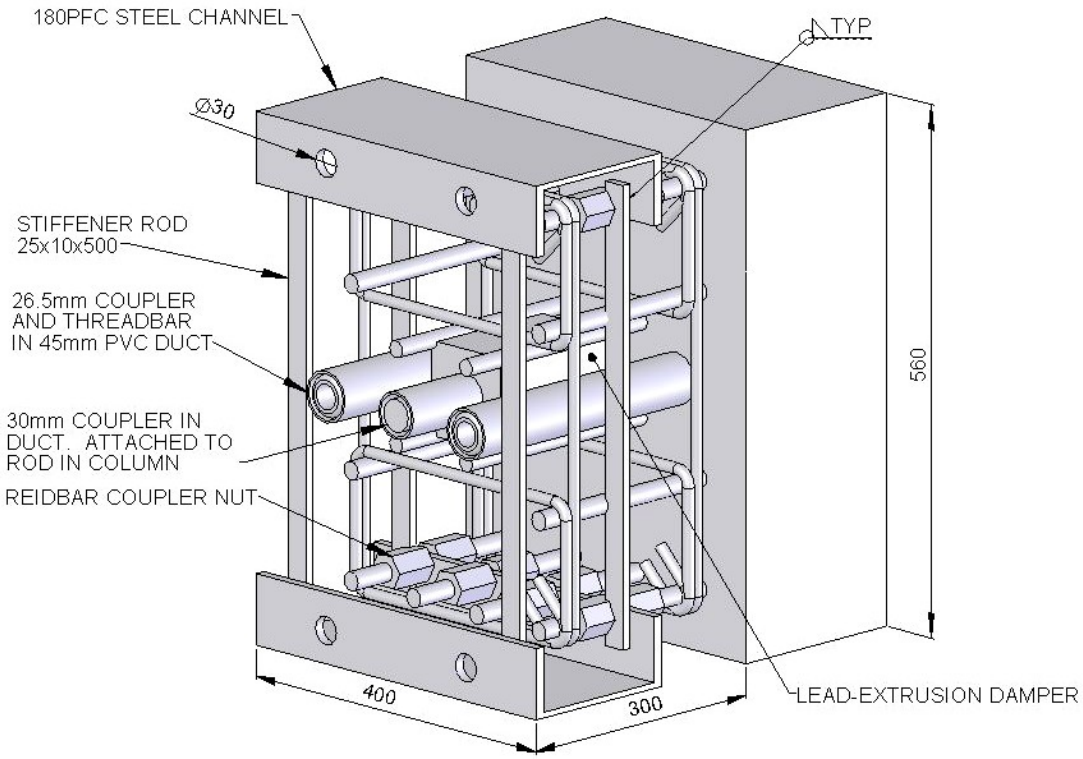

Figure 6-5: Details of the cast-insitu joint of the beam.

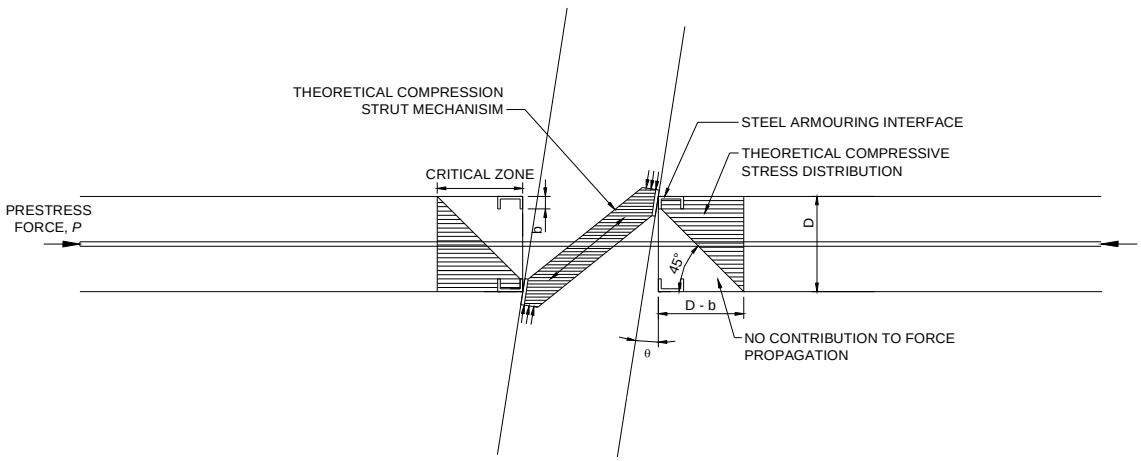

Figure 6-6: Theoretical stress distribution in the high stress zone.

50mm offset from centreline in the gravity beam. A 180PFC channel was used top and bottom to provide the armouring contact surface. This channel was designed so that the expected compression force at the design moment of the joint would be sufficient to prevent crushing of the concrete behind the channel. As illustrated in Figure 6-6, this force was assumed to further propagate through the beam at a 45 degree angle (Davies, 2003). The maximum compressive force was found by:

$$C = P_{diss,\max} + P_{PT,\max} \tag{6-2}$$

where C = total compression point load at the rocking edge; $P_{diss,max}$ = maximum force expected from the dissipation devices (250kN); and $P_{PT,,max}$ = maximum force expected from the prestress (800kN). Therefore the maximum force expected at the rocking joint was 1050kN.

The channels also served as a means of mechanically developing the longitudinal reinforcing. This was accomplished by providing cuts on the interior flange whereby the threaded longitudinal steel could be locked into the channel using nuts. Furthermore, these nuts provided a means of racheting the channel flush with the column face during on-site fabrication. Four 25x10x500mm rods were welded in the corners of each flange. These were provided to help stiffen the joint region to ensure rocking behaviour occurred in a rigid manner. Finally, four 1m threaded rods were spaced at 100mm centres to provide an attachment and anchoring point for the LE damper device.

Shear from gravity and seismic loads were carried by four 30mm shear keys located at each corner of the connecting beam. In the beam, two 30mm holes were drilled in the top and bottom flange to provide a female attachment for the shear keys. The shear keys were tapered inward 5 degrees to prevent binding with the beam during connection opening. In the column, these shear keys were designed to be screwed into a nut located behind a hole in the column's steel plates.

Figure 6-7 illustrates the reinforcing layout in the column. A longitudinal reinforcement ratio of 0.01 was provided by 12 D20 (f_y = 500MPa) longitudinal reinforcing bars. HR12 (f_y = 500MPa) stirrups were provided at a spacing of 250mm. The stirrups were doubled and the spacing was halved within the joint region. A large contribution to shear resistance was provided by the core concrete, due to the axial load in the column. The stirrups in the joint were designed considering the expected overstrength of the rocking connection, given the shear demand illustrated in Figure 6-8. Note that due to the unbonded prestress, there is no shear contribution from longitudinal steel, thus the shear demand in the column joint is primarily a result of the compression point loads due to rocking.

One of the primary objectives of this study was to improve the beam-column joint detailing by improving constructability and reducing materials compared to past designs (Li, 2006). In the column, this was accomplished in several ways, as illustrated in Figure 6-9: (i) the column contact plates were reduced from a single full depth plate to two end plates; (ii) the prestress ducts ran straight, rather than angled, in the joint, thus reducing congestion; (iii) the internal dampers in the beam were connected using a single rod with grouting tubes. The column end plates were sized to provide a full contact surface for the beam's armouring, and to provide a 10mm extension on all sides. This plate was then checked to ensure concrete crushing in the column did not occur at the design strength of the connection. The plate was developed into the core of the joint using weld studs. A photoghraph of the reinforcing in the column is given in Figure 6-4(c).

6.2.3 Specimen construction

The specimen was constructed in several parts. Firstly, the two seismic beams were caged with a cast insitu end on each, as shown in the photograph of Figure 6-10(a). This required providing stubs for the longitudinal steel, the ducts for the prestress system, and the threaded rods for the LE damper (Figure 6-4(b)). Next, the gravity beam and column were

caged and cast. The gravity beam required the drape profile to be located. Note that the damper and tendons were offset from centreline by 30mm and 50mm respectively due to clashes in the column with orthogonal ducts.

The column longitudinal reinforcement was welded to a 20mm steel plate top and bottom. The steel contact armouring plates at the joint were developed into the concrete by two 100mm welds studs welded against the back of each plate. A 50mm recess was provided at the column anchoring ends of the LE damper duct to allow easy bolt clearance. Drossbach tubing was used for the LE damper ducts, with grout tubes provided at each end..

Once the precast elements had sufficiently cured, they were craned into position. The remaining elements were installed so that the final closure pour could be made; this can be seen in the photographs provided in Figure 6-10. Within the closure pour, the damping devices were attached to the threaded rods in the beam. The shaft of the damper was coupled to the threaded rod in the column. The rod in the column was anchored back against a steel washer in the recess on the column face. With the dampers in place, they were prestressed by hand tightening the bolts anchoring the damper to the beam. These bolts can be seen in Figure 6-10(a). The LE damper shaft, coupler, and column threaded rod were all encased in a duct and waterproofed from the concrete. Once the damper was in place the prestress thread-bars were coupled together (Figure 6-10(b)) and encased in ducts (Figure 6-10(c)). Meanwhile, the channel top and bottom was tightened back against the face of the column and locked in place with the longitudinal steel nuts. Finally, a thin sheet was used to provide a barrier between the wet concrete and the column face. This ensured no bonding would occur between the concrete. Note that this measure may not be necessary, since the tensile capacity of the concrete would be negligible. This step was taken merely as a precaution.

A high performance concrete mix was used for the three closure pours. This mix was designed to provide good workability and high strength. Steel fibres (2 percent by weight)

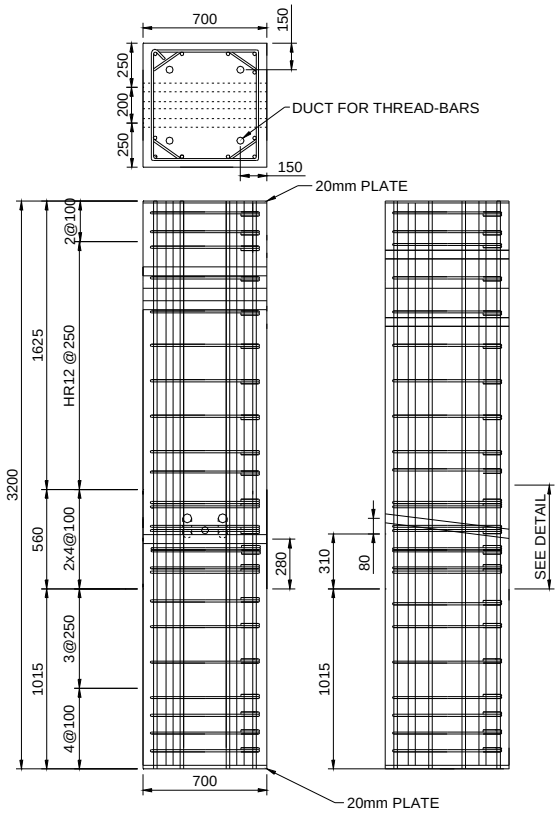

Figure 6-7: Reinforcing details of the column.

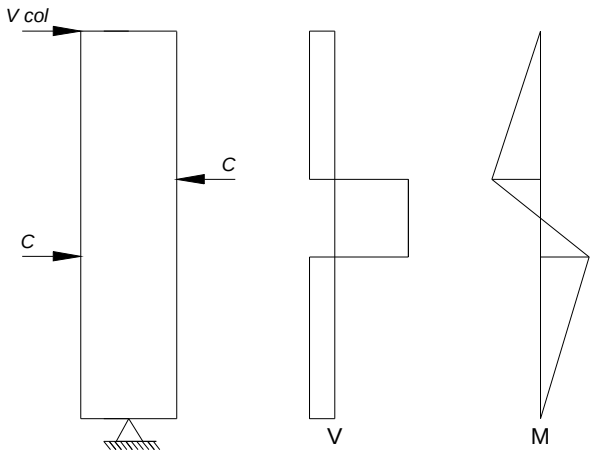

Figure 6-8: The shear and moment demand in the column, given a lateral force, V_{col}.

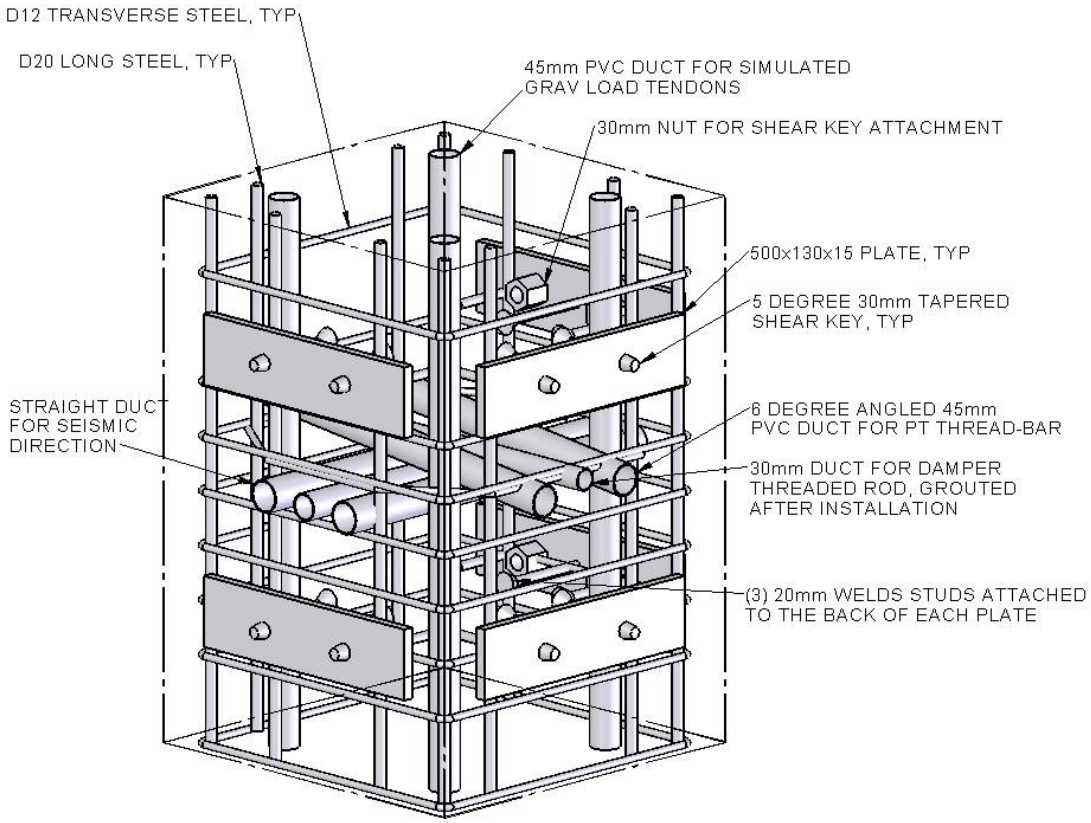

Figure 6-9: Reinforcing in the joint region of the column.

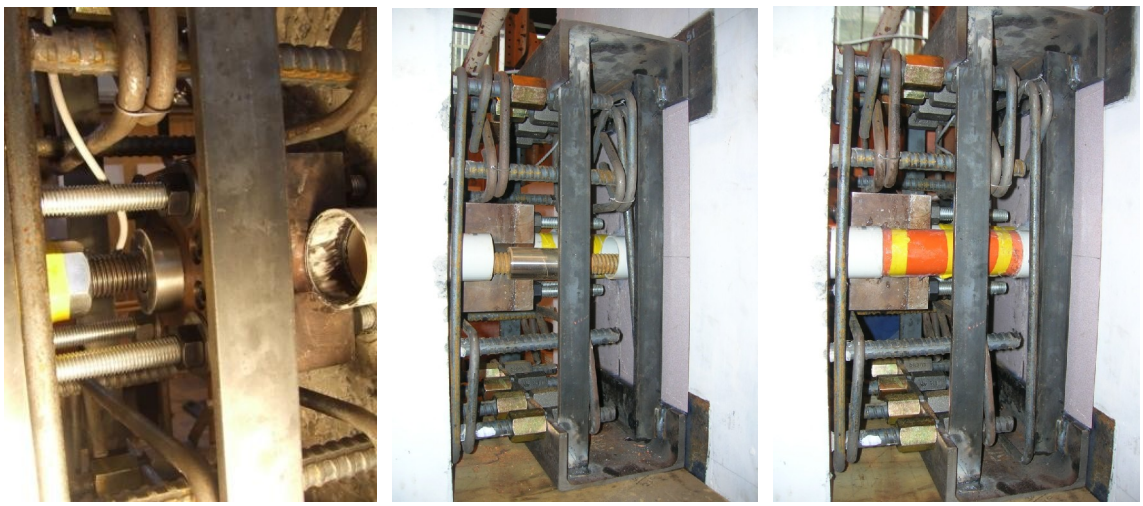

(a) (b) (c)

Figure 6-10: Photographs of the cast insitu joint showing (a) the east beam with the thread-bar exposed; (b) east beam with the thread-bar enclosed in PVC; (c) the west beam showing the damper and coupler.

were incorporated into the mix to help impede crack propagation. This concrete had on average a 28-day compressive strength of 76MPa. The average 28-day strength of the regular concrete was observed to be 50MPa.

6.2.4 The lead-extrusion dampers

Supplemental damping was provided by LE dampers designed in conjunction with the Mechanical Engineering Department at the University of Canterbury (Rodgers, 2006). Several placement options of these devices were considered, including: (i) one damper in the column; (ii) one damper in each beam at centreline; (iii) two dampers in each beam at top and bottom. The second option was chosen because it was considered simpler to install the dampers in the beam than the column. Although two dampers top and bottom may provide better energy dissipation from a longer stroke, a single device would be considerably cheaper than two. Thus, a single LE damper was designed to fit in the centre of the joint. This device is illustrated in Figure 6-11 and photographs are given in Figure 6-12. The device was designed to fit within a 150x150mm square area, at the centre of the beam section. A 30mm rod with one threaded end was used as the damper shaft. This rod was designed to be coupled to a threaded rod in the column of the same size. Four 18mm (f_y = 300MPa) threaded rods at 100mm centres were cast into the precast beam and used to anchor the device within the closure pour. The attachment holes on the devices were oversized to 25mm to allow the device to be adjusted when coupled to the threaded rod in the column.

To ensure the system re-centres, the expected negative moment contribution from the LE damper in compression should not exceed the expected positive moment contribution from the prestress. In other words:

$$\phi M_{PS,i} \geq \Omega_{diss} M_{diss} \tag{6-3}$$

where $M_{PS,i}$ = moment contribution at the joint from the initial prestress force; M_{diss} = moment contribution at the joint from the energy dissipation devices in compression; Ω_{diss} =

overstrength factor of the dissipation devices (taken here Ω_{diss}=1.5); ϕ = understrength factor for the prestress (taken as ϕ=0.85). Rearranging these terms gives a ratio of the moment contribution from prestress and dissipation devices:

$$\lambda = \frac{\phi M_{PS,i}}{\Omega_{diss} M_{diss}} > 1 \qquad (6\text{-}4)$$

Nothe that to ensure the system re-centres, $\lambda > 1$. Given the initial prestress force is 250kN per thread-bar, the dampers were designed for a 250kN yield force. This corresponds to λ = 1.23 and 1.06 in the NS direction for positive and negative moment, respectively, and λ = 1.13 in the EW direction.

Figure 6-13 presents the force-displacement response of the three damping devices. Devices 1, 2 and 3 were installed in the west, east and south joints of the specimen, respectively. Testing of the LE devices was performed using an Avery^{TM} testing machine. The devices were tested by applying a compressive force to the damper shaft while fixing the steel encasing. Once the device reached the end of its stroke, it was flipped and the shaft was compressed in the opposite direction. A linear potentiometer was installed on the steel encasing to measure the displacement of the shaft. As apparent in the figure, the devices provide similar response. The average yield force of the devices is approximately 270kN. One of the devices exhibited a fairly sharp yield point, with an initial stiffness of 400kN/mm. The other two devices had the same initial stiffness until about 50 percent of the yield force at which point the stiffness dropped to about 100kN/mm. This can be attributed to voids forming within the lead as the shaft progressed through several strokes. A thorough discussion addressing this and other aspects of the devices' behaviour can be found in Rodgers (2006).

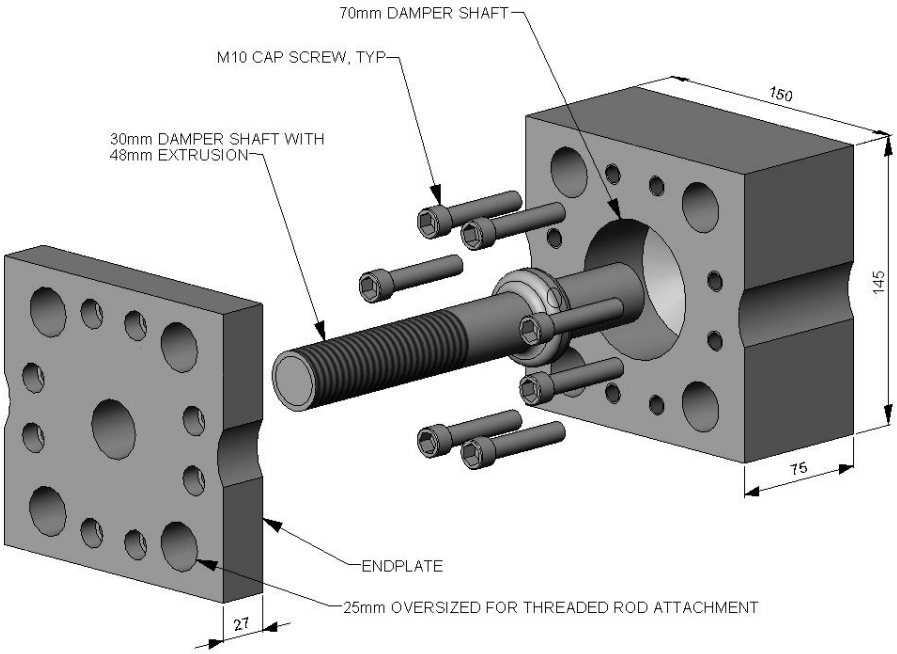

Figure 6-11: Details of the lead-extrusion damper

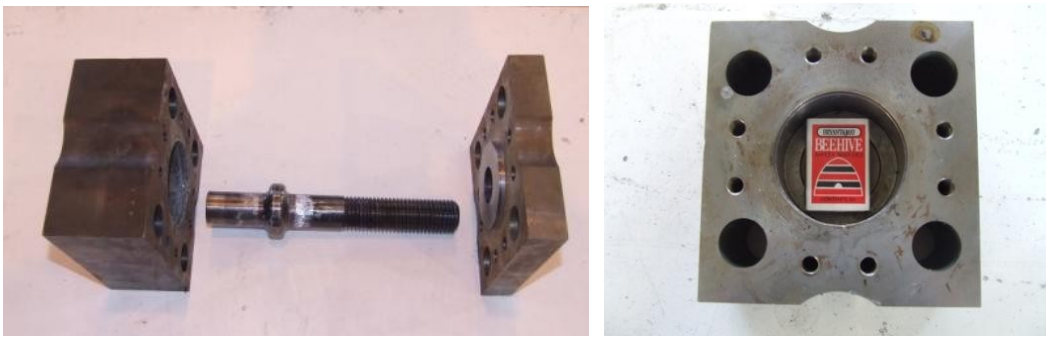

(a) (b)

Figure 6-12: The lead-extrusion damper showing (a) the disassembled device and (b) the lead cavity.

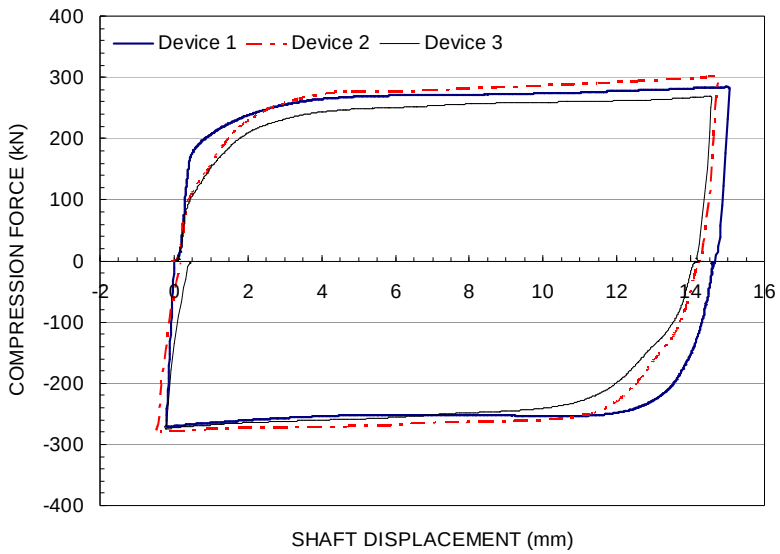

Figure 6-13: Force-displacement response of the lead-dampers.

6.3 PREDICTED RESPONSE

To arrive at the force-displacement response of the subassembly, first the moment capacity of the joint was assessed. By assuming the members behave in a rigid manner, the moment arm can be taken from the edge of the beam, summing each contribution independently:

$$M = \sum M_{PS} + \sum M_{diss} \tag{6-5}$$

given that

$$M_{PS}^{\pm} = P_{PS} e_{PS}\,;\; M_{diss}^{\pm} = P_{diss} e_{diss} \tag{6-6}$$

where e_{PS} = the distance of the from the edge of the beam (280mm in the EW direction, 310mm and 250mm in the NS direction); e_{diss} = the distance of the dissipation device from the edge of the beam (280mm in the EW direction, 330mm and 230mm in the NS direction); P_{PS} = the force in the thread-bars, and P_{diss} = force in the dissipation device. The force in the thread-bars was found by:

$$P_{PS} = P_i + \frac{A_{PS} E_{PS}}{L_t} e_{PS} \theta_{con} n \tag{6-7}$$

where P_i = initial post-tensioning force (250kN); E_{PS} = elastic modulus of the thread-bar (170,000MPa); A_{PS} = cross sectional area of the thread-bar (552mm^2); L_t = unbonded length of the thread-bar (9m); θ_{con} = connection rotation; and n = number of joint openings spanned by the thread-bar (taken as 2 in the EW direction and 1 in the NS direction).

The prediction given in Chapter 4 was calculated assuming the mild steel dissipation devices yielded at the onset of gap opening. Although this was valid in that case, it does not apply to the LE dampers; the stiffness contribution must be considered. The force in the LE dissipation device was found by:

$$P_{diss} = \min \begin{vmatrix} K_{diss} e_{diss} \theta_{con} \\ P_{y,diss} \end{vmatrix} \tag{6-8}$$

where K_{diss} = stiffness of the dissipation device (200kN/mm, taken as an average of the three devices) and $P_{y,diss}$ = yield force of the dissipation device (250kN).

Given the response of the joint, it is possible to identify when the connection begins to open, where the dissipation devices yield, and when the prestress thread-bars yield. In the case of the connection opening, this is assessed by considering the contribution of the initial prestress alone to the moment capacity of the joint. The point at which the dissipation devices yield can be found by setting $P_{diss} = P_{y,diss}$ and solving Equation (6-8) for θ_{con}. Finally, the onset of yielding of the prestress thread-bars can be calculated given Equation (6-7) knowing the yield force of the bars ($P_{PS,yield}$ =650kN).

Given a moment-curvature analysis, the force-displacement response of the subassembly can be evaluated. In the EW direction, the horizontal force at the top of the column, V_{col}, can be found given the moment at the joint by:

$$V_{col} = 2M \frac{L}{L_b L_c} \tag{6-9}$$

where L = length of the beam to centreline of the column (9.8m); L_b = clear support length of the beam (9.1m); and L_c = storey height (2.8m).

The total top displacement of the system given V_{col} can be attributed to localised rotation at the joint and the total elastic deformation of the system:

$$\Delta = \Delta_{elastic} + \theta_{con} \frac{L_b}{L} L_c \tag{6-10}$$

where $\Delta_{elastic}$ is the elastic deformation of the system from flexure. This is defined using the moment area theorem given in Chapter 1 by:

$$\Delta_{elastic} = \frac{V_{col,uplift}}{12} \left[\frac{(L_c - D)^3}{EI^*_{col}} + \frac{L_c^{\,2} L_b^{\,3}}{L^2 EI^*_{bm}} \right] \tag{6-11}$$

where EI^*_{bm} and EI^*_{col} are the effective stiffness of the beam ($0.25EI_{bm,\,gross}$) and column ($0.6EI_{col,\,gross}$), respectively; and D is the depth of the beams (560mm).

The predicted response of the subassembly in the NS and EW direction is given in Figure 6-14. The required moment capacity of the joint (256kNm) was achieved when the column was at a drift of 1 percent. This was due to the initial prestress force and the full

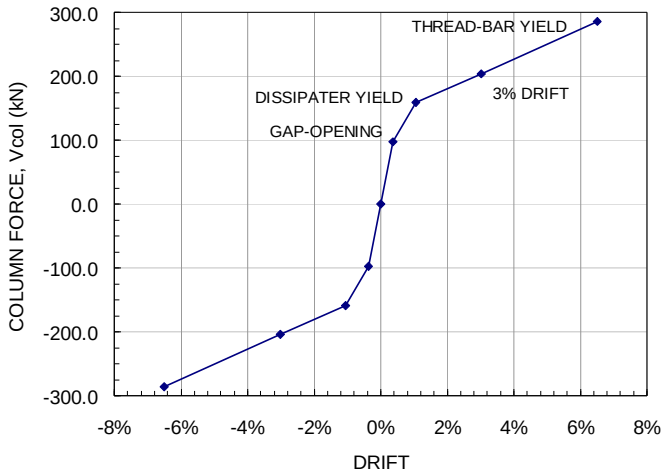

(a)

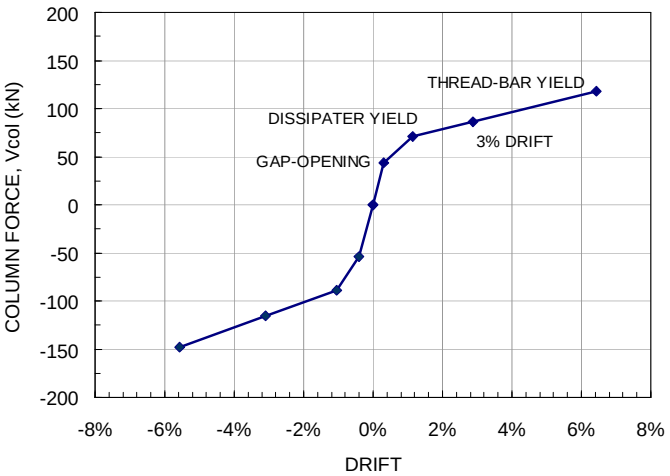

(b)

Figure 6-14: Predicted force-displacement response of the subassembly in the (a) EW and (b) NS direction.

strength of the energy dissipation devices. The localised rotation at the joint at onset of yielding of the prestress thread-bars was found to be 0.052 in the EW direction and 0.53 and 0.43 in the positive and negative NS direction, respectively. This corresponded to a column drift of 6.4 percent in the EW direction and 6.5 and 5.6 percent in the NS direction.

6.4 TEST SETUP

The test setup adopted for this study is almost identical to the setup described in Chapter 4. Figure 6-15 gives a plan view of the test setup, showing the location of the three actuators and the potentiometers located around the specimen. Figure 6-16 gives a south and east elevation view of the test setup, showing the location of the inclinometers and potentiometers. The column was pinned to the floor using a universal joint, additional pins were provided on the struts of each beam. Actuator A and B were located at the top of the east and south face of the column, respectively. Actuator C was located orthogonal to the west face of the gravity beam, in line with the gravity beam's strut. This actuator was primarily used to stabilize the specimen. Rotary potentiometers were installed against the opposite face of each actuator. An additional actuator was installed at mid height of the gravity beam to simulate the presence of precast one-way floor panels. This load was spread over a 1.5m timber block. The load was applied at a constant force of 120kN. The base of the column was pinned with a universal joint, allowing free rotation in both the EW and NS direction. The strut of each beam was pinned, with a load cell located in series.

At one end of each prestress thread-bar anchor, load cells were installed to measure the forces in the thread-bars. Four 32mm high strength thread-bars located along the longitudinal axis of the column were each stressed to 500kN to simulate a total axial load of 2000kN ($0.1f'_cA_g$). Nine rotary potentiometers were installed at various locations around the specimen to measure localized displacement (see Figure 6-15). At each face of the joint, three linear potentiometers were installed 60mm from the top and bottom of the beams, and at the

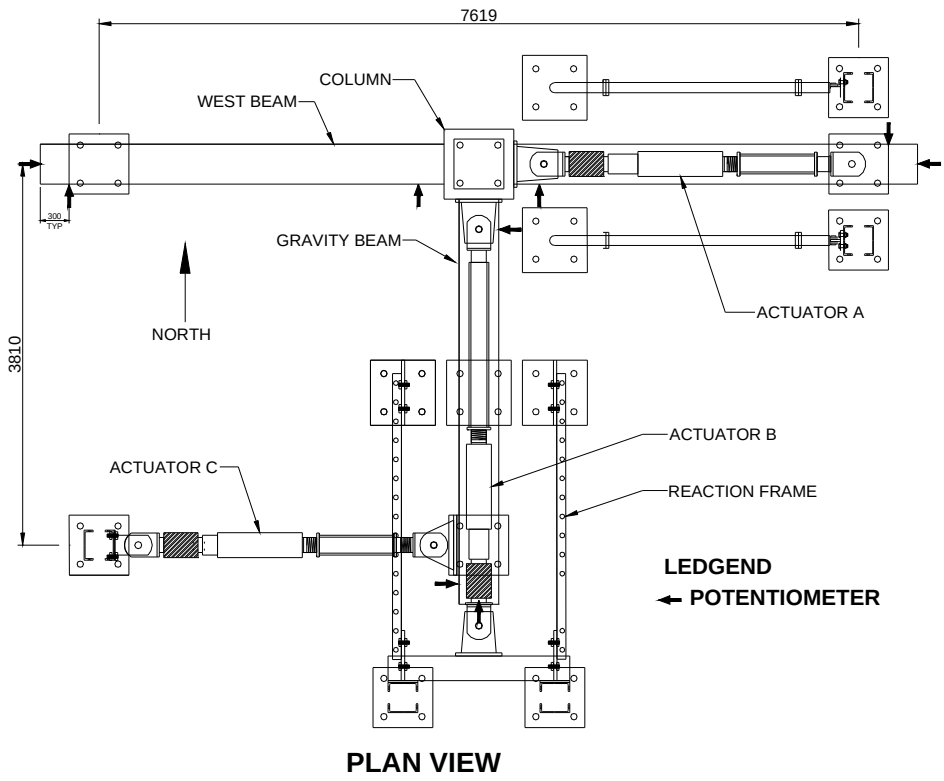

Figure 6-15: Plan view of the bi-directional test setup.

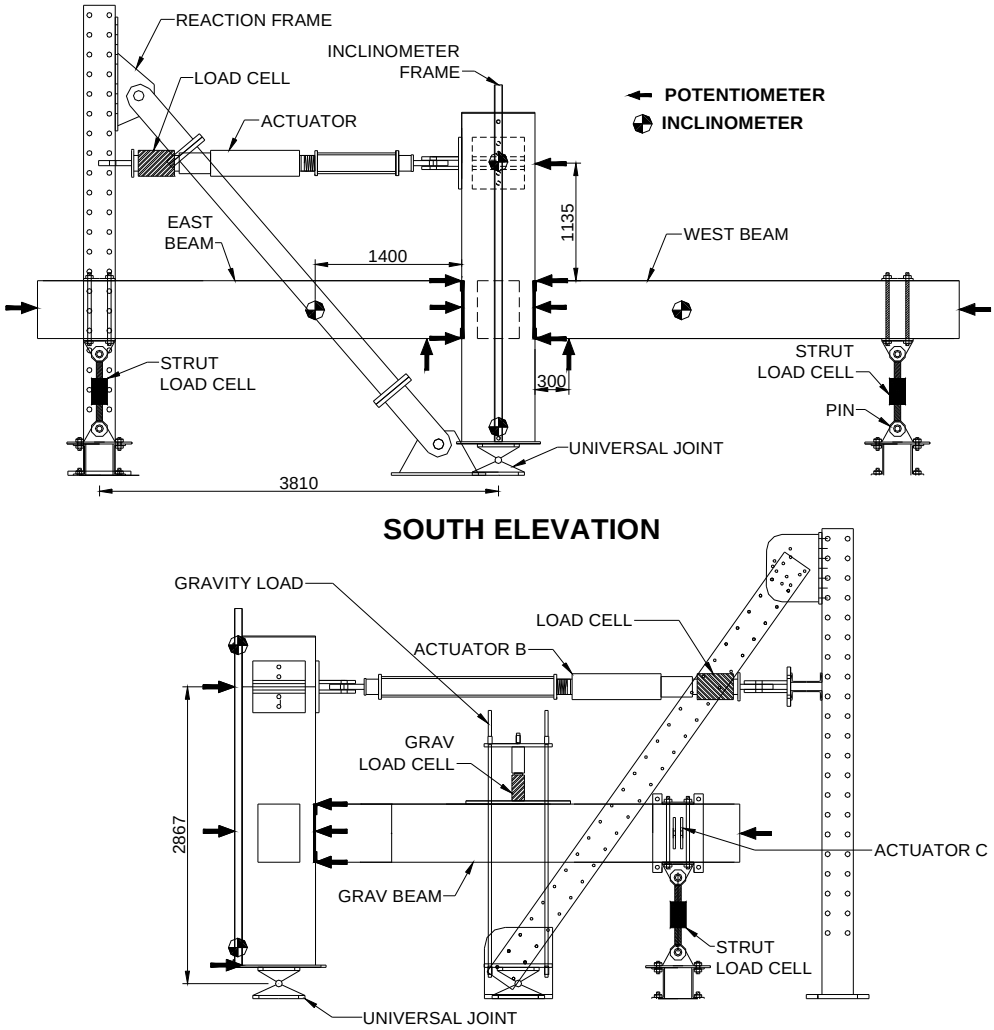

Figure 6-16: South and east elevation view of the test setup.

Figure 6-17: Photograph of the specimen in the testing apparatus.

beam's centreline. Two linear potentiometers were installed underneath each beam to measure any relative movement of the beams along the column face. Within the joint, each coupler connecting the shaft of the LE damper to the threaded rod in the column was converted to a load cell, consisting of eight strain gauges compensating for bending and temperature effects. Four strain gauges were placed on the top and bottom web of the east beam's armouring channel. These were installed to detect potential yielding of the plates upon gap-opening. A photograph of the specimen in the testing apparatus is given in Figure 6-17.

6.5 TEST METHODS

A similar testing strategy was adopted for this specimen as introduced in Chapter 4. This consisted of displacement controlled uni-directional and bi-directional testing. Two methods were adopted: (i) *quasi-static* (QS) testing using cyclic loading patterns; and (ii) *quasi-earthquake displacement* (QED) (Dutta *et al.*, 1999) tests consisting of loading patterns taken directly from dynamic analysis of an analytical model of the prototype structure. The latter method is intended to produce displacement profiles more representative of expected seismic response.

6.5.1 Quasi-static displacement profiles

Preliminary (low drift level) quasi-static tests provided a benchmark from which the behaviour of the specimen was characterized analytically for the QED test. Owing to the damage-free nature of the specimen, it was possible to conduct a few preliminary tests without damaging the specimen. This consisted of uni-directional tests with two cycles at 0.5 percent drift and 1.4 percent drift. This pattern was adopted primarily to capture the behaviour of the specimen and verify the calculated prediction without subjecting it to an excessive number of cycles which may begin to degrade the specimen or the LE damper devices. A drift of 1.4 percent was chosen because it equated to a maximum radial drift of 2

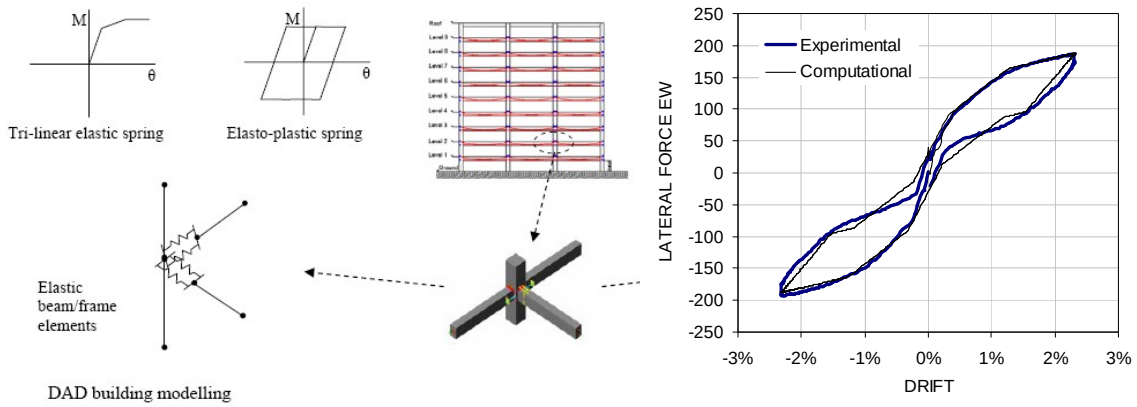

(a) (b)

Figure 6-18: Calibration of the analytical model to experimental data: (a) the modelling procedure adopted; (b) force-displacement response in the EW direction: (Bradley *et al.*, 2006a).

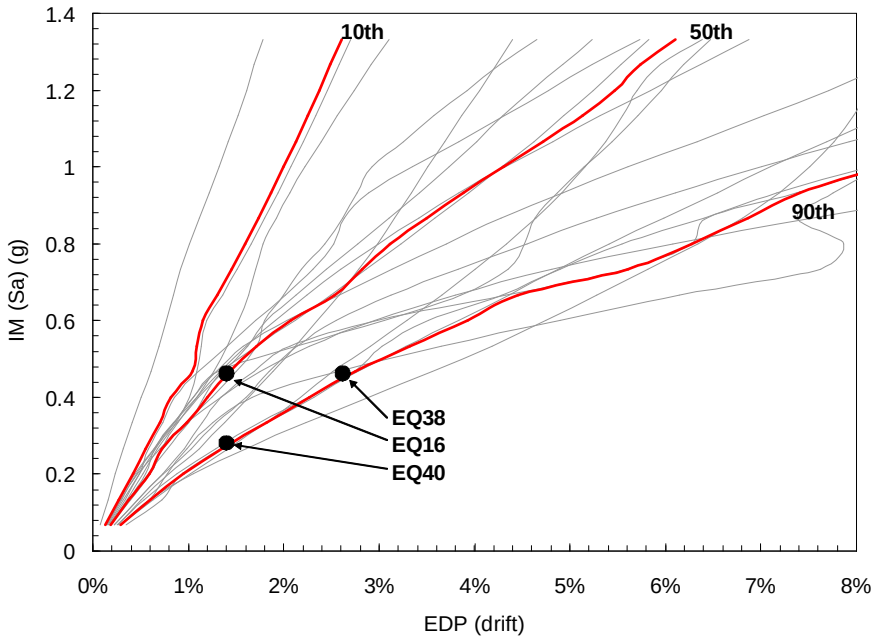

Figure 6-19: Results of Incremental Dynamic Analysis in the EW direction, showing the earthquake records selected for QED testing (Bradley *et al.*, 2006a).

percent, considering displacement in both the EW and NS direction. This allowed a comparison to be made between the uni-directional and bi-directional behaviour of the specimen. Therefore, the next test consisted of the bi-directional "four-leaf clover" cycles to 0.5 percent and 2 percent drift. Finally, two additional uni-directional tests were performed with once cycle at 2.3 percent (equivalent to a radial drift of 3 percent) to verify the energy dissipation provided by the specimen at higher displacement.

Further QS testing was carried out following the completion of QED testing. This consisted of three tests: uni-directional tests in both directions to a maximum drift of 3 percent (equivalent to a radial drift of 4 percent), and a bi-directional test to a maximum (radial) drift of 4 percent.

6.5.2 Quasi-earthquake displacement testing

The QED testing method is intended to serve as a more realistic testing protocol, capturing the behaviour of the specimen under 'real' earthquake ground motion. This has three advantages: (i) unlike QS testing which uses controlled cyclic displacements in ascending order, QED testing will capture small loading cycles following severe displacement demand from initial pulses; (ii) P-Δ effects can be considered in the analytical model, thus capturing any non-uniform displacement due to excessive yielding in a single direction; (iii) the behaviour of the specimen subject to QED displacement profiles can be extrapolated to infer likely damage at multiple levels of excitation.

The data generated from the QS tests was used to create an equivalent analytical model of the specimen. This is illustrated in Figure 6-18, showing the modelling strategy adopted and the hysteretic response in the EW direction. Modelling of the prototype structure was conducted in parallel to this study by a co-researcher; details of the development of the 3D analytical model are given elsewhere (Bradley *et al.*, 2006a). Elasto-plastic and bi-linear elastic springs were used to represent the behaviour of the dampers and prestress at the joint,

respectively. The natural period of the structure was found to be 1.5s. Soil-structure interaction was not considered. With the development of a reliable analytical model of the structure, it was then possible to generate a displacement profile at the node of interest which could be used for physical testing. This required the identification of earthquakes likely to represent various levels of demand, considering both rare and relatively frequent earthquakes. A procedure described by Dhakal *et al.* (2006) was adopted to define three key earthquake records representing multiple levels of seismic demand. This procedure, termed a *Multi-level Seismic Performance Assessment* (MSPA) (Bradley *et al.*, 2006b) consists of performing an *Incremental Dynamic Analysis* (IDA) (Vamvatsikos and Cornell, 2002) to identify the response of the structure from various earthquakes. Using this data, earthquakes representing percentile levels at various intensities can be identified and used for subsequent analysis.

Assuming a firm soil site in Wellington, New Zealand (a high seismic zone) three levels of demand were identified following recommendations given in Dhakal *et al.* (2006). These demand levels were: (i) a 90^{th} percentile *design basis earthquake* (DBE); (ii) a 50^{th} percentile *maximum considered earthquake* (MCE); and (iii) a 90^{th} percentile MCE. The DBE and MCE were defined as an earthquake with a return period of 475 years (10% in 50 years) and 2475 years (2% in 50 years), respectively. For the site of interest, this corresponds to a *peak ground acceleration* (PGA) of approximately 0.4g and 0.8g for the DBE and MCE, respectively, based on the seismic hazard model presented in Stirling *et al.* (2002). Given these levels of demand, several performance objectives can be defined. Following current trends, each level was related to serviceability and life-safety. For the 90^{th} percentile DBE, this corresponded to a high level of confidence that the structure would remain operational following an earthquake of that intensity. After the MCE it would be expected the structure is repairable with a moderate level of confidence (50^{th} percentile MCE) and would not collapse with a high level of confidence (90^{th} percentile MCE).

Earthquake records were selected from a suite of 20 candidates, representing both near-source (large initial acceleration pulses) and medium-source accelerograms, considering both the transverse and orthogonal components. These records are given in Table 6-1. Following current practice, the spectral acceleration (S_a) at the fundamental period of the structure was selected as the *intensity measure* (IM). Thus, the target PGA of 0.4g and 0.8g corresponded to a S_a of 0.27g and 0.48g at the structures fundamental period. The resulting IDA data is plotted in Figure 6-19, showing the 10^{th}, 50^{th}, and 90^{th} percentile fractal curves. The three selected records are noted in Table 6-1. These records corresponded to peak (radial) interstory drifts of 1.6, 1.6 and 2.8 percent for the 90% DBE, 50% MCE, and the 90% MCE, respectively.

6.6 EXPERIMENTAL RESULTS

For clarity, some experimental results have been omitted from this section. This section will present results from the QS testing first, followed by QED test results.

6.6.1 Quasi-static test results

The response of the subassembly in the EW and NS direction is given in Figure 6-20. In this test, the specimen was subjected to two displacement cycles each at column drifts up to 3 percent. The basic analysis method given by Equations (6-5) to (6-11), is plotted on top of the experimental results, showing good agreement. The method predicts the post-gap opening stiffness well. The initial stiffness of the system is slightly higher than observed experimentally. The calculated maximum lateral force at 3 percent drift is within 5 percent of the experimental result. Since the LE dampers exhibited non-linear response, with each damper being slightly different, it was difficult to capture the LE damper contribution; a linear approximation was used in conjunction with the basic analysis method. Actual test data suggests non-linear response, but the linear approximation seems to fit the experimental data well, though it tends to overestimate strength in the EW direction by about 20 percent. In the

Table 6-1: Earthquake records used for Incremental Dynamic Analysis (Bradley, 2006).

Ref	Event	Year	Station	M	R (km)	S_A (g)
1	Imperial Valley	1940	El Centro	6.9	10	0.136
2	Imperial Valley	1940	El Centro	6.9	10	0.041
3	Imperial Valley	1979	Array #05	6.5	4.1	0.210
4	Imperial Valley	1979	Array #05	6.5	4.1	0.180
5	Imperial Valley	1979	Array #06	6.5	1.2	0.172
6	Imperial Valley	1979	Array #06	6.5	1.2	0.210
7	Landers	1992	Barstow	7.3	36	0.180
8	Landers	1992	Barstow	7.3	36	0.093
9	Landers	1992	Yermo	7.3	25	0.074
10	Landers	1992	Yermo	7.3	25	0.470
11	Loma Prieta	1989	Gilroy	7	12	0.170
12	Loma Prieta	1989	Gilroy	7	12	0.160
13	Northridge	1994	Newhall	6.7	6.7	0.190
14	Northridge	1994	Newhall	6.7	6.7	0.097
15[2]	Northridge	1994	Rinaldi	6.7	7.5	0.083
16[2]	Northridge	1994	Rinaldi	6.7	7.5	0.110
17	Northridge	1994	Sylmar	6.7	6.4	0.280
18	Northridge	1994	Sylmar	6.7	6.4	0.021
19	North Palm Springs	1986	North Palm Springs	6	6.7	0.310
20	North Palm Springs	1986	North Palm Springs	6	6.7	0.210
21	Kobe	1995	-	6.9	3.4	1.323
22	Kobe	1995	-	6.9	3.4	0.685
23	Loma Prieta	1989	-	7	3.5	0.550
24	Loma Prieta	1989	-	7	3.5	1.310
25	Northridge	1994	-	6.7	7.5	0.810
26	Northridge	1994	-	6.7	7.5	1.010
27	Northridge	1994	-	6.7	6.4	0.700
28	Northridge	1994	-	6.7	6.4	1.241
29	Tabas	1974	-	7.4	1.2	0.502
30	Tabas	1974	-	7.4	1.2	0.560
31	Elysian Park	-	Simulated	7.1	17.5	1.330
32	Elysian Park	-	Simulated	7.1	17.5	0.930
33	Elysian Park	-	Simulated	7.1	10.7	1.010
34	Elysian Park	-	Simulated	7.1	10.7	1.343
35	Elysian Park	-	Simulated	7.1	11.2	1.694
36	Elysian Park	-	Simulated	7.1	11.2	1.730
37[3]	Palos Verdes	-	Simulated	7.1	1.5	0.850
38[3]	Palos Verdes	-	Simulated	7.1	1.5	1.223
39[1]	Palos Verdes	-	Simulated	7.1	1.5	0.690
40[1]	Palos Verdes	-	Simulated	7.1	1.5	1.370

[1] 90th percentile DBE; [2] 50th percentile MCE; [3] 90th percentile MCE

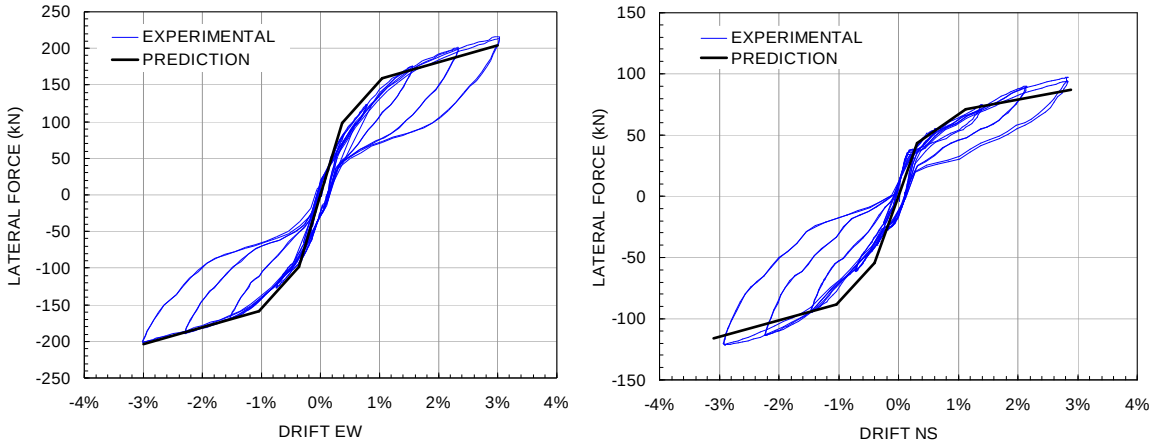

(a) (b)

Figure 6-20: Uni-directional testing to 3 percent drift: Force-displacement response from experimental testing and the hand method prediction: (a)EW direction and (b) NS direction

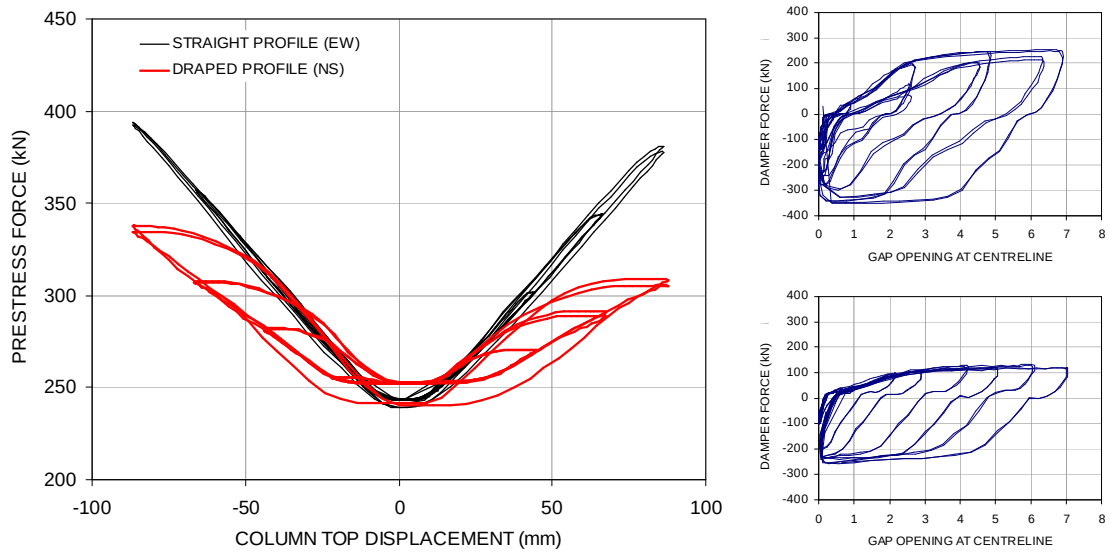

(a) (b)

Figure 6-21: Response of (a) the prestress and (b) the LE dampers in the gravity beam (top) and the east beam (bottom).

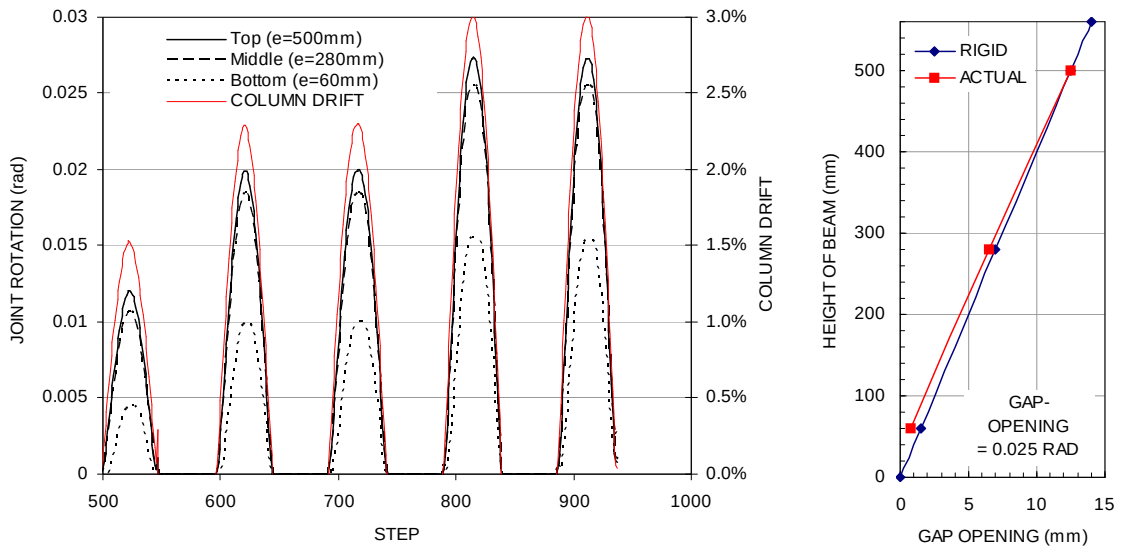

(a) (b)

Figure 6-22: Validation of the rigid-body assumption: (a) joint rotation of east beam measured at three locations along the joint; (b) comparison of rigid versus actual response of the connection. Data is taken from uni-directional QS testing in the EW direction.

(a) (b)

Figure 6-23: Photographs of the specimen after uni-directional QS testing: (a) the specimen at approximately 3 percent drift; (b) the west beam after completion of testing.

NS direction, the prediction was also good. In this case, it was also difficult to predict the contribution from prestress due to its draped profile. This is apparent from Figure 6-21(a) which shows the change in prestress force given column displacement. It is evident that friction between the duct and prestress thread-bars leads to energy dissipation not considered in the original design. This effect is minimised in the EW direction, where the straight ducts prevent the thread-bars from binding.

The basic analysis method assumes the moment arm can be taken from the edge of the beam, therefore it assumes rigid-body connection rotation. To validate this, the rotation of the east connection, as measured from three potentiometers across the joint, is given in Figure 6-22(a). The expected (rigid) opening of the joint and the actual behaviour for the joint at 0.025 radians is plotted in Figure 6-22(b). From these plots, it is apparent the rigid body assumption is reasonable. Connection rotation measured from the middle and top potentiometers varies about 10 percent, whereas the difference between the bottom and top potentiometers varies by about 50 percent. Thus, slight rolling of the connection occurred, although this was minimal.

In the EW direction, excellent hysteretic behaviour is apparent. The specimen does not suffer any noticeable stiffness or strength degradation, and exhibits stable hysteretic energy dissipation. The maximum recorded residual displacement was approximately 0.08 percent, 2.6 percent of the maximum drift of 3 percent. In the NS direction, the behaviour was also good. The specimen exhibits the same stable energy dissipation. The maximum residual drift in this case was recorded to be 0.12 percent, or 4 percent of the maximum drift. This is slightly more than the EW direction, and can be attributed to the draped tendon profile, where friction forces due to binding contribute to this effect.

Figure 6-21(b) shows the response of the LE damper in the east beam and gravity beam. This was recorded using the load cell attached to the coupler and the opening of the

joint recorded in line with the devices. Unfortunately, the load cell connected to the west beam LE damper was damaged during the test setup. Although the device was assumed to be working properly, no results are given for this device. The LE dampers performed reasonably well. In tension, the stiffness of the LE damper was somewhat reduced. This can be attributed to slop within the connecting elements, namely the damper, the threaded rod, and the LE damper itself. This caused the damper to respond to connection-opening much slower. For example, considering only the damper, the device should have reached yield at approximately 0.5mm of elongation. Instead, yield was not observed until 2.5mm of elongation. The east damper did not reach its target yield of 250kN. Instead it appears to yield at approximately 100kN. This may be the reason the initial prediction of response in the EW direction was overestimated. The revised stiffness of the devices, considering the sloppy connecting elements, was about 80kN/mm and 50kN/mm for the gravity and east joint, respectively.

Observed damage to the specimen was minimal. During testing, flexural cracks were detected in the beams, spaced at approximately 250mm. These cracks closed after testing. No flexural cracks were observed in the column. Up to 2 percent drift, virtually no cracking was observed in the joint region. Some small cracks, approximately 50mm in length were observed in the beam's corners from the end of the channel's flange. These cracks formed when this region was in compression from connection opening. Beyond 2 percent drift, some additional cracks were observed, but these were also minor. Again, most cracking was confined to the area around the steel armouring in the beam. No cracks were observed around the armouring in the column, nor were any diagonal shear cracks observed across the joint. No crushing was observed around the column's steel armouring. Upon the completion of testing, there was a prestress loss of about 10kN per thread-bar in both the EW and NS direction. A photograph of the specimen at a drift of 3 percent is given in Figure 6-23(a) and

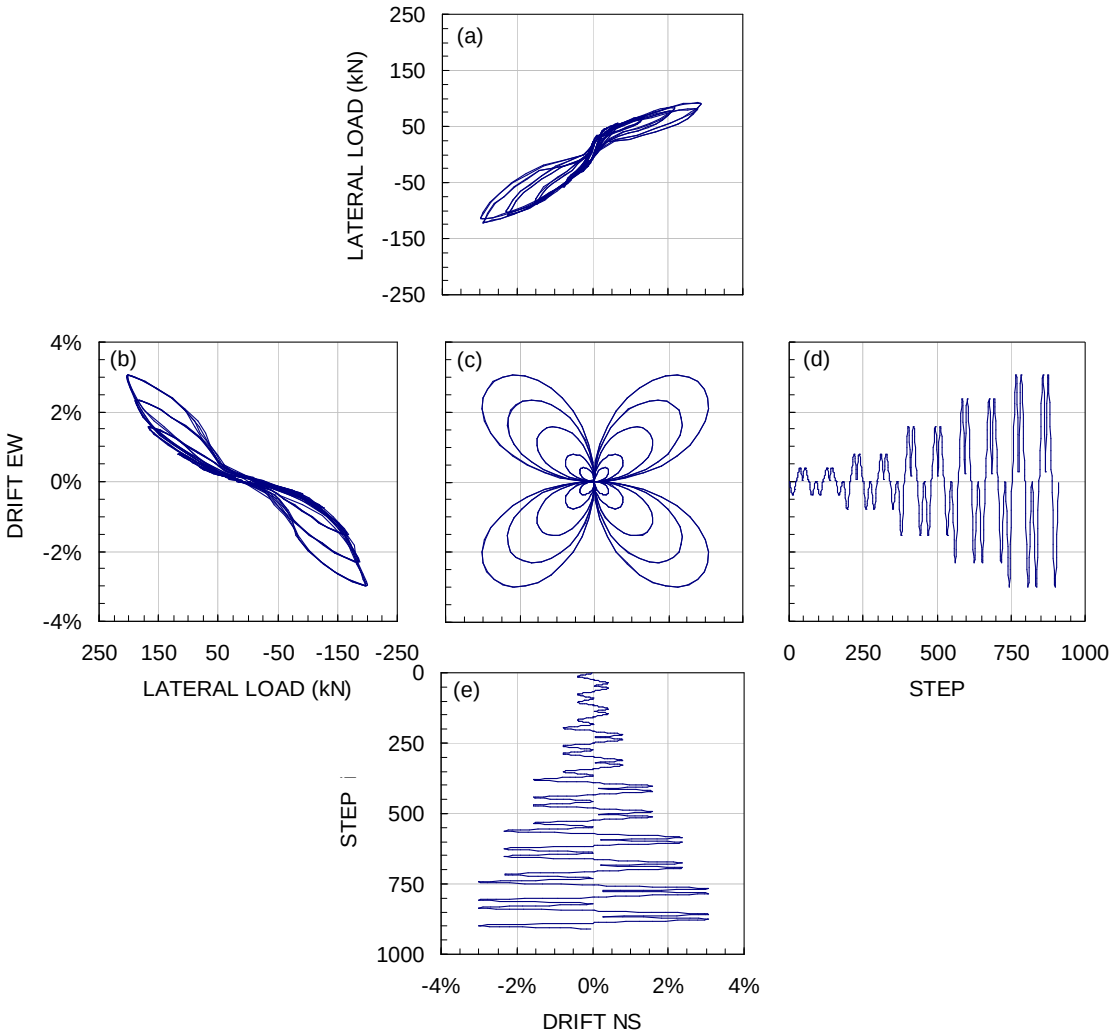

Figure 6-24: Bi-direction QS testing to 4 percent drift: (a) and (b) give the force-displacement response in the NS and EW direction, respectively; (c) shows a plan view of bi-directional orbit; (d) and (e) give the displacement profiles in the EW and NS directions, respectively.

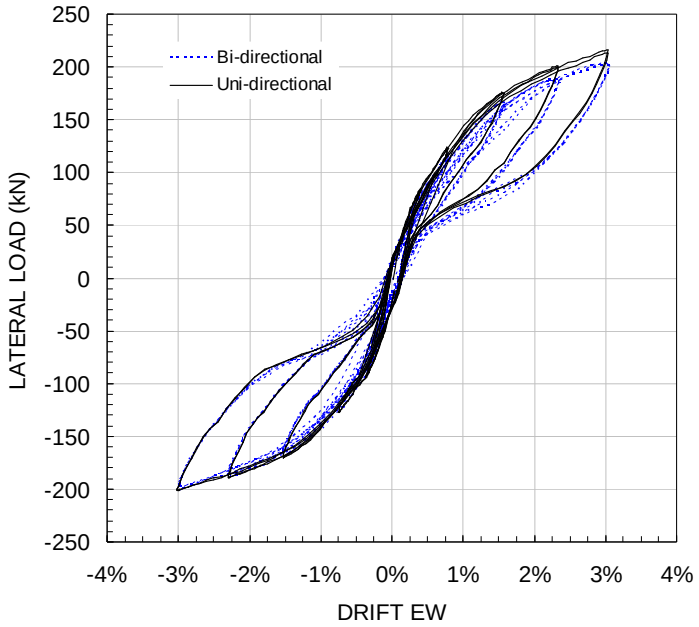

Figure 6-25: Comparison between bi-directional and uni-directional response in the EW direction.

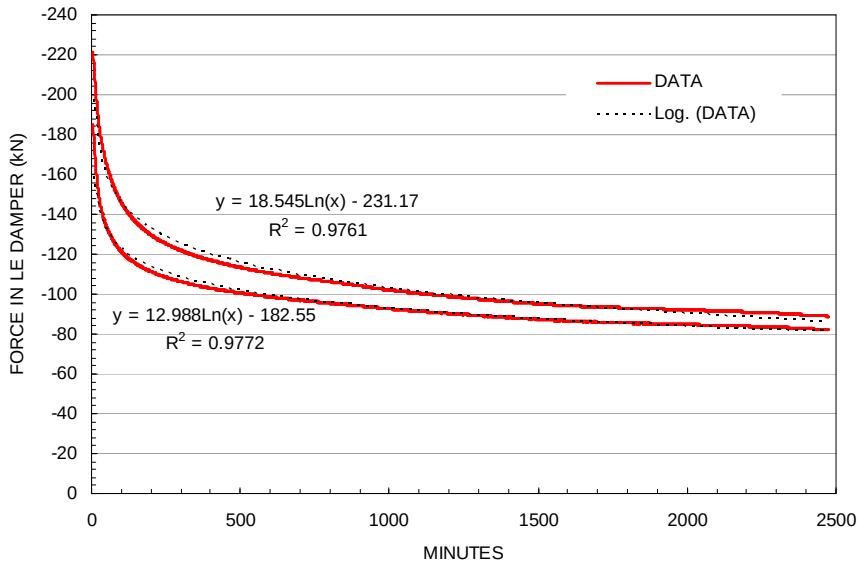

Figure 6-26: Damper force decay over time. Results are plotted for the east and gravity beam damper. The data is fitted to a logarithmic function.

a photograph of the west beam after testing is given in Figure 6-23(b). Note the specimen is essentially damage-free, will all cracks closing upon unloading.

Results from bi-directional testing is given in Figure 6-24, with the bi-directional clover-leaf loading pattern shown in Figure 6-24(c). It this case, the specimen was subjected to two cycles each at 0.5, 1, 2, and 3 percent drift. As with uni-directional testing, the specimen exhibits a good, stable hysteresis loop. There is negligible stiffness or strength degradation. In the NS direction it is apparent the specimen's unloading cycles are less stable than during uni-directional testing. The bi-directional rocking caused some additional damage to the pier in the form of further crack propagation of cracks from previous tests, on the order of 50-100mm. These cracks appeared when the specimen was displaced in the EW and NS directions, causing a significant force concentration at the corner of the beams.

Figure 6-25 presents a comparison in the EW direction between the un-directional and bi-directional testing QS testing. From this figure it is evident that the behaviour of the specimen due to bi-directional loading is essentially the same as uni-directional loading. There is some strength loss from the bi-directional testing, most noticeable at 3 percent drift. This caused a strength loss of approximately 5 percent.

Plotted in Figure 6-26 is the compression force in two of the dampers over time. This was recorded after completion of QS testing to 3 percent drift. Directly after testing, the LE dampers have a compression force of about 200kN. Within the first 8 hours, this force drops to approximately half. After 40 hours, the compression force has reduced to about 85kN, following logarithmic decay.

6.6.2 Quasi-earthquake displacement test results

Results from QED testing in the EW and NS direction are presented in Figure 6-27 and Figure 6-28, respectively. These plots show the force-displacement response, the bi-directional orbit of the column, and the displacement profile versus time. In all cases, the

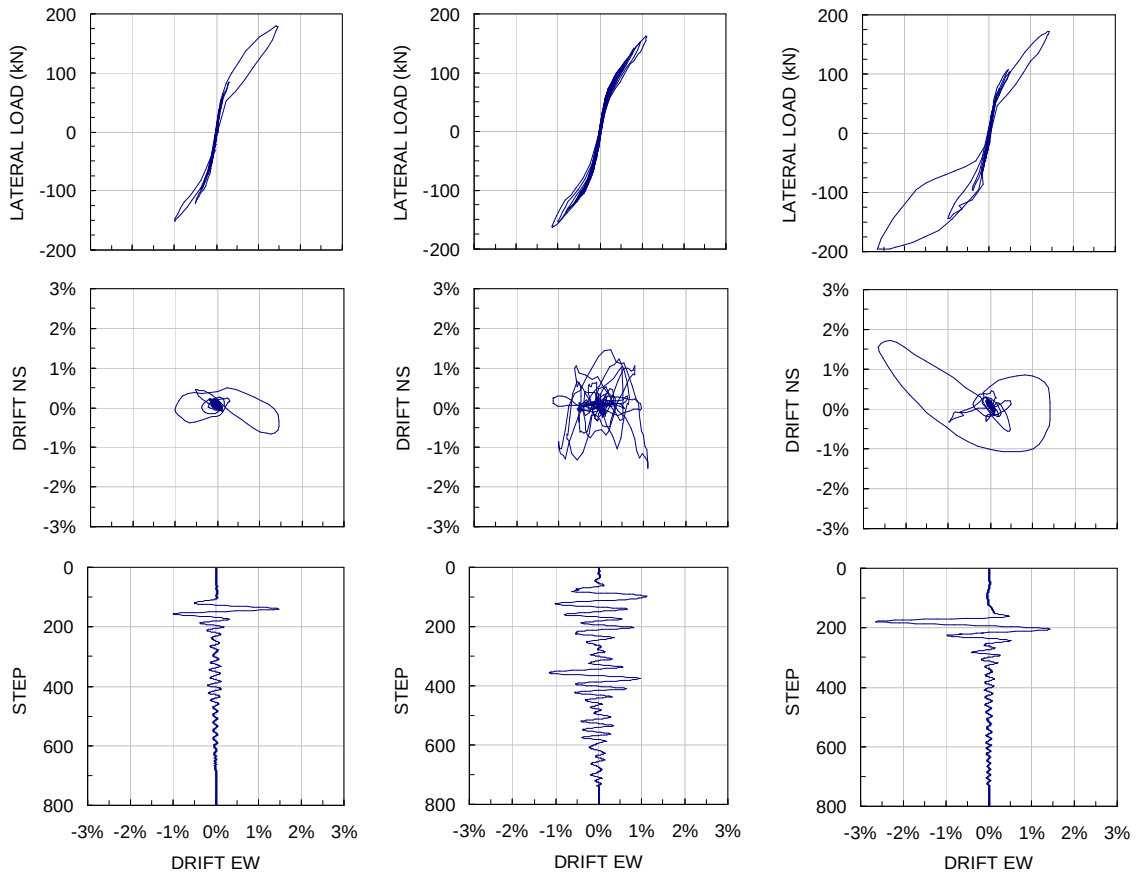

Figure 6-27: Results from QED testing in the EW direction: (a) 90% DBE; (b) 50% MCE; (c) 90% MCE.

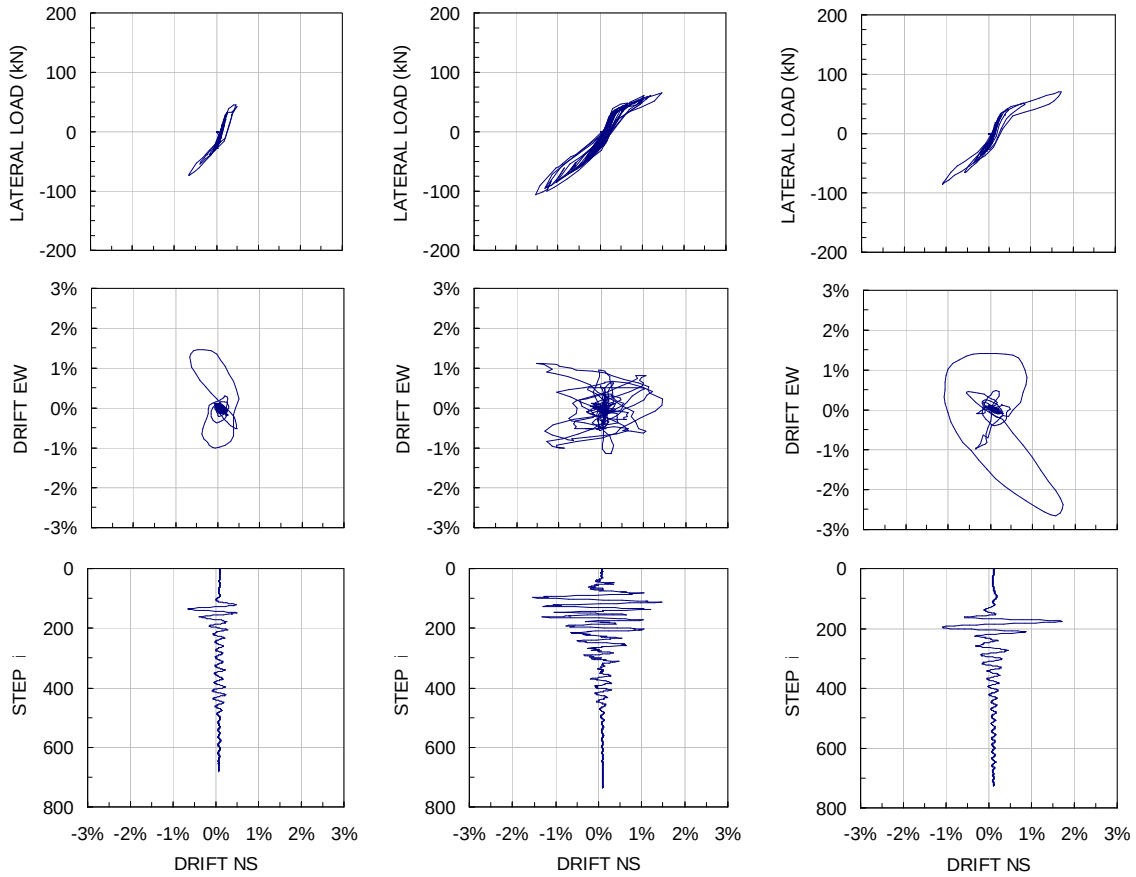

Figure 6-28: Results from QED tesing in the NS direction: (a) 90% DBE; (b) 50% MCE; (c) 90% MCE.

specimen exhibited good hysteretic response, showing a flag-shaped hysteresis loop with good energy dissipation. The response in the NS direction was not as stable as in the EW direction. This was especially the case in for the 50 percent MCE. In this case, the specimen exhibited some stiffness degradation, possibly as a result of bi-directional rocking coupled with non-uniform displacement cycles. Damage to the specimen was minimal. Throughout all tests, only slight cracking near the joint region was observed. These cracks generally closed at the end of testing. Some prestress loss was detected. This was generally on the order of 0-15kN, and may be due to crushing of the concrete around the thread-bar anchorages.

6.7 DISCUSSION

6.7.1 General findings

Overall, the specimen performed well. The specimen exhibited stable hysteresis loops with no stiffness or strength degradation and negligible residual drift. Some minor cracks were observed in the joint region of the beam, ranging in length from 25mm to 150mm. These cracks were confined primarily to the armoured end regions and closed after testing was terminated. No damage (cracking or crushing) was observed in the column.

Testing confirmed that the detailing strategy is sufficient in protecting the members from damage to bi-directional drifts up 4 percent. The joint was shown to "roll" slightly, but this effect was minimal. Given the good agreement between the prediction and experimental results using the rigid body assumption and the negligible rolling of the connection, the basic analysis method is evidently sufficient for predicting response. The design of the joint region was relatively simple, with checks made to ensure the armouring was sufficient for spreading the compressive contact forces to the concrete without damage.

The LE dampers provided stable energy dissipation. They were also shown to effectively "reset" via creep in the lead after testing; the force in the devices was shown to

reduce to approximately half within the first few hours after testing, with further reduction following logarithmic decay. This effect is very desirable in the fact that these devices would not have to be replaced following an earthquake, since the softening seen in mild steel dissipation devices was not observed in this case. Due to the very small opening of the connection (on the order of 5-10mm), the effectiveness of the LE damper is quite sensitive to its stiffness. This includes the contribution to stiffness from the connecting elements of the LE damper. Attempts were made to limit stiffness losses from connecting elements by tightening the LE damper back against the connecting rods and grouting the threaded rod in the column. Although this likely helped, the problem was not entirely eliminated. It was shown that due to slop in the connecting elements this lead to a reduction in stiffness of approximately 60 percent. In further development of these devices, attention should be given to increasing their initial stiffness and carefully considering how different mounting configurations might affect response of the device.

A considerable amount of effort was devoted to identify the most constructible solution possible. Compared to past designs (Li, 2006; Davies, 2004) it is considered that the construction of this specimen was relatively simple. The key to this design is the inclusion of the cast insitu closure pour. This provided a means of ensuring a reliable contact surface at the joint and the ability for elements to be coupled together, thus allowing for segmental pre-cast construction. The construction procedure outlined in Section 6.2.1 is thought to be a good solution, accounting for tolerances comparable to current standards, minimal onsite concrete placement, and design freedom. The cast insitu ends provide a means of placing high performance concrete only in the most vulnerable (end) regions, allowing regular strength concrete to used for the majority of the beam elements.

6.7.2 The Multi-level Seismic Performance Assessment

Earthquakes representing different levels of seismic demand were applied to a subassembly representing an exterior column of a multi-storey building. Using these test results, it is possible to extrapolate observed damage to the whole structure and determine if identified performance objectives were met.

The first performance objective dealt with serviceability. Given a design level earthquake, an engineer must be highly confident that the structure will not sustain damage which causes a disruption to its normal function. The seismic demand associated with this objective was the 90th percentile DBE, corresponding to a PGA of 0.4g (S_a=0.27g) at a 475-year return period. EQ39 and EQ40 (NS and EW directions, respectively) were chosen to represent the 'worst case' displacement demand given the suite of 20 earthquakes considered. The displacement profile consisted mainly of a single large displacement cycle to an interstory drift of 1.6 percent, followed by a slow reduction in displacement. Residual drift was negligible. Observed damage from this level of shaking was minimal. Flexural cracks were observed in the beams and small (50mm) cracks were observed in the beam's joint region. These cracks closed after testing. The LE dampers performed well, with some hysteretic energy dissipation on the first pulse, followed by near-elastic behaviour. The specimen did not suffer any stiffness or strength degradation. Given these results, the specimen satisfied the first requirement of the MSPA; one could be quite confident that the building would remain operational following a DBE.

The second performance objective relates to reparability. In this case, the engineer must be moderately confident the structure is repairable following an very rare earthquake. This relates to the 50th percentile MCE, with a PGA of 0.8g (S_a=0.48g) and a return period of 2475 years. EQ15 and EQ16 were chosen to represent this demand. These records were selected because their displacement demand was closely related to the median response given

by the suite of 20 earthquakes. The displacement demand was most severe in the NS (gravity) direction, corresponding to a maximum interstory drift of 1.6 percent. Again, the specimen performed very well. Only a few additional cracks near the beam's armouring were observed. In the EW direction, the specimen behaved elastically, with no stiffness or strength degradation. In the NS direction, some stiffness degradation was observed. This was attributed to the draped thread-bar profile which would bind within the duct. Nevertheless, this effect was minimal. Therefore the specimen met the second requirement of the MSPA.

The third and final performance objective related to life-safety. With a high level of confidence the structure must not collapse following a very rare earthquake. This objective was related to the 90^{th} percentile MCE, with a PGA of 0.8g (S_a=0.27g) and a return period of 2475 years. EQ39 and EQ40 were selected to represent this level of demand, given these records produced the most severe response. The displacement of the structure consisted of one primary pulse to 2.8 percent interstory drift, followed by several small displacement cycles. As with the previous two earthquakes, damage to the specimen was minimal. Some of the previously developed cracks propagated away from the joint another 100mm. A few additional cracks formed in the armouring region. Most of these cracks closed after testing. During the first pulse, a considerable amount of hysteretic energy dissipation was observed, subsequent displacement cycles were elastic, with the full stiffness and strength of the specimen preserved. Some prestress losses were recorded, in the order of 0 to 5 percent, likely caused by slight crushing in the anchorage regions. These losses were deemed too small to necessitate re-stressing the thread-bars. Given the damage outcome from this level of demand, the structure satisfied the final objective of life-safety.

This MSPA has verified the specimen, and indirectly the structure, is capable of remaining essentially damage-free given severe ground shaking. All performance objectives related to serviceability and life-safety were achieved. This structure, designed to resist

damage by rocking at specially detailed joints, offers an attractive alternative to conventional monolithic design and construction. An equivalent monolithic structure would have likely undergone severe cyclic rotations at its plastic hinges, resulting in severe damage locally and excessive residual displacement of the global system. The suite of 20 earthquake records selected for this study are somewhat generic. Should an MSPA be used to characterize the response of a structure on a specific site, a more thorough selection process should be adopted, considering local effects such as soil-structure interaction and attenuation relationships between the site and the source faults. The MSPA method relies heavily on the analytical model developed in conjunction with the experimental specimen. In order for realistic displacement profiles to be extracted from the model, the response of the two must be reasonably identical. Furthermore, non-structural damage, which constitutes a large portion of overall damage, should be considered for a more complete conclusion to be drawn. Nevertheless, the MSPA method has demonstrated a sound means of experimentally verifying the performance of structures at various levels of seismic demand.

6.8 CONCLUSIONS

A 3D subassembly taken from a typical multi-storey building was designed and tested considering bi-directional effects. The specimen was detailed to resist damage, with energy dissipation provided by internal lead-extrusion damping devices. Displacement-controlled quasi-static and quasi-earthquake displacement testing was used to represent realistic loading conditions. Based on this investigation the following conclusions can be drawn:

1. The specimen satisfied all performance objectives related to serviceability and life-safety. After being subject to displacement profiles representing a design level earthquake and more severe rare earthquakes, the specimen remained virtually damage-free.

2. A basic analysis method for predicting the response of the system was validated by comparing it to experimental results. The method assumes rigid-body behaviour of the members, allowing the moment arm to be taken from the rocking point. Good agreement between the prediction and experimental results was evident, with discrepancies of not more than 5 percent.
3. The lead-extrusion damper was able to provide a reliable form of energy dissipation to the specimen. This damper was mounted internally near the end of each beam. Residual compression forces in the devices at the end of testing were shown to creep back towards zero, with half the force being lost over the first few hours. Therefore, the devices would not have to be replaced following an earthquake.
4. The detailing strategy proved to provide an excellent level of protection from damage while retaining a degree of simplicity and constructability. Closure pours utilizing high-performance concrete were provided at the end joint of each beam. Throughout quasi-static and quasi-earthquake displacement testing up to 4 percent radial drift the specimen suffered nearly any damage. Some small cracks were observed near the steel armouring, which generally closed after testing. Due to the fact that so few cracks were observed, the steel fibres did not significantly contribute to the joint's performance.

REFERENCES

Amaris A, Pampanin S, Palermo A. 2006. Uni and bi-directional quasi-static tests on alternative hybrid precast beam column joint subassemblies. *Proceedings of the 2006 New Zealand Society for Earthquake Engineering* (NZSEE) *Conference*. Napier, New Zealand, Paper #24.

Arnold DM. 2004. Development and Experimental Testing Of a Seismic Damage Avoidance Designed Beam to Column Connection Utilising Draped Unbonded Post-Tensioning. *Master of Engineering Thesis*. University of Canterbury, Christchurch, New Zealand.

Bradley BA, Dhakal, RP, Mander JB. 2006a. Dependency of current Incremental Dynamic Analysis to source mechanisms of selected records. *19th Biennial Conference on the Mechanics of Structures and Materials*; Christchurch, NZ.

Bradley BA,. Dhakal RP, Mander JB. 2006b. Multi-level Seismic Performance Assessment of RC Frame Building Designed for Damage Avoidance through Bi-directional Quasi-Earthquake Displacement Tests, *International Conference on Civil Engineering in the New Millennium* (CENeM-07)*: Opportunities and Challenges*, Kolkata, India.

Cousins WJ and Porritt TE. 1993. Improvements to lead-extrusion damper technology. *Bulletin of the New Zealand National Society for Earthquake Engineering*, **26**:342-348.

Davies MN. 2003. Seismic Damage Avoidance Design of Beam-Column Joints using Unbonded Post-Tensioning: Theory, Experiments and Design Example. *Master of Engineering Thesis*. University of Canterbury, Christchurch, New Zealand.

Dhakal RP, Mander JB, Mashiko N. 2006. Identification of Critical Earthquakes for Seismic Performance Assessment of Structures, *Earthquake Engineering and Structural Dynamics*, **35**(8):989-1008.

Dutta A, Mander JB, Kokorina T. 1999. Retrofit for control and reparability of damage. *Earthquake Spectra*, **15**(4):657-679.

Li L. 2006. Further Experiments on Damage Avoidance design of Beam-to-column joints. *Master of Engineering Thesis*, Dept. of Civil Engineering, University of Canterbury, Christchurch New Zealand

Priestley MJN and Tao JRT. 1993. Seismic Response of Precast Prestressed Concrete Frames with Partially Debonded Tendons. *PCI Journal*, **38**(1):58-69.

Priestley MJN, Sritharan S, Conley JR, Pampanin S. 1999. Preliminary Results and Conclusions from the PRESSS Five-Storey Precast Concrete Test Building. *PCI Journal*, **44(**6):43-67.

Robinson WH and Greenback LR. 1976. An extrusion energy absorber suitable for the protection of structures during an earthquake. *Earthquake Engineering and Structural Dynamics*. **4**:251-259.

Rodgers GW, Denmead CS, Leach NC, Chase JG, Mander JB. 2006. Spectral evaluation of high force-to-volume lead dampers for structural response reduction. *Proc. New Zealand Society for Earthquake Engineering Annual Conference*, Napier, New Zealand, March 10-12.

Rodgers GW. 2006. Next generation structural technologies: implementing high force-to-volume energy absorbers. *PhD Dissertation*. University of Canterbury, Christchurch, New Zealand.

Stanton JF, Stone WC, and Cheok GS. 1997. A Hybrid Reinforced Precast Frame for Seismic Regions. *PCI Journal*, **42**:20-32.

Stirling MW, McVerry GH, Berryman KR. 2002. A New Seismic Hazard Model for New Zealand. *Bulletin of the Seismological Society of America*, **92**(5):1878-1903.

Vamvatsikos, D. and Cornell, C.A. 2002. Incremental Dynamic Analysis. *Earthquake Engineering and Structural Dynamics*, **31**:491–514.

7 Concluding remarks and recommendations

7.1 RESEARCH MOTIVATION, REVISITED

The current trend in earthquake engineering worldwide has been the consideration of multiple performance objectives at various levels of seismic demand. This has come to the forefront of research due to large economic losses associated with recent earthquakes in the United States. Earthquakes such as Loma Prieta in San Francisco (magnitude 6.8; 62 deaths; $6 billion in damage), and Northridge in Los Angeles (magnitude 6.7; 57 deaths; $30 billion in damage) have demonstrated both the strengths and deficiencies of modern ductile design (Scawthorn, 2003). Relative to the size of the population centres where these events occurred, there were very few deaths. Indeed, most deaths can be attributed to non-engineered housing, or pre-seismically engineered bridges. However, the resulting economic losses due to damage were significant. Modern ductile design allows certain types of damage to occur at specially detailed plastic hinges. This is an excellent way of providing economical structures that maintain life-safety and do not collapse, but poor at ensuring structural systems (both buildings and bridges) remain operational following an earthquake. With the introduction of so-called ductile jointed connections in the nineties, engineers now have a new method of detailing structures to resist damage. By accommodating non-linear response by rocking, rather than by the formation of a plastic hinge, damage can be eliminated in the frame. This is very significant in the context of current design objectives which require that a more stringent set of performance objectives be achieved. A summary of past research endeavours, findings of current research, and future possibilities related to ductile jointed connections follows in the next few sections.

7.2 A SUMMARY OF DEVELOPMENTS

7.2.1 Research in the United States

The research presented herein has focused on the further development of ductile jointed precast concrete systems, otherwise known as rocking systems. First developed as part of the PRESSS program, these systems exhibit non-linear response without the formation of plastic hinges. This is accomplished by allowing the members, be it frames or walls, to rock at their connections. The concept of rocking structures is not new; the beneficial effects have been investigated by several early researchers (Housner, 1963; Aslam, 1980). However, with the innovative insight of adding either fully or partially unbonded prestress across the rocking interface, a reliable restoring force is introduced to the system (Priestley and Tao, 1993), resulting in bi-linear elastic force-displacement behaviour. This concept was experimentally verified by Priestley and MacRae (1996); the specimen tested is shown in Figure 7-1. It consisted of unbonded post-tensioning and a concrete interface. The force-displacement response of the subassembly is given in Figure 7-2 and a photograph after testing is shown in Figure 7-3. Note that the observed energy dissipation is due to damage to the specimen, as evident from the photograph. This damage also caused the stiffness degradation shown in Figure 7-2.

Due to the inherent lack of energy dissipation provided by rocking systems, it was noted that peak displacement may be larger than monolithic buildings (Priestley and Tao, 1993). A hybrid solution was introduced by Stanton *et al.* (1997), as illustrated in Figure 7-4. In this case, the unbonded prestress was complemented with yielding mild steel reinforcing across the joint, thus providing both a restoring force and a level of energy dissipation. This resulted in force-displacement behaviour exhibiting a flag-shaped hysteresis loop, which had the very desirable attribute of being both self-centering (i.e. little to no residual displacement) while still dissipating energy in the form of yielding. The results from two of these tests are

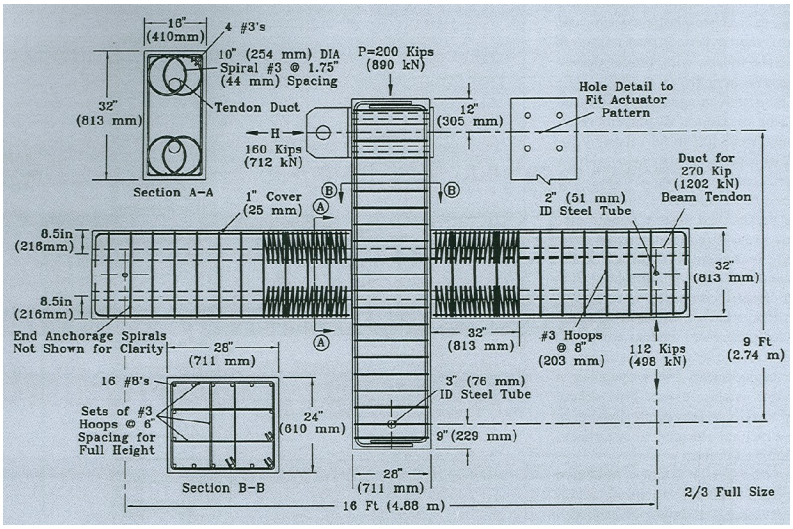

Figure 7-1: Interior joint specimen details (MacRae and Priestley 1996).

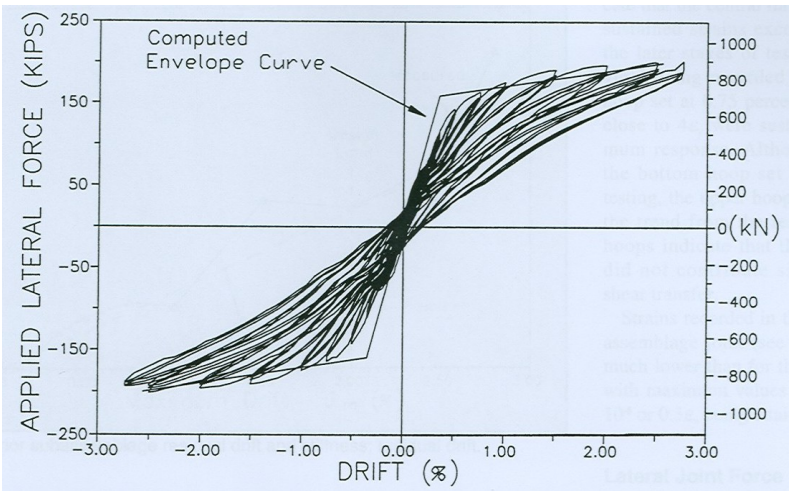

Figure 7-2: Force-displacement response of the subassembly with prestress only and a concrete interface as tested by Priestley and MacRae (1996).

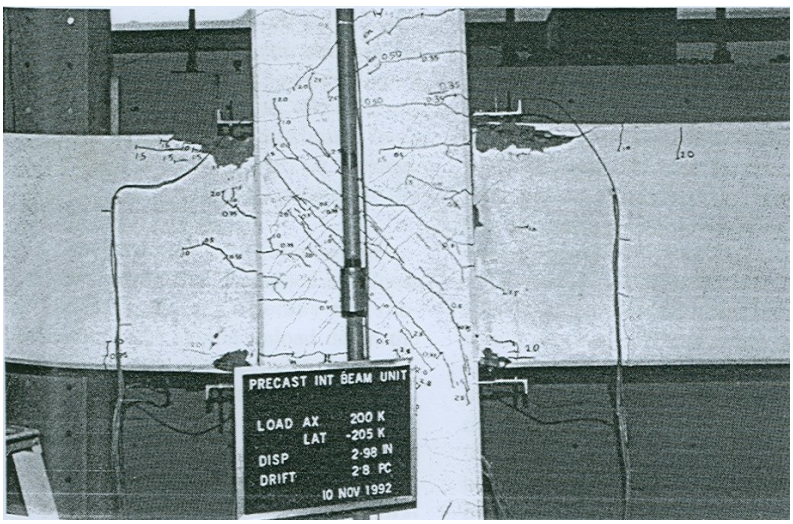

Figure 7-3: Photograph of the Priestley and MacRae (1996) specimen.

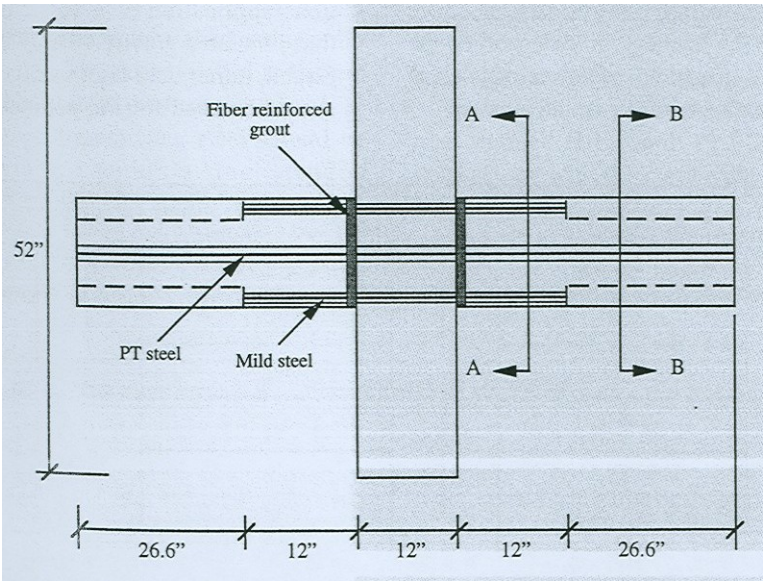

Figure 7-4: A generic detail of the specimens as presented by Stanton *et al.* (1997).

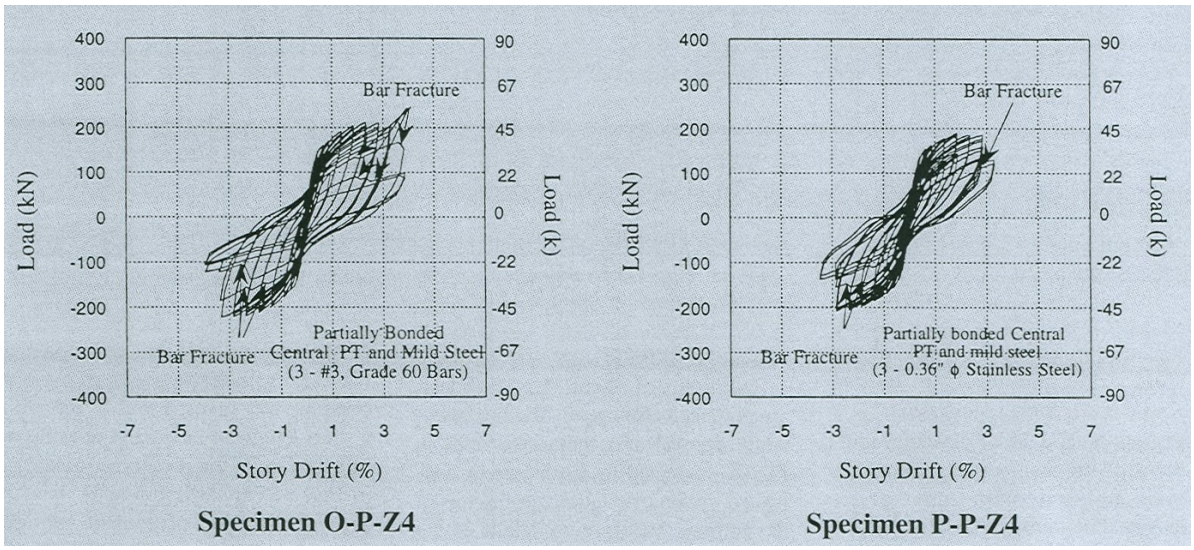

Figure 7-5: Force-displacement response of two of the subassemblies tested by Stanton *et al.* (1997).

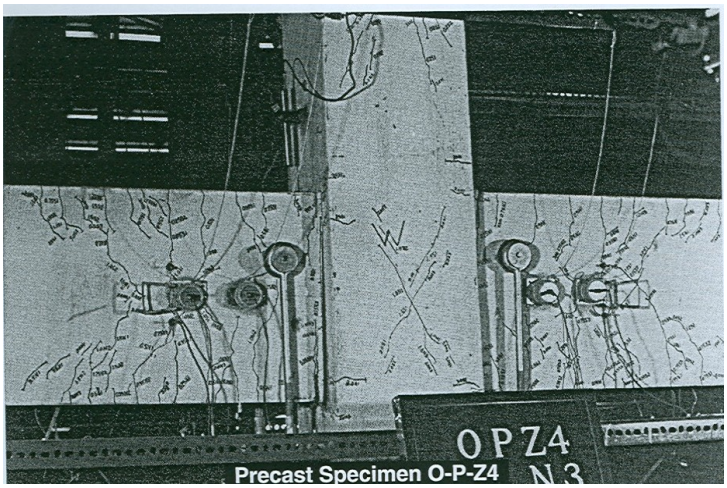

Figure 7-6: Photograph of one of the Stanton *et al.* (1997) precast specimens at failure.

shown in Figure 7-5. Although much improved energy dissipation is apparent from the figure, some stiffness degradation was observed, and finally, bar fracture. This reduced the capacity of the system. Nevertheless, the performance of this system was much better than conventional systems. Visual damage to the specimen is shown in Figure 7-6. These key developments formed the basis of many years of research as part of the PRESSS program, culminating in the testing of a 5 storey frame and wall building (Priestley *et al.*, 1999). One of the key design decisions of these designs was the use of a concrete-concrete interface, where high strength grout was provided to serve as a pad between the connecting members. As a consequence of this, some damage in the form of crushing and cracking was observed, though comparatively much less than expected in conventional monolithic construction. This resulted in some stiffness degradation as the beams essentially began "rolling" due to crushing in their corners. This effect would necessitate the repair of such components following an earthquake.

Accepting that damage is inevitable does not fully account for the potential of these jointed systems. Mander and Cheng (1997) proposed the concept of so-called *Damage Avoidance Design* (DAD) whereby armouring was used to protect the high-stress rocking zones. This was tested on a DAD bridge pier with steel plates at the column ends. The intent in this case was to provide a slightly more costly detailing scheme (in terms of materials and labour) at the benefit of even less (on no) damage. This approach has formed the philosophical backbone of the research presented as part of this thesis.

In the case of all these detailing schemes, there is an added cost due to the inclusion of prestress and supplemental energy dissipation. Across the joint, the supplemental energy dissipation, typically in the form of mild steel, must be sheeted from the beam through ducts in the column, this means access holes are required. If shear must be transferred by corbels or shear keys, these devices must also be locked into position. If external mild steel dissipation

is used, it must be bolted with anchor plates, further complicating the joint, not to mention the aesthetic loss in such a case. The prestress system must be properly accommodated, which may become complicated when considering beams framing from different directions. All of these are examples of the added complexity of rocking systems. Some of these costs may be offset with the ability to cast more concrete off-site. However, steps in reducing the above stated complexities should be taken to ensure rocking systems can be competitive to monolithic concrete construction.

The research presented in this thesis was conducted with the overriding objective of designing a joint to resist all forms of damage (DAD) while still simplifying the joint detailing to address the construction issues outlined above. Through the design, construction, and testing of several specimens, detailing alternatives were investigated, some promising, some not, leading to the recommendations presented in this chapter. In addition, work was devoted to the development of a loss estimation methodology which could be used to highlight the enhanced performance of rocking structures in terms of expected financial seismic risk. A case study comparing the performance of a DAD bridge pier and a ductile monolithic bridge pier found that the DAD bridge had an expected annual loss less than one-quarter the monolithic system.

7.2.2 Research at the University of Canterbury related to Damage Avoidance Design

The research related to beam-column joints as presented in this thesis is part of an evolutionary cycle of research conducted at the University of Canterbury by Arnold (2004), Davies (2003), Li (2006). This section will review the contributions of each researcher and attempt to provide some insight into future research avenues and practical implementation of such systems. Given the foundation of research on ductile jointed connections conducted overseas (Stanton *et al.*, 1997; Mander and Cheng, 1997; Priestley *et al.*, 1999), research at the University of Canterbury has focused on developing specimens with alternative detailing

schemes which resist all forms of damage and testing those specimens under conditions which reflect demand as accurately as possible.

Arnold (2004) and Davies (2003) set out on parallel studies to investigate the performance of a specimen designed for damage avoidance with straight and draped tendon profiles, respectively. In the process, a significant amount of effort was devoted to the design of a prototype structure and practical methods for evaluating its response. In keeping with the goal of resisting all forms of damage, the detailing schemes proposed by the researchers consisted of extensively armoured beam-end sections. This armouring was in the form of full-depth steel plates and stiffeners. This was an expensive and arguably impractical solution which required large amounts of steel and many man-hours to erect. Photographs of these end plates are given in Figure 7-7 and Figure 7-8. The researchers also investigated the application of several different mild steel energy dissipation devices, two of which are given in Figure 7-9. One interesting development of this research, also illustrated in Figure 7-9, is the use of off-site post-tensioning. Instead of sheathing the tendons through the column, in this solution the rocking interface is incorporated into the beam and designed to be bolted to the face of the column. While this is a potentially promising construction alternative, tolerance issues arise from this configuration which further complicate the joint detailing scheme. A sample result from the Davies (2003) testing for a peak drift of 3 percent is given in Figure 7-10 and a photograph of the Arnold (2004) specimen is shown in Figure 7-11. Note that there is some loss in strength due to yielding of the prestress. Neither of these specimens exhibited any damage, which can largely be attributed to the extensive steel armouring.

Although the specimens proposed by Davies (2003) and Arnold (2004) performed very well during testing, their application is limited due to the excessive material and labour requirements to produce them. The steel armouring required the stiffeners be welded across

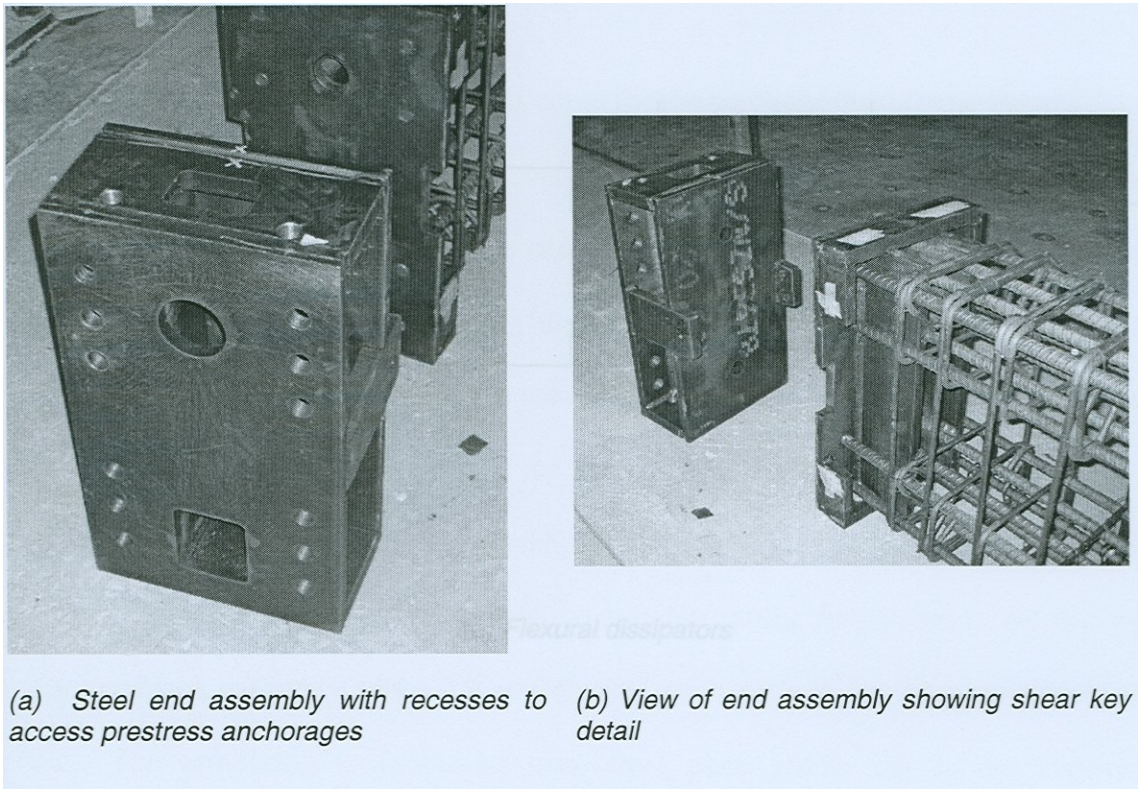

(a) Steel end assembly with recesses to access prestress anchorages

(b) View of end assembly showing shear key detail

Figure 7-7: Photographs of the steel endplate assembly (Davies, 2003).

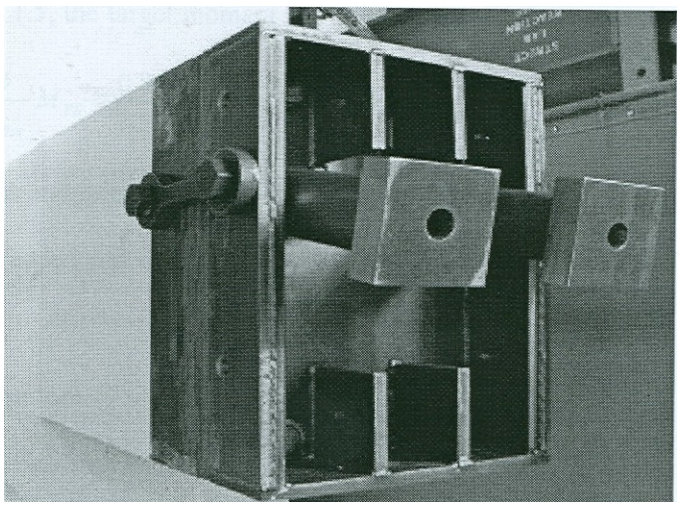

Figure 7-8: The end detail of the specimen (Arnold, 2004)

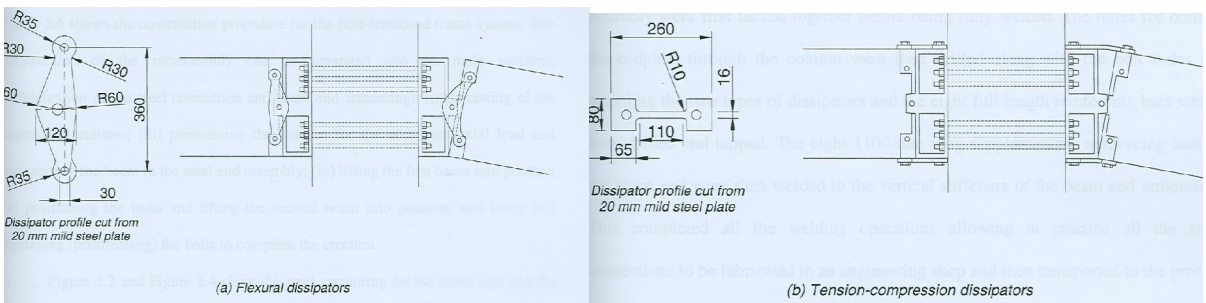

Figure 7-9: A figure taken from Davies (2003) showing two types of energy dissipation devices tested and the off-site post-tensioning method.

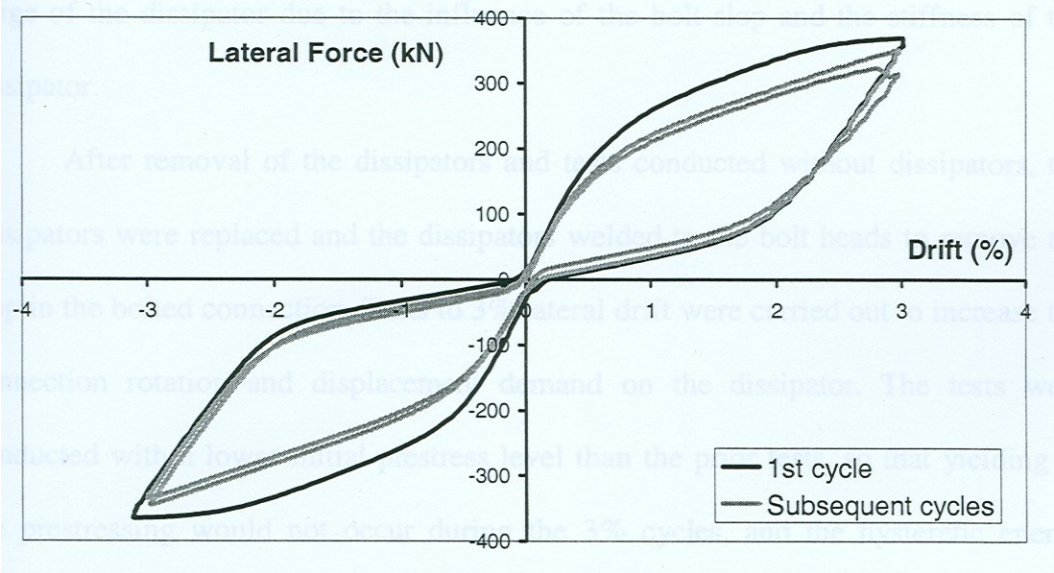

Figure 7-10: Force-displacement response of the Davies (2003) specimen.

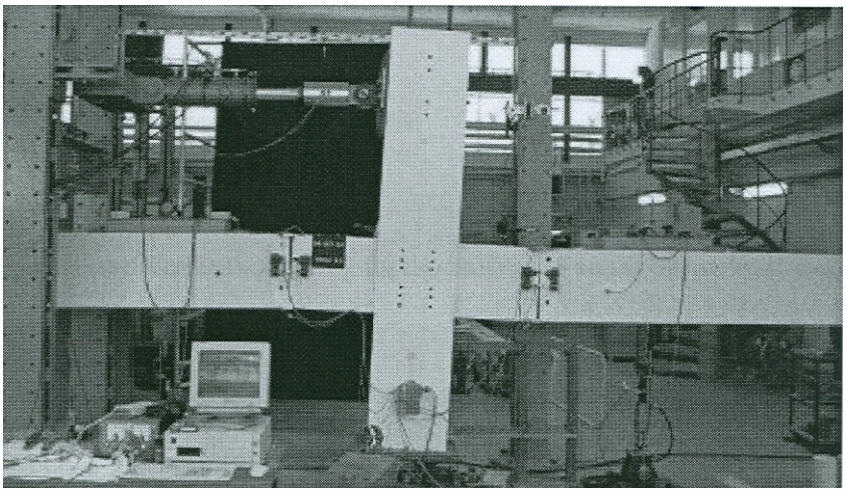

Figure 7-11: The Arnold (2004) specimen at 3 percent drift.

their full length and the beam reinforcing cage be plug welded to it as well. Tolerance requirements are also an issue. The members would have to be cast to a very tight tolerance to ensure the beams properly fit within the column and the connections were flush. In practice this is very difficult to achieve and equates to slower construction. Therefore, these specimens can serve as a benchmark from which more economical designs can be investigated.

Li (2006) set out to address some of the deficiencies identified in Arnold (2004) and Davies (2003). He proposed using a bent coupler system whereby post-tensioning would be anchored at each column, just above the top of the beam. This is illustrated for one of the beams in Figure 7-12. The bent coupler enabled the prestress thread-bars to be pre-installed in the beam and cast full length. Once on-site, a shorter section of thread-bar would be inserted through a diagonal duct in the column and coupled to the beam's thread-bar via the bent coupler. This system had a few distinct advantages: (i) it provided a level of redundancy in the system since each beam was individually post-tensioned; (ii) the shorter thread-bar in the column could act as a fuse for the prestress system if it was machined to a reduced cross-section; (iii) more concrete could be placed off-site; and (iv) the members could (theoretically) be connected together quickly thus speeding up floor cycle time. Several other details were also investigated. To reduce materials and labour, the full-depth steel plate on the beam end was replaced with two angles top and bottom. Shear was accommodated by four shear keys located in each corner of the beam. Mild-steel energy dissipaters, allowed to buckle in compression, were designed to be mounted externally on outrigger plates extruding from the beam. This was done primarily to facilitate rapid post-event replacement and thus accommodate multiple earthquakes (or experimental tests). A sample test result is given in Figure 7-13 and a photograph of the specimen after testing is given in Figure 7-14.

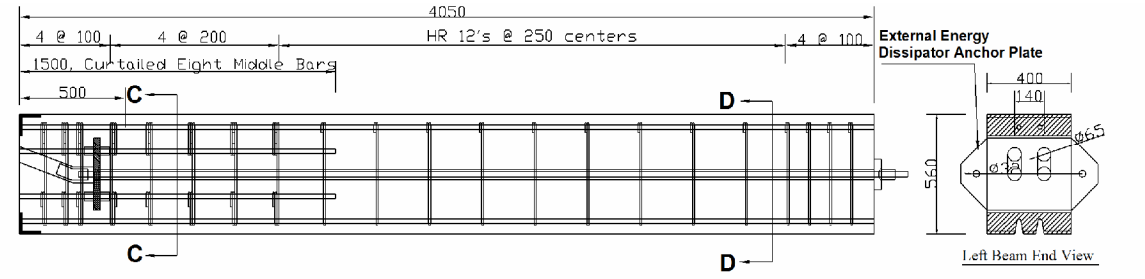

Figure 7-12: Beam detailing given in Li (2006)

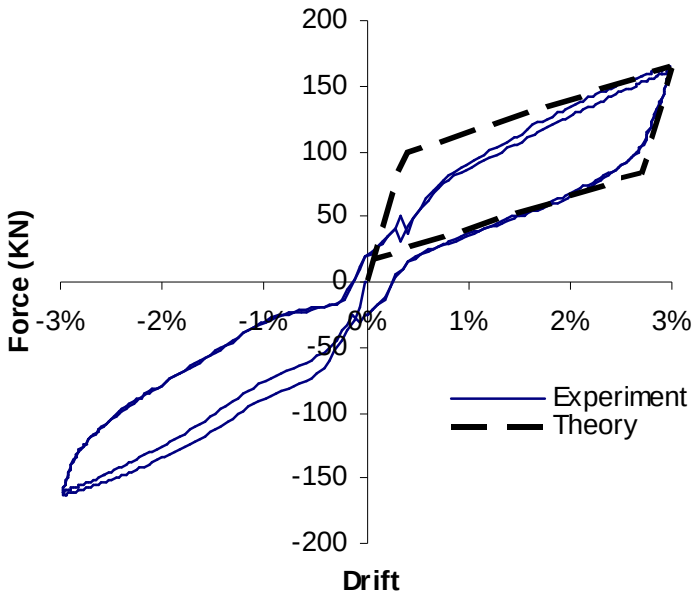

Figure 7-13: Experimental results presented by Li (2006) at 3 percent drift.

Figure 7-14: Photograph of the Li (2006) speciemen after testing.

Although this specimen was an improvement compared to earlier designs, the specimen also had several significant drawbacks. Due to the bent coupler system, very tight tolerances were required in order for the thread-bar to be properly threaded to the coupler. The prestress across the joint was complicated by the angled thread-bars. This resulted in an upward vertical force component which placed additional demand on the shear keys and caused the beam to creep up the face of the column during testing. Although damage was reduced in this region by the inclusion of armouring, the beam still suffered a 'rolling' effect as a result of local tearing in the concrete around the steel angles and crushing behind them. Over many tests, this led to a loss in stiffness. The energy dissipation devices provided were not only impractical from an architectural point of view, but provided only minor energy dissipation due to the fact they were not restrained from buckling. Consequently, these devices would have to be replaced after an earthquake.

Finally, as presented in this thesis, the deficiencies addressed by Li (2006) were considered in a new design approach. This design utilized a new energy dissipation device called a *lead-extrusion* (LE) damper. This device had the unique ability to be reusable following an earthquake and could therefore be mounted internally. An isometric illustration of the joint designed to accommodate the LE damper is given in Figure 7-15. Further efforts were made to simplify the joint region by utilizing a straight tendon profile and using steel channels to serve as armouring. Bi-directional testing revealed the device worked reasonably well and no damage was observed to the beam or column concrete. The force-displacement response of the specimen is given in Figure 7-16, showing good energy dissipation and re-centring characteristics. A photograph of the specimen after testing is given in Figure 7-17.

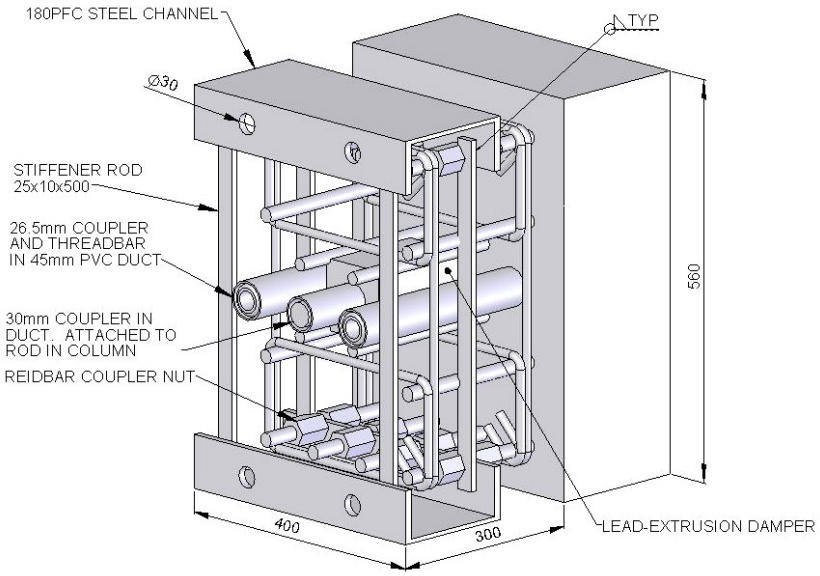

Figure 7-15: The beam jointed designed for the LE damper.

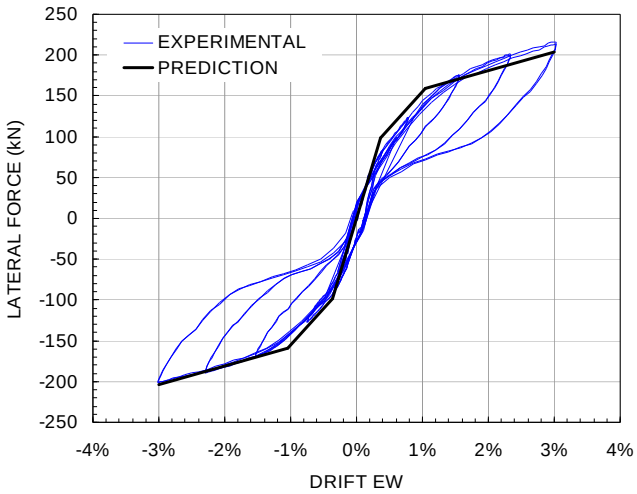

Figure 7-16: Force-displacement response of the subassembly employing internal LE dampers.

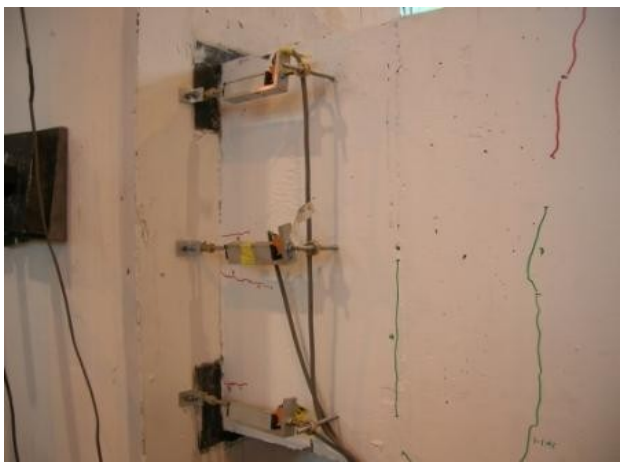

Figure 7-17: Photograph of the subassembly employing internal LE dampers after testing.

7.3 DETAILING OPTIONS

To this point, a brief history of the development of DAD has been given. Research in this area has varied in scale and complexity; many different detailing options have been considered, ranging from some to no damage at large to small cost. The question then becomes which system is best, considering the trade-off between damage and capital cost. This section will attempt to address this question.

7.3.1 Some damage versus no damage

There seem to be two separate schools of thought regarding ductile jointed precast concrete systems. One way of thinking about the design and detailing of these systems is to accept that some damage, mainly in the form of cracking and some crushing/spalling, will occur in the column joint and the beam ends. This will likely lead to a loss of stiffness, with little reduction in strength. This may be acceptable since it is still a significant improvement to damage incurred in typical monolithic systems. Furthermore, it allows for the use of precast concrete in highly seismic regions, which currently is considered a poor material due to its past non-ductile performance.

The other school of thought sees this new system as a means of designing a structure that incurs virtually no damage, even aesthetic damage typical of the 'traditional' PRESSS joint. This is accomplished by detailing the joint region with steel armouring plates to help alleviate the high compression forces at points of rocking. It is considered this can be accomplished with a relatively modest increase in material and labour cost if the joint region is thoughtfully detailed.

In both these cases, no attention is given to the floor slabs (how will they accommodate displacement?) or the expected non-structural damage. The latter form of damage, of course, can be significant. Non-structural damage is a function of both interstory drift and floor accelerations, and can thus be assumed independent of armouring. Repair costs

of this type of damage, coupled with the extensive list of components which are susceptible to damage, is at least equal or greater than damage to the structural system. Assuming this, even if there is no damage to the structural system, the building may still be uninhabitable while repairs are made to glazing, plumbing fixtures, elevators, etc. So is it then reasonable to accept some repairs will be necessary to the structural system as well?

Which system is best? This is a difficult question. From the standpoint of performance based design and the general trend of designing buildings to behave 'better' in moderate to large earthquakes, both systems will perform well, and each may be justified depending on the seismicity of the region. In other words, if the return period for large earthquakes is relatively low, the elimination of structural damage may be very attractive. On the other hand, if the return period is high, meaning there is very little chance such an earthquake will occur, the risk is more reasonable. It also depends highly on the cost of providing armouring at the joint, both in the column and the beam. This adds an additional complexity to the system in the form of increased material cost, congestion in the contact regions, and labour requirements. Although damage to the building in an earthquake may decrease with steel armouring, this savings is not immediate, and may be difficult to justify to an owner who is primarily interested in the capital costs associated with various building systems and materials.

Until such a building is built, it is difficult to say just how much cost, if any, armouring would add to the system. Therefore, this is an unknown that may be roughly estimated by a construction engineer. The life-cycle benefits of armouring can be approximately compared using probabilistic modelling by comparing it to systems without armouring. This may be one such way of determining if the savings are significant enough to justify its use.

Thus the benefits can be reduced to one thing: the time value of money. If the client is willing to initially expend marginally more for improved seismic performance by adding steel armouring, downstream benefits arise in less repairs following small to medium earthquakes. If the owner in not willing to accept the marginal added initial capital cost, one could still expect better behaviour than typical monolithic construction, but be faced with the possibility of repairing structural damage which could otherwise be averted.

7.3.2 Gapping connections versus non-gapping connections

The developments thus far have focused on so-called gapping-floor systems. These systems are designed to allow gaps to form top and bottom due to rocking action, or in other words allows rocking to occur against the top and bottom edge of the members. Several researchers (Gunasekaran *et al.*, 2006) have pointed out this must be accommodated in the flooring system as well, likely resulting in cracking across the floor panels to accommodate the beam growth. This beam growth also has the potential of causing unseating of precast elements which would lead to floor collapse if not properly considered. In response to this, research is currently underway at the University of Canterbury on a detail, termed a non-gapping solution, which pivots entirely at the top of the beam. This ensures a gap will not form across the critical flooring interface and accommodates all rotation by providing a break at the bottom portion of the beam. This system is promising in the fact that is solves many of the problems associated with current frame / slab interaction. By ensuring beam-growth does not occur, the system is more likely to remain damage-free after an earthquake. However this comes at an added cost. The detailing required to ensure such a system re-centres and can support all the shear and moment at the connection is more complicated than a gapping floor solution, and extremely more complicated than a conventional monolithic solution. These costs could prohibit the use of such a system until the frame / slab interaction issues are more widely accepted and understood. In the meantime, gapping floor systems may be the answer

to overcoming current deficiencies in monolithic concrete construction without significant increases in capital cost.

7.4 KEY FINDINGS OF THIS RESEARCH

The research presented in this thesis has covered a range of topics related to the development of rocking systems. Through experimental testing of a bridge pier and several beam-column joints, multiple detailing alternatives have been investigated. The financial implications of these systems has been examined with two new methods developed for calculating *expected annual loss* (EAL). Based on the findings of these studies, the following general conclusions can be drawn:

1. A rapid financial risk assessment method was demonstrated through case studies on bridge piers to provide a means of estimating the expected annual loss of structures. Through the use of simplified formulae, loss studies can be conducted with relative ease, thus eliminating the need for inelastic dynamic analyses.
2. A DAD bridge pier's performance was experimentally verified under bi-directional loading. Given large contact forces at the corner of the pier's base, it was necessary to sufficiently detail the joint region to resist damage. This was accomplished primarily by high-performance concrete.
3. A bent-tendon coupler system was investigated. It was found that high-strength prestressing thread-bars, locally bent to accommodate angled anchorage points in the columns, is a feasible alternative anchoring strategy. Construction complications result from alignment issues due to the coupling system.
4. An externally mounted lead-extrusion damper was used to provide supplemental energy dissipation for a beam-column joint. The damper was shown to provide good energy dissipation at high column drifts (3 percent), but was limited in its effectiveness at low drifts due to slop in the anchoring system.

5. An internally mounted lead-extrusion damper was tested as part of a 3D subassembly. Results indicate the damper provided good hysteretic energy dissipation comparable to typical mild steel devices. The force in the damper crept towards zero upon the completion of testing, verifying the 'resetable' nature of the device. Some inherent slop in the threaded connecting elements caused the dissipater to be ineffective a drift levels less than 1.5 percent.
6. A relatively simple detailing scheme was introduced, where steel channels located top and bottom on the beam provided armouring for the concrete and a means of mechanically developing the longitudinal steel. The system did not suffer damage from bi-directional testing up to 4 percent drift.

7.5 RECOMMENDATIONS FOR FUTURE RESEARCH

The findings of this research suggest a promising alternative to traditional PRESSS systems by introducing a joint which suffers virtually no damage at relatively modest expense. Further studies related to the development of such a connection may help researchers and practitioners to understand its place as a ductile jointed connection. The author feels this can be advanced in the following ways:

1. The dynamic properties of the LE damper have not been fully investigated. With further investigation the potential of these devices can be fully characterized. The relatively low dependence on velocity may ease design and enable the device to pull a force much larger than the restoring force from the prestress. Upon unloading the system would still return to its original state thanks to the force differential under static load.
2. The culmination of research presented in this thesis has focused on the total elimination of damage at the joint. This comes with the cost of slightly more

complicated detailing requirements. In-depth loss studies, addressing the relative difference between capital (construction) cost and life-time cost, plus the inclusion of damage from floor slabs and non-structural components, should be conducted to identify if a completely damage-free joint is economically feasible, and if so, under which situations.

3. Given the beam-column joint of Chapter 4, 5, and 6, a complete lack of damage to the column suggests it may have been unduly conservatively designed. This is also true for the beam; although the beam suffered some minor damage, it was unclear which elements (the stiffeners, the additional confining hoops, the high-performance concrete) contributed most effectively to its performance. Comprehensive modelling studies may reveal more efficient detailing schemes.
4. The gaps which form across the top of the beam must also be accommodated by the flooring system. This would cause cracking (tearing) in the flooring system and potential unseating of the precast elements. These effects may be better understood if a full bay 3D test program was conducted.
5. The Rapid IDA-EAL method developed as part of Chapter 2, though promising, has several limitations which need further investigation. The influence of assumptions on the dispersion, the damping factors used in the capacity spectrum method, and application of the method to more representative multi-degree of freedom systems should be considered in future research.

REFERENCES

Arnold DM. 2004. Development and Experimental Testing Of a Seismic Damage Avoidance Designed Beam to Column Connection Utilising Draped Unbonded Post-Tensioning. *Master of Engineering Thesis*. University of Canterbury, Christchurch, New Zealand.

Aslam M, Goddon WG, and Scalise DT. 1980. Earthquake Rocking Response of Rigid Blocks. *Journal of Structural Engineering, ASCE*, **106**(2), 377-392.

Davies MN. 2003 Seismic Damage Avoidance Design of Beam-Column Joints using Unbonded Post-Tensioning: Theory, Experiments and Design Example. *Master of Engineering Thesis.* University of Canterbury, Christchurch, New Zealand.

Gunasekaran U, MacRae GA, Fenwik R, Carr AJ. 2006. Slab effects on building seismic performance. *Progress in Mechanics of Structures and Materials.* Taylor and Francis Group, London.

Housner GW. 1963. The Behavior of Inverted Pendulum Structure During Earthquake. *Bulletin of the Seismological Society of America*, **53**(2):403-417.

Li L. 2006. Further experiments on the seismic performance of structural concrete beam-column joints designed in accordance with the principals of damage avoidance. *Master of Engineering Thesis*. University of Canterbury, Christchurch, New Zealand.

Mander JB and Cheng CT. 1997. Seismic Resistance of Bridge Piers Based on Damage Avoidance Design. *Technical Report NCEER-97-0014* (National Center for Earthquake Engineering Research), State University of New York, Buffalo, December 10.

Priestley MJN and Tao JRT. 1993. Seismic Response of Precast Prestressed Concrete Frames with Partially Debonded Tendons. *PCI Journal*, **38**(1):58-69.

Priestley MJN and MacRae GA. 1996. Seismic Tests of Precast Beam-to-Column Joint Subassemblages with Unbonded Tendons. *PCI Journal*, **41**(1):64-81.

Priestley MJN, Sritharan S, Conley JR, Pampanin S. 1999. Preliminary Results and Conclusions from the PRESSS Five-Storey Precast Concrete Test Building. *PCI Journal*, **44(**6):43-67.

Scawthorn C. 2003. Earthquakes: A historical perspective. *Earthquake Engineering Handbook*, edited by Chen WF and Scawthorn C, CRC Press, Boca Raton, Florida.

Stanton JF, Stone WC, and Cheok GS. 1997. A Hybrid Reinforced Precast Frame for Seismic Regions. *PCI Journal*, **42**:20-32.

Appendix A: Select material properties

Table A-1: Concrete compression test results.

	Compressive Strength* (MPa)		
	7 day	*28 day*	*at testing*
Chapter 3			
Shoe Block	-	62	-
Chapter 4 & 5			
Seismic Beams	-	37	50
Closure Pour	-	70	-
Chapter 6			
Seismic Beams	35	46	53
Grav Beam, Column	30	39	47
Closure Pour	-	76	76
Grout	-	52	52

* based on 3 cyclinder average

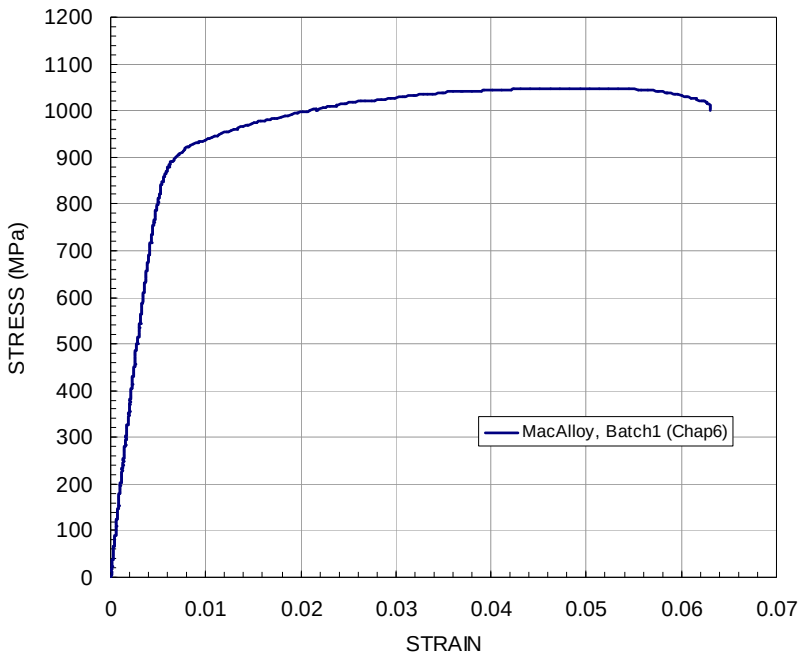

Figure A-1: Steel tension tests.

Appendix B: Complete testing program

CHAPTER 4 & 5 SPECIMEN (BENT TENDON)

Table B-1: Tests performed on the Chapter 4 & 5 beam-column joint subassembly.

Test #	Date	Description	Max Drift	PT %	Dissipater	Gravity Load	Observations / Notes
1	14.03.06	Uni-directional EW	0.5%	50	No	No	
2	14.03.06	Uni-directional EW	2.0%	50	No	No	
3	20.03.06	Bi-directional sine	2.0%	50	No	No	
4	21.03.06	Uni-directional EW	2.0%	50	Yes	No	
		fixed base pin 25-03-06					
5	31.03.06	Uni-directional EW	2.0%	50	No	No	
6	31.03.06	Uni-directional EW	2.0%	50	Yes	No	
7	4.04.06	90% DBE medium	1.2%	50	Yes	Yes	
8	05.04.06	90% DBE high (near-field)	2.1%	50	Yes	Yes	
9	07.04.06	50% MCE medium	1.8%	50	Yes	Yes	
10	11.04.06	50% MCE high (near-field)	2.8%	50	Yes	Yes	
11	13.04.06	Bi-directional cosine	2.0%	50	Yes	Yes	
12	23.05.06	Uni-directional EW	2.0%	50	No	No	
		fixed column endplate 24-05-06					
13	24.05.06	Uni-directional EW	2.0%	50	No	No	much better behavior from specimen
14	25.05.06	Uni-directional EW	2.0%	50	LE Damper	No	first test with new lead-extrusion damper; No dampers attached in NS direction
15	25.05.06	Uni-directional EW	2.0%	50	LE Damper	No	2nd test w/ damper, tightened up bolts during test; No dampers attached in NS direction
16	29.05.06	90% DBE medium	1.2%	50	LE Damper	Yes	No dampers attached in NS direction
17	30.05.06	50% MCE medium	2.1%	50	LE Damper	Yes	No dampers attached in NS direction
18	30.05.06	Uni-directional EW	3.0%	50	LE Damper	No	1%-2%-3% drift, two cycles each
19	31.05.06	Uni-directional EW	3.0%	50	No	No	two cycles at 3% drift only
20	01.06.06	90% MCE high	3.8%	50	Yes	Yes	
21	02.06.06	90% MCE med	4.7%	50	Yes	Yes	
22	-	Uni-directional EW	2.0%	50	2 LE Dampers	-	0.5%-1%-2% drift, two cycles each
23	-	Uni-directional EW	3.0%	50	2 LE Dampers	-	0.5%-1%-2%-3% drift, two cycles each

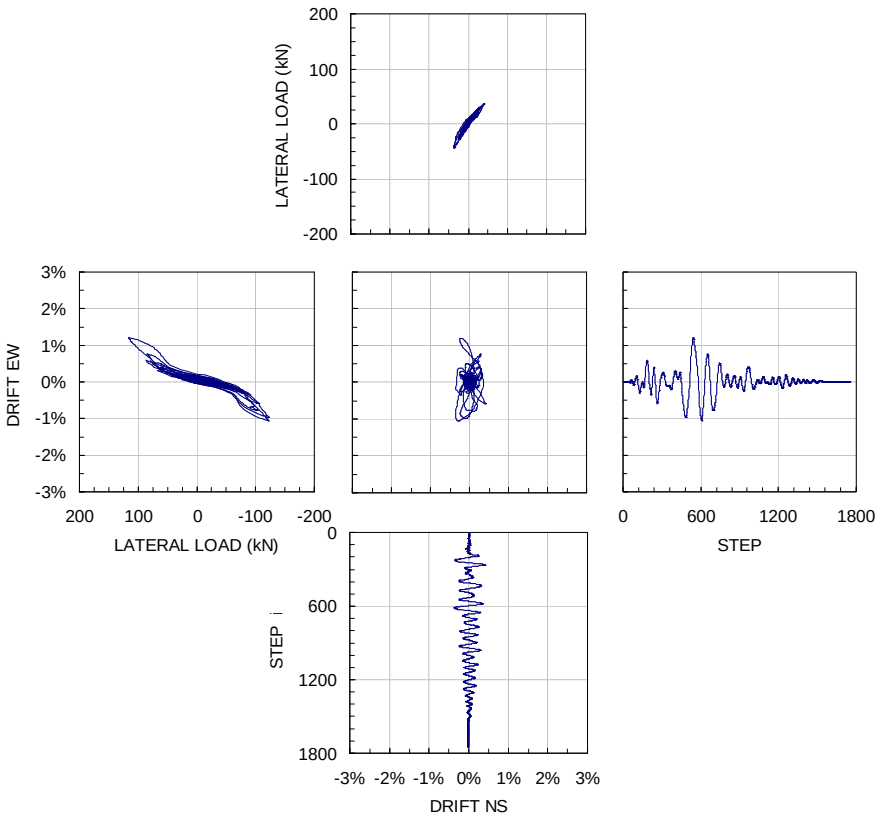

Figure B-1: 90 percent DBE (medium suite)

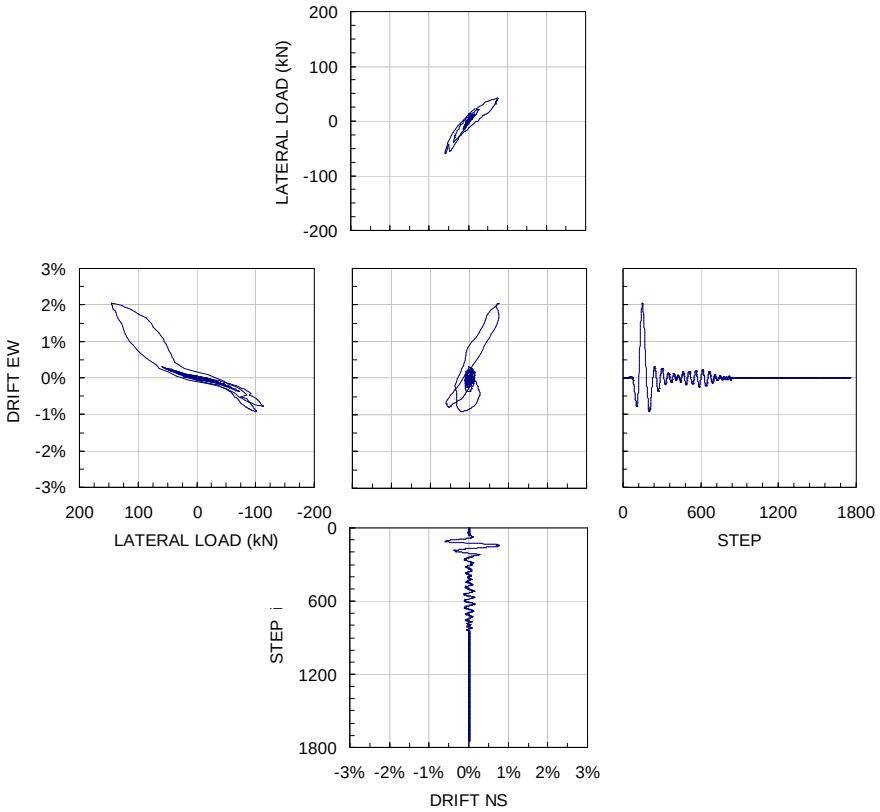

Figure B-2: 90 percent MCE (high suite)

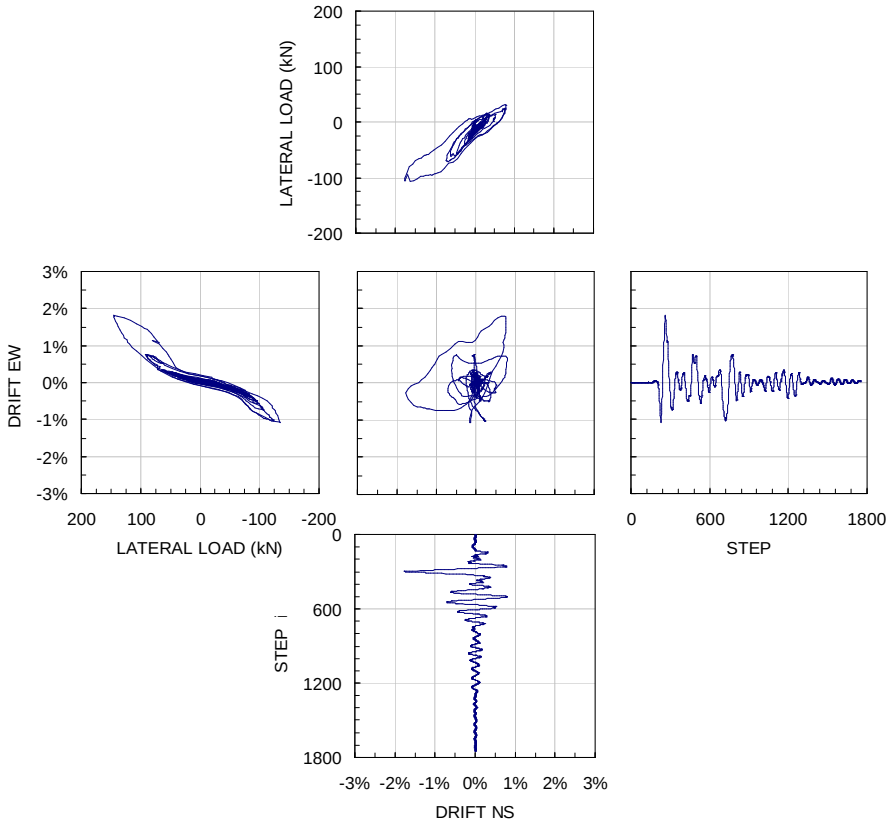

Figure B-3: 50 percent MCE (medium suite)

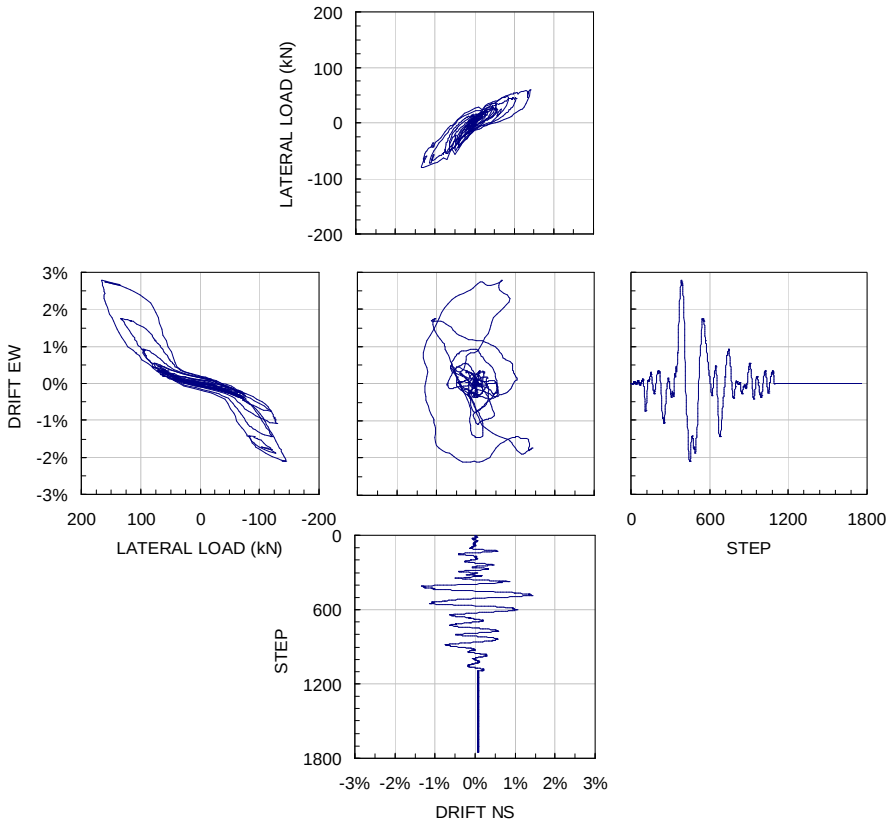

Figure B-4: 50 percent MCE (high suite)

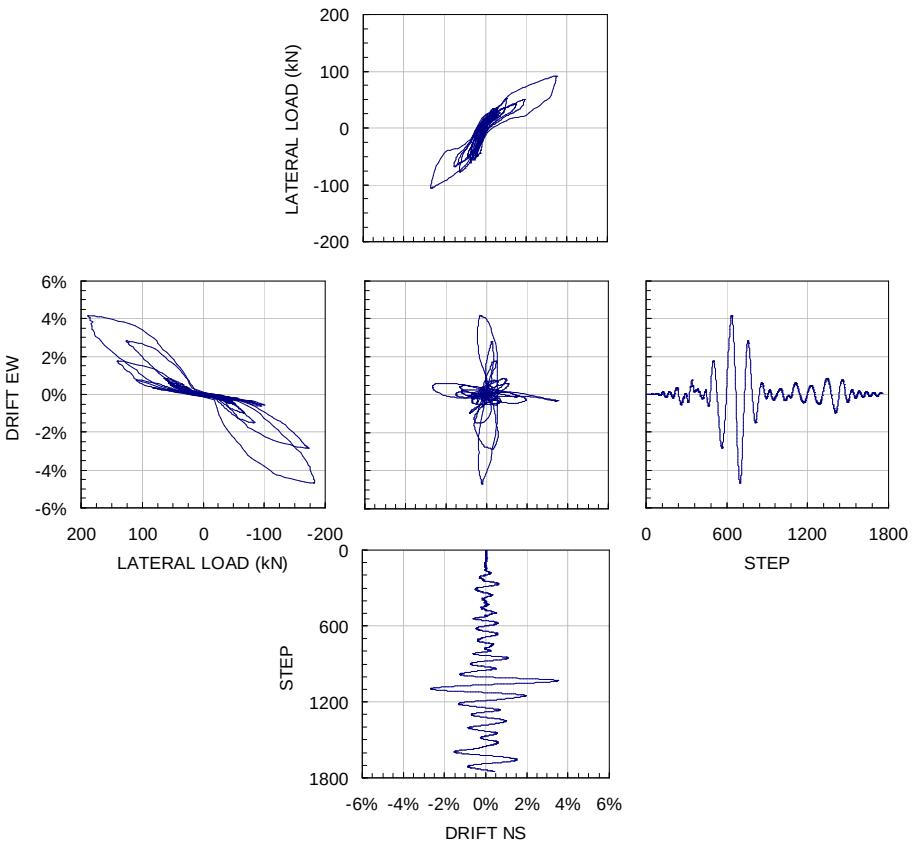

Figure B-5: 90 percent MCE (medium suite)

CHAPTER 6 SPECIMEN (EXT LE DAMPER)

Table B-2: Tests performed on the Chapter 6 beam-column joint subassembly..

Test #	Date	Description	Max Drift	PT (kN)	Dissipater	Gravity Load	Notes / Observations
1	25.10.06	UNI-EW @ 0.5% and 1.4%	1.40%	250	Y	N	
2	25.10.06	UNI-NS @ 0.5% and 1.4%	1.40%	250	Y	N	
3	25.10.06	BI-DIR @ 0.5% and 2% (radial)	1.40%	250	Y	N	
4	13.11.06	UNI-EW @ 2.3% only	2.30%	250	Y	N	
5	13.11.06	UNI-NS @ 2.3% only	2.30%	250	Y	N	
6	22.11.06	90% DBE	1.60%	250	Y	Y	input file created by B. Bradley
7	22.11.06	50% MCE	1.60%	250	Y	Y	input file created by B. Bradley
8	23.11.06	90% MCE	2.80%	250	Y	Y	input file created by B. Bradley
9	23.11.06	UNI-EW .5-1-2-3-4	3.00%	250	Y	N	input file: UNI-EW_.5-1-2-3-4%.csv -- Max Equiv Drifts for Bi-Dir Testing
10	23.11.06	UNI-NS .5-1-2-3-4	3.00%	250	Y	N	unput file: UNI-NS_.5-1-2-3-4%.csv -- Max Equiv Drift of Bi-Dir Testing
11	24.11.06	BI-DIR 0.5-1-2-3-4	3.00%	250	Y	N	seeing several new cracks at 2% drift

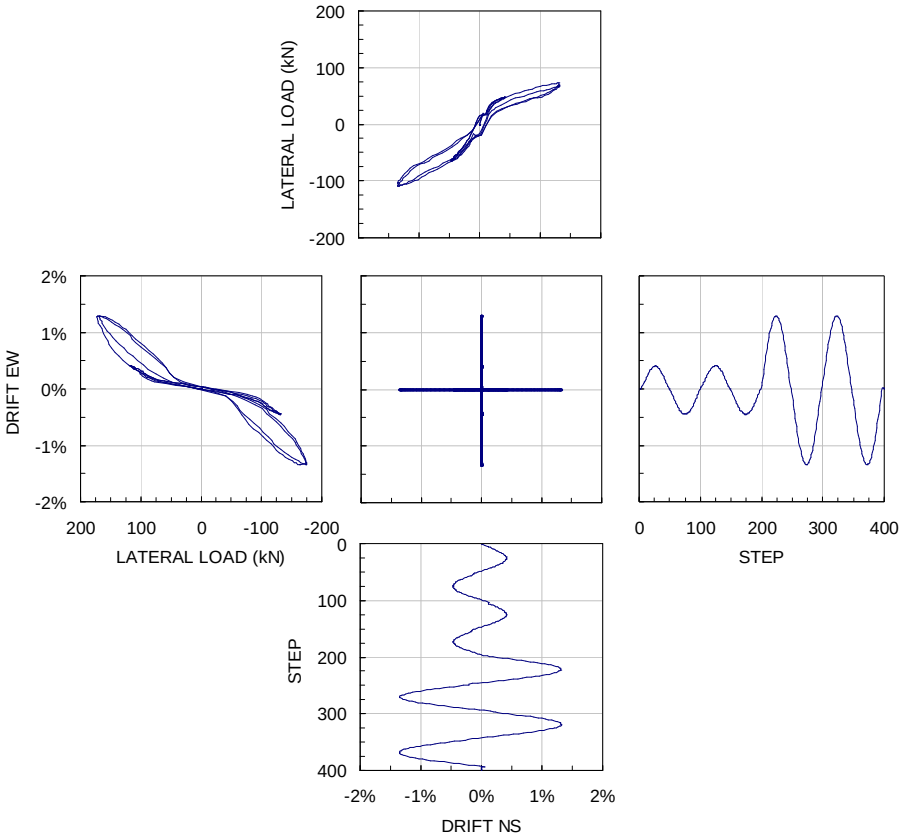

Figure B-6: Uni-directional tests to 1.4 percent drift (test 1 & 2).

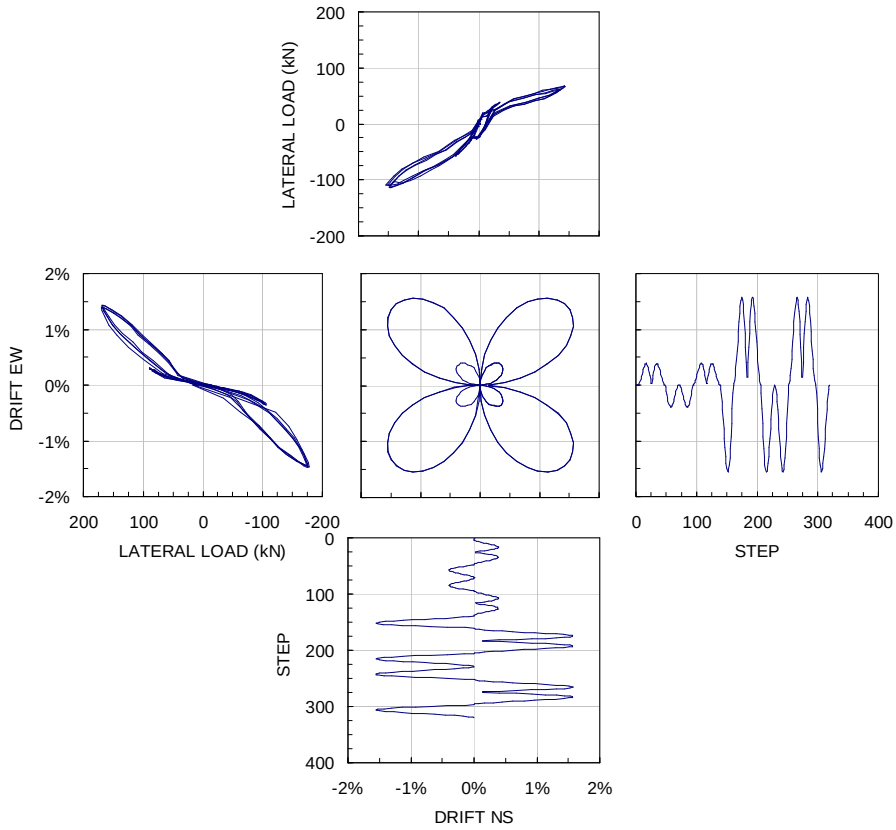

Figure B-7: Bi-directional test to 2 percent drift (test 3).

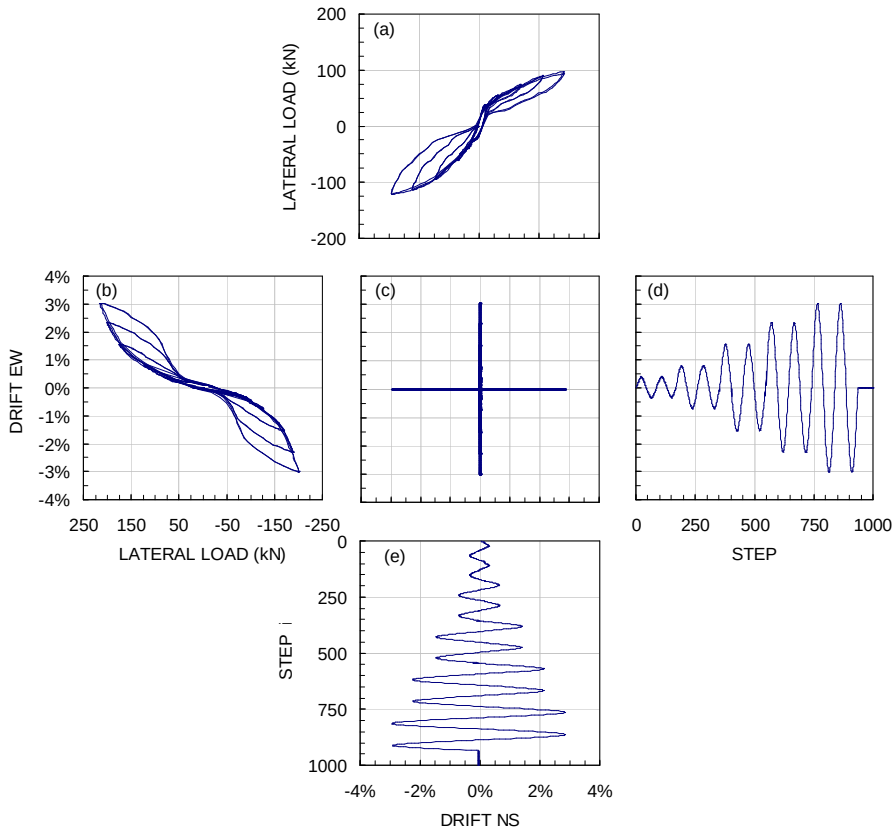

Figure B-8: Uni-directional tests to 4 percent drift (test 9 & 10).

Appendix C: Supplemental photographs

CHAPTER 3: DAD BRIDGE PIER

Strengthened shoe block

Test setup

Looking down on shoe block

Shoe block prior to testing

Crushing in the shoe block corner

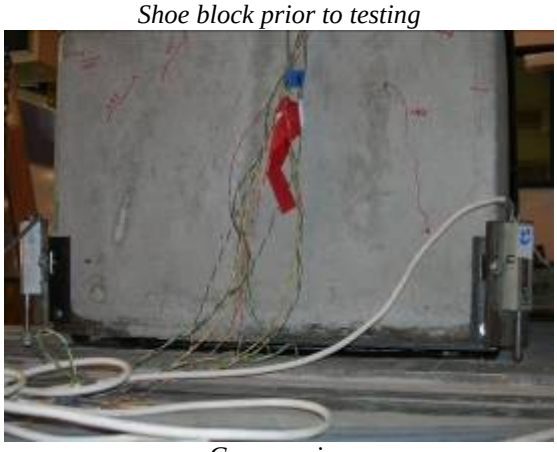

Gap-opening

Flexural cracks in the pier

The ball joint

Mild steel energy dissipater

Shoe block with energy dissipaters

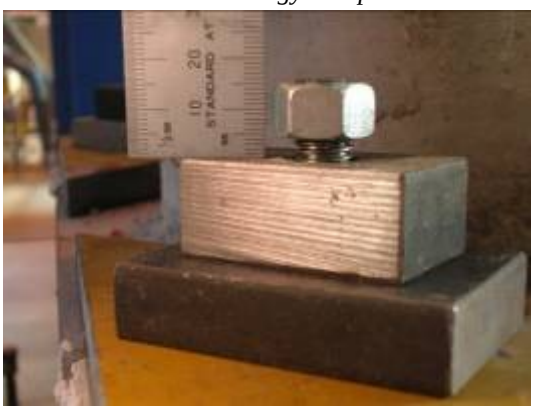

Elongation of a dissipater

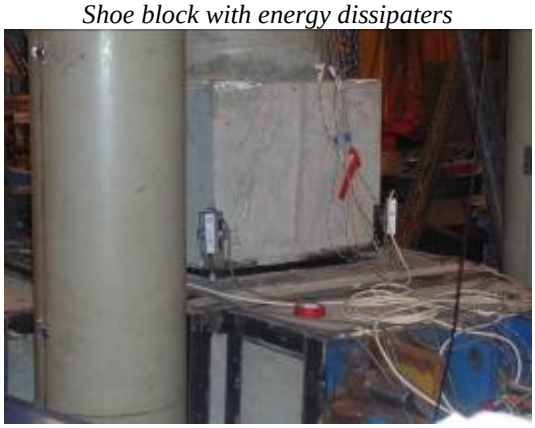

The specimen at 5 percent drift

CHAPTER 4 & 5: BENT TENDON BC JOINT

The beam-column joint reinforcing

Reinforcing

The beam-column joint reinforcing

The beam joint reinforcing

The cast-insitu joint

The column face

The test setup

The test setup

The buckled gravity beam dissipaters

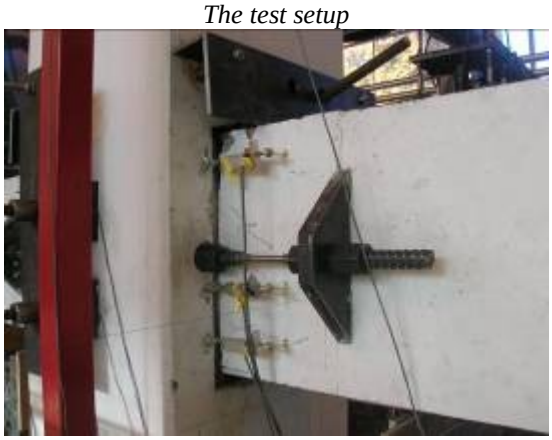

The west beam dissipater

The west beam during testing

The subassembly at 4 percent drift

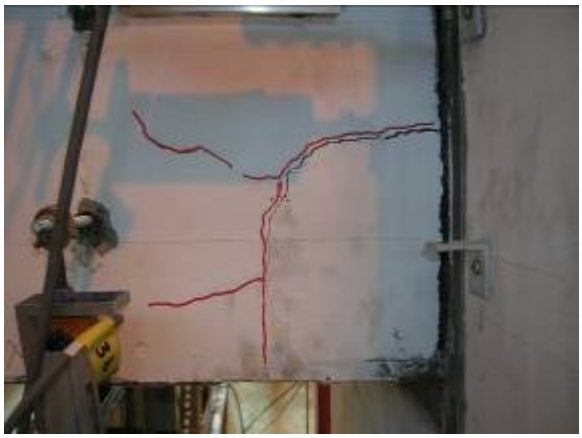

Tearing due to vertical prestress force

The buckled energy dissipaters

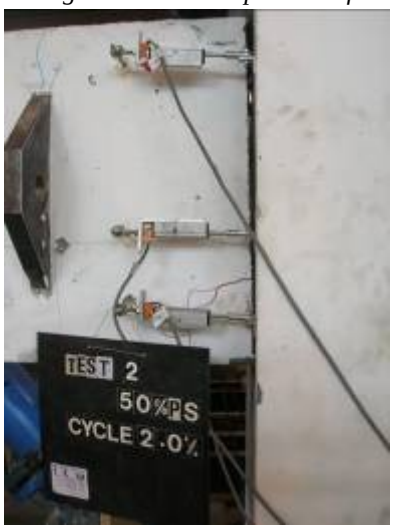

The joint at 2 percent drift

Localized damage

The mounted LE damper

The LE damper

CHAPTER 6: THE INTERNAL LE DAMPER

The seismic beam reinforcing cage

The seismic beam reinforcing cage

The joint region

The gravity beam reinforcing cage

The cast-insitu stub

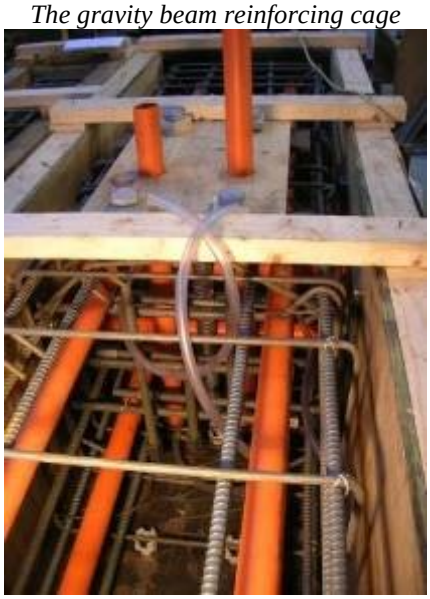

The column joint region

The column reinforcing cage

The column joint region

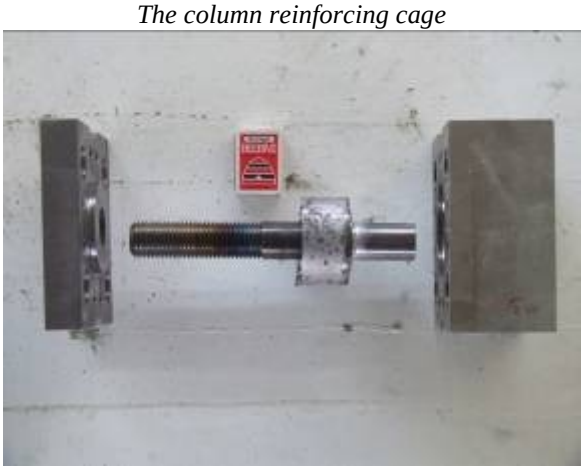

The LE damper disassembled (with lead)

The west joint

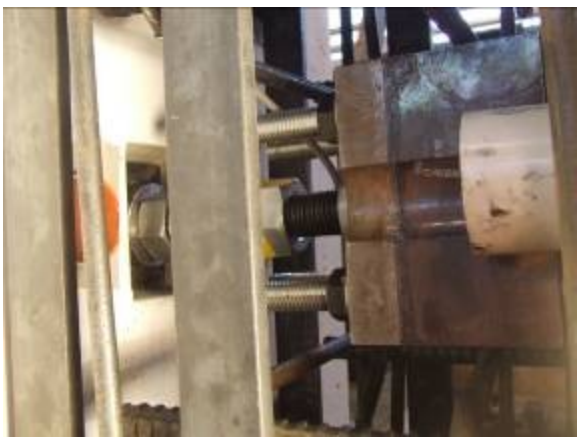

The LE damper connected to the threaded rod

The west joint

The east beam looking down on closure pour

The east joint

The south joint LE damper shaft

The south (gravity beam) joint

The south joint

The south joint

The test setup

Instrumentation setup

The base pin (fixed)

The joint prior to testing

The simulated gravity load

The east joint during testing

The specimen at 3 percent drift

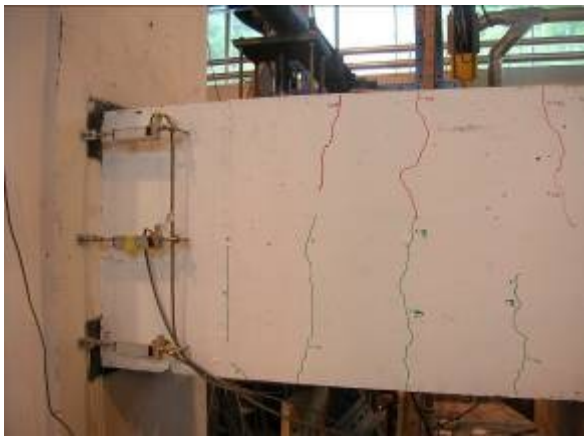

The west beam after testing

Gap-opening at the west beam

The gravity beam during testing

Bi-directional gap-opening at W and S beam

Gap-opening at 2 percent drift

Appendix D: Sample joint design

Given information

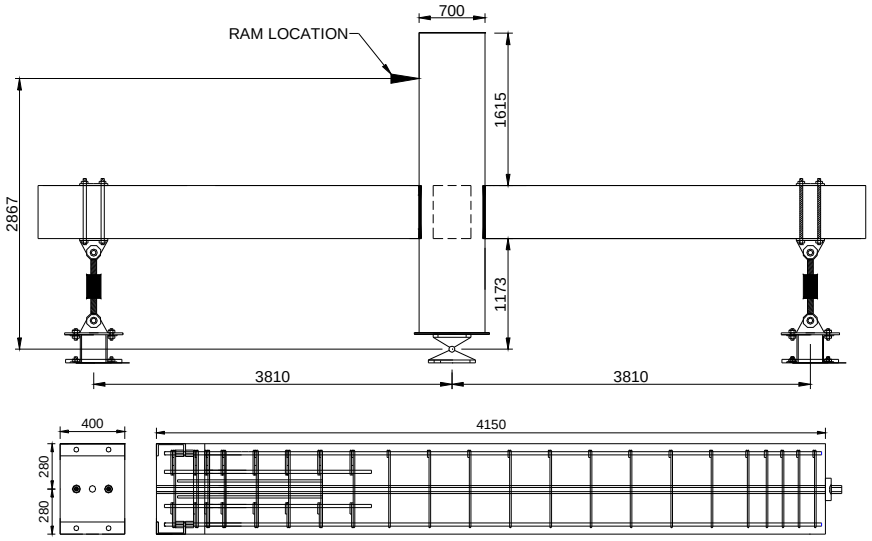

Required moment capacity:	ϕM_n	256 kNm
Concrete compressive strength:	f'_c	45 MPa
Joint concrete strength:	$f'_{c,\,joint}$	60 MPa
Elastic modulus of concrete:	E_c	31530 MPa
Longitudinal steel yield:	f_y	500 MPa
Stiffness of dissipater:	K_{diss}	200 kN/mm
Modulus of elasticity, PT:	E_{PT}	200,000 MPa
Ult. stress of PT (thread-bars):	f_u	1100 MPa

Geometry

$e_{PS} = e_{diss} = 280\text{mm}$ — *Moment arm, taken from rocking edge* (D-1)

$$I_{gross,beam} = \frac{bd^3}{12} = \frac{400 \cdot 560^3}{12} = 5.9\text{E}09mm^4$$ — *Gross moment of inertia, beam* (D-2)

$$I_{gross,col} = \frac{bd^3}{12} = \frac{700 \cdot 700^3}{12} = 2.0\text{E}10mm^4$$ — *Gross moment of inertial, column* (D-3)

$$EI_{eff,beam} = \alpha EI_{gross} = 4.6\text{E}13N - mm^2$$ — *Effective stiffness, beam (α=0.25) (Li, 2006)* (D-4)

$$EI_{eff,col} = \alpha EI_{gross} = 3.8\text{E}14N - mm^2$$ — *Effective stiffness, col (α=0.6)(Paulay & Priestley, 1993)* (D-5)

$L_c = 2867mm$ — *Height of column* (D-6)

$L = 7620mm$ — *Length of beam to centreline of column* (D-7)

$L_b = 6920mm$ — *Length of beam to face of column* (D-8)

$L_t = 9000mm$ — *Unbonded length of tendons (thread-bars)*

Response at gap-opening

$M = P_{PS,initial} \cdot e_{PS} = 500kN \cdot 280mm = 140kNm$ — $P_{PS,initial}$ *=250kN per thread-bar* (D-9)

$$V_{col} = 2M\frac{L}{L_b L_c} = 2 \cdot 140 \cdot \frac{7.6}{2.9 \cdot 6.9} = 106kN$$ — *Horizontal force at top of column* (D-10)

$$\Delta_{elastic} = \frac{V_{col}}{12}\left[\frac{(L_c - D)^3}{EI^*_{col}} + \frac{L_c{}^2 L_b{}^3}{L^2 EI^*_{bm}}\right] = 10.3mm$$ — *Horizontal displacement at top of column due to elastic flexural deformation of the members* (D-11)

Response at dissipater yield

$$\theta_{con} = \frac{P_{diss,yield}}{K_{diss} e_{diss}} = \frac{250}{200 \cdot 280} = 0.0045$$ *Connection rotation at dissipater yield = 250kN* (D-12)

$$P_{PS} = P_i + \frac{A_{PS} E_{PS}}{L_t} e_{PS} \theta_{con} n = 280kN$$ *Force from each thread-bar at given rotation, n = 2 because thread-bar spans two connections. $A_{PS} = 552mm^2$* (D-13)

$$M = \sum M_{PS} + \sum M_{diss} = 2 \cdot 280 \cdot 0.28 + 250 \cdot 0.28 = 227kNm$$ *Moment at joint at dissipater yield* (D-14)

$$V_{col} = 2M \frac{L}{L_b L_c} = 159kN$$ *Horizontal force at top of column* (D-15)

$$\Delta_{rigid} = \theta_{con} \frac{L_b}{L} L_c = 13.4mm$$ *Horizontal displacement at top of column due to rigid body rotation at the connection* (D-16)

$$\Delta_{elastic} = \frac{V_{col}}{12} \left[\frac{(L_c - D)^3}{EI^*_{col}} + \frac{{L_c}^2 {L_b}^3}{L^2 EI^*_{bm}} \right] = 16.7mm$$ *Horizontal displacement at top of column due to elastic flexural deformation of the members* (D-17)

$$\Delta_{total} = \Delta_{elastic} + \Delta_{rigid} = 30.1mm$$ *Total displacement at top of column* (D-18)

Response at θ_{con}=0.02

$$P_{PS} = 250 + \frac{552 \cdot 200000}{9000} 280 \cdot 0.02 \cdot 2 = 387kN$$ *Force from each thread-bar at given connection rotation.* (D-19)

$$M = \sum M_{PS} + \sum M_{diss} = 2 \cdot 387 \cdot 0.28 + 250 \cdot 0.28 = 286kNm$$ *Moment at joint* (D-20)

$$V_{col} = 2M \frac{L}{L_b L_c} = 159kN$$ *Horizontal force at top of column* (D-21)

$$\Delta_{rigid} = \theta_{con} \frac{L_b}{L} L_c = 60.2mm$$ *Horizontal displacement at top of column due to rigid body rotation at the connection* (D-22)

$$\Delta_{elastic} = \frac{V_{col}}{12} \left[\frac{(L_c - D)^3}{EI^*_{col}} + \frac{{L_c}^2 {L_b}^3}{L^2 EI^*_{bm}} \right] = 21.1mm$$ *Horizontal displacement at top of column due to elastic flexural deformation of the members* (D-23)

$$\Delta_{total} = \Delta_{elastic} + \Delta_{rigid} = 81.3mm$$ *Total displacement at top of column* (D-24)

Response at prestress thread-bar yield

$$\delta_u = \frac{f_u}{E_{PT}} L_t - \frac{f_i}{E_{PT}} L_t = 29.1mm$$ *Thread-bar elongation at ultimate (f_u = 1100MPa); where f_i = initial prestress*

$$\theta_{con} = \frac{\delta_u}{e_{PT} n} = \frac{29.1}{280 \cdot 2} = 0.052$$ *Connection rotation required for thread-bar yield* (D-25)

$$P_{PS} = A_{PS} f_u = 607kN$$ *Force in the prestress thread-bar*

$$M = \sum M_{PS} + \sum M_{diss} = 2 \cdot 607 \cdot 0.28 + 250 \cdot 0.28 = 410kNm$$ *Moment at joint at prestress thread-bar ultimate* (D-26)

$$V_{col} = 2M \frac{L}{L_b L_c} = 286kN$$ *Horizontal force at top of column* (D-27)

$$\Delta_{rigid} = \theta_{con} \frac{L_b}{L} L_c = 156.3mm$$ *Horizontal displacement at top of column due to rigid body rotation at the connection* (D-28)

$$\Delta_{elastic} = \frac{V_{col}}{12} \left[\frac{(L_c - D)^3}{EI^*_{col}} + \frac{{L_c}^2 {L_b}^3}{L^2 EI^*_{bm}} \right] = 30.1mm$$ *Horizontal displacement at top of column due to elastic flexural deformation of the members* (D-29)

$$\Delta_{total} = \Delta_{elastic} + \Delta_{rigid} = 186.3mm$$ *Total displacement at top of column* (D-30)

Resulting response

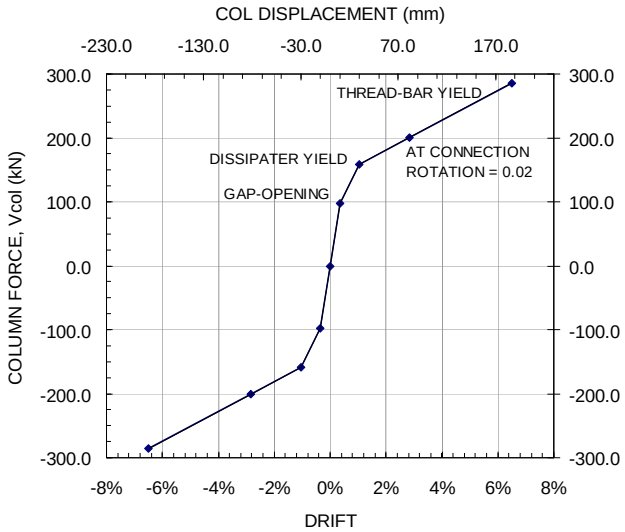

Check beam flexural reinforcement

$M^* = 410\ kNm$ — *Design moment demand at ultimate conditions. This will give (mostly) elastic response.* (D-31)

Try (6) D20 bars top and bottom; — *Four bars bottom layer, 2 bars mid layer*

$\phi M_n = \phi A_s f_y (d\text{-}d') = 373\ kNm < M^*$ — *OK*, use (6) D20 bars* (D-32)

**slightly under at ultimate conditions; some yielding acceptable in this case.*

Check beam transverse reinforcement (D-33)

$$V^* = \frac{2M^*}{L_b} = \frac{410}{3.81} = 107kN$$ — *Maximum shear demand at joint (neglecting beam weight; no tributary floor weight)* (D-34)

Try R12 bars at 100mm

$\phi V_n = 0.85 \cdot 2 \cdot A_s f_y (d/s) = 240kN$ — *OK, use D12 @ s=100 at joint region, minimum otherwise.* (D-35)

Check joint armouring

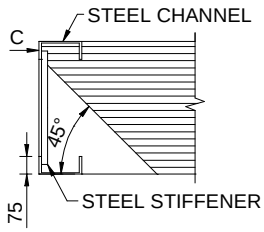

Assume point load, C, is distributed by steel to whole concrete area behind channel.

Assume compression stress propagates at 45 degree angle.

$$C^* = \sum P_{PS} + \sum \Omega P_{diss}$$
$$= 2 \cdot 607 + 1.5 \cdot 250 = 1589kN$$ — *Maximum force at ultimate* (D-36)

$C^* \le (t_f b) f'_c = 75 \cdot 400 \cdot 60 = 1800kN$ — *OK, channel is sufficient* (D-37)

Check shear keys

Self Weight = .56·.4·3.5·23 = 18*kN*	*Gravity load from self-weight beam; 23kN/m^3* **no tributary load in seismic beams*	(D-38)
*V** = 18*kN*+107*kN* = 125*kN*		(D-39)
Try 30mm 8.8 grade (f_y = 880*MPa)* shear key	*Machined from grade 8.8 bolts, considering 1 (of four) will resist shear; conservative*	
$\phi V_n = \phi \cdot 0.6 \cdot A_s f_y = 0.85 \cdot 0.6 \cdot 707 \cdot 880 = 317kN$	*OK*	(D-40)
Check shear key bearing on column armouring plate	*This check ensures load transfer from shear key to column armouring in sufficient*	
$0.85\ f_y\ t\ d_b = 0.85\ 350 \cdot 15 \cdot 30 = 133kN > V^*$	*OK, column armouring plate is 15mm thick; 30mm bolt diameter.*	(D-41)
Check stiffeners can transfer shear forces	*This is to ensure the stiffeners can transfer shear forces, thus transferring forces thru compression to concrete.*	
$0.85\ f_y\ n\ A_s = 0.85 \cdot 350 \cdot 2\ 25 \cdot 10 = 150kN > V^*$	*OK, 2 stiffeners required*	(D-42)
Check joint shear strength		
$V \le 1.25\sqrt{f'_c}A_j = 2100kN > V = 1800kN$	*OK, satisfies joint shear requirement defined in ACI-318 (1989)*	(D-43)

Appendix E: Sample rapid IDA-EAL calculation

Problem statement: Calculate the expected annual loss for the Japanese bridge pier using the methods presented in Chapter 2.

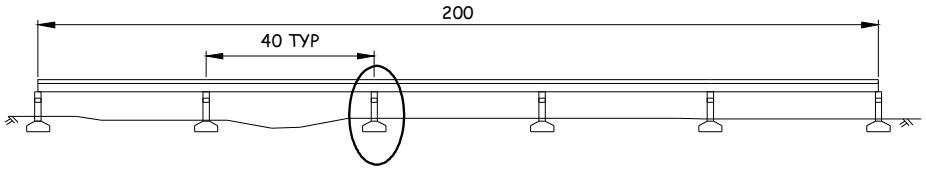

		NZ	Japan	Caltrans
D	mm	1700	2000	2000
D'	mm	1540	1834	1838
PHZ	mm	1700	4000	3000
$P/A_g f'_c$	-	0.15	0.11	0.11
Bar	-	28-D32	28-D51	32-D41
M_n	kN-m	11200	22400	19300
ρ_t	-	0.99%	1.82%	1.34%
Spiral	-	R20@170	R20@115	R20@85
ρ_s	-	0.49%	0.61%	0.78%
T_n	sec	0.86	0.61	0.66

ρ_s = ratio of the volume of the spiral to the volume of the confined concrete
ρ_t = the ratio of the longitudinal bars area to the pier's cross sectional area
T_n = natural period

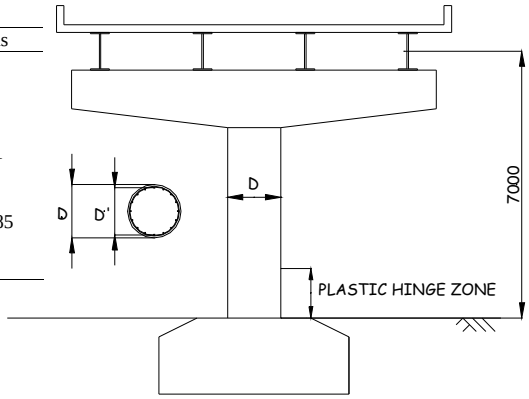

Seismic weight to the pier: W 7000kN

Step 1: Develop pushover curve and calculate damage states

$M_n = 22{,}400kNm;\ V_{col,\ yield} = 3200kN$ — *Determined using the analysis program RESPONSE 2000* (E-1)

$\theta_y = 0.0015\ L/D = 0.5\%$ — *From Priestley et al. (1986)* (E-2)

$K_i = M_n / \theta_y = 4226415\ kNm$ — *Initial stiffness of system* (E-3)

$K_{post\text{-}yiled} = \alpha_s K = 84528\ kNm$ — *Post-yield stiffness where $\alpha_s = 0.02$* (E-4)

$\theta_{DS2\text{-}3} = 1.6\%$ — *Defined as concrete spalling, given $\varepsilon_c = 0.008$ (Paulay & Priestley, 1992). Founding using analysis program RESPONSE 2000* (E-5)

$\theta_{DS3\text{-}4} = 4.6\%$ — *Defined as longitudinal bar buckling using model given in Berry & Eberhard (2005)* (E-6)

$\theta_{DS5} = 5.7\%$ — *Given $\mu_{DS5} = \mu_{DS4} + 2$* (E-7)

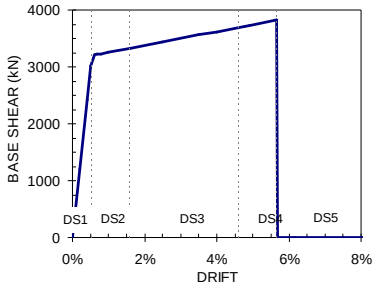

Resulting pushover curve and damage state limits

Step 2: Calculate the median IDA curve

Sample calculation for DS2-3; θ = 1.6%

$\Delta = \theta \cdot H = 0.016 \cdot 7 = 0.112m$ — *Displacement at top of column* (E-8)

$\mu = \theta / \theta_y = 1.6 / 0.5 = 3.2$ — *Ductility at θ* (E-9)

$M = M_y + K_{post\text{-}yield}(\theta - \theta_y) = 23304\ kNm$ — *Moment at θ* (E-10)

$V_{col} = M / H = 3329\ kN$ — *Column force at θ* (E-11)

$C_c = V_{col} / W = 0.48$ — *Normalized force to seismic weight* (E-12)

$$\xi_{eff} = \xi_o + \xi_{hy} = \xi_o + \frac{2}{\pi}\eta\frac{(1-\alpha_s)(1-1/\mu)}{(1-\alpha_s+\mu\cdot\alpha_s)} = 10.0$$

Effective damping where η=0.25 given a modified Takeda hysteresis loop with α=β=0.3 (Carr, 2006); ξ_o = 5 percent (E-13)

$$T = 2\pi\sqrt{\frac{\Delta}{C_c g}} = 2\pi\sqrt{\frac{0.112}{0.48\cdot 9.81}} = 0.97s$$

Period for given secant stiffness (E-14)

$$B_a = \sqrt{\frac{2+\xi_{eff}}{7}} = 1.56$$

Damping reduction factor for constant acceleration range (0.15s<T<0.4s) (E-15)

$$B_d = \sqrt{\frac{8+\xi_{eff}}{13}} = 1.33$$

Damping reduction factor for constant displacement range (T > 3s) (E-16)

$B_v = 1.51$ — *Damping reduction factor for constant displacement range (0.4s<T<3s); found by interpolation* (E-17)

$$F_v S_1 = 2\pi\sqrt{\frac{C_c\cdot\Delta}{g}}\cdot B_v = 2\pi\sqrt{\frac{0.48\cdot 0.112}{9.81}}\cdot 1.51 = 0.70$$

Median IDA curve data point (E-18)

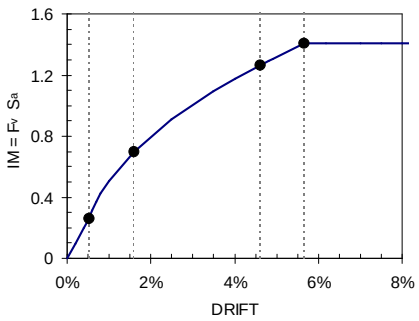

Resulting median IDA curve

Step3: Incorporate uncertainties

$\beta_c = 0.2;\ \beta_u = 0.25$ — *Uncertainty in capacity and modelling (FEMA, 2000)* (E-19)

$\beta_{DBE} = \beta_d = 0.35$ — *Found from IDA analysis; β_d varies with IM* **This parameter needs further investigation* (E-20)

$\beta_{c/d} = \sqrt{\beta_d^{\,2} + \beta_c^{\,2} + \beta_u^{\,2}}$ — *General SRSS method combination of uncertainties* (E-21)

Define hazard-recurrence relationship

$$f_a(IM) = k_o(IM)^{-k} \qquad \textit{Where k=3 for New Zealand seismicity} \qquad \text{(E-22)}$$

Summary of calculations

	θ	IM	f_a	LR	Δ LR	(ΔLR)(f_a)	cont to EAL
DS1				0			*with trunc*
	0.53%	0.261251194	0.007654514		0.03	0.000229635	0.000375753
DS2				0.03			
	1.60%	0.698716227	0.000388368		0.05	1.94184E-05	7.94281E-05
DS3				0.08			
	4.60%	1.264005062	6.44314E-05		0.17	1.09533E-05	8.96037E-05
DS4				0.25			
	5.66%	1.409010853	4.63631E-05		0.75	3.47723E-05	0.000335764
DS5				1			
						SUM	0.000880548
						x1M	**880.5**

EAL = $880 per $1M of asset value (E-23)

REFERENCES

Berry MP and Eberhard MO. 2005. Practical performance model for bar buckling. Journal of Structural Engineering – ASCE; **131**(7):1060-1070.

Carr AJ. 2006. RUAUMOKO: Inelastic Dynamic Computer Program. Computer Program Library, Department of Civil Engineering, University of Canterbury, Christchurch, New Zealand.

Paulay T, Priestley MJN. 1992. *Seismic Design of Reinforced Concrete and Masonry Buildings*. Wiley, New York, NY, 744 pp.

Priestley MJN, Seible F, and Calvi GM. 1986. *Seismic Design and Retrofit of Bridges*. Wiley, New York, NY, 686 pp.

Federal Emergency Management Agency (FEMA). 2000. Recommended seismic design criteria for new steel moment-frame buildings. *Rep. No. FEMA-350*. SAC Joint Venture: Washington, DC.